serial and parallel robotics: energy saving systems and rehabilitation devices

POLITECNICO DI TORINO
Scuola di Dottorato

Dottorato in Meccanica XXVI ciclo

Applied Mechanics

Serial and Parallel Robotics: Energy Saving Systems and Rehabilitation Devices

---

ZHE YIN

TUTOR: GIUSEPPE QUAGLIA

Marzo, 2014

Introduction

This thesis focuses on the design and discussion of robotic devices and their applications. Robotics is the branch of technology that deals with the design, construction, operation, and application of robots as well as computer systems for their control, sensory feedback, and information processing [1]. Nowadays, robotics has been an unprecedented increase in applications of industry, military, health, domestic service, exploration, commerce, etc. Different applications require robots with different structures and different functions. Robotics normally includes serial and parallel structures. To have contribution to two kinds of structures, this thesis consisting of two sections is devoted to the design and development of serial and parallel robotic structures, focused on applications in the two different fields: industry and health.

As we know, robots have a great contribution into industry, especially in manufacturing, welding, and assembly. Robots can improve product quality, reduce manufacturing cost and increase productivity, and so on. However, at the same time, robots consume electrical energy to accomplish tasks. According to annual energy review [2][3], energy consumption increases annually and the industry sector accounts for the biggest percentage in annual energy consumption, among industry, transport, residential and domestic service. Energy saving in industry is therefore becoming very important. The first section of the thesis discusses the energy saving technologies in the industrial application. Specifically, for the widely applied serial robotic structures, the thesis proposes the balancing systems for the energy saving purpose. The balancing system applies the torque compensation technology to counteract the gravity effect of the serial robotic manipulators. The serial robotic structures equipped with the balancing systems can save energy and work in an energy saving way.

Robotic application in health is also a significant area and worth paying attention. Rehabilitation robotics [4] is a field of research dedicated to understanding and augmenting rehabilitation through the application of robotic devices. Over the last two decades, research into robot mediated therapy for the rehabilitation of stroke patients has grown significantly as the potential for cheaper and more effective therapy. Also rehabilitation robotics can be applied to individuals with cerebral palsy, or those recovering from orthopedic surgery [5]. It would be able to carry out exercises, some of which a therapist would provide, but some of which are not so easy to be executed by a human being [6].

The rehabilitation for the human ankle is one of aspects that rehabilitation robotics focuses on. The human ankle is a very complex bony structure in the human skeleton [7]. In fact, the ankle is the most common site of sprain injuries in the human body. In the United States, over 23,000 cases estimated to occur per day [8]. In Australia, about 100,000 emergency department presentations are reported per year. Also in New Zealand, more than 82,000 new claims and 17,200 ongoing claims related to ankle injuries were made in the 2000/2001 year [9]. Additionally, ankle disabilities are common in neurological disorders, such as stroke, traumatic brain, and spinal cord injuries. Every year, more than 795 000 Americans suffer a stroke and the stroke is the leading cause of permanent disability in the United States [10]. Rehabilitation robotics is beneficial for the recovery of ankle disabilities. With rehabilitation robotics, a patient

can repeat the process or exercise as many times as he wishes. Another positive aspect is the fact that exact measurements of the patient's improvement or decline can be obtained, through the sensors on the device. The rehabilitation robotics can apply constant therapy for long periods. The rehabilitation robot is a wonderful device to use according to many therapist and patients that have gone through the therapy [6]. The second part of this thesis will focus on the rehabilitation of the human ankle and propose a robotic device with a parallel structure for the training and recovery of the ankle. The rehabilitation device can be applied for the improvement of the ankle performance and muscle functions.

References:

[1] Robotics. Oxford Dictionaries. Retrieved 4 February 2011.

[2] International Energy Outlook 2013. U.S. Energy Information Administration. DOE/EIA-0484(2013).

[3] BP Statistical Review of World Energy. June, 2013.

[4] Brewer, BR; McDowell, SK; Worthen-Chaudhari, LC (2007 Nov-Dec). "Poststroke upper extremity rehabilitation: a review of robotic systems and clinical results." Topics in stroke rehabilitation14 (6): 22–44.

[5] Hillman, M. (2004). Rehabilitation robotics from past to present: A historical perspective. In Z.Z. Bien & D. Stefanov (Eds.), Advances in Rehabilitation Robotics (25-44). Berlin: Springer-Verlag.

[6] Carrera, I., Moreno, H., Saltarén, R., Pérez, C., Puglisi, L., & Garcia, C. (2011). ROAD: domestic assistant and rehabilitation robot. Medical & Biological Engineering & Computing, 49(10), 1201-1211.

[7] Tejima N. Rehabilitation robotics: a review. Advanced Robotics 2000, 14: 551-564.

[8] Hertel J: Functional anatomy, pathomechanics, and pathophysiology of lateral ankle instability. J Athl Train 2002, 37:364–375.

[9] Brukner P, Khan K: Clinical sports medicine. 3rd edition. Sydney: McGraw Hill; 2006.

[10] American Heart Assoc. (2009). Heart Disease and Stroke Statistics, 2009.

Section I Energy Saving Systems for Serial Robotic Structures

Section I discusses the design and development of energy saving systems for the serial robotic structures. The robotic structures presented in this section are commonly used in industrial automation and production. The energy saving systems apply the balancing technology to save the energy which is used to keep the static gravity of the manipulators in non-balanced counterparts. A manipulator is statically balanced if its torque caused by the static gravity during its working is counteracted by its balancing system.

The balancing technology is an old topic and there are many research organizations and people working on it. Counterweight and spring are the main tools for the static balance of manipulators. Compared with the counterweight approach, the balancing approach with springs introduces little mass and benefits the manipulator performances, therefore, it is preferable applied by researchers. Using this approach, they have proposed many excellent and genius solutions for the static balance of the various robotic structures. However, most of them discuss the balancing issues theoretically and ideally. Among published results, they lack of feasible solutions in real applications. Some researchers only focus on the feasible solutions for their respective robotic structures and for their specific usages. As the supplement and development of the balancing topic, this section of the thesis discusses feasible solutions for industrial robotic devices which are articulated and serial manipulators with two rotational degrees of freedom. This kind of structures is commonly applied in industry and their feasible solutions are also valuable for similar structures and serial structure with more than two degrees of freedom. The design process of the balancing systems have an emphasis on practical considerations and the realization of perfect torque compensation.

To illustrate the design process and the feasible solutions in a clear way, the content of this section is organized in this way:

In Section I.1, an investigation on the state of the art for balancing systems using springs is presented.

In Section I.2, two serial robotic structures are introduced respectively. The first model has a parallelogram structure and the two motors are mounted on the base. The second model has two articulated connected linkages with two motors mounted on their respective joints. After that, their kinematic and dynamic analysis are presented and compared. Simulation tools are applied and their movement performances are plotted.

In Section I.3, the two balancing systems for the two serial structures are proposed. Energy transfer principle is illustrated to support the introduction of the balancing system. The first balancing system consists of linkages and mechanical springs. The structure of the balancing system is evolved based on practical considerations. Springs' design is followed to satisfy the static equilibrium. Numerical examples are shown to classify approximate and perfect equilibrium. Another feasible balancing strategy is

demonstrated, consisting of cross mechanism, pulley and cable mechanism. Perfect balance is realized. Pneumatic and hydro-pneumatic springs are discussed to provide with constant forces. The three dimensional array for the structure is also shown graphically.

In Section I.4, the spring distribution is discussed for the layout arrangement of the first balancing system. This part focuses on feasible solutions considering the volume of the whole balancing system. This is the valuable work since many researchers consider the balancing system only with ideally ‘zero length spring’ (the spring produces zero force when its length is zero). The two influence factors are discussed and the whole volume is graphically shown.

In Section I.5, the conclusions are collected and featured results are highlighted.

Section I.1 State of the Art for Balancing System

Saving energy is becoming increasingly important in recent years [1]. In manufacturing and processing industry, energy consumption normally accounts for a majority of the production cost [2]. Therefore, energy saving is considered by designers of mechanical mechanisms as a principal aspect. Serial manipulators, as effective machining tools, have a wide range of applications in production lines [3]. However, they have massive linkages requiring extra actuator efforts to compensate their gravity during working. Much research [4-6] has been done to decrease energy consumption caused by the gravity of manipulators, including applying light-weight materials, improving the structure, and static balancing strategies. A machine is statically balanced if it can move freely in every configuration of its workspace without spending energy from any actuator to keep its equilibrium [7]. In other words, gravity effect from massive linkages is counteracted by balancing mechanisms, therefore the introduction of balancing mechanisms saves the energy which is used to drive manipulators in non-gravity balanced counterparts. Static balancing is a feasible technology to realize the energy saving target and many mechanical systems need to be equipped with balancing devices [4-10]. A system statically balanced can move during its workspace in an energy-saving way.

I.1.1 Counter-weight approach

Two types of static balancing [5] are applied in balancing systems: the mass balancing by means of counterweights and the elastic balancing by means of springs. The mass balancing by counterweights is an old topic and there are many valued work done in this field [4, 8-11]. Adding a counter weight to a mechanical system brings the center of the mass coincident with a vertical joint axis. In this way, energy efficiency is improved. However, greater mass of the system has bigger volume and greater inertia, degrades dynamic performance and the ability to resist external forces. The greater mass also means larger amounts of power consumed in resisting gravity of the system. Normally, a counter load is amounted at the opposite end of a link, compensation torque balancing with gravitational torque is therefore generated [4, 11]. Moreover, accurate compensation torque requires counter weights to be adjusted according to different postures of links and mass change on an end effector. So counter weights are not applied for all joints' balance but only for some ones around the base.

I.1.2 Spring approach

Balancing by means of springs avoids the disadvantages mentioned in 'Counter-weight approach' Part because of little mass of springs. The introduction of spring elements can balance gravitational potential energy. It adds little mass, inertia or complexity. With reasonable design, spring compensation can accurately match nonlinear joint torques induced by link motion, therefore, simplify control strategy, reduce actuator torque demand, lower power consumption and improve dynamic behaviours [12]. Using auxiliary devices, such as parallelogram linkages or pulleys, a spring device normally can be designed in a well connection with a mechanical system [13]. If the design of a balancing device is done based on good investigation of a system's structure, perfect

equilibration can be realized in which gravity effect of a system (with a balancing device in it) can be eliminated by the system itself. Any configuration of the system will be statically balanced under a perfect equilibrating situation without spending energy from any actuator for keeping its equilibrium [14].

I.1.2.1 Spring approach in theory

Many researchers [15-19] proposed theoretical solutions for the balance of mechanisms. Their work focused on the discrete and continuous balancing, multi solutions of balancing equation set, schematic possibilities, computerized algorithms et al.

Simionescu and Ciupitu [15] presented strategies of the static balancing for a rotating link around a horizontal fixed axis, by means of helical springs and other auxiliary devices. Discrete solutions for several positions' balancing were demonstrated. A simple system was firstly introduced, as shown in Figure I.1. 1 .

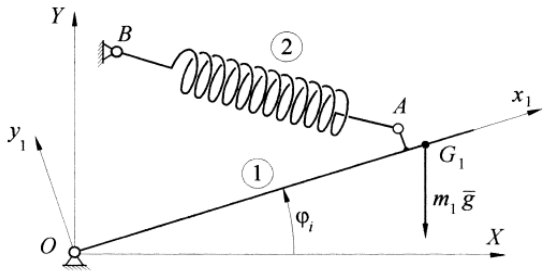

Figure I.1. 1 the spring balancing for a rotating link[15]

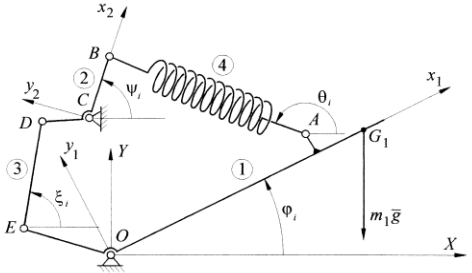

Figure I.1. 2 the balancing system with four linkages[15]

Its equilibrium of the forces moments is expressed as,

$$(m_1 OG_1 \cos\varphi_i + m_{2A} X_A)g + F_s a = 0, \quad i = 1,...,6. \qquad (I.1.1)$$

Where F_s is the spring force, $F_s = F_0 + k(AB - l_0)$,

$$a = \frac{X_B Y_A - X_A Y_B}{AB}, \quad \left\| \begin{matrix} X_A \\ Y_A \end{matrix} \right\| = R_{\varphi i} \left\| \begin{matrix} x_{1A} \\ y_{1A} \end{matrix} \right\|, \quad R_{\varphi i} = \left\| \begin{matrix} \cos\varphi_i & -\sin\varphi_i \\ \sin\varphi_i & \cos\varphi_i \end{matrix} \right\|,$$

$$AB = \sqrt{(X_A - X_B)^2 + (Y_A - Y_B)^2}, \quad m_{2A} = \frac{BG_2}{AB} m_2 .$$

(X_A, Y_A) and (X_B, Y_B) are the positions described in the coordinate XOY. (x_{1A}, y_{1A}) is the position in the local coordinate x_1Oy_1. $R_{\varphi i}$ is the transfer matrix between the two coordinates. m_1 and m_2 are the masses of the link 1 and the spring 2.

For six discrete values of φ_i, the unknown variables x_{1A}, y_{1A}, X_B, Y_B, F_0 and k can be calculated at the six positions. In a general case, y_{1A} and X_B are not equal to null, which reduce the value of the initial length l_0 of the spring. From the constructional point of view, an acceptable length l_0 can be achieved if the fixed point B is replaced by a movable mechanism. The movable mechanism moving around a fixed axis, a parallel plane or a translational guide may be referred in following situations.

(i) Figure I.1.2 shows a possibility characterised by a kinematic loop. The spring is articulated by a link 2. A link 3 is introduced to connect the link 2 with the link 1. The balancing description is followed as,

$$(m_1 OG_1 \cos\varphi_i + m_{4A} X_A)g + F_s(Y_A \cos\theta_i - X_A \sin\theta_i) + R_{31X} Y_E - R_{31Y} X_E = 0, \qquad i = 1,...,12, \tag{I.1.2}$$

Where,

$$\theta_i = \arctan\frac{Y_B - Y_A}{X_B - X_A}, \quad m_{4A} = \frac{BG_4}{AB} m_4, \quad m_{4B} = m_4 - m_{4A},$$

$$\begin{Vmatrix} X_E \\ Y_E \end{Vmatrix} = R_{\varphi i} \begin{Vmatrix} x_{1E} \\ y_{1E} \end{Vmatrix}, \quad \begin{Vmatrix} X_B \\ Y_B \end{Vmatrix} = \begin{Vmatrix} X_C \\ Y_C \end{Vmatrix} + R_{\psi i} \begin{Vmatrix} BC \\ 0 \end{Vmatrix}, \quad R_{\psi i} = \begin{Vmatrix} \cos\psi_i & -\sin\psi_i \\ \sin\psi_i & \cos\psi_i \end{Vmatrix}.$$

Then, some complementary equations are added and 12 distinct variables are collected. Finally, the solution is realized in an iterative manner.

(ii) Figure I.1.3 presents another possibility with a translational guide. A slide 2 is driven by the link 1 through a connecting rod 3. The balancing is described as,

$$(m_1 OG_1 \cos\varphi_i + m_{4A} X_A)g + F_s(Y_A \cos\theta - X_A \sin\theta) - R_{13X} Y_E + R_{13Y} X_E = 0, \ i = 1,...,11, \tag{I.1.3}$$

Where R_{13X} and R_{13Y} are reaction forces acting on the link 1 by a connecting rod 3.

$$R_{13X} = \frac{[(m_2 + m_3 + m_{4B})g\sin\alpha - F_s\cos(\theta - \alpha)]DE - m_3 gDG_3 \sin\alpha}{DE\cos(\alpha - \psi_i)}\cos\psi_i;$$

$$R_{13Y} = \frac{m_3 gDG_3 \cos\alpha\cos\psi_i - [(m_2 + m_3 + m_{4B})g\sin\alpha - F_s\cos(\theta - \alpha)]DE\sin\psi_i}{DE\cos(\alpha - \psi_i)};$$

$$\psi_i = \alpha + \arcsin\frac{X_E\sin\alpha - Y_E\cos\alpha - b - e}{DE};$$

$$X_B = e\sin\alpha + (S_i + d)\cos\alpha, \qquad Y_B = (S_i + d)\sin\alpha - e\cos\alpha.$$

Among these conditions, 11 variables are collected as x_{1A}, y_{1A}, x_{1D}, y_{1D}, CD, d, b, e, α, F_0 and k. If the work field is symmetrical with respect to the axis OY, the number of the unknowns decreases to six but high accuracy is required.

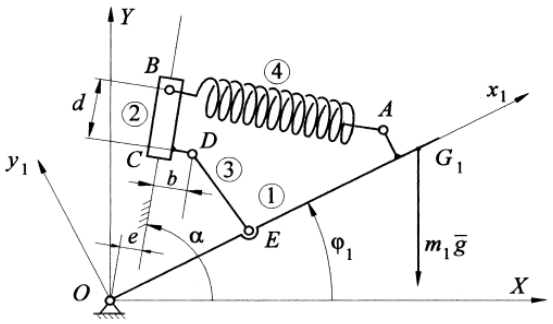

Figure I.1.3. the balancing system with a possible slider I[15]

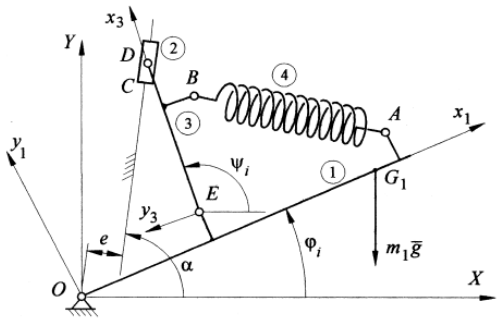

Figure I.1.4. the balancing system with a possible slider II[15]

Alternatively, the static balancing can be achieved in Fig. I.1.4. In this way, the reaction forces between the link 1 and the connecting rod 3 are changed as,

$$R_{13X} = \frac{[(m_2 + m_3 + m_{4B})g\sin\alpha + F_s\cos(\theta-\alpha)]\cos\psi_i}{\cos(\alpha-\psi_i)} + \frac{[m_3(X_{G3}-X_D) + m_{4B}(X_B-X_D)]g + F_s[(X_B-X_D)\sin\theta-(Y_B-Y_D)\cos\theta]}{DE\cos(\alpha-\psi_i)}\sin\alpha \quad ;$$

$$R_{13Y} = \frac{[(m_2 + m_3 + m_{4B})g\sin\alpha + F_s\cos(\theta-\alpha)]\sin\psi_i}{\cos(\alpha-\psi_i)} - \frac{[m_3(X_{G3}-X_D) + m_{4B}(X_B-X_D)]g + F_s[(X_B-X_D)\sin\theta-(Y_B-Y_D)\cos\theta]}{DE\cos(\alpha-\psi_i)}\cos\alpha \quad ;$$

$$\begin{Vmatrix} X_B \\ Y_B \end{Vmatrix} = \begin{Vmatrix} X_D \\ Y_D \end{Vmatrix} + R_{\psi i}\begin{Vmatrix} x_{3B} \\ y_{3B} \end{Vmatrix}, \qquad \psi_i = \alpha + \arcsin\frac{X_E\sin\alpha - Y_E\cos\alpha - e}{DE}.$$

11 variables are collected as x_{1A}, y_{1A}, x_{1D}, y_{1D}, x_{3B}, y_{3B}, CD, e, α, F_0 and k.

(iii) Figure I.1.5. introduces another structure for the balancing system. A connecting rod 3 has a translational joint with a rotating link 2. The two ends of the rod 3 are connected with the spring 4 and the link 1 respectively. The rod 3 has a plane-parallel movement during the motion of the system. Similarly, 11 variables are collected and solved using the same strategy mentioned before.

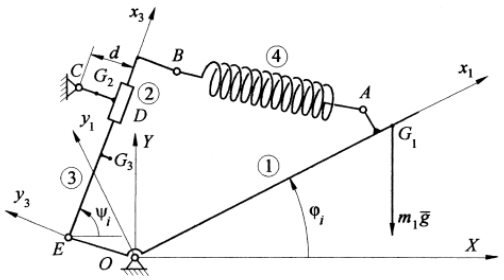

Figure I.1.5. a balancing system with a rotating slider[15]

After these study of balancing systems, an example is illustrated as an application of a discrete balance.

Then, Simionescu and Ciupitu[16] presented structures which balance was realized by the introduction of high pair mechanisms in a continuous way for the whole workspace. Figure I.1.6 shows a possibility for a continuous balance. The balancing spring 4 connects the link 1 with a cam mechanism which has a curve pathway on the link 1. The equations describing the directrix curves of the cam are,

$$x_1 = Y_C \sin\varphi \mp \frac{R(dY_C / d\varphi \cos\varphi - Y_C \sin\varphi)}{P} \quad ,$$

$$y_1 = Y_C \cos\varphi \pm \frac{R(dY_C / d\varphi \sin\varphi + Y_C \cos\varphi)}{P}$$

Where R is the radius of the follower 3,

$$P = \sqrt{\left(\frac{dY_C}{d\varphi}\right)^2 + Y_C{}^2} .$$

The equilibrium condition can be expressed as,

$$(OG_1 m_1 + OAm_{4A})g\cos\varphi + F_s \cdot OA\sin(\varphi - \theta) + Y_C R_{31}\sin\alpha = 0 \qquad \text{(I.1.4)}$$

Where R_{31} is the reaction force between the cam 1 and the roll 3,

$$R_{31} = [F_s \sin\theta + (m_2 + m_3 + m_{4B})g]\frac{P}{Y_C}, \quad X_A = OA\cos\varphi, \quad Y_A = OA\sin\varphi, \quad X_B = 0,$$

$$Y_B = Y_C + BC \quad , \qquad \alpha = \arctan\frac{dY_C / d\varphi}{Y_C} \quad , \qquad \theta = \arctan\frac{Y_B - Y_A}{-X_A} \quad ,$$

$$AB = \sqrt{(X_A - X_B)^2 + (Y_A - Y_B)^2} \ .$$

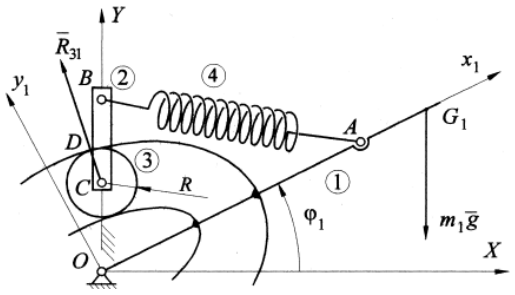

Figure I.1.6. a balancing system with a movable cam[15]

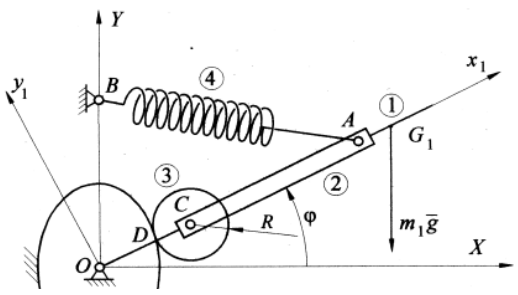

Figure I.1.7. a balancing system with a fixed cam[15]

In Fig. I.1.7, a cam is fixed and a follower moves along the link 1. In this case, the equations for the directrix curves are:

$$x_1 = X_C \mp \frac{R(dOC/d\varphi \sin\varphi + X_C)}{Q}, \qquad y_1 = Y_C \pm \frac{R(dOC/d\varphi \cos\varphi - Y_C)}{Q}$$

Where,

$$X_C = OC\cos\varphi, \qquad Y_C = OC\sin\varphi, \qquad Q = \sqrt{(dX_C/d\varphi)^2 + (dY_C/d\varphi)^2}\ .$$

Another structure is proposed in Fig. I. I.1.8. The cam is articulated and its follower is a part of the link 1. The relative position between the roll 3 and the cam 2 is:

$$x_{2D} = x_{2E} \pm \frac{RQ}{\sqrt{P^2+Q^2}}, \qquad y_{2D} = y_{2E} \mp \frac{RP}{\sqrt{P^2+Q^2}}$$

Where

$$P = y_{2E}\frac{d\psi}{d\varphi} + x_{1E}\sin(\psi-\varphi) - y_{1E}\cos(\psi-\varphi) \quad ,$$

$$Q = x_{2E}\frac{d\psi}{d\varphi} - x_{1E}\cos(\psi-\varphi) - y_{1E}\sin(\psi-\varphi)\ .$$

The reaction force in the touching point D is:

$$R_{31} = \frac{(m_1 OG_1\cos\varphi + m_{4A}X_A)g + F_s(Y_A\cos\theta - X_A\sin\theta)}{y_{1E}\cos(\psi-\phi-\varphi) - x_{1E}\sin(\psi-\phi-\varphi)}.$$

Figure I.1.9 shows another variant. A cam is a part of the link 1 and its follower can rotate around a fixed joint C.

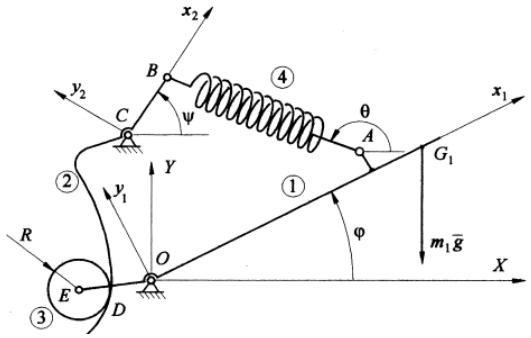

Figure I.1.8. a balancing system with a rotating cam mechanism I[15]

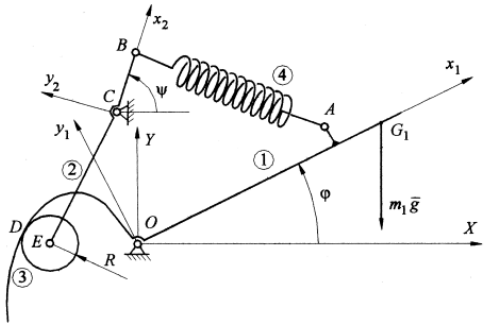

Figure I.1.9. a balancing system with a rotating cam mechanism II[15]

The active surfaces of the cam can be described as:

$$x_{1D} = x_{1E} \pm \frac{RP}{\sqrt{P^2+Q^2}}, \qquad y_{1D} = y_{1E} \mp \frac{RQ}{\sqrt{P^2+Q^2}}$$

Where,

$$P = x_{1E} - [x_{2E}\cos(\psi - \varphi) - y_{2E}\sin(\psi - \varphi)]\frac{d\psi}{d\varphi} \quad ,$$

$$Q = y_{1E} - [x_{2E}\sin(\psi - \varphi) + y_{2E}\cos(\psi - \varphi)]\frac{d\psi}{d\varphi} .$$

The balancing conditions for these structures were also analyzed in their work. After that, a concept 'efficaciousness coefficient' was introduced to evaluate the effect of a balancing system. The value of the coefficient depends on the ratio of the mechanical work for moving an unbalanced arm and an balanced one. A balancing mechanism is acceptable if the value is greater than one.

A motion function was presented as a standard for calculation of consumed mechanical power. The mechanical work for an unbalanced arm, a discrete balancing system and a continuous balancing system was formulated. Friction effect among mechanical joints was also included. Examples showed the effectiveness for balanced systems.

Kurt Hain's work[17] focused on graphical methods about the design of springs in discrete (point) and continuous balancing. For discrete balancing, a linear spring was assumed and it can produce an oppositely equal torque to balance the load or manipulator at some positions.

Figure I.1.10 shows a simple example to explain the design of an extension spring. Geometric relation can be obtained as,

$$r\sin(180° - \phi) = (a + f)h / b \qquad \text{(I.1.5)}$$

Where a is the free length of spring, f is the elongation.

The torque applied on the joint O is,

$$m_F = Ph = cfh = cf\frac{rb\sin\phi}{a+f} = crb\sin\phi\frac{f}{a+f} =$$

$$= crb\sin\phi(1 - \frac{a}{a+f}) = crb\sin\phi(1 - \frac{a}{\sqrt{r^2 + b^2 - 2rb\cos\phi}}) \qquad \text{(I.1.6)}$$

Where c is the coefficient of the spring. ϕ is the only variable in the balancing moment. c can be decided through the physical parameters of the spring,

$$c = \frac{P}{f} = \frac{Gd^4}{8D^3n} \qquad \text{(I.1.7)}$$

Where d is the diameter of the spring coil. D is the diameter of the spring. n is the number of the coils. G is shear modulus for the spring material. A numerical example is shown to clarify the design.

Balancing a given load with two springs are applied due to limited space. Two springs require shorter lever and give better flexibility (Fig. I. 1.11). A resultant spring can be an alternative choice if necessary, whose moment is equal to the algebraic sum of the two spring moments (Fig. I. 1.12).

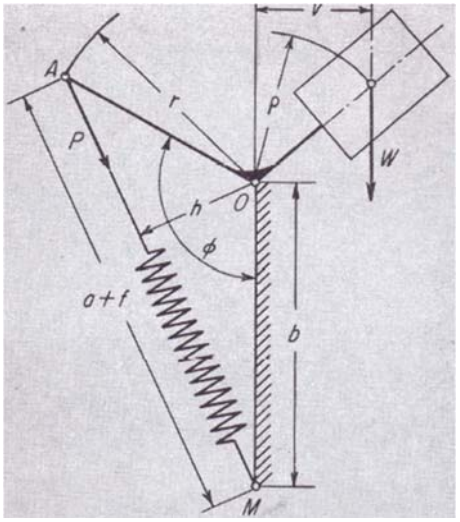

Figure I.1.10. spring attached to lever arm[17]

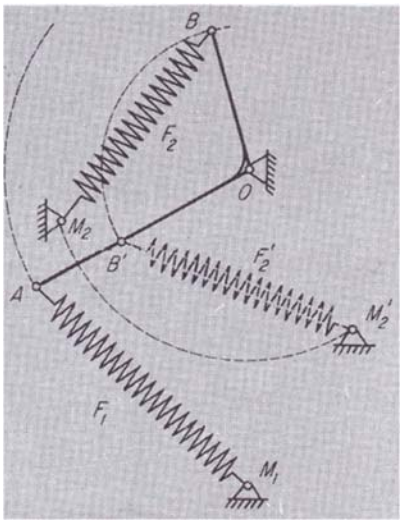

Figure I.1.11. two springs for balancing[17]

With a pulley, two springs can also be combined in the way shown in Fig. I. 1.13. the torque supplied by the springs is,

$$m_F = Ph = P_1h_1 + P_2h_2 = P_1(h_1 + h_2) \qquad (I.1.8)$$

Assuming negligible friction, it is known that $P_1 = P_2$. The two springs connected in series have stiffness c_1 and c_2 respectively, and its resultant stiffness c is,

$$\frac{1}{c} = \frac{1}{c_1} + \frac{1}{c_2} \qquad (I.1.9)$$

Balancing torques can be obtained graphically. A differential pulley is also used to balance a load torque (Fig. I. 1.14). In this case, the pulley itself must be in equilibrium, which requires two springs applied on it with the relation,

$$P_1R_0 = P_2r_0 \qquad (I.1.10)$$

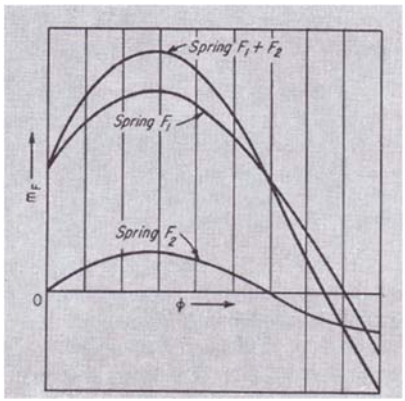

Figure I.1.12. to replace two springs with one[17]

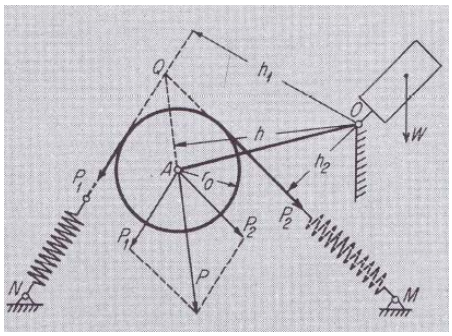

Figure I.1.13. springs with a pulley[17]

Then, the resultant is,

$$m_F = Ph = P_1h_1 + P_2h_2 \qquad (I.1.11)$$

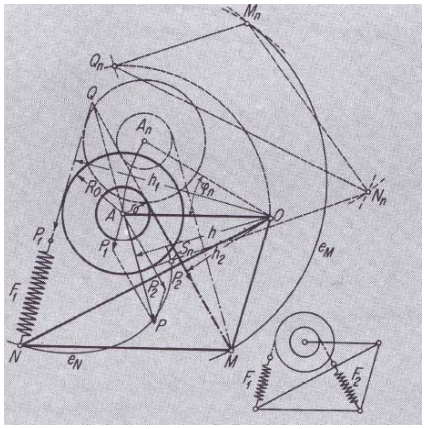

Figure I.1.14. two springs with a differential pulley[17]

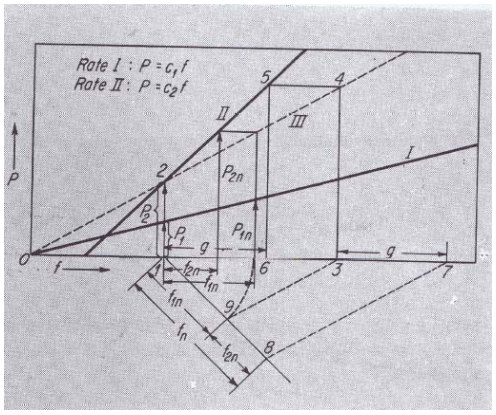

Figure I.1.15. spring force curve layouts[17]

The relation of spring forces can be illustrated in Fig. I. 1.15. With the figure, the deflections and forces can be clearly demonstrated.

Graphical methods also show the way to design springs in lever mechanisms for several points' balancing and continuous balancing.

For point balancing, it can be known from Eq. (I.1.6) that if a, b, c and r are four variables, four equations can be solved with four known pairs of m_F and ϕ. With the solution (a, b, c, r), the spring can balance a load moment at most four points defined by ϕ.

But in some practical cases, a balance at two or three points is enough. For that, the balancing torque m_F and the load moment m_W can be considered separately, as shown in Figure I.1.16. For some points required to be matched accurately, two curves coincide exactly. For other points, only approximate balancing is realized.

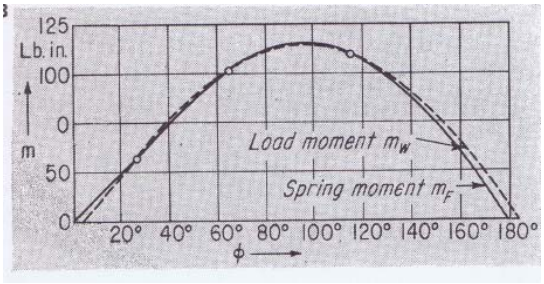

Figure I.1.16. load moment and spring moment[17]

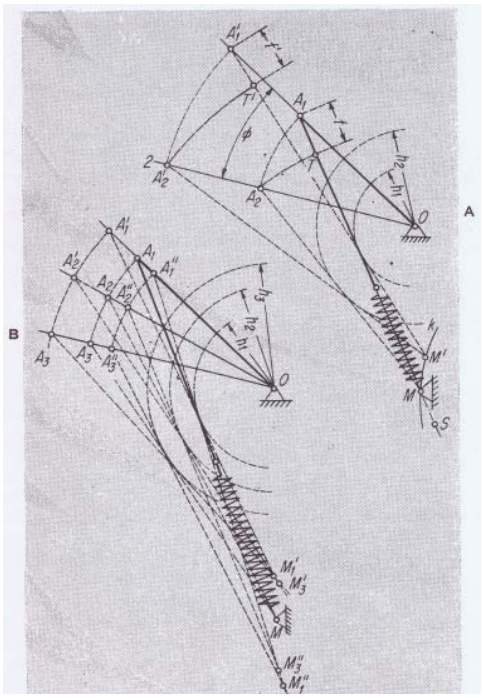

Figure I.1.17. graphical solutions for two-point (A) and three-point (B) balance[17]

Take two points' balancing as an example, procedures are shown graphically in Figure I.1.17. Firstly, draw an arc with a radius h_1, around O. Then, a range of the angle ϕ is described by two rays. In the area, A_1 and A_2 are chosen with an equal distance from O. After that, starting from A_1, a line is drawn tangent to the arc. Cut the desired elongation f from A_1 and find T. Next, h_2 is obtained from,

$h_2 = m_{w2}/P_2, \quad P_2 = P_1 - cf.$ (I.1.12)

Another arc is drawn with a radius h_2 around O. Then, a tangent to this arc is starting from A_2. the two tangent lines intersect at M, which is the pivot position for the spring. Figure I.1.17 also shows the similar design for three-point balancing.

Another strategy is illustrated for three-point balancing design (Fig. I. 1.18). Three points are marked on rays OA_1, OA_2, OA_3 with the same distance from O. Along the extension of A_2A_3 finds a point M and makes $A_2A_3 = f_{32}$. with the known h_2 (h_3), P_2 and P_3 can be calculated and drawn on the curve line in Figure I.1.19. Then, on the line A_2A_3, a point S is chosen near M to make sure that an arc around S with a radius SA_2 can cut SA_1 at T and $A_1T = f_{21}$. After that, f_{21} is marked on the curve and P_1 can be found. With the known m_{w1} and P_1, h_1 is obtained. Next, draw another arc around O with a radius h_1. through A_1, a tangent to this arc has a point of intersection with A_2A_3 extension. The point is the pivot position of the spring. An arbitrary selection of point S needs more trials to find a proper one with an elongation f_{21}. In Figure I.1.19, stiffness of the spring can be evolved,

$$c = \frac{P_2 - P_3}{f_{32}} = \frac{P_1 - P_2}{f_{21}}. \qquad \text{(I.1.13)}$$

Another possible point M can be also found along the A_1A_2 or A_1A_3 if $h_1 = h_2$ or $h_1 = h_3$ is assumed.

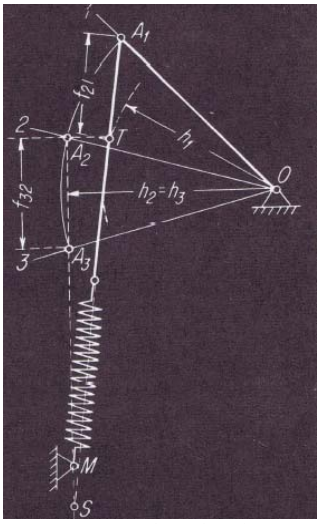

Figure I.1.18. graphical solution for 3-point balance[17]

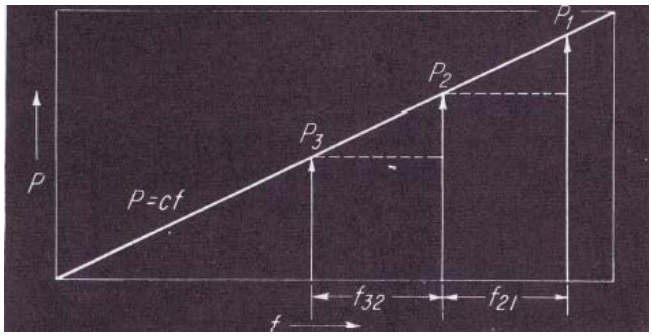

Figure I.1.19. spring-rate curve for 3-point balance[17]

Similar design with four-point balance is shown in Figure I.1.20. More than four-point balance is impossible with this graphical method and continuous balance is therefore proposed for multi-point balance.

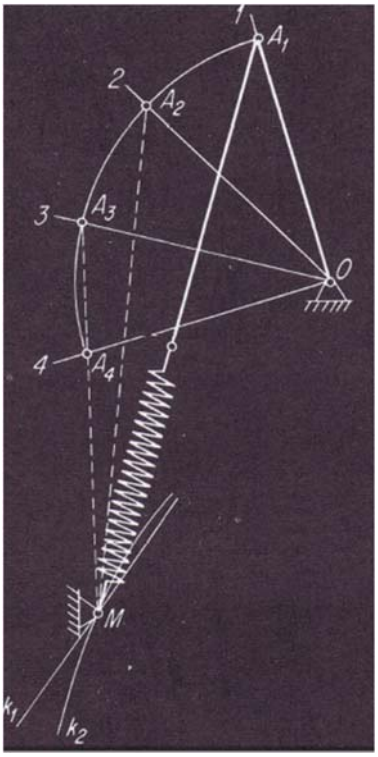

Figure I.1.20. graphical solution for 4-point balance[17]

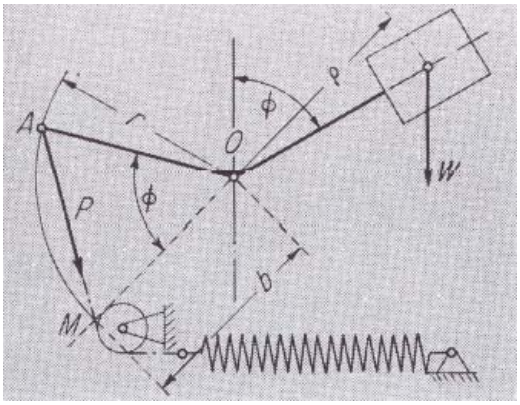

Figure I.1.21. a scheme for continuous balance[17]

For continuous balancing, a possibility is shown in Figure I.1.21 with special conditions a = 0, r = b and $\phi = \phi'$ (ϕ' is the angle of load moment) in Equation (I.1.6), then the equation can be evolved as,

$$m_F = rbc \sin\phi = m_w \sin\phi' \quad \text{(I.1.14)}$$

The continuous balancing is only correct when the load moments change as a sine function.

However, if a cam with an irregular shape is applied, continuous balancing can be realized in a more general way. The method is applied when the range of spring forces is limited or a spring fails to produce required torque variation. Figure I.1.22 supplies a solution with an odd-shape cam and a variable arm of force. It is easily known,

$P_1a_1 = P_2a_2$, $m_F = P_1h_1+P_2h_2 = P_1(h_1+h_2a_1/a_2)$. (I.1.15)

The spring elongation N_nS_n is drawn with the same way described before.

With an odd-shape convex, a pulley can supply any precise balancing moments according to any required spring rate. Figure I.1.23 shows an example to design the convex of a pulley. With the required moments shown in Figure I.1.23 (A), any arbitrary spring is selected and its force curve is marked in Figure I.1.23 (B). Then, matched force arms h_i are drawn in Figure I.1.23 (D) with an arbitrary distance OM_1 as a trial. For the same spring, if a series of forces with larger spring forces are chosen from P_1' to P_5' in Figure I.1.23 (B), the final result looks like Figure I.1.23 (F). If another spring with different stiffness is used in Figure I.1.23 (C), with a trial of the same distance OM_1, the result is drawn in Figure I.1.23 (E). The shadow areas in Figure I.1.23 (B) and (C) are the same, which means the same work done by the spring to balance the load moments in Figure I.1.23 (A).

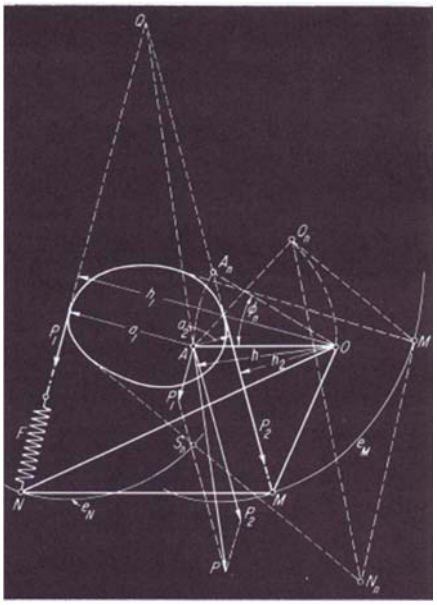

Figure I.1.22. an odd-shape pulley for continuous balance[17]

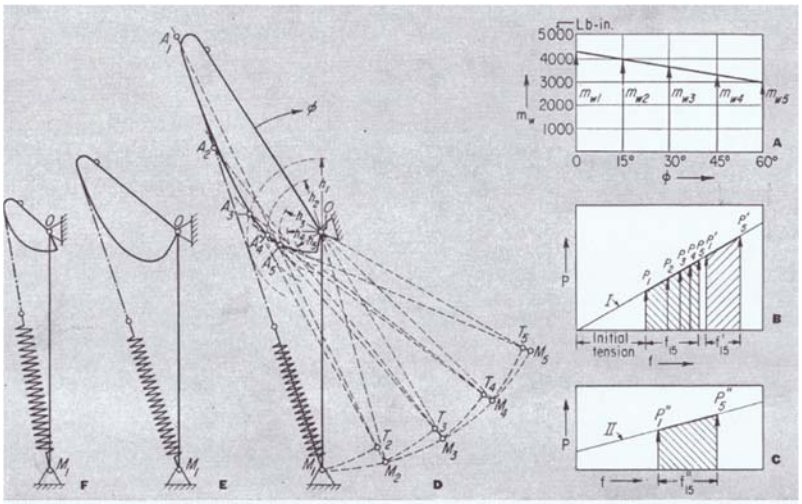

Figure I.1.23. design of pulley convex for continuous balancing applied in continuous balancing[17]

S. Segla et al. [18, 19] discussed optimization problems about physical parameters of the 'APR20' robot (Fig. I. 1.24). In their work, the 'APR20' robot was balanced by mean of springs. For the optimization of balancing effect in whole workspace, an objective function was built to describe an average force applied by the robot (Fig. I. 1.25). Then, all parameters were analysed with following mathematic strategies: Genetic algorithm, the Monte Carlo method, Conjugate gradient method, Fletcher-Reeves method, Elitist Non-dominated Sorting Genetic Algorithm, Differential evolution.

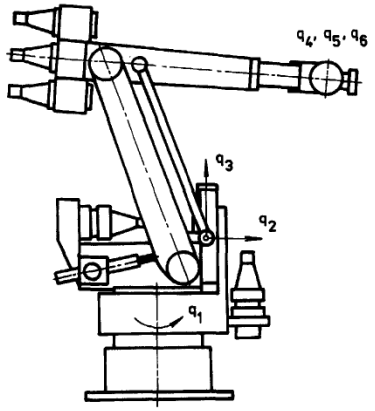

Figure I.1.24 'APR20' robot[18,19]

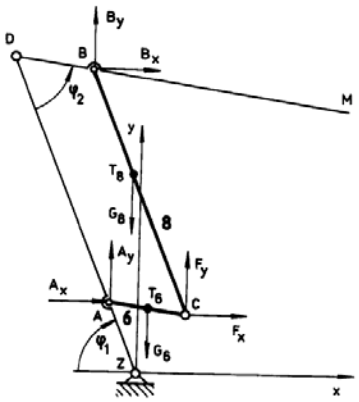

Figure I.1.25 the forces F_x and F_y[18,19]

After balancing strategy is shown and force analysis are expressed in equations, objective function is obtained in the form :

$$fav = \sum_{i=1}^{N} \frac{\sqrt{Fxi^2 + Fyi^2}}{N}$$

Where F_x and F_y are component forces in horizontal and vertical directions. N is the number of sample data in the workspace of the robot. F_x and F_y are decided by a list of independent variables (Fig I.1.26, Fig. I.1.27):

$e1, l01, k1, lx1, ly1, \phi 10, e2, l02, k2, lx2, ly2, \phi 20$

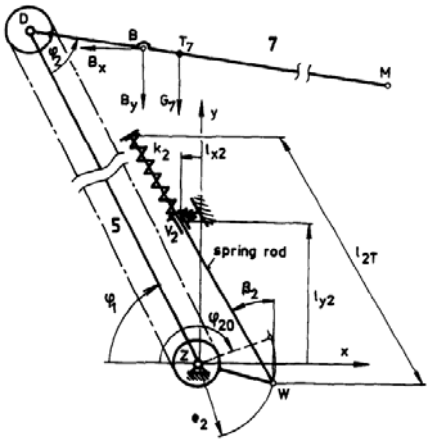

Figure I.1.26 static equilibrium for link 7 [18,19]

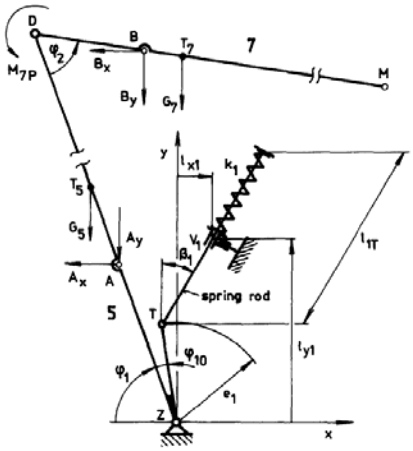

Figure I.1.27 static equilibrium for links 5 and 7 [18,19]

They have different domains of definition with different search intervals in algorithms (Table I.1). All these variables are the physical properties of the model robot 'APR20'. With these variables, a mathematical model is built.

Table I.1. Search Intervals[18,19]

Variable	Units	Lower bound	Upper bound

k_1	N/m	0	4,000,000
l_{01}	m	0.15	0.4
l_{x1}	m	-0.08	0.08
l_{y1}	m	0.035	0.234
φ_{10}	rad	-0.3491	0.3491
k_2	N/m	0	600,000
l_{02}	m	0.1	0.45
l_{x2}	m	-0.04	0.04
l_{y2}	m	0.024	0.18
φ_{20}	rad	2.7925	3.4906

With different values in variables, the result 'fav' is collected as a function of the varibles.

$$fav = \sum_{i=1}^{N} \frac{\sqrt{Fxi^2 + Fyi^2}}{N}$$

.

Then, set $g(i) = \sqrt{Fxi^2 + Fyi^2}$, consider fav as an 'estimator' of its theoretical value $g(i)$. The optimal result in discrete spectrum is then discussed .

Now assume that the values of fav is in normal distribution. The probability of every result can be estimated as p_i. In the Monte Carlo method, the estimator can be evaluated as:

$$\langle g \rangle = \sum_{i=1}^{N} g(i)\, p_i$$

Since a theoretical expectation value of any random variable may be approximated by a mathematical average of N random samplings.

$$S = \frac{1}{N} \sum_{i=1}^{N} g(i)$$

, where N is the number of samplings.

For the second estimator, we evaluate the error ΔS between S and real values. It is known from the central-limit theorem that the estimated value is distributed according to a normal distribution and its deviation from the theoretical value S is given in terms of the statistical error:

$$\Delta S = \sqrt{\frac{\mathrm{var}(g)}{N}}$$

ΔS can be estimated as:

$$\left\langle \frac{1}{N}\sum_{i=1} g_i^2 - \left(\frac{1}{N}\sum_i g_i\right)^2 \right\rangle = \left\langle g^2 \right\rangle - \frac{1}{N^2}\left\langle \sum_{i=1} g_i^2 + \sum g_i g_i' \right\rangle$$

$$= (1-\frac{1}{N})\left\langle g^2 \right\rangle - \frac{N(N-1)}{N^2}\left\langle g \right\rangle^2$$

$$= \frac{N-1}{N}\mathrm{var}(g) = (N-1)\Delta S^2$$

So,

$$\Delta S = \sqrt{\frac{1}{N-1}\left[\frac{1}{N}\sum_{i=1} g_i^2 - \left(\frac{1}{N}\sum_i g_i\right)^2\right]}$$

Choose s1= $\sum_i g_i$, s2= $\sum_{i=1} g_i^2$ as two estimators. Initialize the two estimators for S and ΔS. Update the two estimators with $s1 = s1 + e_i$, $s2 = s2 + e_i^2$, where $e_i = g(i)/p_i$. Finally, S and ΔS can be evaluated as:

$$S = \frac{s1}{N}, \quad \Delta S = \sqrt{\frac{1}{N-1}[\frac{s_2}{N} - (\frac{s_1}{N})^2]}$$

The final optimal force fav=3.15N is obtained by the Monte Carlo program.

The values for independent variables were also listed in their work. Results from the applications of other algorithms were also concluded and compared in their work.

The work from these researchers are mainly focused on the theoretical solutions for different mechanisms. For achieving ideal balance, they applied parallel guide, irregular shaped cam, computational algorithms, which are difficult to be realized in practice. Especially for cam and prismatic guide, high manufacturing accuracy is required and abrasion during use should also be considered seriously.

I.1.2.2 Spring approach in practice

Much work [5-7, 20-30] has been done for the balance of linkage mechanisms. They applied ingenious balancing systems into wide applications in industrial [6, 20-29], orthosis[22, 23,28], robot's safety[6], human-robot interaction[13, 30] and so on. Some of the work are detailed below.

Agrawal and Abbas Fattah [7, 20] concluded a general theory to balance anthropomorphic robots. They applied different balancing strategies according to different joints and architectures. The possible joints in robots are revolute (R), prismatic (P) or spherical (S) ones, played as trunk, should and elbow. Normally, the axis of the trunk joint is parallel to the gravity acceleration. Therefore, the trunk joint has no effect

for gravity balancing. Only other joints are classified and balanced in Table I.2. The principle of balancing mainly is to connect springs to the centre of mass of distal parts of the robot and to make the total potential energy of the system invariant in all configurations after locating the centre with parallelograms.

Table I.2. architectures of spatial industrial robots[7]

Type	Trunk	Shoulder	Elbow	Comment
(i) RR	R	R	R	Last two Rs are parallel
(ii) RRR	R	RR	R	Last two Rs are parallel
(iii) SR	R	S	R	Joint axes are not parallel or perpendicular
(iv) PP	R	P	P	Two Ps are perpendicular
(v) RRP	R	R	RP	Last two Rs are parallel
(vi) RRP	R	R	RP	Last two Rs are not parallel

Consider a spatial robot with two R joints as an example to show how joints are balanced (Fig. I. 1.28). θ_2 and θ_3 describe the position of the robot. a_2, d_3 and a_3 show the physical dimensions of the robot. The parameter θ_1 is not shown since θ_1 is used to describe the trunk along gravity vector and it has no influence on gravity balancing. Here O_1 can be considered as a reference point for further balancing study.

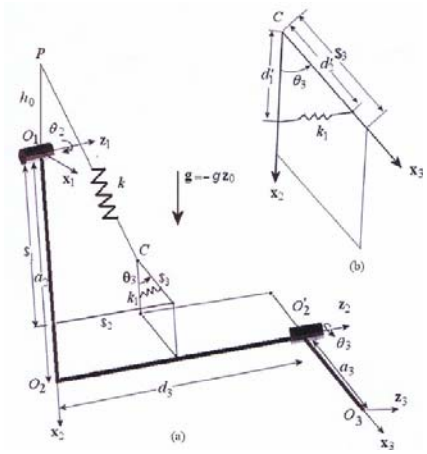

Figure I.1.28. (a) the balance of a RR robot.(b) connection points of spring k_1[7]

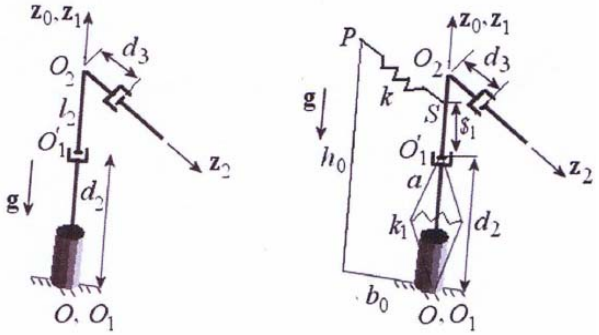

Figure I.1.29. (a) a schematic of a PP robot (b) the balance of the PP robot[7]

With respect to O_1, the centre of mass (COM) is shown as,

$$\mathbf{r}_{O1C} = (m_2\mathbf{r}_{O1C2}+m_3\mathbf{r}_{O1C3})/m, \quad \text{(I.1.16)}$$

where $m = m_2+m_3$, m_2 and m_3 are the masses of link 2 and link 3. $\mathbf{r}_{O1C2}$ and $\mathbf{r}_{O1C3}$ are position vectors of the COM of link 2 and link 3. describe Eq. (I.1.16) in another way,

$$\mathbf{r}_{O1C} = \$_1\mathbf{x}_2+\$_2\mathbf{z}_2+\$_3\mathbf{x}_3, \quad \text{(I.1.17)}$$

where $\$_i$ is the function of physical parameters assuming link i is located in its local $\mathbf{x}_i\mathbf{z}_i$ plane. In Figure I.1.28(a), the links' COM is located by a parallelogram. In this way, the gravitational energy is,

$V_g = -m\mathbf{g}\,\mathbf{r}_{O1C}$ (I.1.18)

With Eq. (I.1.17) and $\mathbf{g} = -g\mathbf{z}_0$, Eq. (I.1.18) can be evolved as,

$\mathbf{V}_g = mg(\$_1\mathbf{z}_0\mathbf{x}_2+\$_2\mathbf{z}_0\mathbf{z}_2+\$_3\mathbf{z}_0\mathbf{x}_3)$ (I.1.19)

A spring is introduced to compensate the gravitational energy. Its energy is,

$\mathbf{V}_s = k\mathbf{r}_{PC}\mathbf{r}_{PC}/2$ (I.1.20)

Where, $\mathbf{r}_{PC} = \mathbf{r}_{O1C}-\mathbf{r}_{O1P}$, $\mathbf{r}_{O1P} = h_0\mathbf{z}_0$. Zero-free length spring is assumed here. Considering the Cartesian coordinate, Eq. (I.1.20) can be evolved as,

$\mathbf{V}_s = -kh_0(\$_1\mathbf{z}_0\mathbf{x}_2+\$_2\mathbf{z}_0\mathbf{z}_2+\$_3\mathbf{z}_0\mathbf{x}_3)+k(\$_1^2+\$_2^2+\$_3^2+h_0^2+2\$_1\$_3\mathbf{x}_2\mathbf{x}_3)/2$ (I.1.21)

The total potential energy is

$\mathbf{V} = \mathbf{V}_g+\mathbf{V}_s = (mg-kh_0)(\$_1\mathbf{z}_0\mathbf{x}_2+\$_2\mathbf{z}_0\mathbf{z}_2+\$_3\mathbf{z}_0\mathbf{x}_3)+k(\$_1^2+\$_2^2+\$_3^2+h_0^2+2\$_1\$_3\mathbf{x}_2\mathbf{x}_3)/2$ (I.1.22)

From Eq. (I.1.22), to make it invariant, variable items must be vanished. The first item vanishes if $mg = kh_0$. the second variable item $V_{var} = k\$_1\$_3\mathbf{x}_2\mathbf{x}_3$ disappears after the second spring is introduced (shown in Fig 1.28(b)). The variable part now is,

$\mathbf{V}_{var}+k_1x_1^2/2 = k\$_1\$_3\mathbf{x}_2\mathbf{x}_3-k_1d_1'd_2'\mathbf{x}_2\mathbf{x}_3+k_1(d_1'^2+d_2'^2)/2$ (I.1.23)

Where x_1 is the extension of spring k_1. When $k_1 = k\$_1\$_3/(d_1'd_2')$, the total potential energy is constant and the robot is gravity-balanced.

With the skill mentioned above, the first three types can be balanced perfectly.

Prismatic joints are considered in Types (iv)-(vi). For Type (iv) PP architecture, in Figure I.1.29(a), d_2 and d_3 are joint variables. The joint axis of the link 2 is parallel to gravity vector. The first joint is not discussed since its non-effect in gravity balancing. The location of COM is

$\mathbf{r}_{OC} = \mathbf{r}_{OS}+\mathbf{r}_{SC} = (d_2+\$_1)\mathbf{z}_1+\$_2\mathbf{z}_2,$ (I.1.24)

where $\$_1 = (m_2l_{2c}+m_3l_2)/m$, $\$_2 = m_3l_{3c}/m$, $m = m_2+m_3$. l_{2c} is the distance between the COM of the moving part in link 2 and the point O_1' and l_{3c} is the distance between the COM of link 3 and the point O_2. The axes of two prismatic pairs are perpendicular. The gravitational energy is

$V_g = -m\mathbf{g}\,\mathbf{r}_{OC} = mg(d_2+\$_1)$. (I.1.25)

Two springs are introduced to compensate V_g in Figure I.1.29(b). The first spring k is from the point S to a fixed point P as a height h_0 above the base. The second spring k_1 is on a moving rhombus. The total potential energy is

$V = V_g+V_k+V_{k1}= mg(d_2+\$_1)+k(b_0^2+(h_0-(d_2+\$_1))^2)/2+k_1(4a^2-d_2^2)/2$. (I.1.26)

Eq(I.1.26) can be also re-written as

$V = (mg-k(h_0-\$_1))d_2+(k-k_1)d_2^2/2+mg\$_1+k(b_0^2+h_0^2+\$_1^2)/2+2k_1a^2-kh_0\$_1$. (I.1.27)

When $k = mg/(h_0-\$_1)$ and $k_1 = k$ are assumed, the system is balanced perfectly with the total energy invariant.

For Type (v) RRP architecture, Figure I.1.30 is shown as an example. Notice that link 3 is only a revolute joint with zero mass and length. As the method mentioned above, the COM vector is

$\mathbf{r}_{O1C} = \$_1\mathbf{x}_2+\$_2\mathbf{z}_3=\$_1\mathbf{x}_2+(\$_{21}+\$_{22}d_4)\mathbf{z}_3$ (I.1.28)

where $\$_1 = m_2l_{c2}/m$, $\$_{21} = (m_{41}l_{c41}+m_{42}l_{c42})/m$, $\$_{22} = m_{42}/m$. The COM of the robot is shown in Figure I.1.31 with an introduction of a parallelogram. The gravitational energy is

$V_g = -m\mathbf{g}\,\mathbf{r}_{O1C}$ (I.1.29)

Where $\mathbf{g} = -g\mathbf{y}_1$. With Eq. (I.1.28), Eq. (I.1.29) can be rewritten as

$V_g = mg(\$_1s_2+\$_2s_{23})$ (I.1.30)

Where s_2 and s_{23} stand for sin (θ_2) and sin ($\theta_2+\theta_3'$), and $\theta_3' = \theta_3-\pi/2$.

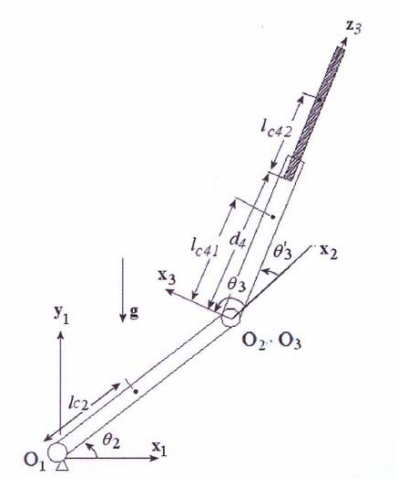

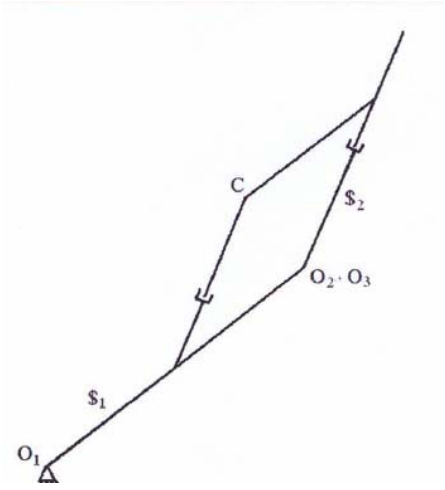

Figure I.1.30. a schematic of the RRP robot with geometric parameters[7]

Figure I.1.31. location of COM of the RRP robot[7]

A spring k_1 is added for balancing in Figure I.1.32(a) and its energy is

$$V_{k1} = \frac{1}{2}k_1\overrightarrow{PC}^2 = \frac{1}{2}k_1(\overrightarrow{O_1C} - \overrightarrow{O_1P})^2 = \frac{1}{2}k_1(\$_1 x_2 + \$_2 z_3 - h_0 y_1)^2 = \\ = \frac{1}{2}k_1(h_0^2 + \$_1^2 + \$_2^2 - 2h_0\$_1 s_2 - 2h_0\$_2 s_{23} + 2\$_1\$_2 c_3) \quad \text{(I.1.31)}$$

Where c_3 stands for $\cos\theta_3'$. The total potential energy is

$$V = V_g + V_{k1} = mg(\$_1 s_2 + \$_2 s_{23}) - k_1 h_0(\$_1 s_2 + \$_2 s_{23}) + k_1(h_0^2 + \$_1^2 + \$_2^2 + 2\$_1\$_2 c_3)/2 \quad \text{(I.1.32)}$$

When $k_1 = mg/h_0$, the left variable part is

$$V_{var} = k_1(\$_2^2 + 2\$_1\$_2 c_3)/2 \quad \text{(I.1.33)}$$

Then springs k_2 and k_3 are added to balance the variable part, shown in Figure I.1.32(b). the variable part is therefore evolved as

$$V_{var} + k_2((l_1 - \$_1)^2 + \$_2^2 - 2(l_1 - \$_1)\$_2 c_3)/2 + k_3(4a^2 - \$_2^2)/2 = \\ = (k_1 + k_2 - k_3)\$_2^2/2 + (k_1\$_1 - k_2(l_1 - \$_1))\$_2 c_3 + k_1\$_2^2/2 + 2k_3a^2. \quad \text{(I.1.34)}$$

Assuming $k_2 = k_1\$_1/(l_1 - \$_1)$ and $k_3 = k_1 + k_2$, all items become invariant. Finally, the robot is balanced by three springs.

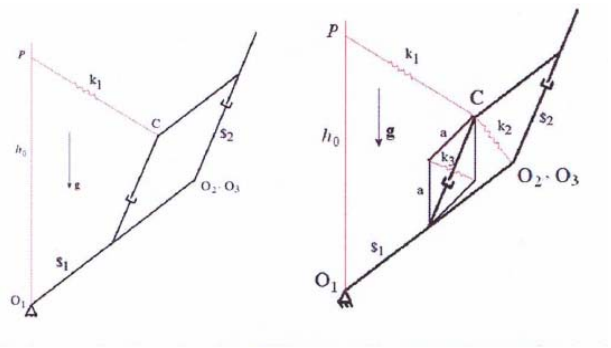

Figure. 1.32 (a) the RRP robot with the spring k1(b) the balance of the RRP robot[7]

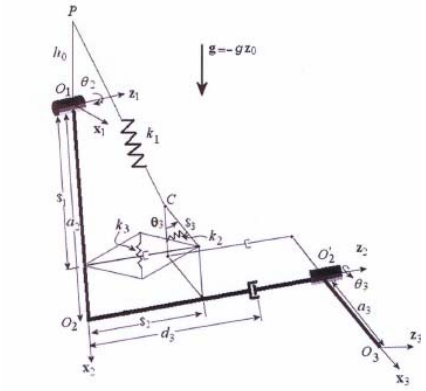

Figure. 1.33 the balance of a spatial RRP robot[7]

For the Type (vi) RRP architecture (Fig. I. 1.33), the similar balancing skill can be applied to balance the robot perfectly.

Rizk et al.[23] designed a gravity-balanced orthosis for the recovery of upper limb. The balanced orthosis comprised an arm and a forearm with five DOF in 3D space. There are 3 DOF at the connection 'shoulder' between the arm and the frame and 2 DOF at the connection 'elbow' between the arm and the forearm.

The arm is connected to the frame with a spherical joint, which makes the model move in 3D space (Fig. I. 1.34). Between the arm and the forearm, a revolute joint is applied to connect them. Two springs S1 and S2 are used to balance torques applying on the two joints respectively. Especially, the gravity of the forearm is balanced by the spring S2 through a pulley-and-cable mechanism. The axes of both pulleys P1 and P2 are parallel. The mechanism transfers the balancing effect from the spring S2 on the frame to the forearm. The rotation around the axis y_0 has no effect. Although the device has 5 DOF, three parameters θ_1, θ_2 and φ are enough to define it in every configuration. Therefore, the device is kinematical redundant and the redundancy allows a patient to have strong control on more muscles in his rehabilitation.

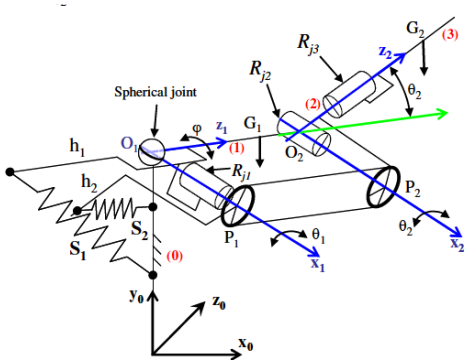

Figure I.1.34. the scheme of the device and notations[23]

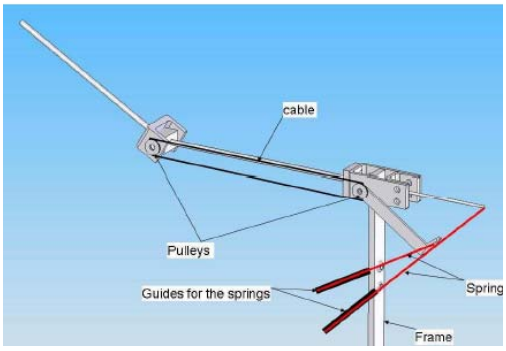

Figure I.1.35. the CAD model[23]

Spring design is based on the principle that the total potential energy is invariant. In detail, energy is stored and exchanged in forms of gravitational and elastic potential ways. But the amount of energy is unchanged. That is to say, the increase of gravitational energy is equal to the decrease of elastic energy and vice versa. To follow the principle, coordinates associated to the frame, the arm and the forearm are defined as (x_0, y_0, z_0), (x_1, y_1, z_1) and (x_2, y_2, z_2). The transformation matrices between the coordinates are,

$$ {}^{2}T_{1} = \begin{bmatrix} \cos\theta_2 & -\sin\theta_2 & 0 & l_1 \\ \sin\theta_2 & \cos\theta_2 & 0 & 0 \\ 0 & 0 & 1 & 0 \\ 0 & 0 & 0 & 1 \end{bmatrix}, \quad {}^{1}T_{0} = \begin{bmatrix} \cos\theta_1 & -\sin\theta_1 & 0 & 0 \\ \cos\varphi\sin\theta_1 & \cos\varphi\cos\theta_1 & -\sin\varphi & 0 \\ \sin\varphi\sin\theta_1 & \sin\varphi\cos\theta_1 & \cos\varphi & 0 \\ 0 & 0 & 0 & 1 \end{bmatrix} $$

(I.1.35)

Then, the centres of the masses for the arm and the forearm are located as,

$$O_1G_1 = \begin{bmatrix} \frac{l_1}{2}\cos\theta_1 \\ \frac{l_1}{2}\cos\varphi\sin\theta_1 \\ \frac{l_1}{2}\sin\varphi\sin\theta_1 \\ 1 \end{bmatrix}, \qquad O_0G_2 = \begin{bmatrix} \frac{l_2}{2}\cos(\theta_1+\theta_2)+l_1\cos\theta_1 \\ \cos\varphi(\frac{l_2}{2}\sin(\theta_1+\theta_2)+l_1\sin\theta_1) \\ \sin\varphi(\frac{l_2}{2}\sin(\theta_1+\theta_2)+l_1\sin\theta_1) \\ 1 \end{bmatrix}$$

(I.1.36)

In order to getting a general expression for potential energies, springs' extremities should be defined. f_1 and f_2 are their coordinates,

$$f_1 = \begin{bmatrix} u_1 \\ v_1 \\ 0 \end{bmatrix}, \qquad f_2 = \begin{bmatrix} u_2 \\ v_2 \\ 0 \end{bmatrix} \qquad \text{(I.1.37)}$$

The variation of the gravitational and elastic potential energies is measured respectively between the initial configuration $\theta_1=\pi/2$, $\theta_2=\varphi=0$ and an arbitrary configuration,

$$\Delta E_g = (m_1\Delta y_{G1} + m_2\Delta y_{G2})g =$$

$$= \left[m_2\left(\frac{l_2}{2}+l_1-\cos\varphi(\frac{l_2}{2}\sin(\theta_1+\theta_2)+l_1\sin\theta_1)\right)+m_1\frac{l_1}{2}(1-\cos\varphi\sin\theta_1)\right]g \qquad \text{(I.1.38)}$$

$$\Delta E_e = \frac{1}{2}\begin{bmatrix} k_1(u_1^2+v_1^2+h_1^2+2u_1h_1\cos\theta_1+2v_1h_1\cos\varphi\sin\theta_1) \\ +k_2(u_2^2+v_2^2+h_2^2+2u_2h_2\cos(\theta_1+\theta_2)+2v_2h_2\cos\varphi\sin(\theta_1+\theta_2)) \end{bmatrix} \qquad \text{(I.1.39)}$$

k_1 and k_2 are stiffness of the springs S1 and S2. h_1 and h_2 are level arms of the arm and the forearm. Eq. (I.1.38, 1.39) are the same in every configuration and the coefficients of each item should be identical in both expressions. Compare Eq.(I.1.38) and Eq.(I.1.39), we know that,

$u_1=u_2=0$, $v_1=-h_1$, $v_2=-h_2$, $k_1=(m_2+2m_1)gl_1/(2h_1^2)$, $k_2=m_2gl_2/(2h_2^2)$ (I.1.40)

k_1 and k_2 are constant and two linear and zero-initial-length springs are applied. The model in equilibrium is statically balanced whatever the configuration.

After the design, balancing forces in the spherical joint are emphasized. The force along the x_0-axis is dependent by the extension without the abduction. The force along y_0 is always negative. The force along z_0 is positive or negative decided by θ_1 and θ_2 and its amplitude depends on φ.

The friction effect was also discussed in the paper. Dry friction was considered as a constant torque. With the analysis of friction applied on the two joints, friction was proved that it required more effort to move the device and increased the balance of the device. Finally, an example showed a possibility of the CAD model in Fig. I. 1.35.

Streit and Shin[14, 26, 27] developed the balance theory from Hain[12], Nathan[24] and Pracht[25] and illustrated two methodologies of equilibrator theory for planar linkage mechanism with revolute joints.

The first method was originated from Hain's work. One degree of freedom linkage was shown as an introduction. Its relationship between spring and linkage is: mgr=kbc, shown in Fig. I. 1.36 .

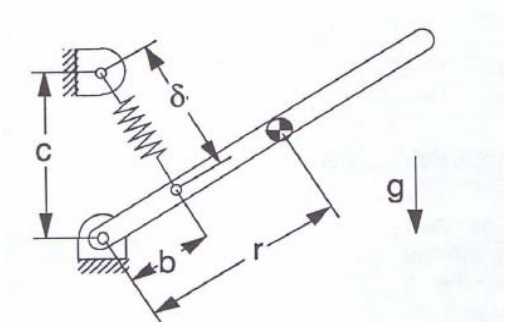

Figure I.1.36. One degree of freedom rotatable linkage[14]

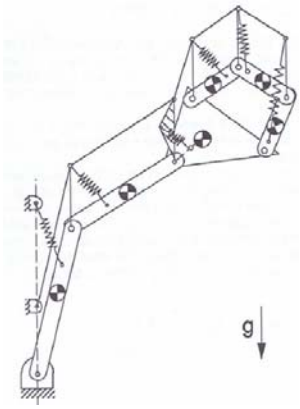

Figure I.1.37. equilibrating a general chain with planar revolute joints[14]

The mechanism can be applied to balance any revolute joint kinematic chain[24], shown in Fig. I. 1.37. During perfect balance, potential energy is exchanged between springs and links throughout the whole motion range. In detail, the i-th link can be balanced by the i-th spring.

The second method was introduced by Pracht[25] as an equilibrator design for 2 dof (degree of freedom) system, as shown in Figure I.1.38. The mathematical description is following as,

$[m_1r_1+m_3r_3+m_4l_1+m_5l_1]g=k_1b_1c_1$
$[m_2r_2+m_3l_2-m_4r_4-m_5r_5]g=k_2b_2c_2$

In this design, zero-free-length-spring is applied. Zero-free-length-spring supplies the force that is proportional to this body length, instead of its elongation. The balancing system in Fig. I. 1.38 can be also used to balance distributed mass. When it is applied as an equilibrator of a distributed mass, the balancing system is considered as 2 dof constant force generation mechanism. In this case, the constant force is produced at the end of the system, which direction is vertically upward. Considering the force generation mechanism as a unit, multi-dof mechanism can be balanced, shown in Fig. I. 1.39. the balancing system is called 'vertical link system'[24]. This design strategy requires zero free length springs K=n-1, and links L =2(n-m-1). n is the number of links in original linkage including ground. m is the number of links in original linkage which are pinned to ground.

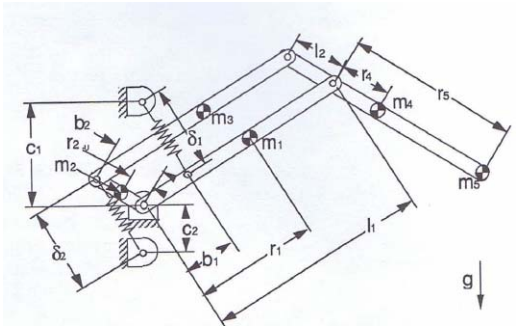

Figure I.1.38. 2 dof equilibrator[14]

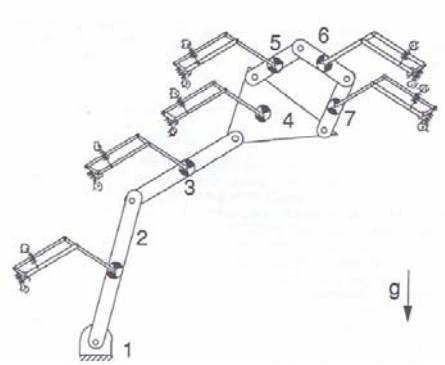

Figure I.1.39. equilibrating a general planar linkage[14]

The strategy can be also applied as a part of parallelogram to balance a system in Fig. I. 1.40. In this case, K and L are obtained from the equations below,

K=n-1

$$L=\sum_{i=1}^{n} j_i(j_i+1)$$

n is the number of links in original linkage including ground. j_i is the minimum number of links between the ith link and ground. i is the number of the link whose weight is to be equilibrated.

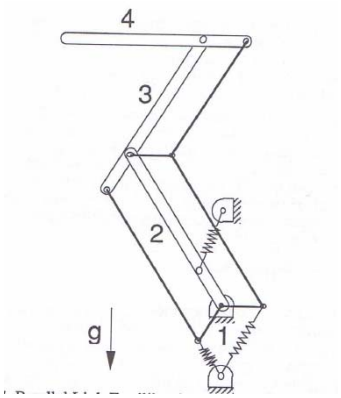

Figure I.1.40. parallel link equilibration[14]

the issue about the balance of prismatic pair was also discussed. For the device only with prismatic pair, Neg'ator spring was presented in Figure I.1.41. This spring provides a constant force using a pre-stressed strip of spring material. However, this spring equilibrates gravitational potential energy perfectly when there is only pure prismatic pair working, relative to fixed coordinates. When planar linkages have a combination of prismatic and revolute pairs, Figure I.1.42 illustrates a balance strategy.

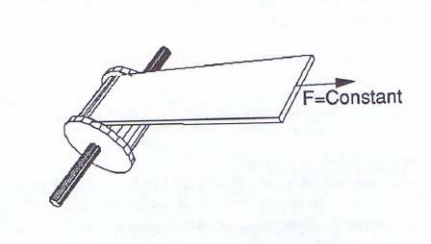

Figure I.1.41. Neg'ator Spring[14]

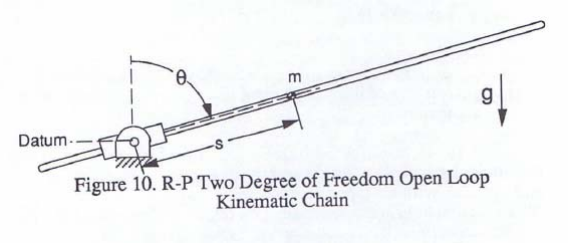

Figure 10. R-P Two Degree of Freedom Open Loop Kinematic Chain

Figure I.1.42. R-P joints kinematic chain[14]

Potential energy in the device is a function of revolute angle θ and prismatic coordinate s,

$V_g=mgs\cos\theta$

The device is balanced by the springs in Figure I.1.43. The elastic potential energy is ,

$$V_e=\frac{1}{2}k_1(s^2+c^2-2sc\cos\theta)+\frac{1}{2}k_2(4a^2-s^2)$$

When $k_1=k_2=k$,

$$V_e=\frac{1}{2}kc^2+2ka^2-ksc\cos\theta$$

The total potential energy is given as,

$$V=V_g+V_e=(mg-kc)s\cos\theta+\frac{1}{2}kc^2+2ka^2$$

When mg=kc is satisfied, the total energy is constant and perfect balancing is realized. During the motion of the device, energy exchange is happened between gravitational energy and elastic energy from two zero-free-length springs. When the prismatic pair moves, energy from the gravity of the link and elongation of springs changes and the total energy is unchanged.

Spring mass is also considered. Figure I.1.44 shows the centre of spring mass and linkage. The total gravitational energy is,

$$V_g=mgr\cos\theta+m_sg(\frac{b}{2}\cos\theta+\frac{c}{2})$$

And the elastic energy is

$$V_e=\frac{1}{2}k\delta^2=\frac{1}{2}k(b^2+c^2-2bc\cos\theta)$$

So the total amount is

$$V = \frac{1}{2}k(b^2 + c^2) + m_s g\frac{c}{2} + (mgr + m_s g\frac{b}{2} - kbc)\cos\theta$$

If $(mr + m_s\frac{b}{2})g = kbc$, V keeps constant for all θ. The mass of the spring also has a contribution to the static balancing of the whole device.

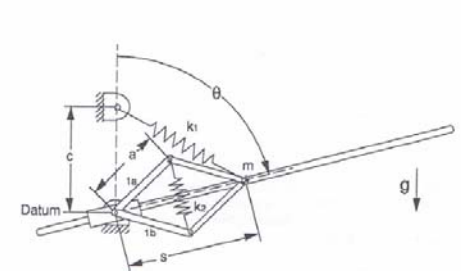

Figure I.1.43. Equilibration of an R-P kinematic chain[14]

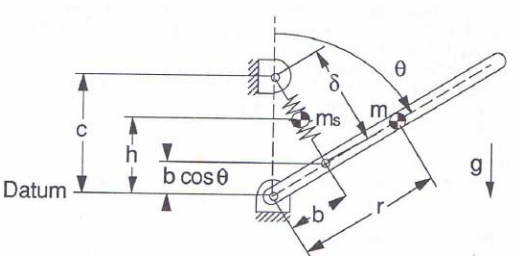

Figure I.1.44. Equilibration of spring mass[14]

Nathan[12] presented a method of passive compensation balancing mechanical gravity of robot manipulators with cable, pulley and built-in spring. With appropriate pulley profiles, cables accurately transferred changes of gravitational potential energy caused by link motion to changes of elastic potential energy in strain spring.

A single-joint illustration is introduced to explain the balancing strategy. Fig. I. 1.45 shows the connection between cables and the linkage. With the special pulley shape, a non-linear change of gravity torque is mapped to a linear behaviour of balancing spring. The gravity torque is perfectly compensated by the spring torque,

$$mgL\sin\theta = Tr = -kxr \qquad \text{(I.1.41)}$$

Where m: the link mass, concentrated at the end of the linkage.
g: gravitational acceleration.
T: the spring force.
r: the effective radius of the pulley.
k: the effective spring constant of springs.
x: the linear displacement of the cable.

Dynamic behaviours of the whole system can be described as,

$$kr^3 - mgL\sin\theta\frac{dr}{d\theta} + mgLr\cos\theta = 0 \quad \text{(I.1.42)}$$

The solution of Eq. 1.42 is,

$$r(\theta) = \sqrt{\frac{mgL}{k}}\sin\frac{\theta}{2} \quad \text{(I.1.43)}$$

Eq. 1.43 shows the effective pulley radius. But r(θ) is not the actual shape $r_p(\theta)$ of the pulley. Fig 1.46 illustrates the relation between the effective pulley profile and the actual shape. In other words, the point P, where the cable and the pulley separates, is the actual trajectory of the pulley profile that is not always coincident with that of the effective radius.

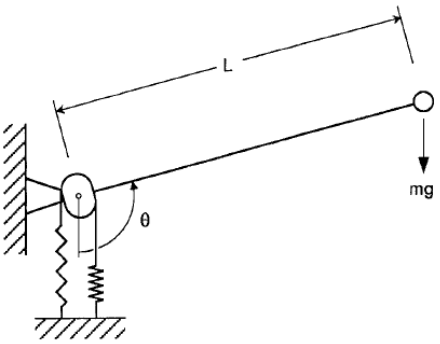

Figure I.1.45. a mechanism with cable, pulley and spring[12]

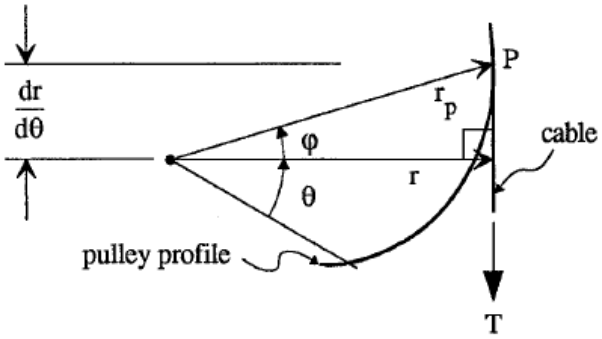

Figure I.1.46. effective versus actual pulley radius[12]

The actual shape $r_p(\theta)$ of the pulley is shown in Eq.(I.1.44),

$$r_p(\theta) = \sqrt{\frac{mgL}{k}\left(\frac{1}{4}\cos^2\frac{\theta}{2} + \sin^2\frac{\theta}{2}\right)} \quad \text{(I.1.44)}$$

The shape described by Eq. (I.1.44) can be approximately substituted by the profile r_0 in a range of 240 degrees.

$$r_0 = \sqrt{\frac{mgL}{2k}} \quad \text{(I.1.45)}$$

With Eq. (I.1.45), the cam is built and the experimental result shows the acceptable error. Possible sources of the error is analyzed and the according solutions are proposed. Firstly, the cable has a diameter and the action line of the cable tension applies at half a diameter away from the cam surface. The compensation torque error is caused by the discrepancy. The error can be solved if the cable profile is changed. Secondly, the error is caused by the realistic non-linearity in spring behaviour. The second error can be improved by lowering the maximum stress in springs. Thirdly, some error happens when the springs incline because that one end of the spring is fixed on the ground while the other end moves with the motion of the linkage. Increasing the length of the cable is helpful for reducing the error.

The approach is then easily extended to deal with multiple links. In multiple DOF situation, all joints actuated by tension element pairs on idler pulleys fixed on the base

frame are assumed. Consider the last (n-th) link in a manipulator (Fig. I. 1.47), the conditions under static balance are,

$$X_n = 0 \qquad Y_n = m_n g \qquad \tau_n = m_n g L_{cm,n} \cos\theta_n \quad \text{(I.1.46)}$$

τ_n is the torque to be compensated by the balancing system applied in Fig. I. 1.47. The previous (n-1 th) link is considered assuming that the tension elements actuating joint n are amounted on the joint n and an idler pulley on the joint (n-1), as showed in Fig. I. 1.48. The pulley is free to rotate with respect to the previous link. The conditions satisfying the static equilibrium are ,

$$X_{n-1} = 0 \qquad Y_{n-1} = m_{n-1} g + Y_n = (m_n + m_{n-1}) g \qquad \tau_{n-1} = (m_n L_{n-1} + m_{n-1} L_{cm,n-1}) g \cos\theta_{n-1}$$

(I.1.47)

Where L_{n-1} is the distance between joints n and (n-1).

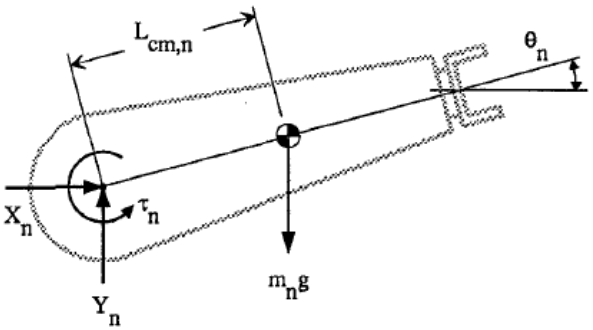

Figure I.1.47. free body diagram for the last link[12]

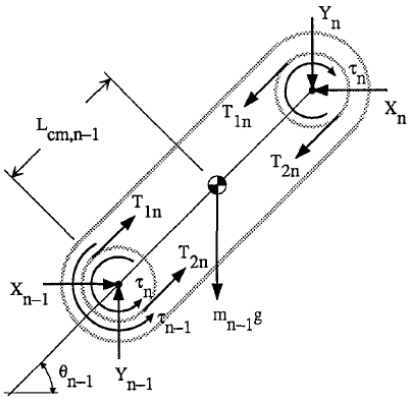

Figure I.1.48. free body diagram of the (n-1)th link[12]

With the some way, each previous joint can be decomposed into two parts: the gravity torque at every joint and the weight of every link. The first component is transferred to the base by the balancing system. The second one is vertical reaction force applied on each joint. The general solution is evolved for an arbitrary joint j. The total torque is,

$$\tau_j = (m_j L_{cm,j} + L_j \sum_{k=j+1}^{n} m_k) g \cos\theta_j \quad \text{(I.1.48)}$$

This method can be applied on each independent joint without considering other influence from other joint angles.

T. Morita et al.[29] presented a balancing strategy for a four-DOF articulated manipulator (Fig. I. 1.49). The motion range is limited by the repeated structure and precise gravity compensation is difficult to generate since the accuracy is dependent on the posture of the link under geometrical constraints.

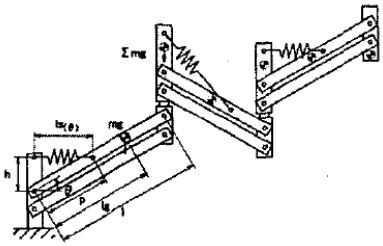

Figure I.1.49. parallelogram link with spring[29]

A mechanism named 'Pseudo-Parallelogram Mechanisms' is applied to replace the parallelogram links and release more workspace for the manipulator, as showed in Fig. I. 1.50, 1.51. In the pseudo-parallelogram, a tension of the belt is used to keep the upper link a constant posture.

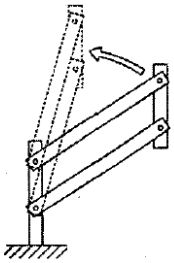

Figure I.1.50. parallelogram link mechanism[29]

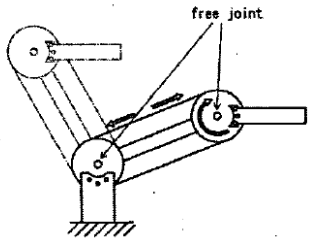

Figure I.1.51. Pseudo-Parallelogram Mechanism[29]

Further, springs are used for the generation of accurate torque. From Fig. I. 1.52, it is known that,

$$Gl\cos\theta = Fp\sin\phi, \quad F = k\Delta l_s(\theta) \quad \text{(I.1.49)}$$

$$Gl\cos\theta = \frac{kp\Delta l_s(\theta)}{l_s(\theta)}\cos\theta = kph(1-\frac{l_{s0}}{l_s(\theta)})\cos\theta \quad \text{(I.1.50)}$$

Due to the nonlinear term $l_s(\theta)$ in denominator from Eq. (I.1.50), the usual spring mechanism (Fig. I. 1.52) fails to obtain accurate compensation in every configuration. To solve this problem, Fig. I. 1.53 and 1.54 show two possibilities to eliminate the natural spring length l_{s0}. In Fig. I. 1.53, p = h is constrained and the spring keeps initial length when θ = 90 degrees. Then, Eq. (I.1.50) can be derived as,

$$Gl\cos\theta = kph\cos\theta, \quad k = \frac{Gl}{ph} \quad \text{(I.1.51)}$$

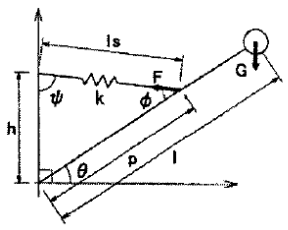

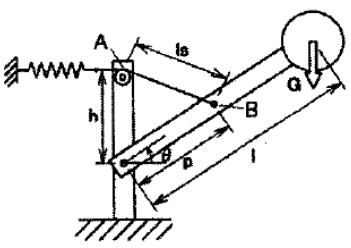

Figure I.1.52. spring-link mechanism of single joint[29]

Figure I.1.53. link model for pitch axis (type I) [29]

The stiffness of the spring is decided, based on Eq. (I.1.51). Fig. I. 1.54 shows a more compact way to place the spring. Different from the previous way, the geometric constraint is expressed in Eq. (I.1.52) so that Eq. (I.1.51) is satisfied for the accurate balance.

$$\Delta l_{s-90^\circ} = p - h \quad \text{(I.1.52)}$$

Then, the design is extended into three orthogonal dimensions in the workspace, as showed in Fig. I. 1.55. The fixed point A is above the intersection point of three orthogonal axes. The place of the spring is adopted for a pitch rotation. The roll rotation is geometrically similar with the pitch one. The compensation torque is not necessary for the yaw axis since the yaw axis is parallel to the direction of gravity.

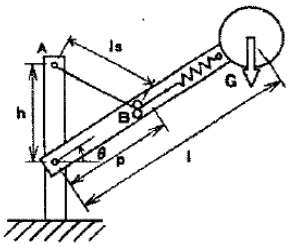

Figure I.1.54. link model for pitch axis (type II) [29]

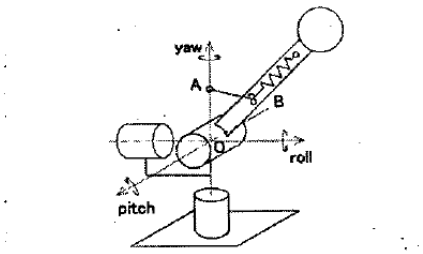

Figure I.1.55. module for three-orthogonal axes[29]

After that, kinematic and dynamic analysis are presented to show that all joint angles are decoupled well and the gravity torque is perfectly balanced by the compensation torque from the spring. Some examples are simulated to show good results. With the proposed method, some dynamic parameters, such as the mass of payload, the acceleration and the velocity are improved, compared with conventional mechanisms.

T. Lens, O. Stryk[6] showed a combination of counterweights and springs as balancing strategies. A mechanical structure with four revolute joints was studied as an application in human environments. Therefore, safety was considered firstly and lightweight design and active compliance was applied to improve the safety.

The model is shown in Fig. I. 1.56, 1.57, consisting of cables and linkages. The built-in springs are connected directly to the two electrical motors fixed on the base. The springs can store some gravitational energy from the 1st linkage during working. The other two motors controlling upper linkages are amounted on the movable linkage and acted as a counterweight. After that, the mass centre of the 2nd link is located around the axis of the 2nd revolute joint which connects the 2nd link with the 1st one.

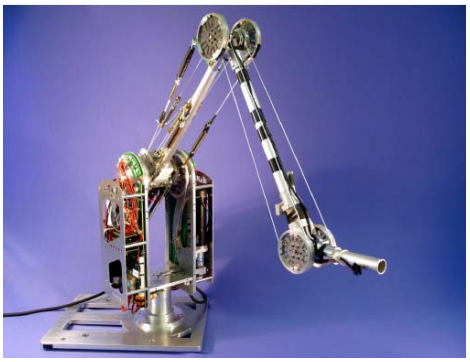

Figure I.1.56. BioRob-X4 (4 dof) arm without gripper[6]

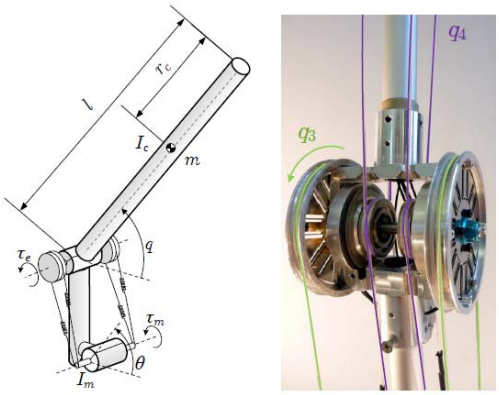

Figure I.1.57. BioRob arm joint actuation details. Actuation for joints 1-3(left). Actuation of joint 4 spanning two joints(right) [6]

The joint equilibrium positions $\hat{\mathbf{q}}$ are described by motor positions $\boldsymbol{\theta}$. The position of the last joint has a shift $\boldsymbol{\alpha}$ caused by the mechanical structure,

$$\hat{\mathbf{q}}(\boldsymbol{\theta},\mathbf{q}) = \begin{pmatrix} \theta_1 \\ \theta_2 \\ \theta_3 \\ \theta_4 - \frac{r_3}{r_4}\theta_3 \end{pmatrix} = \boldsymbol{\theta} - \boldsymbol{\alpha} \qquad \text{(I.1.53)}$$

r_3 and r_4 are the radii of the deflection pulley in the third joint and the pulley in the forth joint. The links and motors are decoupled by the built-in translational springs in cables, therefore, causing a link inertia lower than other motor inertia in links without springs. The motors with lower transmission ratio z and rotor inertia I are allowed to apply in, which leads to lower reflected rotor inertia. The robot with the lower inertia can move very fast (6.88m/s) and consume power low (54W).

Under a collision situation, all kinetic energy of the robot is assumed to transformed into elastic potential energy in springs. For a clamping case, quasi-static clamping produces high contact forces near singular positions. This problem can be improved using lightweight structure and low-power motors. Springs, in collision and clamping cases, play a role of absorber, store potential energy in elastic way and reduce potential risk when the robot has collision or high forces during clamping.

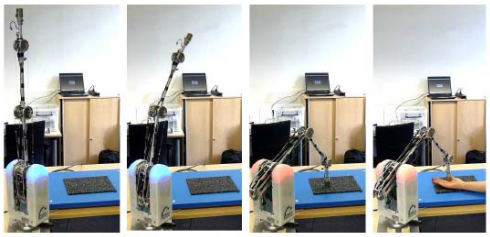

Figure I.1.58. collision experiments without (frame 1-3) and with clamping a human hand (frame 4) using a force plate. [6]

In experimental test (Fig. I. 1.58), collision is simulated with a typical pick-and-place trajectory. A force plate is used to sense forces and placed above the desired end effector position so that a colliding path is generated. The experiment shows a better result with little force and little energy collision, compared with a robot having no balancing strategies. Moreover, no torque and velocity peaks happened during the collision. Clamping effect is also measured in the experiment. The maximum clamping force is 24.7N. But without balancing device, the force would reach up to 453N. It is concluded that the existence of the balancing device stores some energy and reduces greatly the force on the end effector. In non-self-locking motors, the stored energy in springs can be transferred to the motors and dissipated, which makes springs working more efficiently. The balanced robot features high intrinsic safety and low power consumption.

Mathijs Vermeulen and Martijn Wisse[13] considered intrinsic safety and mechanical interaction between robot and humans. Their work featured a robot model with a strict limit to protect humans from any unexpected hurting or pain, even if an absolute collapse of the control system happens during working.

The robot design mentioned in their work is applied in fruit/vegetable processing and other domestic tasks. Pinching safety is evaluated as 50 N, the result of multiply of pain tolerance [kPa] and minimum contract area [cm^2], which value is used to restrict actuator torques and manipulator acceleration. For impact safety, a pain pressure threshold (PPT = 250 kPa) and a pressure application rate (500 kPa/s) are assumed. With these assumptions, a compromise is obtained between a maximum velocity and an effective mass. Then, geared DC motors are selected to drive joints. To satisfy the requirements, static balancing becomes necessary.

Two balancing strategies were presented(Fig. I. 1.59). The second one (in Fig. I. 1.59(b)) with two springs below the shoulder and a parallelogram structure above the shoulder is adopted since this distribution saves more space and shows more flexibility. Then, the gravitational and elastic energies are expressed respectively and the total potential energy is therefore concluded,

$$V_{tot} = (mgl_1 - k_1 r_1 a)(\sin\varphi_2 \cos\varphi_4 + \cos\varphi_2 \cos\varphi_3 \sin\varphi_4 + (mgl_2 - k_2 r_2 a)\sin\varphi_2 + \frac{1}{2}k_2 a^2 + \frac{1}{2}k_1 a^2 + \frac{1}{2}k_2 r_2^2 + \frac{1}{2}k_1 r_1^2 \quad \text{(I.1.54)}$$

When $mgl_1 = ak_1r_1$ and $mgl_2 = ak_2r_2$, perfect equilibrium is realized. Easy adjustment is possible in this case: once m is changed, the fixed point of the springs can be moved upward and downward to change the dimension a and recover equilibrium.

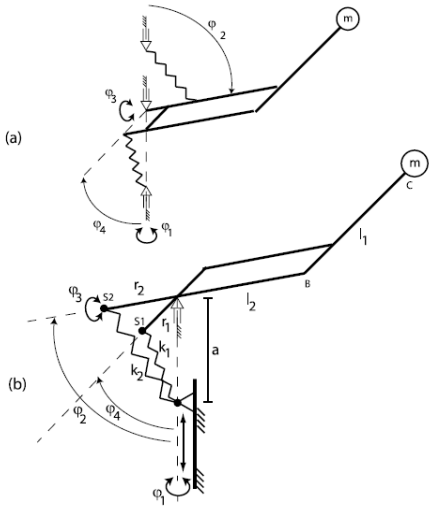

Figure I.1.59. two static balancing models with four-DOF[13]

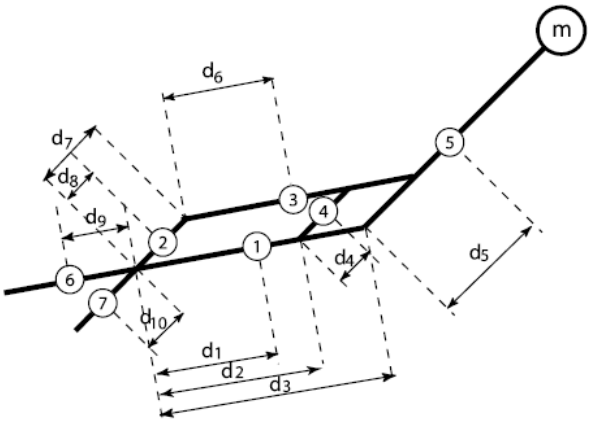

Figure I.1.60. full dimensions of all links[13]

After perfect balance is realized with only the mass of the end effector, other masses of links are also taken into account. a_1 and a_2 are used to describe two different springs k_1 and k_2. Masses and dimensions of all links are showed in Figure I.1.60. the new equilibrium equations are,

$$(m_1d_1 + m_3d_3 + m_4d_9 + m_5d_{10} + m_6d_6 + ml_2)g = k_2r_2a_2 \qquad \text{(I.1.55)}$$

$$(m_2d_2 + m_3d_8 + m_4d_4 + m_5d_5 + m_7d_7 + ml_1)g = k_1r_1a_1 \qquad \text{(I.1.56)}$$

After that, motors were selected based on assumed data. For spring compensation system, the authors used a CAD model to produce some results. $k_1 = k_2$ and $r_1 = r_2$ were assumed, and in that case, the length a can be adjusted as required. Two parallel springs were applied. With a spring stroke amplifier subsystem, a prototype was built, shown in Figure I.1.61. Experiments were followed to show the robot behaves well in industrial task and safety.

Figure I.1.61. the manipulator prototype[13]

Researchers from the work showed their valued design for balance purpose. However they presented little information about how a balancing system is developed and connected with unbalanced mechanisms. Normally they proposed a combination of a balancing device and a mechanical model in their start of their papers[6, 12, 14, 18, 19, 23, 24, 26, 27, 29], but how the combination is built is lack of discuss in their work. Especially, when they tried to introduce auxiliary devices, such as parallelogram devices, pulleys, cams, to connect springs to mechanisms, they mentioned little any reasons why the devices were applied and how they were introduced. Moreover, the placement of a balancing system is not discussed yet. They did not investigate other possible places in 3D space for the placement of the balancing system. All these problems should be illustrated clearly for research work.

In this research thesis, the author tries to present two proposals for the static balance of an anthropomorphic robot. After detailed investigation of its kinematic and dynamic properties, balancing systems are introduced to equilibrate the robot's gravity. This thesis shows a clear way how a balancing system is gradually developed and built to connect to the robot. Positions to place the balancing system in 3D space are also discussed and optimized positions are selected for the static balance. For the thesis, another feature is the way to obtain springs' parameters. Many researchers follow the same way to find springs' parameters: after showing an investigated model balanced by springs, gravitational and elastic potential energies were expressed in equations respectively. Then, to satisfy an assumption that the total potential energy is kept invariant, spring stiffness was obtained and some examples were supplied to support conclusions. Here, springs' parameters are obtained from the torque compensation point of view. Numerical examples are shown finally to support conclusions.

References:

[1] BP: Statistical Review of World Energy, Workbook , London, 2013.

[2] Annual Energy Review 2011. U.S. Department of Energy's Energy Information Administration. DOE/EIA-0384(2011), September, 2012.

[3] Musson, Robinson. Science and Technology in the Industrial Revolution. University of Toronto Press, 1969. pp. 491–500.

[4] Luca Bruzzone, Giorgio Bozzini. Energetic efficiency of a statically balanced hybrid industrial manipulator, 9th international workshop on research and education in Mechatronics, 2008, Bergamo, Italy.

[5] L. Bruzzone, G. Bozzini. Elastic Balancing of a SCARA-Link Hybrid Industrial Manipulator, 28th IASTED International Conference Modelling, Identification and Control (MIC 2009), February 16-18, 2009, Innsbruck, Austria.

[6] T. Lens, O. Stryk, Investigation of Safety in Human-Robot-Interaction for a Series Elastic, Tendon-Driven Robot Arm, Proceedings of the IEEE-RSJ International Conference on Intelligent Robots and Systems (IROS), 2012.

[7] Sunil. A, Abbas F. Gravity-balancing of Classes of Industrial robots, Proceedings of the IEEE International Conference on Robotics and Automation, May, 2006.

[8] M. J. Walkert, K. Oldham. A General Theory of Force Balancing Using Counterweights. Mechanism and Machine Theory, Vol. 13, pp. 175-185, 1978.

[9] H. Diken. Effect of Mass Balancing on the Actuator Torques of a Manipulator. Mech. Mach. Theory Vol. 30, No. 4, pp. 495-500, 1995.
[10] G.G. Lowen, F.R. Tepper and R. S. Berkof, Balancing of Linkages - an update, Mech. Mach. Theory, 18(3), 213-220, 1983.
[11] S. Hirose, T. Ishii, A. Haishi. Float Arm V: Hyper-Redundant Manipulator With Wire-Driven Weight-Compensation Mechanism. Proceedings of the IEEE International Conference on Robotics & Automation. Taipei, Taiwan, September 14-19, 2003.
[12] Nathan Ulrich, Vijay Kumar. Passive mechanical gravity compensation for robot manipulators. IEEE international conference on robotics and automation, Sacramento, California, April 1991.
[13] Mathijs Vermeulen, Martijn Wisse. Intrinsically safe robot arm: Adjustable static balancing and low power actuation. Int J Soc Robot No. 2, 275-288, 2010.
[14] Streit, D.A., and Shin. E. Equilibrators for Planar Linkages, J. Mech. Des. Vol. 115, No. 3, pp. 604-610, 1993.
[15] Ion Simionescu, Liviu Ciupitu. The static balancing of the industrial robot arms Part I: Discrete balancing. Mech. Mach. Theory. Vol. 35, pp. 1287-1298, 2000.
[16] Ion Simionescu, Liviu Ciupitu. The static balancing of the industrial robot arms Part II: Continuous balancing. Mech. Mach. Theory. Vol. 35, pp. 1299-1311, 2000.
[17] Hain, K. 'Force Analysis', 'Spring Mechanism-Point Balancing' and 'Spring Mechanisms-Continuous Balancing', Spring Design and Application, Chironis N. P., McGraw- Hill, New York, 1961, pp. 268-275.
[18] S. Segla, Kalker-Kalkman and Schwab. Statically Balancing of a robot mechanism with the aid of a genetic algorithm Mech. Mach. Theory Vol. 33, pp. 163-174, 1998.
[19] R. Saravanan, S. Ramabalan and P. Badu. Optimum static balancing of an industrial robot mechanism. Engineering Application of Artificial Intelligence 21. pp. 824-834, 2008.
[20] Sunil. Agrawal, G. Gardner, S. Pledgie, Design and fabrication of a gravity balanced planar mechanism using auxiliary parallelograms, Journal of Mechanical Design, Transactions of the ASME 123 (4) (2001) 525 – 528.
[21] Sunil Agrawal, Abbas Fattah. Gravity-balancing of spatial robotic manipulators. Mech. Mach. Theory. Vol 39, pp. 1331-1344, 2004.
[22] Sai K. Banala, Sunil K. Agrawal, Abbas Fattah, et al. Gravity-Balancing Leg Orthosis and Its Performance Evaluation. IEEE Trans. Robot. Vol. 22, NO. 6, 2006.
[23] R. Rizk, S. Krut, E. Dombre. Design of a 3D Gravity Balanced Orthosis for Upper Limb, IEEE International Conference on Robotics and Automation, May 19-23, 2008.
[24] Nathan R. H. A Constant Force Generation Mechanism, ASME J. of Mechanisms, Transmissions and Automation in Design, Dec. Vol. 107, No.4, pp. 508-512, 1985.
[25] Pracht P., Minotti P. and Dahan M. Synthesis and Balancing of Cam-Modulated Linkages. Advances in Design Automation, Vol. 10, No. 2, pp. 221-226, 1987.

[26] Streit D.A., Gilmore B.J., Perfect Spring Equilibrators for Rotatable Bodies. ASME Journal of Mechanisms, Transmissions, and Automation in Design, Dec, Vol. 111, pp. 451-458, 1989.
[27] Walsh G.J., Streit D.A. and Gilmore B.J. Spatial Spring Equilibrators Theory. Mech. Mach. Theory. Vol. 26, pp. 155-170, 1991.
[28] Boudewijn M. W., Wouter D., Rogier B., Just L. Energy-free Adjustment of Gravity Equilibrators Using the Virtual Spring Concept. Proceeding of the IEEE International Conference on Rehabilitation Robotics, June, Noordwijk, The Netherlands.
[29] T. Morita, F. Kuribara and Y. Shiozawa. A Novel Mechanism Design for Gravity Compensation in Three Dimensional Space, Proceeding of the IEEE/ASME International Conference on Advanced Intelligent Mechatronics, 2003.
[30] Sami Haddadin, Alin Albu-Schäffer and Gerd Hirzinger. Requirements for Safe Robots: Measurements, Analysis and New Insights. The International Journal of Robotics Research. Vol. 28, No. 11–12, November/December , pp. 1507–1527, 2009

Section I.2 Kinematic and Dynamic Analysis for Articulated Robotic Devices

Nomenclature:

m_i	kg	the mass of Link i
G_i	--	the center of the gravity of Link i
O_i	--	the revolute joint i
b_2	m	the length of a part for Link 2
l_i	m	length of a part of Link i
r_i	m	distance between O_i and G_i
θ_i	rad	angle between Link i and the horizontal plane
$\dot{\theta}_i$, ω_i	rad/s	angular velocity of Link i
$\ddot{\theta}_i$, α_i	rad/ s^2	angular acceleration of Link i
g	m/ s^2	the gravity acceleration
$\vec{a}_{Oi}$	m/ s^2	acceleration of point O_i
$\vec{a}_{Gi}$	m/ s^2	acceleration of Link i
$\vec{a}_{G_i/O_iT}$, $\vec{a}_{G_i/O_iN}$	m/ s^2	tangential and normal components of acceleration for Link i with respect to O_i
$\vec{a}_{O_2/O_1T}$, $\vec{a}_{O_2/O_1N}$	m/ s^2	tangential and normal components of acceleration for the joint O_2 with respect to O_1
a_{G_ix} , a_{G_iy}	m/ s^2	x and y axes components of acceleration for Link i
H_{Oi} , V_{Oi}	N	horizontal and vertical force components at joint O_i
I_{Gi}	Kg.m^2	moment of inertia for Link i with respect to G_i , $I_{Gi} = m_i l_i^2 / 12$
I_{Oi}	Kg.m^2	moment of inertia for Link i with respect to O_i , $I_{Oi} = m_i l_i^2 / 3$
M_i	N.m	motor torque by the motor M_i

In this chapter, a robot is introduced as an object needed to be balanced. This robot has an articulated structure with two degrees of freedom (DOF). It has two variants due to the motor positions. The structure in Figure I.2. 1 shows a variant when two motors M1 and M2 are placed on the base. A parallelogram mechanism in this structure transfers power for the upper link from the motor M2. Figure I.2. 2 shows another structure that the motor M2 is mounted on the second joint for the upper link. The motion of the two variants will be analyzed in this chapter since they are widely applied in industry and worth paying attention. The articulated structure is analyzed in terms of kinematics and dynamics with the help of the software Matlab.

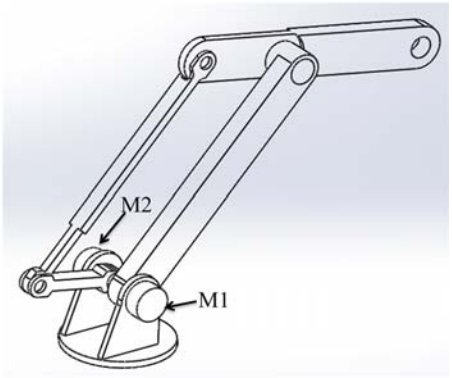

Figure I.2. 1. The robotic structure I.

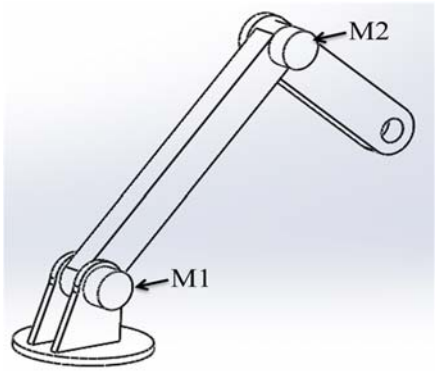

Figure I.2. 2. The robotic structure II.

I.2.1 The kinematic analysis for the articulated structure

For the robotic structure I, the parallelogram device only transfers power for the upper link, therefore, its weight is negligible, compared with the Link 1 and Link 2 (Figure I.2. 3). The revolute joint O1 is fixed, while other three joints are moving. Especially for Link 2, its mass is mainly distributed in the part O_2G, the part O_2O_4 accounts for little mass. With the above assumption, the robotic structure I shares the same kinematic model with the robotic structure II, as shown in Figure I.2. 4 and Figure I.2. 5.

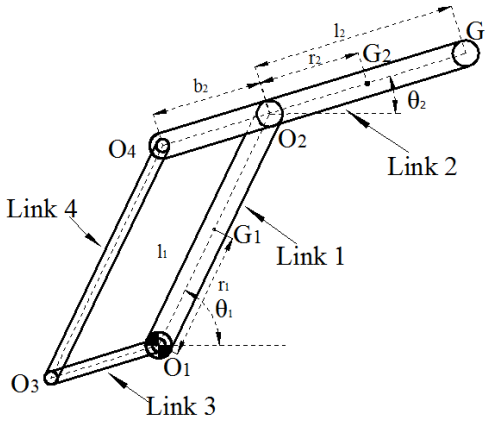

Figure I.2. 3. Dimensions for the robotic structure I

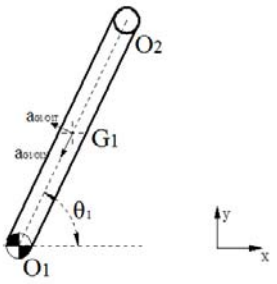

Figure I.2. 4. Kinematic analysis for Link 1

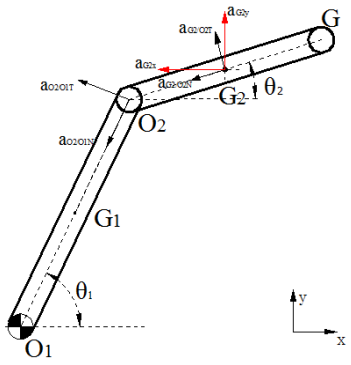

Figure I.2. 5. Kinematic analysis for Link 2

For Link 1,

$$\vec{a}_{G1} = \vec{a}_{O1} + \vec{a}_{G_1/O_1T} + \vec{a}_{G_1/O_1N} \tag{I.2. 1}$$

Table I.2. 1 acceleration magnitudes for Link 1

Components	$\vec{a}_{O1}$	$\vec{a}_{G_1/O_1T}$	$\vec{a}_{G_1/O_1N}$
magnitudes	0	$\ddot{\theta}_1 r_1$	$\dot{\theta}_1^2 r_1$

For Link 2,

$$\begin{aligned}\vec{a}_{G2} &= \vec{a}_{O2} + \vec{a}_{G_2/O_2} \\ &= \vec{a}_{O_2/O_1N} + \vec{a}_{O_2/O_1T} + \vec{a}_{G_2/O_2N} + \vec{a}_{G_2/O_2T}\end{aligned} \tag{I.2. 2}$$

Table I.2. 2 acceleration magnitudes for Link 2

components	$\vec{a}_{O_2/O_1N}$	$\vec{a}_{O_2/O_1T}$	$\vec{a}_{G_2/O_2N}$	$\vec{a}_{G_2/O_2T}$
magnitudes	$\dot{\theta}_1^2 l_1$	$\ddot{\theta}_1 l_1$	$\dot{\theta}_2^2 r_2$	$\ddot{\theta}_2^2 r_2$

$\vec{a}_{G2}$ can be expressed as two components for simplicity. Project this equation into x-axis and y-axis, $a_{G_{2x}}$ and $a_{G_{2y}}$ can be obtained as,

$$\begin{aligned}a_{G_{2x}} &= -a_{O_2/O_1N}\cos\theta_1 - a_{O_2/O_1T}\sin\theta_1 - a_{G_2/O_2N}\cos\theta_2 - a_{G_2/O_2T}\sin\theta_2 \\ &= -\dot{\theta}_1^2 l_1\cos\theta_1 - \ddot{\theta}_1 l_1\sin\theta_1 - \dot{\theta}_2^2 r_2\cos\theta_2 - \ddot{\theta}_2 r_2\sin\theta_2\end{aligned} \tag{I.2. 3}$$

$$\begin{aligned}a_{G_{2y}} &= -a_{O_2/O_1N}\sin\theta_1 + a_{O_2/O_1T}\cos\theta_1 - a_{G_2/O_2N}\sin\theta_2 + a_{G_2/O_2T}\cos\theta_2 \\ &= -\dot{\theta}_1^2 l_1\sin\theta_1 + \ddot{\theta}_1 l_1\cos\theta_1 - \dot{\theta}_2^2 r_2\sin\theta_2 + \ddot{\theta}_2 r_2\cos\theta_2\end{aligned} \tag{I.2. 4}$$

I.2.2 The dynamic analysis for the articulated structure

For the robotic structure I, the Motor M2 controls the motion of Link 2 through a parallelogram mechanism. For the robotic structure II mounted on the joint O2 controls the Link 2 directly. Therefore, the dynamics of the Link 1 is more complicated than that of the Link 2.

For the Link 1, its dynamic description in Structure I (Figure I.2. 6) is,

Along x axis, $H_{O1} + F_{T1} \cdot \sin\theta_1 + F_{N1} \cdot \cos\theta_1 + H_{O2} = 0$ (I.2. 5)

Along y axis, $V_{O1} - m_1 g - F_{T1} \cdot \cos\theta_1 + F_{N1} \cdot \sin\theta_1 + V_{O2} = 0$ (I.2. 6)

Where $F_{T1} = m_1 a_{G1/O1T}$, $F_{N1} = m_1 a_{G1/O1N}$.
Around O1 axis,

$$M_1 - m_1 g \cdot r_1 \cdot \cos\theta_1 - F_{T1} \cdot r_1 - I_{G1} \cdot \alpha_1 - H_{O2} \cdot l_1 \cdot \sin\theta_1 + V_{O2} \cdot l_1 \cdot \cos\theta_1 = 0 \quad \text{(I.2. 7)}$$

For Structure II, since the Motor M2 is mounted on the joint O2, the moments of forces for Link 1 are different (Figure I.2. 7), as:

$$M_1 - m_1 g \cdot r_1 \cdot \cos\theta_1 - F_{T1} \cdot r_1 - I_{G1} \cdot \alpha_1 - H_{O2} \cdot l_1 \cdot \sin\theta_1 + V_{O2} \cdot l_1 \cdot \cos\theta_1 - M_2 = 0 \quad \text{(I.2. 8)}$$

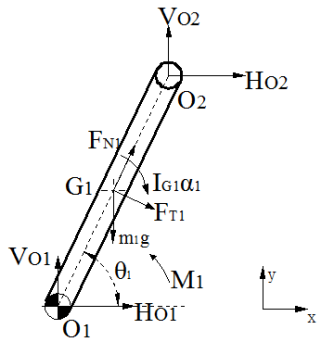

Figure I.2. 6. Dynamic model of Link 1 in Structure I

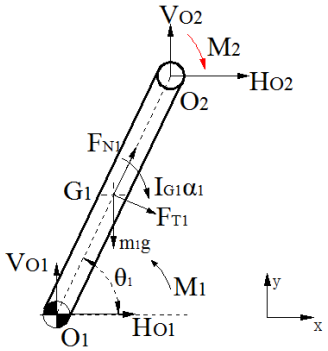

Figure I.2. 7. Dynamic model of Link 1 in Structure II

Figure I.2. 8 and Figure I.2. 9 show the dynamics of Link 2 in both structures. For the first structure, we have:

$$M_2 - F_{O_3O_4} \cdot b_2 \sin(\theta_1 - \theta_2) = 0 \quad \text{(I.2. 9)}$$

Along x axis, $-F_{O_3O_4} \cdot \cos\theta_1 + F_{G_2x} - H_{O2} = 0$ (I.2. 10)

Along y axis, $-F_{O_3O_4} \cdot \sin\theta_1 - F_{G_2y} - V_{O2} - m_2 g = 0$ (I.2. 11)

Where $F_{G_{2x}} = m_2 a_{G2x}$, $F_{G_{2y}} = m_2 a_{G2y}$.

Around G2 axis,

$$F_{O_3O_4} \cdot b_2 \sin(\theta_1 - \theta_2) - H_{O_2} \cdot r_2 \cdot \sin\theta_2 + V_{O_2} \cdot r_2 \cdot \cos\theta_2 - I_{G2} \cdot \alpha_2 = 0 \quad \text{(I.2. 12)}$$

For the second structure (Figure I.2. 9), we have:

Along x axis, $F_{G_{2x}} - H_{O2} = 0$ (I.2. 13)

Along y axis, $-F_{G_{2y}} - V_{O2} - m_2 g = 0$ (I.2. 14)

Around G2 axis,

$$M_2 - H_{O_2} \cdot r_2 \cdot \sin\theta_2 + V_{O_2} \cdot r_2 \cdot \cos\theta_2 - I_{G2} \cdot \alpha_2 = 0 \quad \text{(I.2. 15)}$$

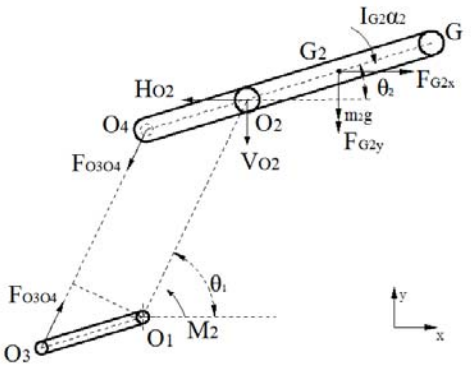

Figure I.2. 8. Dynamics of Link 2 in Structure I

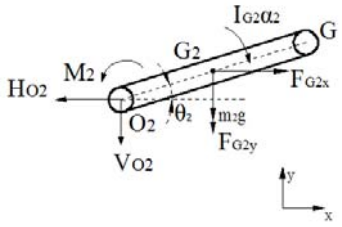

Figure I.2. 9. Dynamics of Link 2 in Structure II

I.2.2.1. The integration of the dynamic description for the structure I

For the structure I, we can get the integration of its dynamics in this way. Arrange the equation (I.2. 10) in this way,

$$H_{O2} = -F_{O_3O_4} \cdot \cos\theta_1 + F_{G_{2x}} \quad \text{(I.2. 16)}$$

Arrange the equation Along y axis, $-F_{O_3O_4} \cdot \sin\theta_1 - F_{G_{2y}} - V_{O2} - m_2 g = 0$ (I.2. 11) in this way,

$$V_{O2} = -F_{O_3O_4} \cdot \sin\theta_1 - F_{G_{2y}} - m_2 g \quad \text{(I.2. 17)}$$

Consider the equation (I.2.7) with the equations (I.2.10) and (I.2.11), we can have:

$$M_1 - m_1 g \cdot r_1 \cdot \cos\theta_1 - F_{T1} \cdot r_1 - I_{G1} \cdot \alpha_1 - (-F_{O_3O_4} \cdot \cos\theta_1 + F_{G_2x}) \cdot l_1 \cdot \sin\theta_1 + (-F_{O_3O_4} \cdot \sin\theta_1 - F_{G_2y} - m_2 g) \cdot l_1 \cdot \cos\theta_1 = 0 \quad \text{(I.2. 18)}$$

With the kinematic conclusions (I.2. 3) and (I.2. 4), the equation (I.2. 18) can be evolved as:

$$M_1 - m_1 g \cdot r_1 \cdot \cos\theta_1 - m_2 g \cdot l_1 \cdot \cos\theta_1 + m_2 \cdot r_2 \cdot l_1 \sin(\theta_2 - \theta_1) \cdot \dot{\theta}_2^2 - m_2 \cdot r_2 \cdot l_1 \cos(\theta_1 - \theta_2) \cdot \ddot{\theta}_2 - (m_1 \cdot r_1^2 + \frac{1}{12} m_1 \cdot l_1^2 + m_2 l_1^2) \cdot \ddot{\theta}_1 = 0 \quad \text{(I.2. 19)}$$

With the equations (I.2. 9), (I.2. 16), (I.2. 17), Eq. (I.2. 12) can be evolved as:

$$M_2 - m_2 g \cdot r_2 \cdot \cos\theta_2 + m_2 \cdot l_1 \cdot r_2 \sin(\theta_1 - \theta_2) \cdot \dot{\theta}_1^2 - m_2 \cdot l_1 \cdot r_2 \cos(\theta_1 - \theta_2) \cdot \ddot{\theta}_1 - (\frac{1}{12} m_2 \cdot l_2^2 + m_2 \cdot r_2^2) \ddot{\theta}_2 = 0 \quad \text{(I.2. 20)}$$

The equations (I.2.19) and (I.2. 20) are the dynamic description for Link 1 and Link 2 respectively.

I.2.2.2. The integration of the dynamic description for the structure II

The integration conclusions can be obtained in the same way we did in 2.2.1. Firstly consider the Link 1. From the equations (I.2.13) and (I.2.14), Eq. (I.2. 8) can be evolved as:

$$M_1 - M_2 - m_1 g \cdot r_1 \cdot \cos\theta_1 - m_2 g \cdot l_1 \cdot \cos\theta_1 + m_2 \cdot r_2 \cdot l_1 \sin(\theta_2 - \theta_1) \cdot \dot{\theta}_2^2 - m_2 \cdot r_2 \cdot l_1 \cos(\theta_1 - \theta_2) \cdot \ddot{\theta}_2 - (m_1 \cdot r_1^2 + \frac{1}{12} m_1 \cdot l_1^2 + m_2 l_1^2) \cdot \ddot{\theta}_1 = 0 \quad \text{(I.2. 21)}$$

From the equations (I.2.13) and (I.2.14), Eq. (I.2. 15) can be evolved as:

$$M_2 - m_2 g \cdot r_2 \cdot \cos\theta_2 + m_2 \cdot l_1 \cdot r_2 \sin(\theta_1 - \theta_2) \cdot \dot{\theta}_1^2 - m_2 \cdot l_1 \cdot r_2 \cos(\theta_1 - \theta_2) \cdot \ddot{\theta}_1 - (\frac{1}{12} m_2 \cdot l_2^2 + m_2 \cdot r_2^2) \ddot{\theta}_2 = 0 \quad \text{(I.2. 22)}$$

The equations (I.2.21), (I.2.22) are the dynamic description for Link 1 and Link 2 respectively. Notice that the both structures have very similar dynamic description for Link 1 and the same dynamic description for Link 2.

I.2.3 Structure simulation

With the software Matlab, we can study the robotic motion using Simulink and SimMechanics modules. The study model is simulated gradually from one DOF to two DOF structures. For every situation, the simulation results from Simulink and

SimMechanics modules are compared. Since we focus on the motion characters of different robotic structures caused by extra torques, every situation is considered at the horizontal plane for simplicity. Therefore, the gravity effect for different structures is neglected.

I.2.3.1 One DOF situation

At this situation, a linkage with a fixed revolute joint is controlled by a motor. The linkage can be driven by the motor (the torque is 100 Nm) and its dynamic parameters can be obtained. The linkage itself is simulated as a cylinder with 100 kg weight and 1.2 meters long. Its section radius is 0.06 m and its dense is 7930 kg/m^3 (steel). Results (Figure I.2. 10 and Figure I.2. 11) show the responses (displacement, velocity, acceleration and torque) from Simulink and SimMechanics modules are the same under the same conditions.

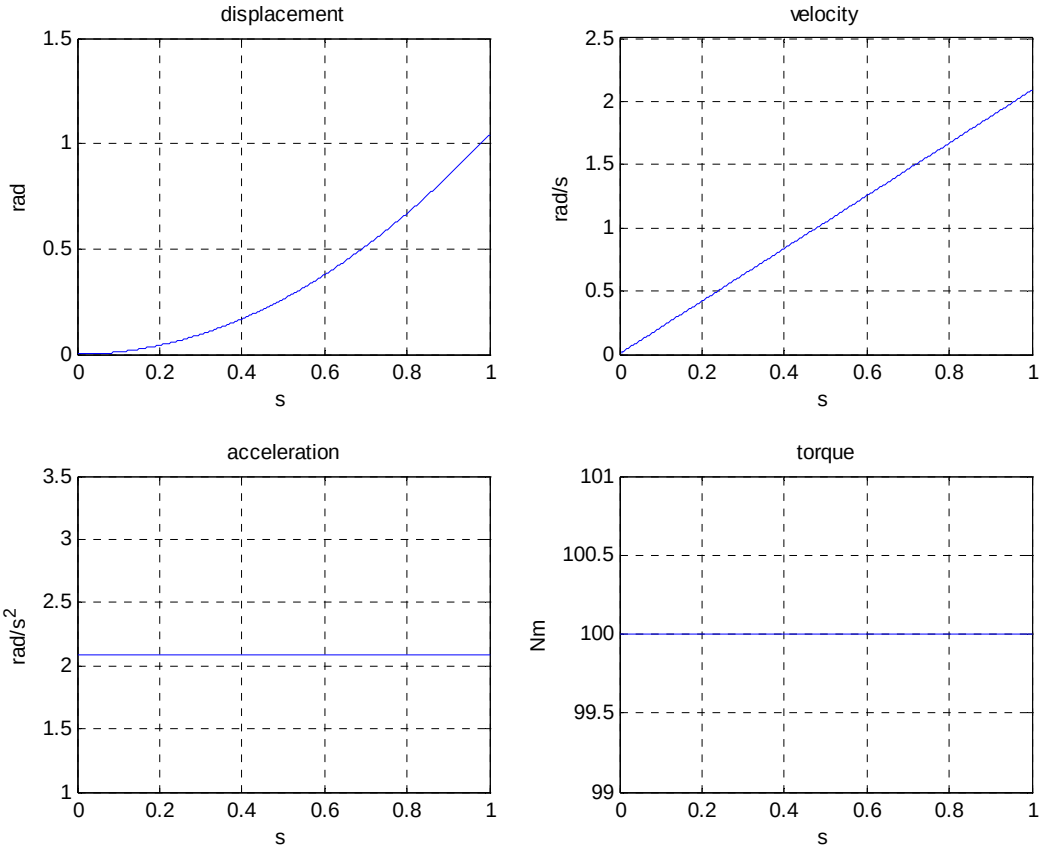

Figure I.2. 10. One DOF simulation in Simulink

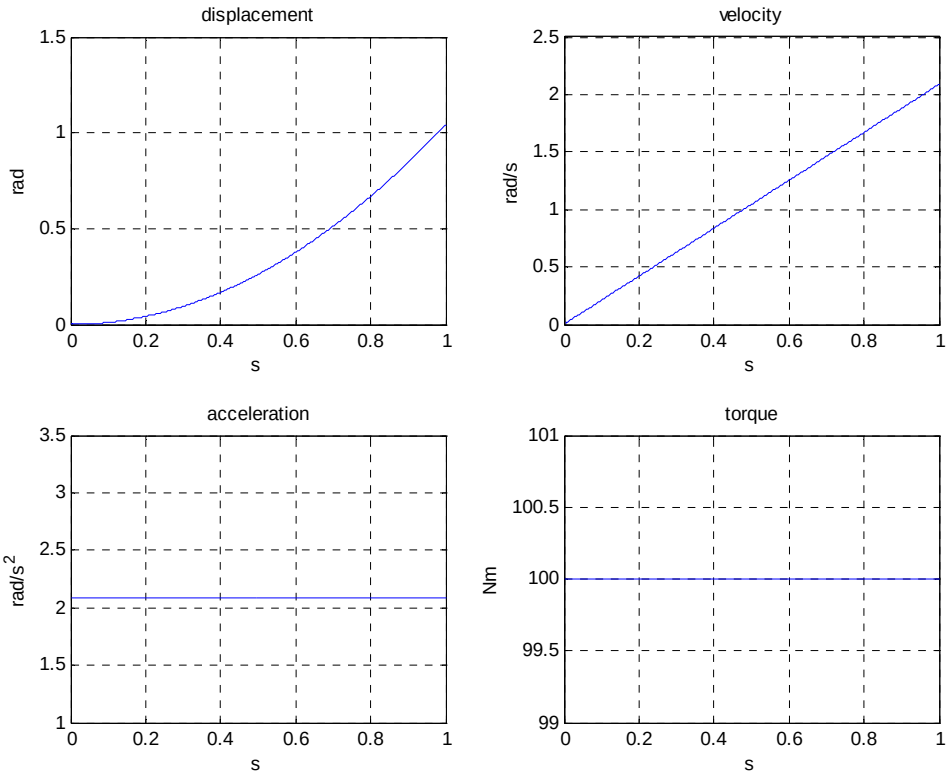

Figure I.2. 11. One DOF simulation in SimMechanics

I.2.3.2 Two DOF situation

The robotic structure II (Figure I.2. 2) is simulated in this situation. The model consists of two linkages with motors on their revolute joints. Here, we follow the same conditions for Link 1 in One DOF situation. The Link 2 is simulated with 40 kg weight and 1 m long. The two links are driven by the two motors (M1 = 100 Nm, M2 = 50 Nm). Then, we can build the model (Figure I.2. 12) and get the simulation results (Figure I.2. 13 and Figure I.2. 14) in the SimMechanics module.

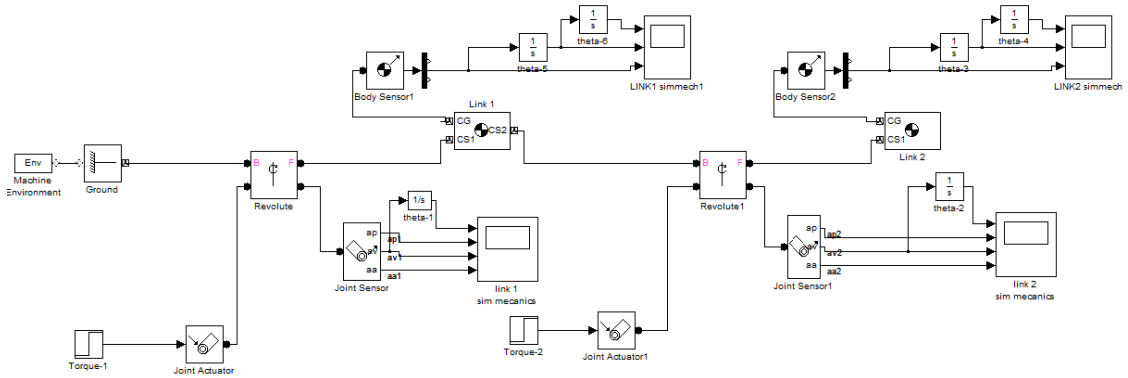

Figure I.2. 12. SimMechanics layout for the robotic structure II

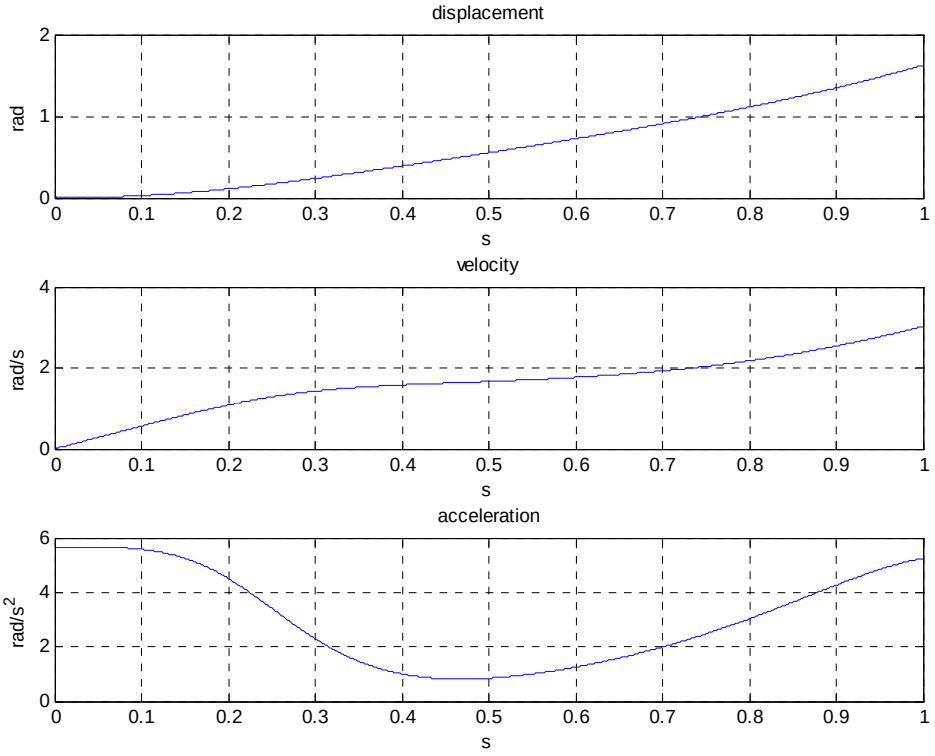

Figure I.2. 13. Simulation results for the first link in SimMechanics

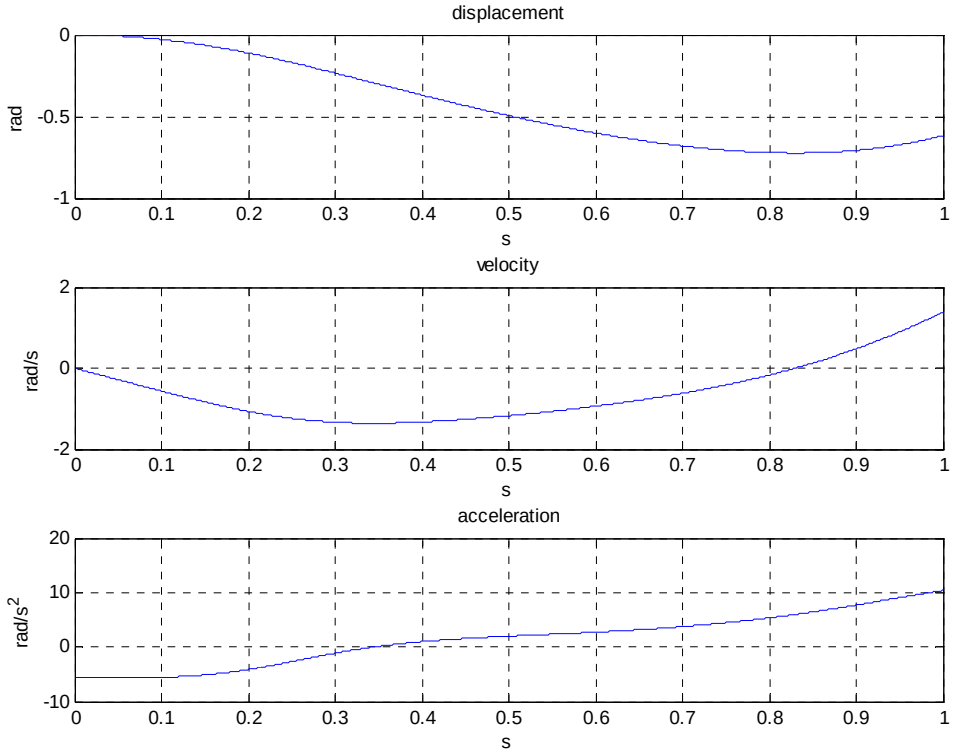

Figure I.2. 14. Simulation results for the second link in SimMechanics

In the Simulink module, the model is built with its kinematic and dynamic relation. From Figure I.2. 5, we can get the vector relation as:

$$\vec{L}_{O1O2} + \vec{L}_{O2G} = \vec{L}_{O1G} \tag{I.2. 23}$$

Project this equation into x and y axis, the dimension relation is obtained as:

$$\begin{cases} x: L_{O1Gx} = l_1 \cdot \cos\theta_1 + l_2 \cdot \cos\theta_2 \\ y: L_{O1Gy} = l_1 \cdot \sin\theta_1 + l_2 \cdot \sin\theta_2 \end{cases} \tag{I.2. 24}$$

With this relation, velocity and acceleration relation can be evolved as:

$$\begin{cases} x: \dot{L}_{O1Gx} = -l_1 \cdot \sin\theta_1 \cdot \omega_1 - l_2 \cdot \sin\theta_2 \cdot \omega_2 \\ y: \dot{L}_{O1Gy} = l_1 \cdot \cos\theta_1 \cdot \omega_1 + l_2 \cdot \cos\theta_2 \cdot \omega_2 \end{cases} \tag{I.2. 25}$$

$$\begin{cases} x: \ddot{L}_{O1Gx} = -l_1 \cdot \cos\theta_1 \cdot \omega^2{}_1 - l_1 \cdot \sin\theta_1 \cdot \alpha_1 - l_2 \cdot \cos\theta_2 \cdot \omega^2{}_2 - l_2 \cdot \sin\theta_2 \cdot \alpha_2 \\ y: \ddot{L}_{O1Gy} = -l_1 \cdot \sin\theta_1 \cdot \omega^2{}_1 + l_1 \cdot \cos\theta_1 \cdot \alpha_1 - l_2 \cdot \sin\theta_2 \cdot \omega^2{}_2 + l_2 \cdot \cos\theta_2 \cdot \alpha_2 \end{cases} \tag{I.2. 26}$$

The equation (I.2. 19) can be arranged in this way:

$$l_1 \cdot \sin\theta_1 \cdot \alpha_1 + l_2 \cdot \sin\theta_2 \cdot \alpha_2 + \ddot{L}_{O1Gx} = -l_1 \cdot \cos\theta_1 \cdot \omega^2{}_1 - l_2 \cdot \cos\theta_2 \cdot \omega^2{}_2 \quad \text{(I.2. 27)}$$

$$-l_1 \cdot \cos\theta_1 \cdot \alpha_1 - l_2 \cdot \cos\theta_2 \cdot \alpha_2 + \ddot{L}_{O1Gy} = -l_1 \cdot \sin\theta_1 \cdot \omega^2{}_1 - l_2 \cdot \sin\theta_2 \cdot \omega^2{}_2 \quad \text{(I.2. 28)}$$

From the equation (I.2. 1), it is known:

$$\begin{aligned} a_{G_1x} &= -a_{G_1/O_1T} \sin\theta_1 - a_{G_1/O_1N} \cos\theta_1 \\ &= -\alpha_1 r_1 \sin\theta_1 - \omega^2{}_1 r_1 \cos\theta_1 \end{aligned}$$

$$\begin{aligned} a_{G_1y} &= a_{G_1/O_1T} \cos\theta_1 - a_{G_1/O_1N} \sin\theta_1 \\ &= \alpha_1 r_1 \cos\theta_1 - \omega^2{}_1 r_1 \sin\theta_1 \end{aligned}$$

Make the two equations in this order:

$$a_{G_1x} + \alpha_1 r_1 \sin\theta_1 = -\omega^2{}_1 r_1 \cos\theta_1 \quad \text{(I.2. 29)}$$

$$a_{G_1y} - \alpha_1 r_1 \cos\theta_1 = -\omega^2{}_1 r_1 \sin\theta_1 \quad \text{(I.2. 30)}$$

Also, make the equations (I.2. 3) and (I.2. 4) for Link 2 in this order:

$$a_{G_2x} + \alpha_1 l_1 \sin\theta_1 + \alpha_2 r_2 \sin\theta_2 = -\omega_1^2 l_1 \cos\theta_1 - \omega_2^2 r_2 \cos\theta_2 \quad \text{(I.2. 31)}$$

$$a_{G_2y} - \alpha_1 l_1 \cos\theta_1 - \alpha_2 r_2 \cos\theta_2 = -\omega_1^2 l_1 \sin\theta_1 - \omega_2^2 r_2 \sin\theta_2 \quad \text{(I.2. 32)}$$

We can obtain the force relation for Link 1 from Figure I.2. 15.

x axis: $H_{O1} + H_{O2} = m_1 \cdot a_{G_1x}$

Or: $-m_1 \cdot a_{G_1x} + H_{O1} + H_{O2} = 0 \quad \text{(I.2. 33)}$

y axis: $V_{O1} + V_{O2} = m_1 \cdot a_{G_1y}$

Or: $-m_1 \cdot a_{G_1y} + V_{O1} + V_{O2} = 0 \quad \text{(I.2. 34)}$

around O1 axis, we can have:

$$M_1 - M_2 - H_{O2} \cdot l_1 \cdot \sin\theta_1 + V_{O2} \cdot l_1 \cdot \cos\theta_1 = I_{O1} \cdot \alpha_1$$

Where $I_{O1} = \frac{1}{3} m_1 l_1^2$.

Or: $I_{O1} \cdot \alpha_1 + H_{O2} \cdot l_1 \cdot \sin\theta_1 - V_{O2} \cdot l_1 \cdot \cos\theta_1 = M_1 - M_2$ (I.2. 35)

For Link 2, we can obtain its force relation from Figure I.2. 16.

x axis: $-H_{O2} = m_2 \cdot a_{G_2x}$

Or : $m_2 \cdot a_{G_2x} + H_{O2} = 0$ (I.2. 36)

y axis: $-V_{O2} = m_2 \cdot a_{G_2y}$

Or: $m_2 \cdot a_{G_2y} + V_{O2} = 0$ (I.2. 37)

around G2 axis, we can have:

$-H_{O2} \cdot r_2 \cdot \sin\theta_2 + V_{O2} \cdot r_2 \cdot \cos\theta_2 + M_2 = I_{G2} \cdot \alpha_2$

Where $I_{G2} = \frac{1}{12} m_2 l_2^2$.

Or: $I_{G2} \cdot \alpha_2 + H_{O2} \cdot r_2 \cdot \sin\theta_2 - V_{O2} \cdot r_2 \cdot \cos\theta_2 = M_2$ (I.2. 38)

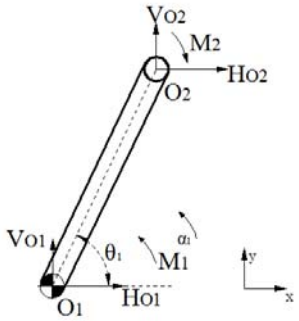

Figure I.2. 15. Force analysis of Link 1 for Structure II in Simulink simulation

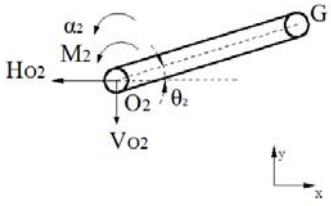

Figure I.2. 16. Force analysis of Link 2 for Structure II in Simulink simulation

With the kinematic relation (I.2.20)-(I.2. 25) and the dynamic relation (I.2. 26)-(I.2. 31), we can obtain the motion description of the model in the matrix form:

$A_{12\times12} \cdot u_{12\times1} = B_{12\times1}$ (I.2. 39)

Where,

$$A=\begin{bmatrix}
l_1\cdot\sin\theta_1 & l_2\cdot\sin\theta_2 & 1 & & & & & & & & & \\
-l_1\cdot\cos\theta_1 & -l_2\cdot\cos\theta_2 & & 1 & & & & & & & & \\
r_1\cdot\sin\theta_1 & & & & 1 & & & & & & & \\
-r_1\cdot\cos\theta_1 & & & & & 1 & & & & & & \\
l_1\cdot\sin\theta_1 & r_2\cdot\sin\theta_2 & & & & & 1 & & & & & \\
-l_1\cdot\cos\theta_1 & -r_2\cdot\cos\theta_2 & & & & & & 1 & & & & \\
 & & & & -m_1 & & & & 1 & & 1 & \\
 & & & & & -m_1 & & & & 1 & & 1 \\
I_{O1} & & & & & & & & & & l_1\cdot\sin\theta_1 & -l_1\cdot\cos\theta_1 \\
 & & & & & & m_2 & & & & 1 & \\
 & & & & & & & m_2 & & & & 1 \\
 & I_{G2} & & & & & & & & & r_2\cdot\sin\theta_2 & -r_2\cdot\cos\theta_2
\end{bmatrix}$$

$$u=\begin{bmatrix}
\alpha_1 \\ \alpha_2 \\ \ddot{L}_{O1Gx} \\ \ddot{L}_{O1Gy} \\ a_{G_1x} \\ a_{G_1y} \\ a_{G_2x} \\ a_{G_2y} \\ H_{O1} \\ V_{O1} \\ H_{O2} \\ V_{O2}
\end{bmatrix},\quad B=\begin{bmatrix}
-l_1\cdot\cos\theta_1\cdot\omega^2{}_1-l_2\cdot\cos\theta_2\cdot\omega^2{}_2 \\
-l_1\cdot\sin\theta_1\cdot\omega^2{}_1-l_2\cdot\sin\theta_2\cdot\omega^2{}_2 \\
-\omega^2{}_1\cdot r_1\cdot\cos\theta_1 \\
-\omega^2{}_1\cdot r_1\cdot\sin\theta_1 \\
-\omega_1{}^2\cdot l_1\cdot\cos\theta_1-\omega_2{}^2\cdot r_2\cdot\cos\theta_2 \\
-\omega_1{}^2\cdot l_1\cdot\sin\theta_1-\omega_2{}^2\cdot r_2\cdot\sin\theta_2 \\
0 \\ 0 \\ M_1-M_2 \\ 0 \\ 0 \\ M_2
\end{bmatrix}$$

The simulation results are obtained in the Simulink module (Figure I.2. 17 and Figure I.2. 18).

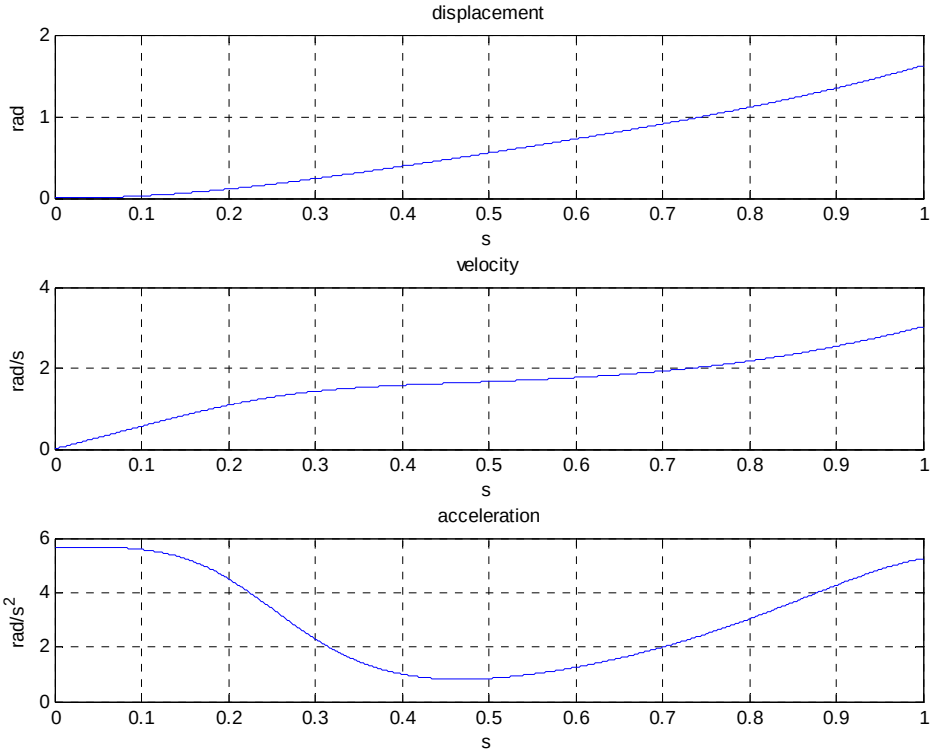

Figure I.2. 17. Simulation results for the first link in Simulink

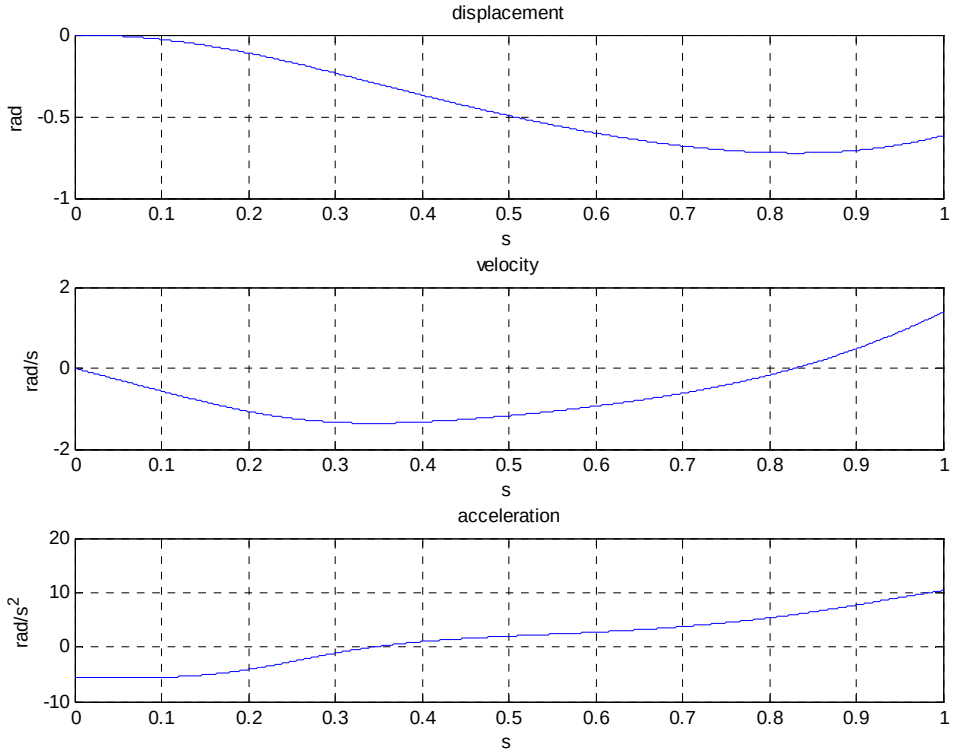

Figure I.2. 18. Simulation results for the second link in Simulink

Compare Figure I.2. 17 and Figure I.2. 18 with Figure I.2. 13 and Figure I.2. 14, the Simulink and SimMechanics modules can meet the same results if the known conditions are the same.

I.2.3.3 Two DOF situation with a parallelogram mechanism

The robotic structure I (Figure I.2. 1) is simulated in this situation. For the SimMechanics module, the model is firstly drawn in the 3D software 'Pro-Engineer', as seen in Figure I.2. 1. Then, the drawing data are exported from the 3D software and imported into SimMechanics as the simulation object (Figure I.2. 19). Finally we can get the simulation results (Figure I.2. 22 and Figure I.2. 23).

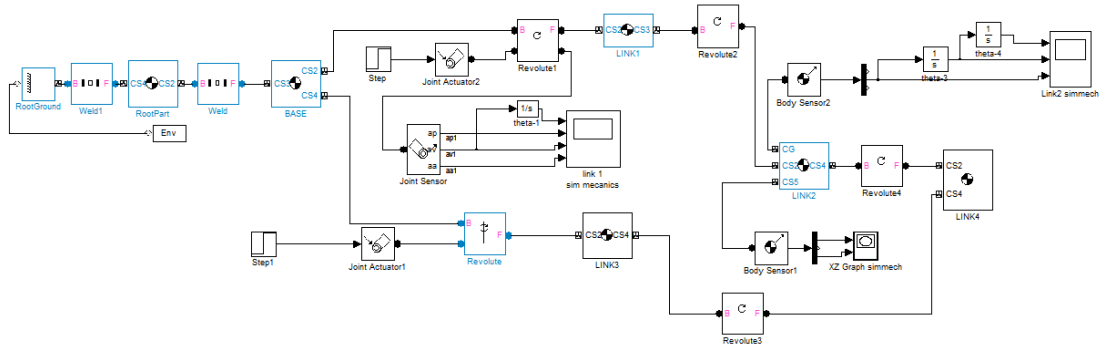

Figure I.2. 19. SimMechanics layout for the robotic structure I

For the Simulink module (Figure I.2. 20 and Figure I.2. 21), we have the following equations:

For Link 1,

$$M_1 - H_{O2} \cdot l_1 \cdot \sin\theta_1 + V_{O2} \cdot l_1 \cdot \cos\theta_1 = I_{O1} \cdot \alpha_1 \qquad \text{(I.2. 40)}$$

Where $I_{O1} = \frac{1}{3} m_1 l_1^{\,2}$.

For Link 2,

$$-F_{O_3O_4} \cdot \cos\theta_1 - H_{O2} = m_2 a_{G2x} \qquad \text{(I.2. 41)}$$

$$-F_{O3O4} \cdot \sin\theta_1 - V_{O2} = m_2 \cdot a_{G_2y} \qquad \text{(I.2. 42)}$$

$$F_{O3O4} \cdot b_2 \cdot \sin(\theta_1 - \theta_2) - H_{O_2} \cdot r_2 \cdot \sin\theta_2 + V_{O_2} \cdot r_2 \cdot \cos\theta_2 = I_{G2} \cdot \alpha_2 \qquad \text{(I.2. 43)}$$

Where $I_{G2} = \frac{1}{12} m_2 l_2^2$. From the equation (I.2. 9), we know,

$$F_{O_3O_4} \cdot b_2 = M_2 / \sin(\theta_1 - \theta_2)$$

When $\theta_1 \neq \theta_2$.

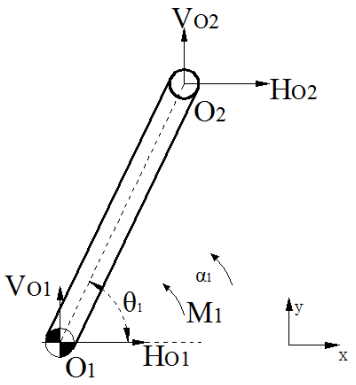

Figure I.2. 20. Force analysis of Link 1 for Structure I in Simulink simulation

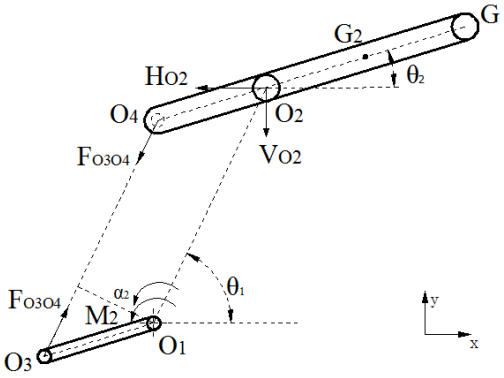

Figure I.2. 21. Force analysis of Link 2 for Structure I in Simulink simulation

Then, we replace the equations (I.2. 28)-(I.2. 31) with the equations (I.2. 33)-(I.2. 36) in the equation (I.2. 32) to obtain the motion description for the structure I. Figure I.2. 22 and Figure I.2. 23 show the results.

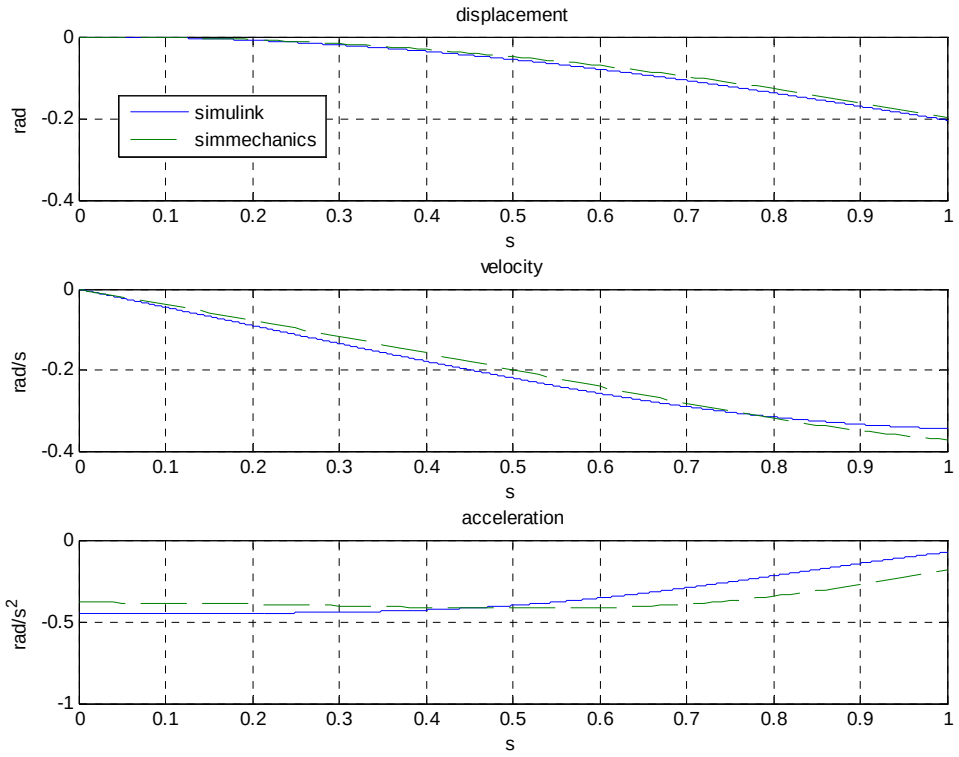

Figure I.2. 22. Simulation results for the first link in Simulink and SimMechanics

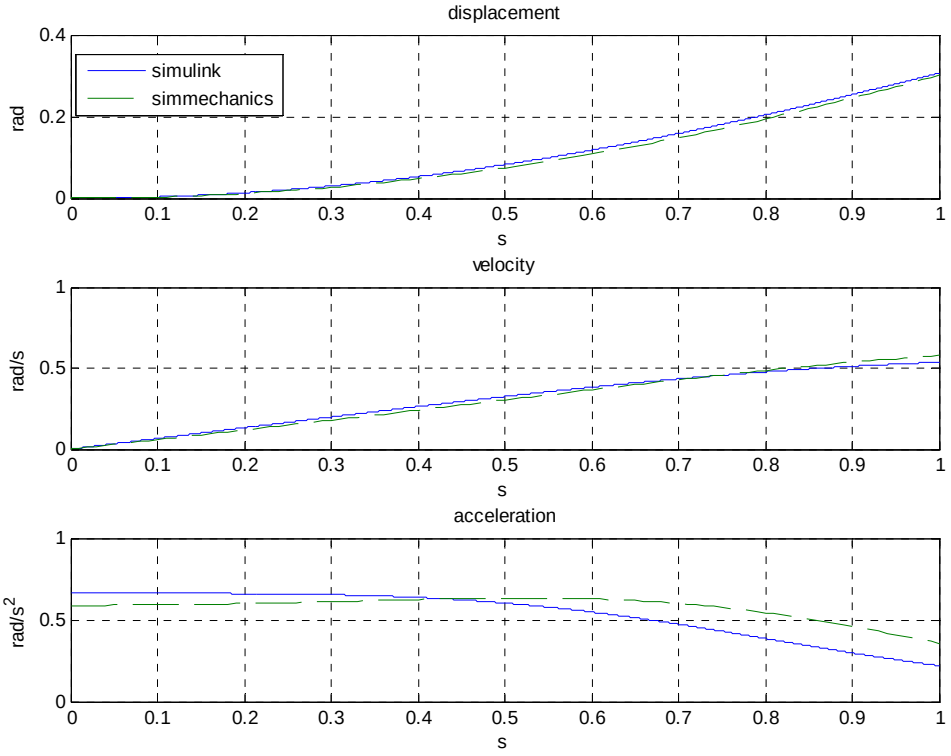

Figure I.2. 23. Simulation results for the second link in Simulink and SimMechanics

In the Simulink method, we show an ideal model where the masses of Link 3 and Link 4 are considered as zero and the component 'O_2O_4' (the length is b_2) of Link 2 is also set as zero. But in the Simmechanics method, the parallelogram mechanism is drawn in 3D software and closer to the practical model. So every component in this model has its weight and the centre of the gravity for Link 2 is different from that in the Simulink model. Figure I.2. 22 and Figure I.2. 23 show the error between the ideal and the practical models.

I.2.4 Conclusions

The two robotic structures with 2 DOF are investigated in this chapter. The first has a parallelogram structure and two motors are mounted on the base. The other has a serial structure with two motors mounting on their joints respectively. After the study of their kinematic and dynamic characters, the simulation tool Matlab is applied to simulate the motion of the structures. For the 1 DOF situation, the model is simple and the simulation results are the same between the Simulink and the SimMechanics modules of Matlab. For the simulation of the second robotic structure, the model layout is shown in the SimMechanics module with functional blocks and the results are produced under the extra motor torques. In the Simulink module, the kinematic and dynamic relation is collected in the matrix form, the simulation results are obtained through solving the matrix equation and compared with results from the SimMechanics method. Finally, the

robotic structure I is simulated in an ideal way with the Simulink module and in a practical way with the SimMechanics module, respectively. This chapter has a compared study about the two structures. Based on the motion study, the balancing systems for the both structures will be proposed in the next chapter.

Section I.3 Static Balancing for Articulated Robots

Nomenclature:

m_i	kg	the mass of Link i
h_i	m	height of gravity centre of Link i
b_i	m	connecting link length
l_i	m	length of a part of Link i
r_i	m	distance between O_i and G_i
θ_i	rad	rotational angle between Link i and the horizontal plane
a_i	m	the distance between the connecting link end O_{bi} and its according fixed revolute joint.
α_i	rad	rotational angle between the connecting link and the vertical plane
F_i	N	the spring force
E_e	J	elastic potential energy
E_g	J	gravitational potential energy
g	m/ s^2	the gravity acceleration, 9.8 m/ s^2
H_{Oi} , V_{Oi}	N	horizontal and vertical force components at joint O_i
I_{Gi}	Kg.m^2	moment of inertia for Link i with respect to G_i , $I_{Gi} = m_i l_i^2 / 12$
I_i	Kg.m^2	moment of inertia for Link i with respect to O_i , $I_{Oi} = m_i l_i^2 / 3$
C_{Mi} , M_i	N.m	motor torque by the motor M_i
C_i	N.m	torque by the Link i
P_0	Pa	initial pressure
V_0	m^3	initial volume
A_1	m^2	effective area
V_{aux}	m^3	volume of auxiliary bladder
x_1	m	position of piston

Static balancing for a manipulator's weight is necessary in terms of energy saving and performance improvement. This chapter proposes a method to design balancing devices for articulated robots in industry. The methodology is firstly presented in this chapter. The robotic dynamics is demonstrated for the balancer design. Full design details for the balancing system using springs are presented from two aspects. One is the optimization for the position of the balancing system. The other is the design of the spring parameters. Then, as examples, this chapter shows details of the balancer design for the both robotic structures that are studied in the previous chapter. For the first structure, the balancing system with linkages and springs is introduced and discussed from two aspects. The perfect torque compensation is realized and illustrated with numerical examples. For the second structure, a balancing system with pulleys, cross mechanisms and pneumatic

springs is proposed. The comparison between the two robotic structures is made. Conclusions and future work are also mentioned.

I.3.1. Methodology

This section demonstrates the methodology for the design of the balancing system. Robotic dynamics is introduced. The design target is to develop a balancing system which can produce the proper torque and counteract the gravity torque of the robot. The external motors in the balanced system do not compensate the gravity torque of the robot, therefore, they can save energy. Two design aspects based on the theory are considered. The one is to design and place a balancer to satisfy the torque requirements and the other is to decide the spring parameters to produce the matched spring forces.

I.3.1.1. Robotic dynamics

It is well known that the matrix equation describing robotic dynamics [1] is,

$$\mathbf{C} - \left[\mathbf{I}(\boldsymbol{\theta})\ddot{\boldsymbol{\theta}} + \mathbf{q}\left(\boldsymbol{\theta}, \dot{\boldsymbol{\theta}}\right) + \mathbf{G}(\boldsymbol{\theta})\right] = \mathbf{0} \qquad \text{(I.3. 1)}$$

Where **C** is the column vector of actuator torques, **I** is the manipulator inertia matrix, **q** is from kinetic effect. The gravity effect **G** is a non-linear function and the objective of gravity compensation. The aim of designing a balancing device is to reduce or eliminate the gravity effect during the workspace of the robot model.

For a non-balanced robot, actuators should actively supply all torques to counteract every item in the equation (I.3.1). In this case, **C** can be assumed consisting of two components, $\mathbf{C_a}$ and $\mathbf{C_b}$. $\mathbf{C_a}$ is assumed to be the torque component to counteract the system's inertia **I** and kinetic effect **q**, while $\mathbf{C_b}$ is assumed to be the component to counteract the gravity effect **G**,

$$\begin{cases} \mathbf{C_a} = [\mathbf{I}(\boldsymbol{\theta})\ddot{\boldsymbol{\theta}} + \mathbf{q}(\boldsymbol{\theta}, \dot{\boldsymbol{\theta}})] \\ \mathbf{C_b} = \mathbf{G}(\boldsymbol{\theta}) \end{cases}$$

For a balanced robot, $\mathbf{C_b}$ can be replaced by a passive compensator. In this case, the introduction of the passive compensator can reduce or eliminate the consumption of actuator torques for the gravity effect item. If it happens, assuming that the torque from the passive compensator is $\mathbf{C_s}$, it is known,

$$\begin{cases} \mathbf{C_a} = [\mathbf{I}(\boldsymbol{\theta})\ddot{\boldsymbol{\theta}} + \mathbf{q}(\boldsymbol{\theta}, \dot{\boldsymbol{\theta}})] \\ \mathbf{C_s} = \mathbf{G}(\boldsymbol{\theta}) \\ \mathbf{C_b} = \mathbf{0} \end{cases}$$

In this way, actuators only need to supply the torque $\mathbf{C_a}$, therefore, the total energy consumption is saved. Eq. (I.3.1) can be evolved as,

$$\mathbf{C_a} - \left[\mathbf{I}(\boldsymbol{\theta})\ddot{\boldsymbol{\theta}} + \mathbf{q}\left(\boldsymbol{\theta}, \dot{\boldsymbol{\theta}}\right)\right] + \mathbf{C_s} - \mathbf{G}(\boldsymbol{\theta}) = \mathbf{0} \qquad \text{(I.3. 2)}$$

The passive compensator producing $\mathbf{C_s}$ is the balancing device we try to design for the energy saving target. It is known from Eq. (I.3.2), a torque $\mathbf{C_s}$ supplied by the passive compensator is dependent on the item **G**.

From an energy exchange point of view, in an unbalanced robot, an actuation system must provide the energy required to shift from one level of gravitational potential energy to another according to robotic positions. Once equipped with a balancing mechanism, a balanced robot can transfer energy during motion. Specifically, Figure I.3. 1 shows the detail. Take an articulated robot with two degrees of freedom as an example. When θ_1 (or θ_2) decreases, the potential energy is transferred from the robot into the balancing mechanism and vice versa. The target is to design a device that is able to obtain or give energy according to this way. In this way the global energy required from an actuation system in order to perform a specific task can be significantly reduced.

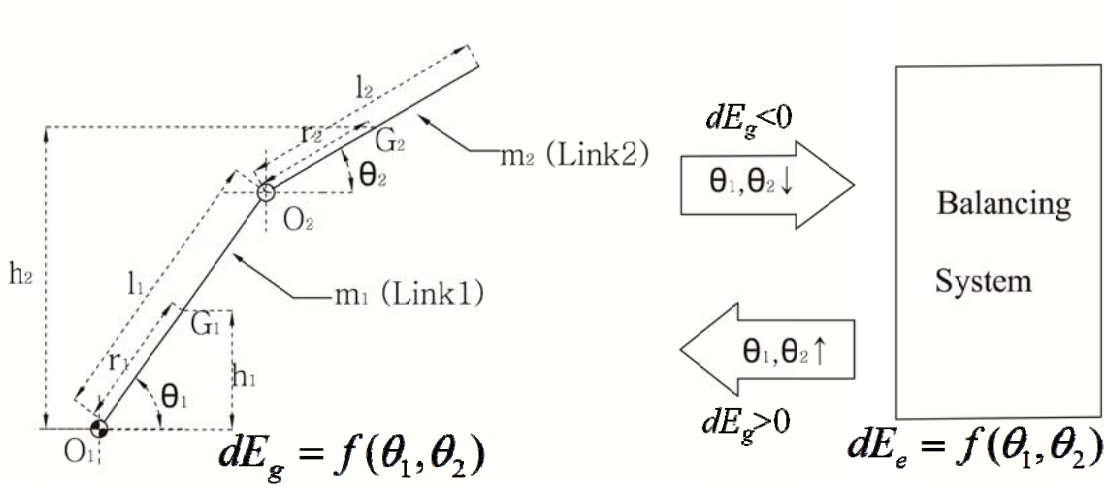

Figure I.3. 1. Energy transfer between the robot and the balancing mechanism

I.3.1.2. Design steps

Based on the dynamics, a balancing system can be designed from two aspects. The first aspect is the choice for the balancer position. Firstly, we propose a direct way to balance the gravity effect of the robot and satisfy the dynamic requirement. Then, considering practical applications, the balancer proposed should be moved and improved to clear the ambient for the robotic motion. The second aspect is to study the torque from the balancer proposed in the first aspect. To realize perfect balance, the spring parameters are designed to make the spring produce the proper torque to compensate the gravity effect of the robot. With the combination of the two aspects, the perfect balance can be realized.

I.3.2. The balancer design for the robotic structures I and II

This section presents the design process of the static balancer for the robotic structures I and II (Figure I.2.1 and Figure I.2.2). The two structures are the study objects needed to be equipped with proper balancing systems. Their kinematic and dynamic is studied in Section I.2. We know the dynamic description for the structure I.

Link 1 in Structure I:

$$\begin{aligned} &M_1 - m_1 g \cdot r_1 \cdot \cos\theta_1 - m_2 g \cdot l_1 \cdot \cos\theta_1 + m_2 \cdot r_2 \cdot l_1 \sin(\theta_2 - \theta_1) \cdot \dot{\theta}_2^2 \\ &-m_2 \cdot r_2 \cdot l_1 \cos(\theta_1 - \theta_2) \cdot \ddot{\theta}_2 - (m_1 \cdot r_1^2 + \frac{1}{12} m_1 \cdot l_1^2 + m_2 l_1^2) \cdot \ddot{\theta}_1 = 0 \end{aligned} \tag{I.3. 3}$$

Link 2 in Structure I:

$$\begin{aligned} &M_2 - m_2 g \cdot r_2 \cdot \cos\theta_2 + m_2 \cdot l_1 \cdot r_2 \sin(\theta_1 - \theta_2) \cdot \dot{\theta}_1^2 - m_2 \cdot l_1 \cdot r_2 \cos(\theta_1 - \theta_2) \cdot \ddot{\theta}_1 \\ &-(\frac{1}{12} m_2 \cdot l_2^2 + m_2 \cdot r_2^2) \ddot{\theta}_2 = 0 \end{aligned} \tag{I.3. 4}$$

Link 1 in Structure II:

$$\begin{aligned} &M_1 - M_2 - m_1 g \cdot r_1 \cdot \cos\theta_1 - m_2 g \cdot l_1 \cdot \cos\theta_1 + m_2 \cdot r_2 \cdot l_1 \sin(\theta_2 - \theta_1) \cdot \dot{\theta}_2^2 \\ &-m_2 \cdot r_2 \cdot l_1 \cos(\theta_1 - \theta_2) \cdot \ddot{\theta}_2 - (m_1 \cdot r_1^2 + \frac{1}{12} m_1 \cdot l_1^2 + m_2 l_1^2) \cdot \ddot{\theta}_1 = 0 \end{aligned} \tag{I.3. 5}$$

The dynamics of Link 2 in Structure II is the same as that of Link 2 in Structure I. These dynamic equations follow the format of the equation (I.3.1). So the target is to design balancers to produce the torque $\mathbf{C_s}$ to counteract the gravity effect **G**. For the both structures, we can obtain $\mathbf{C_s}$ as:

$$\mathbf{C_s} = \begin{bmatrix} C_{s1} \\ C_{s2} \end{bmatrix} \tag{I.3. 6}$$

Where C_{s1} is the balancing torque for Link 1 and C_{s2} is for Link 2.

$$C_{s1} = (m_1 r_1 + m_2 l_1) g \cdot \cos\theta_1$$

$$C_{s2} = m_2 r_2 g \cdot \cos\theta_2$$

Since in both structures, the masses of Link 1 and Link 2 are only considered. From the energy point of view, the potential energy for both structures can be expressed in the same way:

$$E_g = m_1 g h_1 + m_2 g h_2 = m_1 g(r_1 \sin\theta_1) + m_2 g(r_2 \sin\theta_2 + l_1 \sin\theta_1). \quad \text{(I.3. 7)}$$

Therefore,

$$\frac{dE_g}{d\theta_1} = m_1 g r_1 \cos\theta_1 + m_2 g l_1 \cos\theta_1, \quad \frac{dE_g}{d\theta_2} = m_2 g r_2 \cos\theta_2. \quad \text{(I.3. 8)}$$

$$dE_g = \frac{dE_g}{d\theta_1} \cdot d\theta_1 + \frac{dE_g}{d\theta_2} \cdot d\theta_2 = (m_1 g r_1 \cos\theta_1 + m_2 g l_1 \cos\theta_1) \cdot d\theta_1 + (m_2 g r_2 \cos\theta_2) \cdot d\theta_2. \quad \text{(I.3. 9)}$$

I.3.2.1. Design of a balancer for the robotic structure I

In this section, we propose a balancing system for the first structure. The system consists of springs and linkages. We design the system from two aspects, based on the robotic dynamics in Section I.3.1. After perfect torque balance is realized, numerical examples verify the conclusion [2].

I.3.2.1.1 Evolution of a balancing structure for the structure I

Firstly, we propose a direct way to balance the gravity effect of the robot and satisfy the dynamic requirement, as shown in Figure I.3. 2 and Figure I.3. 3. Two springs are applied to balance the first and the second links respectively. From Eq. (I.3.8), the gravity-effect component of the robot described by θ_1 is $(m_1 r_1 + m_2 l_1) g * \cos\theta_1$, and the component described by θ_2 is $m_2 g r_2 * \cos\theta_2$. The compensating torque from the first spring is $F_1 b_1 \cos\theta_1$ and the torque from the second spring is $F_2 b_2 \cos\theta_2$. Both torques are described by robotic positions (θ_1 and θ_2), therefore they have a close connection with the gravity effect of the robot. For the Link 1, we can have:

$$\begin{aligned} &M_1 + F_1 \cdot b_1 \cdot \cos\theta_1 - m_1 g \cdot r_1 \cdot \cos\theta_1 - m_2 g \cdot l_1 \cdot \cos\theta_1 + m_2 \cdot r_2 \cdot l_1 \sin(\theta_2 - \theta_1) \cdot \dot{\theta}_2^2 \\ &- m_2 \cdot r_2 \cdot l_1 \cos(\theta_1 - \theta_2) \cdot \ddot{\theta}_2 - (m_1 \cdot r_1^2 + \frac{1}{12} m_1 \cdot l_1^2 + m_2 l_1^2) \cdot \ddot{\theta}_1 = 0 \end{aligned} \quad \text{(I.3. 10)}$$

The dynamic description of the Link 2 can be evolved as:

$$\begin{aligned} &M_2 + F_2 \cdot b_2 \cdot \cos\theta_2 - m_2 g \cdot r_2 \cdot \cos\theta_2 + m_2 \cdot l_1 \cdot r_2 \sin(\theta_1 - \theta_2) \cdot \dot{\theta}_1^2 \\ &- m_2 \cdot l_1 \cdot r_2 \cos(\theta_1 - \theta_2) \cdot \ddot{\theta}_1 - (\frac{1}{12} m_2 \cdot l_2^2 + m_2 \cdot r_2^2) \ddot{\theta}_2 = 0 \end{aligned} \quad \text{(I.3. 11)}$$

To balance the gravity effect, springs should produce constant forces. This requirement can be approximated by means of low stiffness mechanical spring or by means of

pneumatic spring connected to big auxiliary volume. In detail, passive compensators are expected to balance the gravity effect of the robot in a perfect way which means the compensating torques exactly counteract the gravity torques and actuators do not need power to contribute the gravity effect. The perfect balance can be realized if,

$$\begin{cases} F_1 b_1 \cos\theta_1 = (m_1 r_1 + m_2 l_1) g \cos\theta_1 \\ F_2 b_2 \cos\theta_2 = m_2 g r_2 \cos\theta_2 \end{cases} \quad \text{(I.3. 12)}$$

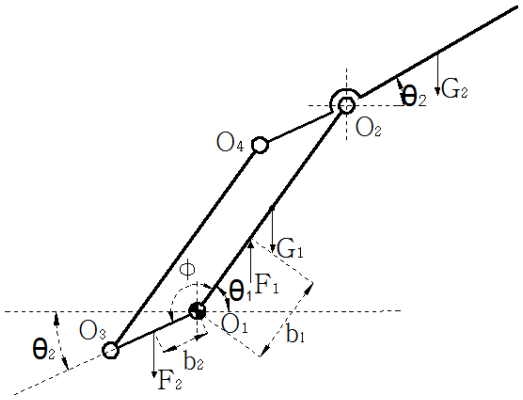

Figure I.3. 2. the design of the balancing system

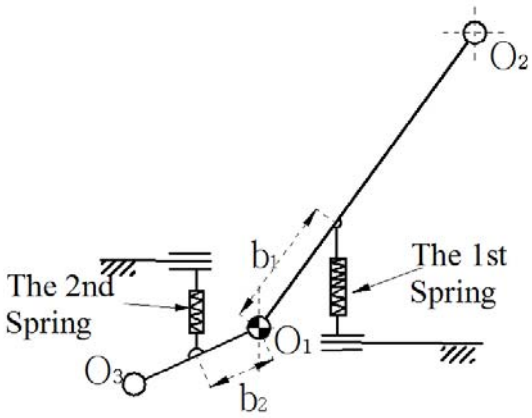

Figure I.3. 3. The spring positions

From Figure I.3. 3, it is realized that the existence of spring devices interrupts the robotic motion. To release more space, it is better to move the balancing system far away from the robot. Figure I.3. 4 presents a solution to move the first spring. The choice of the angle δ_1 is arbitrary. δ_1 and θ_1 are distributed in different ways, but both ways share the same range ($\delta_1+\theta_1$). A prismatic guide is placed parallel to a new datum line O_1-P_1 for θ_1 so that the 1st spring is perpendicular to the line O_1-P_1, therefore the spring produces a spring torque $F_1 b_1 \cos\theta_1$. Using this way, whatever a value of δ_1, a proper position can be always found for the 1st spring to produce a spring torque $F_1 b_1 \cos\theta_1$ decided by the angle θ_1. With this skill, we can decide δ_1 and the length of the connecting link b_1 so that the spring is placed at a proper position. The second spring can also be placed at a proper position using the same approach (Figure I.3. 5). Here, we choose $\delta_1 = \pi/2$, $\delta_2 = \pi/2$ to place the two springs, shown in Figure I.3. 6.

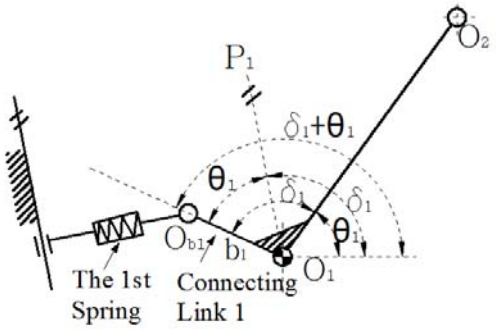

Figure I.3. 4. A solution to place the 1st spring

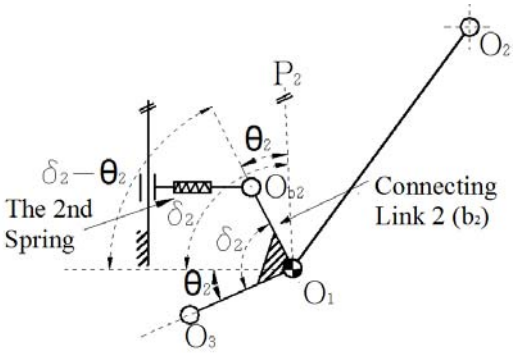

Figure I.3. 5. A solution to place the 2nd spring

Since the prismatic guides normally require much space for placing the guides, they are substituted with revolute joints, as shown in Figure I.3. 7. With the substitution, torque errors happen since with revolute joints, a torque produced by a spring is not always $F_1b_1\cos\theta_1$ (or $F_2b_2\cos\theta_2$). During the robotic motion, the springs rotate and the torques are decided not only by robotic positions, but also by relative positions of the springs with respect to the robot.

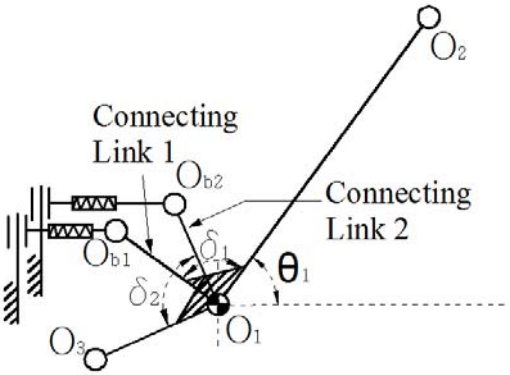

Figure I.3. 6. The Placement of the two springs

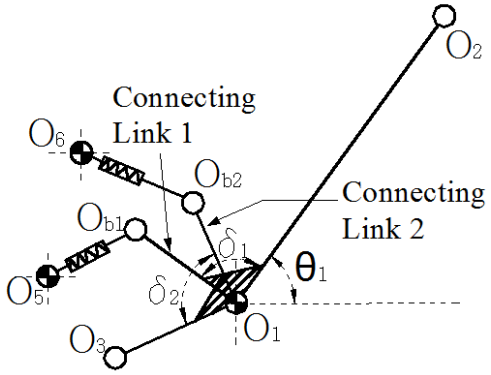

Figure I.3. 7. A feasible design using revolute joints

In detail, after the robotic structure is equipped with the springs, the dynamics for the Link 1 (Figure I.3. 8) can be expressed as:

$$\begin{aligned} &C_1 + F_1 \cdot \cos\beta_1 \cdot b_1 \cdot \cos\theta_1 + F_1 \cdot \sin\beta_1 \cdot b_1 \cdot \sin\theta_1 - m_1 g \cdot r_1 \cdot \cos\theta_1 \\ &-F_{T1} \cdot r_1 - I_1 \cdot \alpha_1 - H_{O2} \cdot l_1 \cdot \sin\theta_1 + V_{O2} \cdot l_1 \cdot \cos\theta_1 = 0 \end{aligned} \qquad \text{(I.3. 13)}$$

With the kinematic conclusions in the Section I. 2 and the equations (2.10) and (2.11), this equation can be evolved as:

$$C_1 + F_1 \cdot \cos\beta_1 \cdot b_1 \cdot \cos\theta_1 + F_1 \cdot \sin\beta_1 \cdot b_1 \cdot \sin\theta_1 - m_1 g \cdot r_1 \cdot \cos\theta_1 - m_2 g \cdot l_1 \cdot \cos\theta_1$$
$$+ m_2 \cdot r_2 \cdot l_1 \sin(\theta_2 - \theta_1) \cdot \dot{\theta}_2^2 - m_2 \cdot r_2 \cdot l_1 \cos(\theta_1 - \theta_2) \cdot \ddot{\theta}_2 - (m_1 \cdot r_1^2 + \frac{1}{12} m_1 \cdot l_1^2 + m_2 l_1^2) \cdot \ddot{\theta}_1 = 0 \quad \text{(I.3. 14)}$$

From Figure I.3. 9, it is known that,

$$C_2 + F_2 \cdot \cos\beta_2 \cdot b_2 \cdot \cos\theta_2 + F_2 \cdot \sin\beta_2 \cdot b_2 \cdot \sin\theta_2 - F_{O_3O_4} \cdot b_2 \sin(\theta_1 - \theta_2) = 0 \quad \text{(I.3. 15)}$$

$$F_{O_3O_4} \cdot b_2 \sin(\theta_1 - \theta_2) - H_{O_2} \cdot r_2 \cdot \sin\theta_2 + V_{O_2} \cdot r_2 \cdot \cos\theta_2 - I_2 \cdot \alpha_2 = 0 \quad \text{(I.3. 16)}$$

With the equations (I.2.10), (I.2.11), (I.3.15), the equation (I.3.16) is evolved as:

$$M_2 + F_2 \cdot \cos\beta_2 \cdot b_2 \cdot \cos\theta_2 + F_2 \cdot \sin\beta_2 \cdot b_2 \cdot \sin\theta_2 - m_2 g \cdot r_2 \cdot \cos\theta_2$$
$$+ m_2 \cdot l_1 \cdot r_2 \sin(\theta_1 - \theta_2) \cdot \dot{\theta}_1^2 - m_2 \cdot l_1 \cdot r_2 \cos(\theta_1 - \theta_2) \cdot \ddot{\theta}_1 - (\frac{1}{12} m_2 \cdot l_2^2 + m_2 \cdot r_2^2) \ddot{\theta}_2 = 0 \quad \text{(I.3. 17)}$$

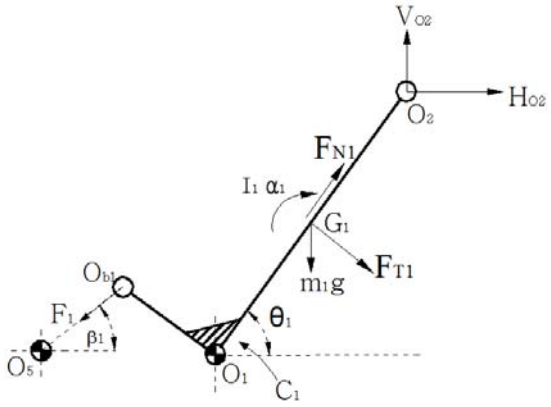

Figure I.3. 8. The force analysis of Link 1 considering the spring effect

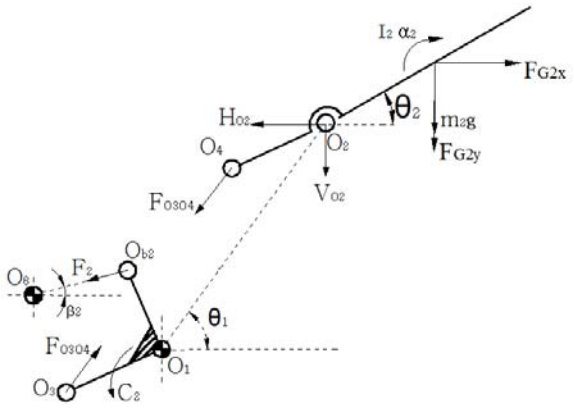

Figure I.3. 9. The force analysis of Link 2 considering the spring effect

In the following part, we will discuss how to find the best position for the fixed pivot O_5 (or O_6) so that the error between the torque caused by the 1st (or 2nd) spring and the gravity torque of Link 1 (or Link 2) is as little as possible. Also, spring parameters are studied to decrease or eliminate the error. It is perfectly static balancing if the spring torques can compensate the gravity torque of the robot in every configuration.

I.3.2.1.2. Analysis of torque compensation and design of spring parameters

In this part, spring torques are analyzed with the choice of spring parameters. We start the design of a balancing device from Link 1. In Figure I.3. 10, the position of the fixed pivot O_5 can be described with r_5 and α_5 in polar coordinate. A spring is possibly designed in two ways (Figure I.3. 10), depending on spring force and space dimensions. In the first way, a spring is connected by two articulated joints O_5 and O_{b1}. In the second way, a

spring is guided to avoid the separation of the spring and the link articulated with the joint O_5. In following research, the second design is taken as an example. In the triangle $\Delta O_1O_{b1}O_5$, the varied length of the 1st spring a_1 is expressed:

$$a_1 = a_1(\theta_1) = \sqrt{r_5^2 + b_1^2 - 2b_1 r_5 \cos(\alpha_5 - \theta_1)}\,, \quad a_1 \sin\mu_1 = b_1 \sin(\alpha_5 - \theta_1) \tag{I.3. 18}$$

The moment arm of the 1st spring is:

$$b_{1F} = r_5 \sin\mu_1 \tag{I.3. 19}$$

So the torque applied by the balancing system is:

$$C_{1F}(\theta_1) = F_{1F} \cdot b_{1F} \tag{I.3. 20}$$

Here, we classify the force F_{1F} applied by the spring into two cases: (i) constant force and (ii) variable force. Both cases can be realized in reality, using different devices.

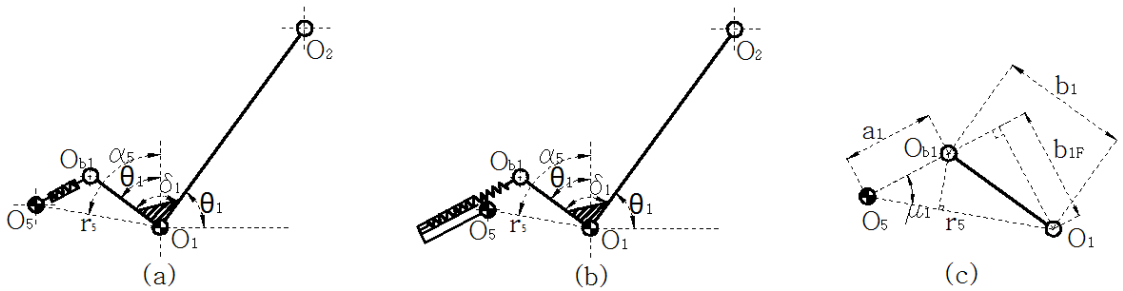

Figure I.3. 10. Design of a balancing device for Link 1

(i) Constant force. Assume that F_{1F} is the constant force which value equals the one when the maximum torque from Link 1 is compensated. It is known, from Eq. (I.3.12), that:

$$C_{1max} = C_1(\theta_1 = 0) = (m_1 r_1 + m_2 l_1)g\,, \quad F_{1F} \cdot b_{1F(\theta_1=0)} = C_{1max} \tag{I.3. 21}$$

Therefore,

$$F_{1F} = \frac{C_{1max}}{b_{1F(\theta_1=0)}} \tag{I.3. 22}$$

The error needed to be compensated by an actuator is,

$$e_c = C_1(\theta_1) - C_{1F}(\theta_1) \tag{I.3. 23}$$

The target is to reduce the error as much as possible. From Eq. (I.3.23), the error depends on the angle θ_1: different angles imply different errors and different positions of Link 1.

(ii) Variable force. In this case, we set the force F_{1FK} on the spring is variable, which value depends on the spring deformation. It is known that,

$$F_{1FK} = F_{1F0} + k_{1id} \cdot \Delta a_1 \tag{I.3. 24}$$

Where $\Delta a_1 = a_1 - a_{10}$, a_{10} is the spring deformation when F_{1F0} is produced by the spring at $\theta_1 = 0$. Then the balancing torque is:

$$\begin{aligned} C_{1FK} &= F_{1FK} \cdot b_{1F} = (F_{1F0} + k_{1id} \cdot \Delta a_1) \cdot b_{1F} \\ &= [F_{1F0} + k_{1id} \cdot (a_1 - a_{10})] \cdot \frac{r_5 \cdot b_1}{a_1} \sin(\alpha_5 - \theta_1) \end{aligned} \tag{I.3. 25}$$

Especially, if $\alpha_5 = \pi/2$, considering Equations (7), (8), Equation (14) can be evolved as:

$$\begin{aligned} C_{1FK} &= F_{1FK} \cdot b_{1F} \\ &= F_{1F0} \cdot \frac{r_5 \cdot b_1}{a_1} \cdot \cos\theta_1 + k_{1id} a_1 \cdot \frac{r_5 \cdot b_1}{a_1} \cdot \cos\theta_1 - k_{1id} a_{10} \cdot \frac{r_5 \cdot b_1}{a_1} \cdot \cos\theta_1 \\ &= (F_{1F0} - k_{1id} a_{10}) \cdot \frac{r_5 \cdot b_1}{a_1} \cdot \cos\theta_1 + k_{1id} r_5 b_1 \cdot \cos\theta_1 \end{aligned} \tag{I.3. 26}$$

The value of the balancing torque must be equal to the value of the torque from the link, then a perfect balancing can be realized, as shown in the equation (I.3.27),

$$C_{1FK} = C_1 = C_{1max} \cdot \cos\theta_1 \tag{I.3. 27}$$

In this case, we can obtain the conditions satisfying the equation (I.3.27):

$$F_{1F0} = k_{1id} \cdot a_{10} \ , \ \ k_{1id} r_5 b_1 = C_{1max} \tag{I.3. 28}$$

Therefore, the spring can be deformed by a_{10} to obtain the force F_{1F0}. We have the spring stiffness as:

$$k_{1id} = \frac{C_{1max}}{r_5 b_1} \tag{I.3. 29}$$

In this way, no error exits and Link 1 can be compensated perfectly.

Now assume an arbitrary spring with the stiffness k_1 applied in the balancing mechanism, the torque error can be defined in percentage as,

$$e_{C\%} = \frac{C_{1FK} - C_1}{C_{1max}} \cdot 100 \qquad \text{(I.3. 30)}$$

Considering Eq. (I.3.26), Eq. (I.3.30) can be evolved as,

$$\begin{aligned} e_{C\%} &= \frac{F_{1F0} \cdot \frac{r_5 \cdot b_1}{a_{10}} \left(\frac{a_{10}}{a_1} - \frac{k_1 a_{10}^2}{F_{1F0} \cdot a_1} + \frac{k_1 a_{10}}{F_{1F0}}\right) \cdot \cos\theta_1 - C_{1max} \cdot \cos\theta_1}{C_{1max}} \cdot 100 \\ &= \left[\left(\frac{a_{10}}{a_1} - \frac{k_1 a_{10}^2}{F_{1F0} \cdot a_1} + \frac{k_1 a_{10}}{F_{1F0}}\right) - 1\right] \cdot \cos\theta_1 \cdot 100 \end{aligned} \qquad \text{(I.3. 31)}$$

It is known from Eq. (I.3.28), the ideal spring must have a deformation a_{10} to obtain the proper force F_{1F0} for the torque compensation of the manipulator.

Since a_{10} is the distance between the connection points of the spring, when $\theta_1 = 0$. This means that the spring must have an initial length of the same order of a_{10} and this means also that the encumbrance of the spring can lead to practical installation problems (like in fig. 10 b). To solve this problem, a spring with a bigger value of the stiffness can produce the required force in the initial condition ($\theta_1 = 0$) with shorter deformation but it will have the error in torque in the other positions. The following analysis is done to evaluate this error. For example, if we have:

$$k_1 = n \cdot k_{1id} = n \cdot \frac{F_{1F0}}{a_{10}} \qquad \text{(I.3. 32)}$$

In this case, the deformation is shortened as 1/n of the previous one. Then the Eq. (I.3.31) is evolved as,

$$e_{C\%} = \left(\frac{a_{10}}{a_1} - n\frac{a_{10}}{a_1} + n - 1\right) \cdot \cos\theta_1 \cdot 100 \qquad \text{(I.3. 33)}$$

Considering Eq. (I.3.18), if we introduce the ratio $ra_1 = r_5/b_1$ to have a non-dimensional evaluation, Eq.(I.3.33) is evolved as,

$$e_{C\%} = \left(\frac{\sqrt{1 + ra_1^2}}{\sqrt{1 + ra_1^2 - 2 \cdot ra_1 \sin\theta_1}} - n \cdot \frac{\sqrt{1 + ra_1^2}}{\sqrt{1 + ra_1^2 - 2 \cdot ra_1 \sin\theta_1}} + n - 1\right) \cdot \cos\theta_1 \cdot 100 \qquad \text{(I.3. 34)}$$

Figure I.3. 11 shows that when the balancer is located at $\alpha_5 = \pi/2$, the error $e_{C\%}$ changes as the spring stiffness varies. It means that a designer can choose the proper stiffness with the matched deformation according to different practical requirements. If n=1 Eq. (I.3.34) represents the ideal case of perfect balance and $e_{C\%}$ is equal to zero. It is realized that even if n = 2, the stiffness k_1 is twice than the ideal stiffness k_{1id}, the error is no more than around 15%. We can also observe that the error figure is not globally

symmetric within the range (0, 2π), but local symmetric within areas (0, π) and (0, -π). After we take the absolute value of $e_{C\%}$, the error is then evaluated in a mean value way $e_{C\%mean}$, as shown in Figure I.3.12.

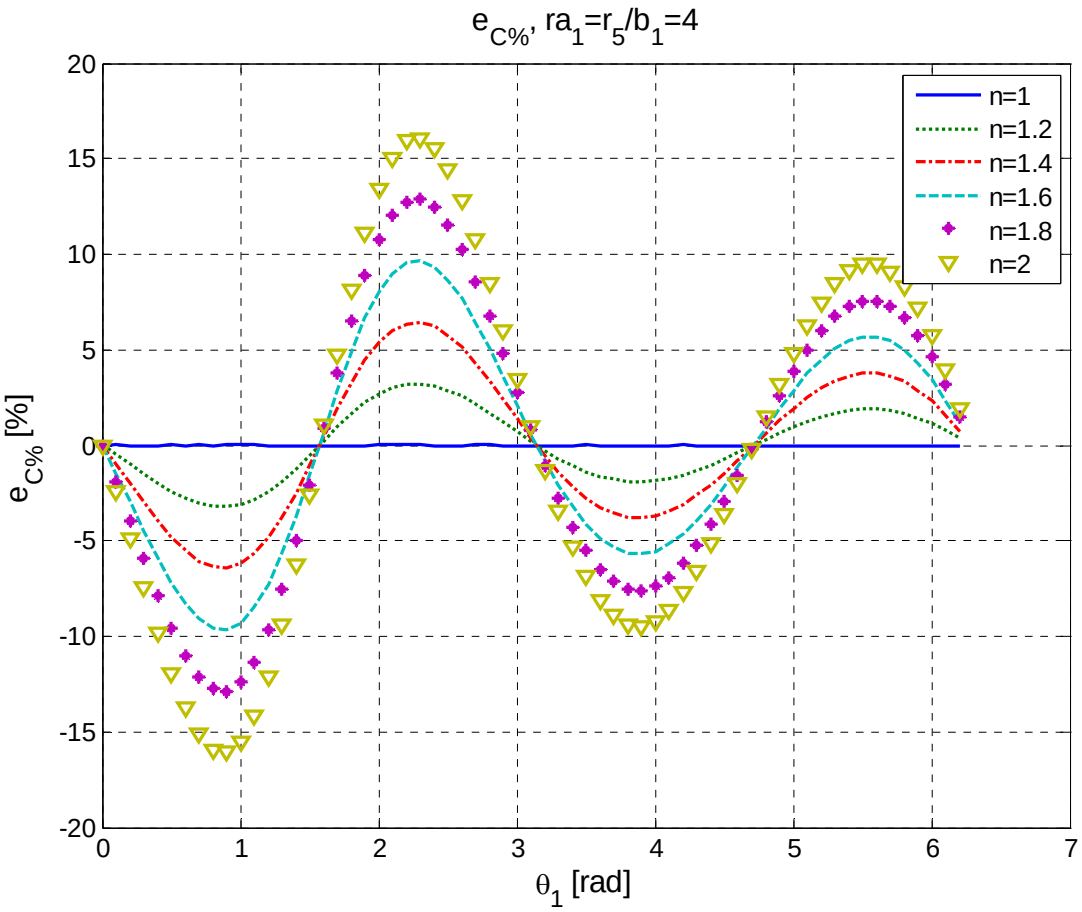

Figure I.3. 11. The error between the 1st spring torque and the torque from the Link 1 when ra_1=4 and the spring stiffness is varying.

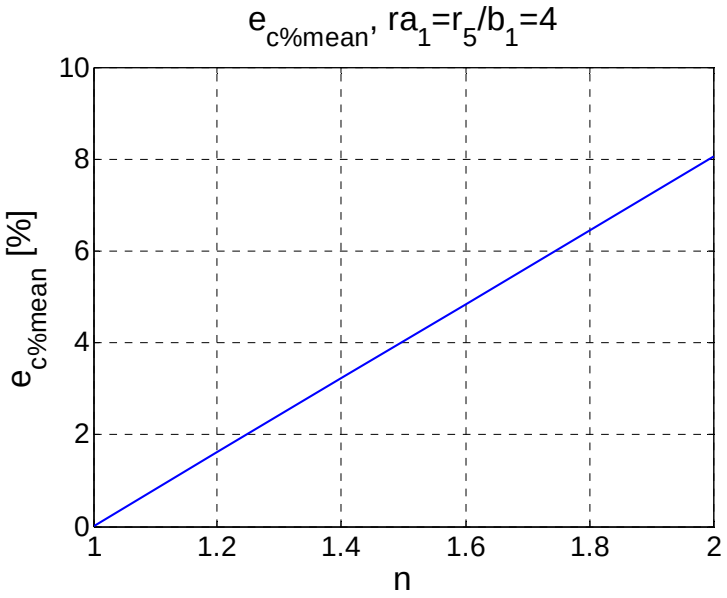

Figure I.3. 12.The error between the 1st spring torque and the torque from the Link 1 in the mean value.

Next, we discuss how to realize the static balancing for Link 2 in a feasible way. The process is the same as before if we change subscript '1' with '2' for the Link 2. In Figure I.3.13, the position of the fixed pivot O_6 is described with r_6 and α_6 in polar coordinate. Also the maximum torque is,

$$C_{2\max} = C_2(\theta_2 = 0) = m_2 r_2 g$$

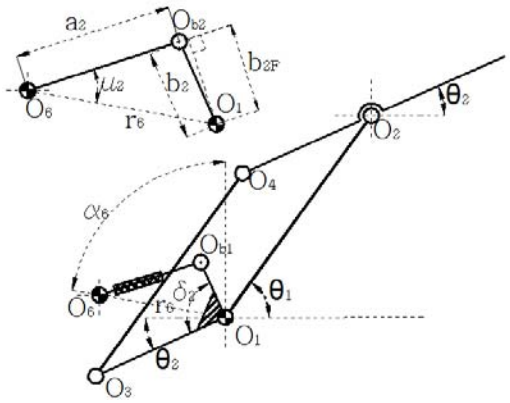

Figure I.3. 13. Design of a balancing device for Link 2

In this part, we define the spring parameters to make the spring torques in the situation of the revolute joints exactly counteract the gravity effect from the robot.

I.3.2.1.3 Considerations about the structure singularity

In the robotic structure I, since the parallelogram device is introduced, the angle φ is unavoidable followed (Figure I.3. 14). Due to the equation (I.2. 9), the force on the Link 4 is:

$$F_{O_3O_4} = C_2 / b_2 \sin(\theta_1 - \theta_2)$$

When $\theta_1 = \theta_2$, the force F_{O3O4} becomes infinitely large. This is the singularity position for this structure, which should be avoided.

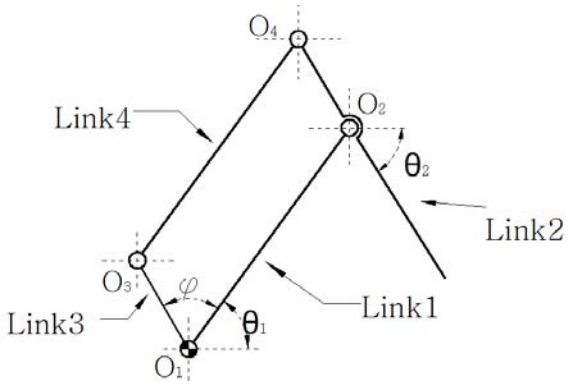

Figure I.3. 14. The angle φ introduced between Link1 and Link 3

To avoid the overlapped position of Link 3 and Link 1, we can assume that the motion range of Link 3 is $\varphi_{min} \leq \varphi \leq \varphi_{max}$. Figure I.3. 15 and Figure I.3. 16 show the extreme positions.

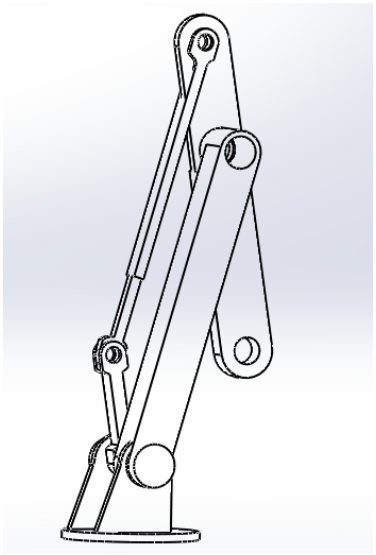

Figure I.3. 15. The extreme position when $\varphi = \varphi_{min}$

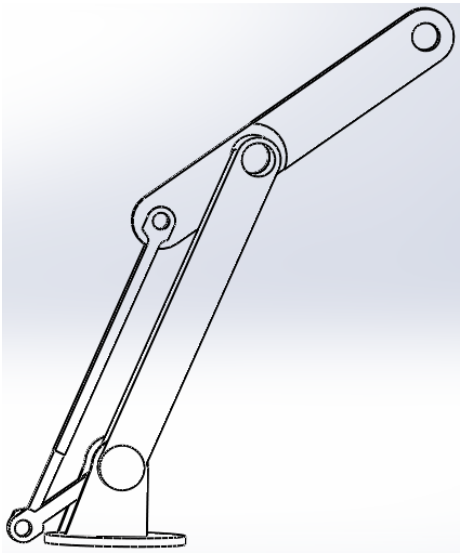

Figure I.3. 16. The extreme position when $\varphi = \varphi_{max}$

With extreme positions, the motion range of Link 2 is limited with respect to Link 1. For every position of Link 1, the motion range of Link 2 is fixed as $\Delta\varphi = \varphi_{max} - \varphi_{min}$, as shown in Figure I.3. 17.

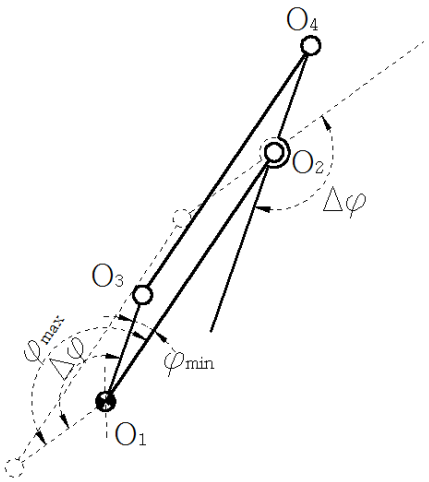

Figure I.3. 17. The motion range of Link 2

I.3.2.1.4. Numerical examples

This part shows numerical examples to test and verify the balancing effect of the balancer mentioned above. Weight and dimensions are listed in Table I.3.1

Table I.3.1. Robot physical parameters

physical parameters	m_1	m_2	l_1	l_2	r_1	r_2	b_1	b_2
values	100	40	1.2	1	0.6	0.5	0.2	0.2

(i) Constant force for Link 1.

For the 1st link, when the spring provides with a constant force and the range of θ_1 is $(-\pi/2, \pi/2)$. Figure I.3.18 shows the spring torque C_{1F}, compared with the gravity torque C_1 as a function of θ_1 in a constant-force case, when α_5 is different and $ra_1 = r_5/b_1 = 6$. ra_1 is used to describe the non-dimensional position for the pivot O_5. Every smooth curve means the spring torque at every position described by α_5 and ra_1. The dotted curve means the gravity torque. From the figure, for the curve $\alpha_5 = 84^o$, for example, the spring torque is firstly bigger than the gravity torque and the error is therefore positive. Then, as θ_1 increases, the curve gets closer to the gravity torque and finally less than the gravity torque with the error becoming negative. We can observe the curve with α_5=86° is the best result among the batch of curves: this curve goes along the dotted curve, which means the torque supplied by the spring almost compensates the gravity torque. Here only torque changes at $ra_1 = 6$ are shown in this paper. In Figure I.3.19 conclusions about

different ra_1 are shown. A bigger value of ra_1 shows little error between the spring torque and the gravity torque. It is not difficult to know that with a bigger value of ra_1, the error becomes little, because the bigger value of ra_1 implies the position of the fixed pivot O_5 goes further away from the point O_1. At an infinite position, the revolute joint will ideally evolve into a prismatic guide and there is no error for a prismatic pair. It is known from Figure I.3.19, when α_5=86° and $ra_1=r_5/b_1$=6, the least error is obtained as about 2.8%.

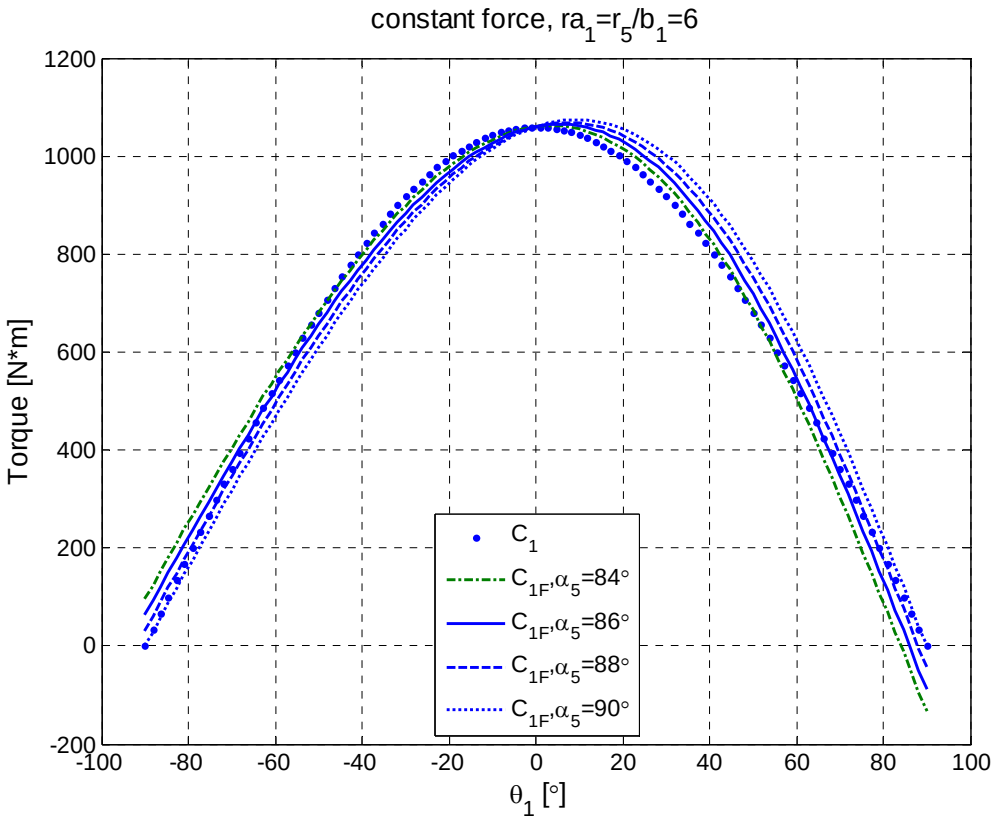

Figure I.3. 18. The 1st spring torque and the torque from the Link 1 in a constant-force case.

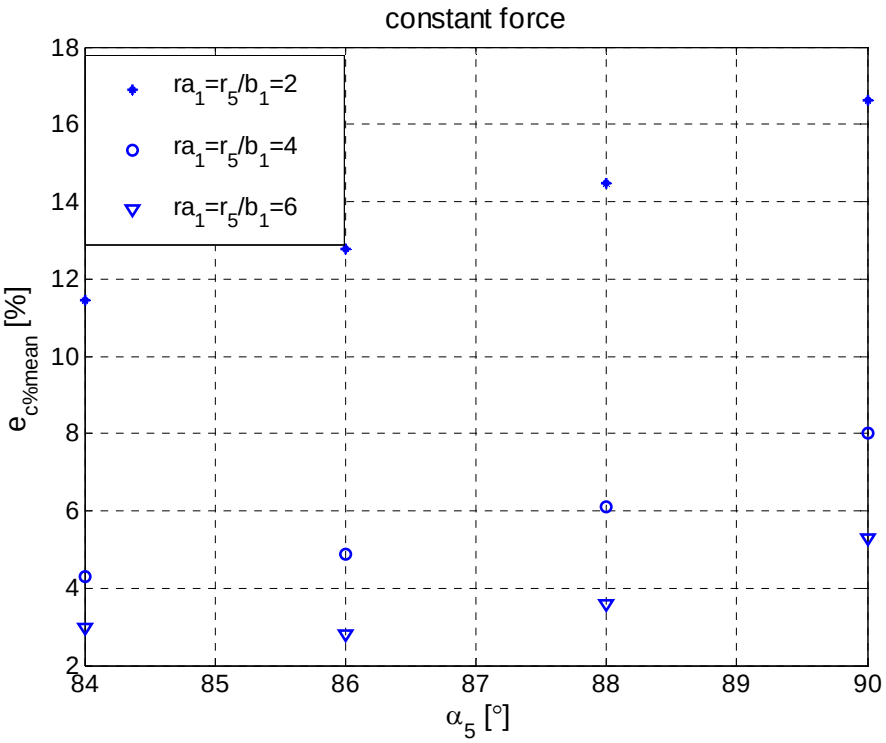

Figure I.3. 19. The error between the 1st spring torque and the torque from the Link 1 in a constant-force case.

(ii) Variable force for Link 1.

Figure I.3.20 shows the 1st spring torque, compared with the gravity torque described by θ_1 in a variable-force case. The spring stiffness, the initial length and the initial force are decided by the requirements of the torque compensation discussed above. The perfect balance is realized at α_5=90° where Figure I.3.21 shows the error is zero. Also, the ratio ra_1 has no influence on the error, which means, when a spring produces a variable force with ideal parameters defined in the equations (I.3.28), (I.3.29), the error is only dependent on the orientation of the spring, not on the distance away from the point O_1.

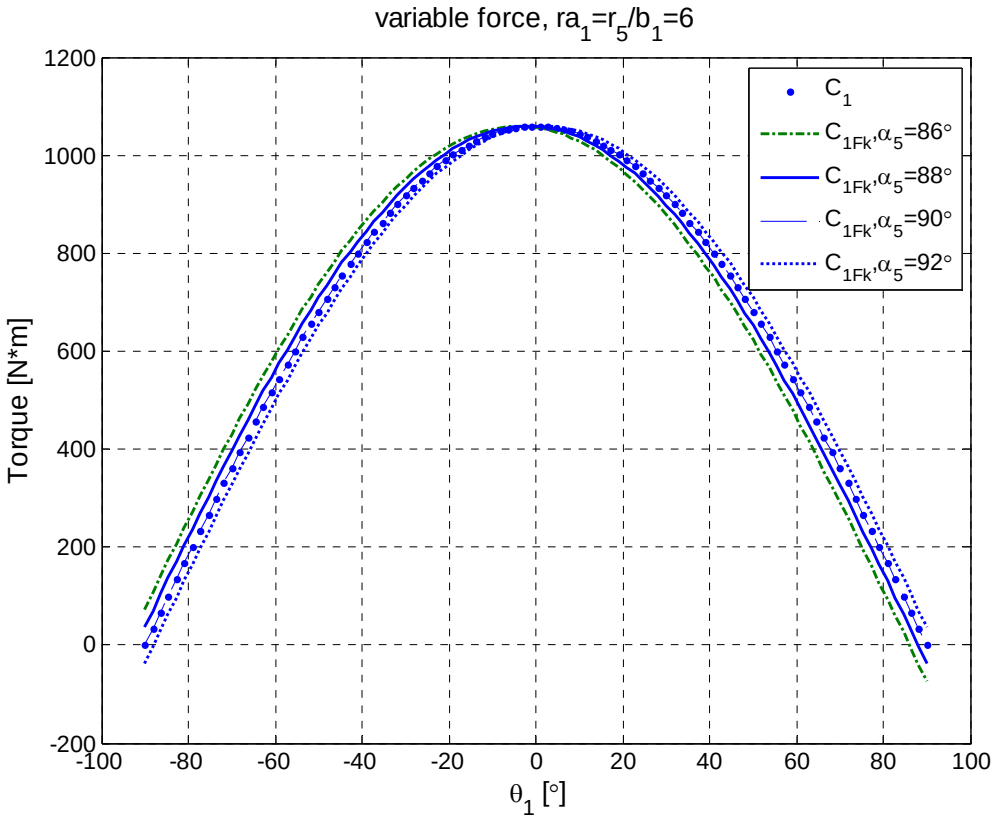

Figure I.3. 20. The 1st spring torque and the torque from the Link 1 in a variable-force case.

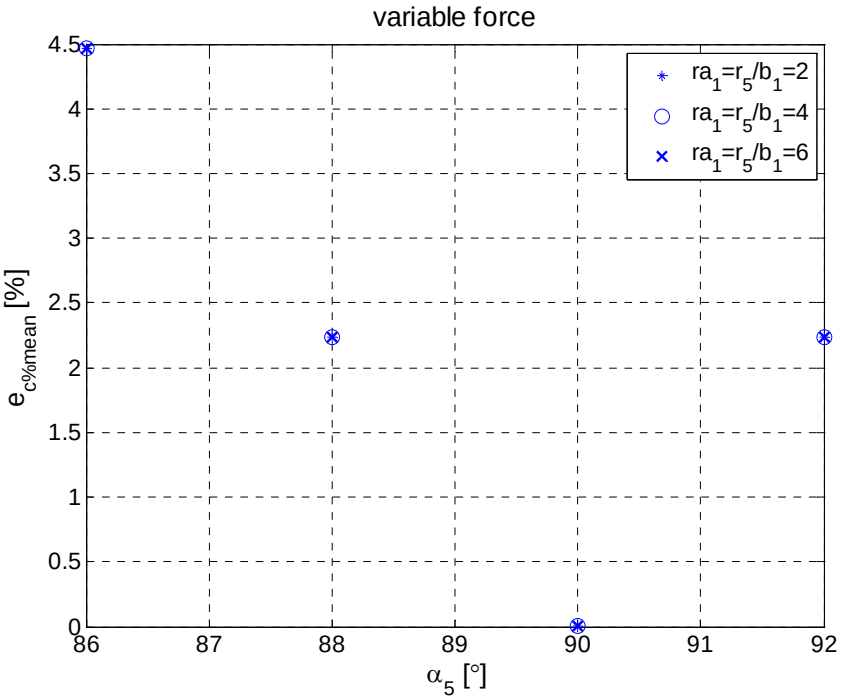

Figure I.3. 21. The error between the 1st spring torque and the torque from the Link 1 in a variable-force case.

(iii) Constant force for Link 2.

For the study of the 2nd link, it is known that the gravity torque is influenced by the position of the 1st link. So if we assume the range of θ_2 is controlled by θ_1 and ϕ (Figure I.3.2), θ_2 can be known from the relation: $\theta_2 = \phi+\theta_1-\pi$. The choice of ϕ should consider the singularity problem. When ϕ equals 0 or π, the singularity is happened. Here, ϕ varies from 18° to 162° as an example. Figure I.3.22 shows a batch of curves in a constant-force situation in the conditions $ra_2 = r_6/b_2 = 6$, $\alpha_6 = 92°$. When the θ_1 is fixed and ϕ changes, θ_2 is therefore changed. During the change of θ_2, the spring torques and the required balancing torque are drawn as smooth and dotted curves respectively. Then with other values of θ_1, we follow the same way to define θ_2 and produce torque changes. Figure I.3.23 shows, among different positions of the joint pivot O_6 described by α_6 and ra_2, the optimization result for the error is least as about 5%, when $\alpha_6 = 90°$ and $ra_2 = 6$.

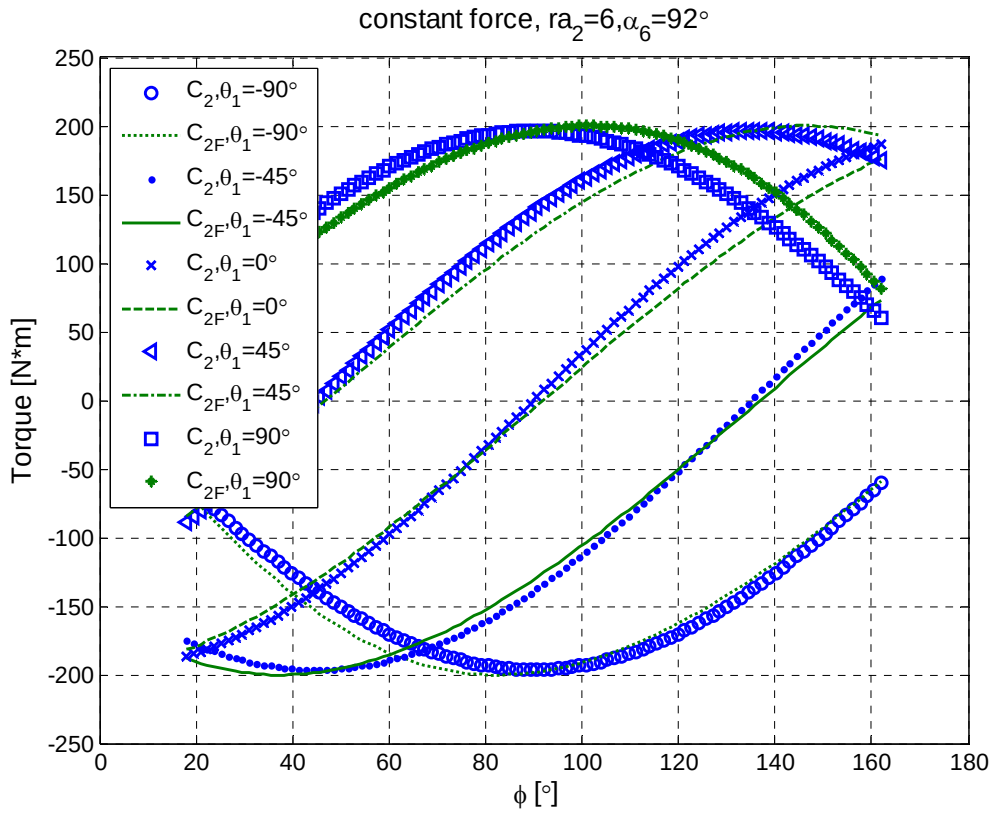

Figure I.3. 22. The 2nd spring torque and the torque from the Link 2 in a constant-force case.

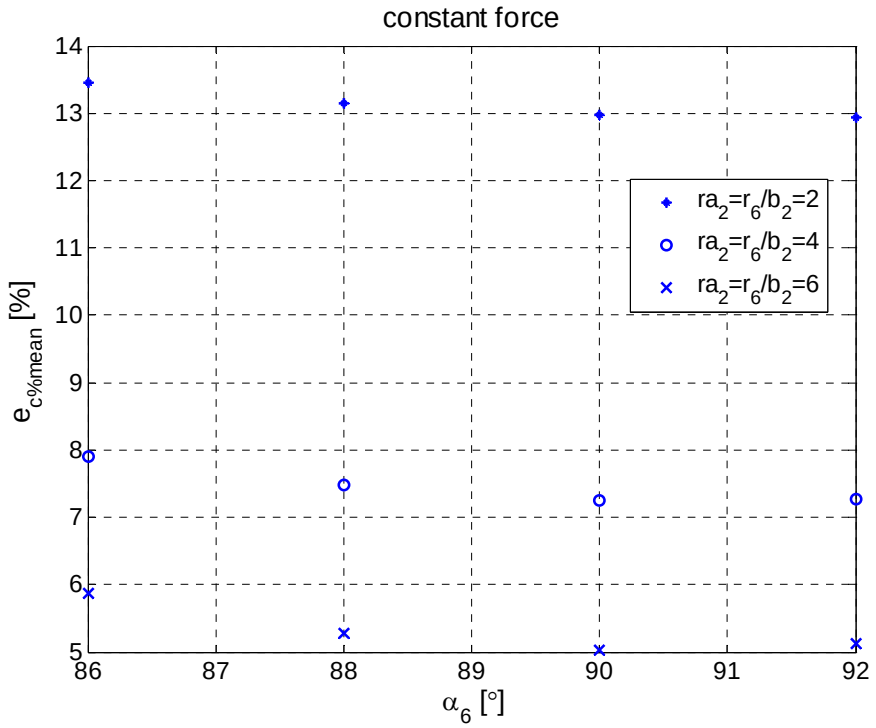

Figure I.3. 23. The error between the 2nd spring torque and the torque from the Link 2 in a constant-force case.

(iv) Variable force for Link 2.

Figure I.3.24 shows the 2nd spring torque, designed according to ideal parameters of eq. 17 but referred to the second link, compared with the gravity torque from Link 2 in a variable-force case, when α_6=92°. Figure I.3.25 shows the error $e_{C\%mean}$ as a function of α_6, and it is zero when α_6=90°. Also, the error has no relation with the value of the ratio ra_2.

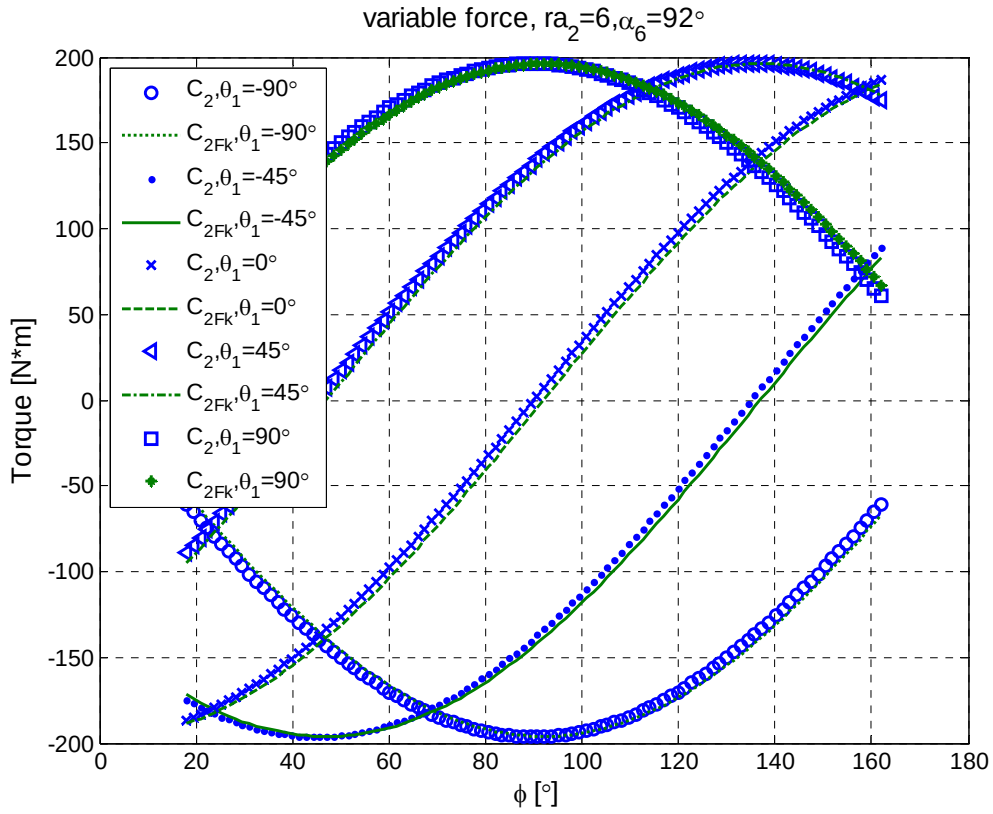

Figure I.3. 24. The 2nd spring torque and the torque from the Link 2 in a variable-force case.

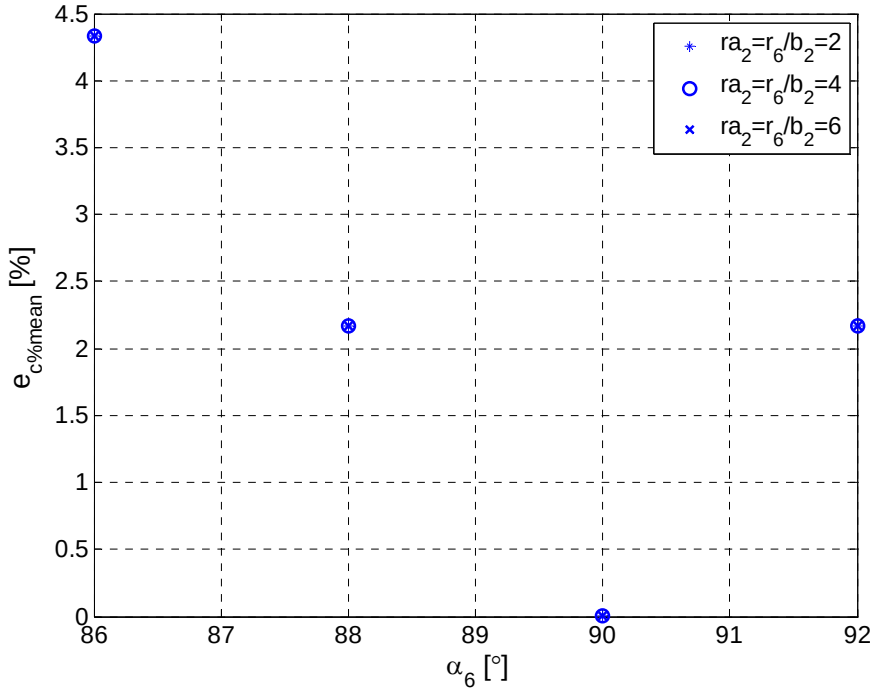

Figure I.3. 25. The error between the 2nd spring torque and the torque from the Link 2 in a variable-force case.

I.3.2.2. Design of a balancer for the robotic structure II

This part focuses on the design of the balancing system for the robotic structure II. The balancing system consists of cable, pulleys, cross mechanisms and springs [3]. The two design aspects, the position of the balancer and the design of spring parameters, are discussed. For spring choice, pneumatic and hydro-pneumatic springs are studied.

I.3.2.2.1 Evolution of a balancing structure for the structure II

Consider the first link as a 1 DOF situation without the connection of Link 2. The balancing device consists of the cross mechanism and the spring. Figure I.3. 26 shows two possibilities to place a balancing device. The position of the balancing device can be decided by δ_1 and b_1, considering free volume around the robot. With a cross mechanism, rotational movement is transferred into translational one. F1 is a constant force applied by the spring, which can be realized by a pneumatic spring introduced later. M1 is Motor 1 driving the first link.

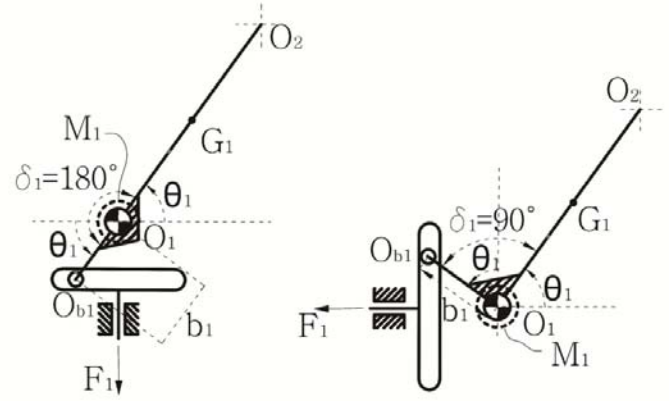

Figure I.3. 26. A balancing device for the first link.

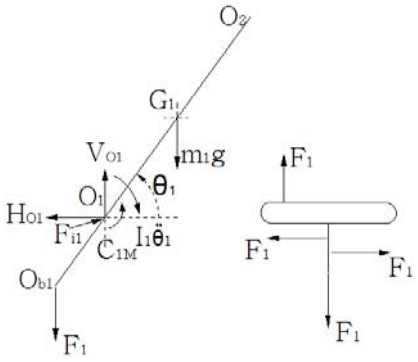

Figure I.3. 27. Free body diagram for Link 1 and the cross mechanism in 1 DOF situation.

Take the left part of Figure I.3. 26 as an example. From its free body diagram (Figure I.3. 27), it is known the dynamic description of Link 1 is

$$F_1 b_1 \cos\theta_1 + C_{1M} = m_1 g r_1 \cos\theta_1 + I_1 \ddot{\theta}_1. \qquad \text{(I.3. 35)}$$

Under the perfectly static balancing situation $\ddot{\theta}_1 = 0$, the torque provided by the motor M_1 must be null, i.e. $C_{1M} = 0$, then,

$$F_1 b_1 \cos\theta_1 = m_1 g r_1 \cos\theta_1. \qquad \text{(I.3. 36)}$$

If we assume that,

$$F_1 b_1 \cos\theta_1 = \frac{dE_e}{d\theta_1},\ \ m_1 g r_1 \cos\theta_1 = \frac{dE_g}{d\theta_1}. \qquad \text{(I.3. 37)}$$

Then we have,

$$\frac{dE_e}{d\theta_1} d\theta_1 = \frac{dE_g}{d\theta_1} d\theta_1. \qquad \text{(I.3. 38)}$$

Compared with Eq. (I.3.9), an ideal balancing device is realized if we develop a system that is able to produce a constant force and to obtain or provide energy according to Eq.(I.3.37).

Figure I.3. 28 shows the synthesis of the balancing devices for Link 1 and Link 2. The motor M_1 provides a torque C_{1M} between the frame and Link 1, motor M_2 provides a torque C_{2M} between the links 1 and 2. Considering Link 1 as a part of the robot (Figure I.3. 29 and Figure I.3. 30), it is known,

$$F_1 b_1 \cos\theta_1 + C_{1M} - C_{2M} - m_2 r_2 l_1 \sin(\theta_1 - \theta_2)\dot{\theta}_2^2 - m_2 r_2 l_1 \cos(\theta_1 - \theta_2)\ddot{\theta}_2 = \\ = (m_1 r_1 + m_2 l_1) g \cos\theta_1 + (I_1 + m_2 l_1^2)\ddot{\theta}_1. \quad \text{(I.3. 39)}$$

Under perfectly static balancing situation $\dot{\theta}_2 = 0$ and $\ddot{\theta}_1 = \ddot{\theta}_2 = 0$, the torques provided by the motors M_1 and M_2 must be null, i.e. $C_{1M} = C_{2M} = 0$, then we can have:

$$F_1 b_1 \cos\theta_1 = (m_1 r_1 + m_2 l_1) g \cos\theta_1. \quad \text{(I.3. 40)}$$

$$F_1 b_1 \cos\theta_1 = \frac{dE_e}{d\theta_1}, \ (m_1 r_1 + m_2 l_1) g \cos\theta_1 = \frac{dE_g}{d\theta_1}. \quad \text{(I.3. 41)}$$

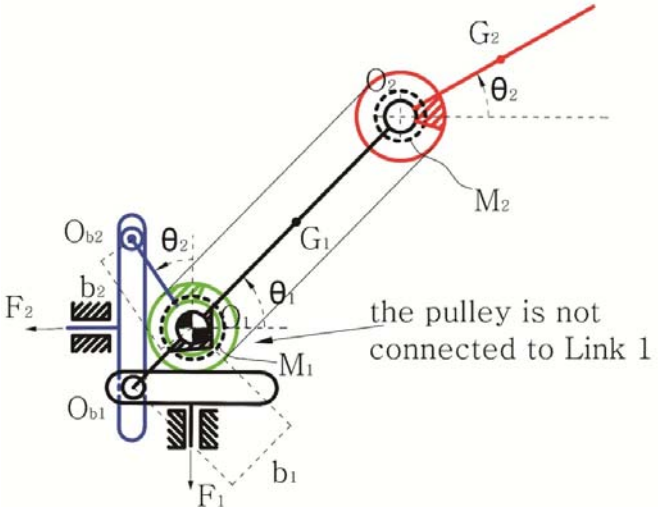

Figure I.3. 28. Balancing device for the two DOF robot.

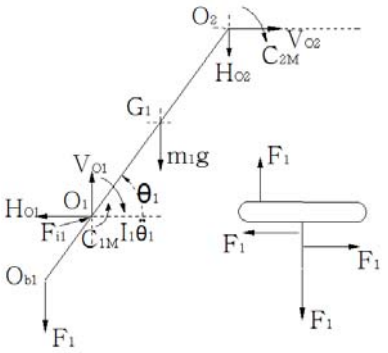

Figure I.3. 29. Free body diagram for Link 1 and the cross mechanism in 2 DOF situation.

For Link 2, Figure I.3. 28 shows a possibility of the balancing device for the second link. The rotation of the link 2 is transferred by means of the cable-pulleys mechanism to the rotation of the link O_1-O_{b2} that is fixed on the lower pulley. The pulley is not connected to the link 1, but has the same rotational axis as Link 1. F_2 is a constant force applied by a spring device. It is known the dynamic description of Link 2,

$$F_2 b_2 \cos\theta_2 + C_{2M} = m_2 g r_2 \cos\theta_2 + I_2 \ddot{\theta}_2. \quad \text{(I.3. 42)}$$

Under perfectly static balancing situation, $C_{2M} = 0$ and $\ddot{\theta}_2 = 0$, then,

$$F_2 b_2 \cos\theta_2 = m_2 g r_2 \cos\theta_2. \quad \text{(I.3. 43)}$$

If we assume that,

$$F_2 b_2 \cos\theta_2 = \frac{dE_e}{d\theta_2}, \quad m_2 g r_2 \cos\theta_2 = \frac{dE_g}{d\theta_2}. \tag{I.3. 44}$$

Then we have,

$$\frac{dE_e}{d\theta_2} d\theta_2 = \frac{dE_g}{d\theta_2} d\theta_2. \tag{I.3. 45}$$

An ideal balancing device is realized if we develop a system that can work according to Eq. (I.3.7). Combining Eq.(I.3.7), Eq.(I.3.38), and Eq.(I.3.41) – (I.3.45), Eq. (I.3. 46) is evolved. In this way, the energy can be transferred between the robot and the balancing system.

$$dE_g = \frac{dE_g}{d\theta_1} \cdot d\theta_1 + \frac{dE_g}{d\theta_2} \cdot d\theta_2 = \frac{dE_e}{d\theta_1} \cdot d\theta_1 + \frac{dE_e}{d\theta_2} \cdot d\theta_2 = F_1 b_1 \cos\theta_1 d\theta_1 + F_2 b_2 \cos\theta_2 d\theta_2 = dE_e. \tag{I.3. 46}$$

Also, there is a screw that fixes the link O_1-O_{b2} to the lower pulley. This solution represents the possibility of adjusting the relative position between the lower pulley and the link, which adapts the system to different positions of the centre of the gravity for Link 2, due to different types of payloads and an end effector on Link 2, as shown in Figure I.3. 31.

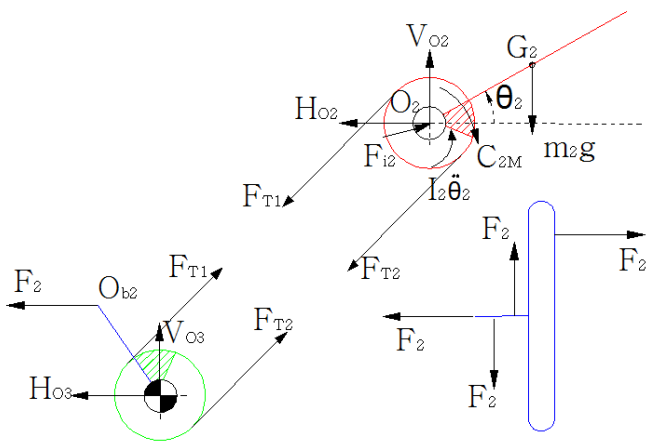

Figure I.3. 30. Free body diagram of two pulleys and a cross mechanism.

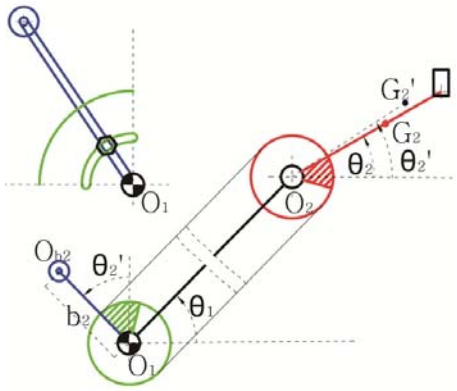

Figure I.3. 31. Little adjustment for the new center of gravity.

I.3.2.2.2. (Hydro-) Pneumatic spring and design of spring parameters

A mechanical spring can be designed to satisfy force and torque requirements. However a mechanical spring with large dimensions takes much space. A pneumatic or hydro-

pneumatic spring with a compact working chamber takes little space and allows much space for the robot. The pneumatic or hydro-pneumatic spring with an auxiliary volume is used to apply almost constant forces.

A pneumatic spring consists of a working chamber and an auxiliary bladder both filled with gas, which works in an adiabatic condition, with negligible friction effects. Figure I.3. 32 illustrates its work principle. Assume P_0 and V_0 are the initial pressure and volume in the spring. P_0 can be controlled to make the system produce the constant force required. It is known that in an adiabatic condition,

$$P_1V_1 = P_0V_0, \quad V_1 = V_{aux} + x_1A_1. \tag{I.3. 47}$$

Here, assume that the volume of the bladder is much bigger than that of the chamber. So,

$$F_1 = P_1A_1 = \frac{P_0V_0}{V_1}A_1 = \frac{P_0V_0}{V_{aux} + x_1A_1}A_1 \approx \frac{P_0V_0}{V_{aux}}A_1 = \text{const.} \tag{I.3. 48}$$

In this way, the pneumatic spring supplies an approximately constant force to support a manipulator. The bladder can be placed far away from the robot, therefore, the robot can have much space for its tasks.

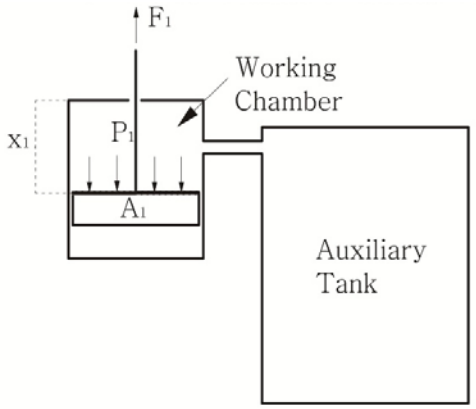

Figure I.3. 32. the pneumatic spring

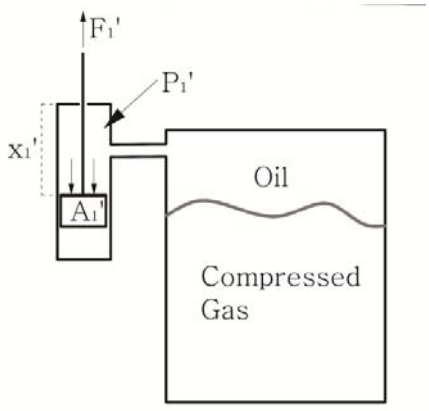

Figure I.3. 33. Hydro-pneumatic spring

A hydro-pneumatic spring can also do the same job. This kind of spring has a bladder as a separation element comprising oil and gas. Since oil can take more pressure than gas, the hydro-pneumatic spring can produce a bigger constant force in a more compact structure with smaller dimensions (Figure I.3. 33), compared with the pneumatic spring. The pressure that the spring can supply can reach up highly to 200 bars. Moreover, the spring allows charging and discharging at a high frequency. Oil is practically incompressible therefore cannot store pressure energy. The compressed gas is utilized in the bladder for storing energy. The oil in the bladder is connected to the hydraulic circuit so that the bladder accumulator can draw or release oil during work.

I.3.3. Discussion and Conclusions

This chapter shows how to design a balancing system for an articulated robot. After the dynamic analysis, the position of the balancing system and the design of spring parameters are discussed. As examples, two variants I and II of an articulated robotic structure are equipped with proper balancing systems. Both links of the robot are balanced by means of different springs and auxiliary devices. For the first structure, numerical examples show the balancing effect when the positions of the springs are different and the springs are provided with constant or variable forces. For a constant-force case, the robot can be approximately statically balanced with low-stiffness mechanical springs or pneumatic springs. For a variable-force case, the perfect balance is realized through the spring design and the torque error only depends on the orientation α_5 (or α_6), regardless of the ratio. Numerical results prove that with the proper design using the methodology presented in this chapter, an articulated robot can be statically balanced perfectly in all configurations. For the second structure, pulley, cable and cross mechanisms, (hydro-) pneumatic springs compose the balancer. Pneumatic, and hydro-pneumatic springs are discussed for torque compensation.

There are pros and cons between the two variants. For the first structure, the robot with a parallelogram has a limited workspace. Motors and the balancing system mounted on the base give the robot more elasticity. For the second structure, the direct drive on joint makes the second link of the robot bulky and increase the mass and inertia. With pulley and cable mechanism, the robot has wider workspace. The load on the end effector is also taken into consideration when the static gravity is balanced.

In 3 DOF robotic structures, the third degree of freedom which axis is parallel to the gravity vector need not to be considered in the robotic static balance. Therefore, the static balance of spatial industrial robots in this situation is also included in this part.

According to the methodology presented in this chapter, articulated robots can be perfectly statically balanced in all configurations. This chapter shows a feasible way to design balancing devices and define their parameters based on considerations of practical requirements. This chapter tries to provide a design method of the balancing system for other similar structures. Future work should focus on articulated robots with multi-degrees of freedom. Also robotic structures with prismatic pairs should be discussed as an extended application of the methodology shown in this part.

References

[1] Tsai, L. W Robot Analysis: The mechanics of Serial and Parallel Manipulators, Wiley-Intersecience Publication, John Wiley and Sons, 1999.

[2] Giuseppe Quaglia, Zhe Yin. Optimization of static balancing for an anthropomorphic robot. Proceedings of the 3rd IFToMM International Symposium on Robotics and Mechatronics, Singapore, October, 2013.

[3] Giuseppe Quaglia, Zhe Yin. A Balancing Mechanism for An Anthropomorphic Robot. Advanced Materials Research Vols. 774-776 (2013) pp. 1397-1403.

Section I.4 Discussion about Space Distribution of Balancing Systems

Nomenclature:

m_i	kg	the mass of Link i
D	m	the spring diameter
d	m	the diameter of spring wire.
I	--	the spring index, I = D/d
n	--	the number of spring coils
L	m	the length of an extensive spring
L_i	m	the length of the spring in natural status, when no force applies on it
a_i	m	the distance between the connecting link end O_{bi} and its according fixed revolute joint.
m	m	the part distance between the fixed joint O_5 and one eng of the spring in its natural status.
n	--	the number of spring coils.
G	Pa	Young modulus in torsion
Δ	m	the spring elongation, L- L_i
θ_i	rad	angle between Link i and the horizontal plane
l_i	m	length of a part of Link i
k_i	N/m	the stiffness of the balancing spring for Link i
r_i	m	the distance between the two points
b_i	m	the length of the connecting link O_1-O_{bi}.
ra_1	--	the ratio r_5/b_1.
ra_3	--	the ratio b_1/r_1.
S	Pa	the tensile strength, a property of spring material
S_i	Pa	the initial tension, associated with the spring index I
F_1	N	the force applied by the balancing spring for Link 1
F_{1i}	N	the initial force in the spring, matched with S_i
γ	rad	the motion range of the spring during work
g	m/ s^2	the gravity acceleration

In the Section I.3, the design of the balancing system is discussed in details. To realize the perfect balance, the balancing system is designed to provide the proper torque according to the torque requirement from the serial manipulators. As we know, mechanical spring properties are normally decided by the spring material, the diameter (D), the number of coils (n), the spring wire size (d), etc. Also, in many cases, a spring needs to have a preload and an initial length to realize the required force. Many works focusing on the design of balancers neglect this kind of issues about the spring design. They normally introduce the 'zero-free length' spring when they talk about the balancer consisting of springs ([1]-[5]). In several cases, when manipulators require the balancing

spring to provide much balancing torque or force, the spring that can do this job normally has to be designed with huge spring diameter and long initial length. This results in the balancing system becoming bulky and physically unrealized. Especially for complex manipulator structures, the practical balancing system and layout have the potential possibility to interfere with the work of the balanced manipulator. Take the first structure we studied in the Section I. 3 as an example, it has a parallelogram structure and the two connecting linkages for the introduction of the balancers. If the balancing spring takes much space with a long initial length or many spring coils or a large spring diameter, it would make the balancing system bulky and even interrupt the manipulator tasks. So problems about how to design the spring balancer with a compact volume and satisfied functions are worth paying attention.

This chapter focuses on the discussion of the practical spring design and layout in space. Since the first structure is more complicated than the second model we studied in the Section I. 3, it is more necessary to discuss the spring distribution around the manipulator. Conclusions for the first structure are also helpful for the second model. In the first structure, the balancing mechanism for the Link 1 and Link 2 is designed based on the same principle and approach. Therefore, we only discuss the spring design details about the first link. The way to choose a spring for a compact design discussed in this chapter is also effective for the balancer layout of the second link.

I.4.1 Problem Proposal

For a mechanical spring design, we normally would like it to produce the proper force with a compact structure. In this balancing system, the spring is used to provide the proper force for the torque compensation. The amount of the torque should be balanced is decided by the manipulator linkage. To balance it, we can design the spring to produce heavy force which requires large volume with big spring diameter D and thick wire size d. Alternatively, if the spring is made with a long initial length and a big number of spring coils, this solution also takes much volume. In applications, it also needs to consider the spring material, the cost problem and so on. Among these aspects, a compromised solution is finally put into practice. Especially in this spring design for the first link, there are many factors that influence the spring design. Except these parameters mentioned above, we can also change the ratios ra_1 and ra_3 (therefore r_5 and b_1 in Figure I.4. 1 and Figure I.4. 2) to control the arm of the compensated torque. If the arm becomes long, light force is enough to realize the required torque and vice versa. However, if the connecting link b_1 is kept long or r_5 is designed long, the whole balancing system becomes heavy and bulky. Here, we try to comprehensively consider all factors, the ratios ra_1, ra_3 and the physical parameters of the spring, to arrange the balancer matched with the serial manipulator in a compact way. There are many solutions using various springs. The extension spring with preload in it will be applied for the spring design in this chapter.

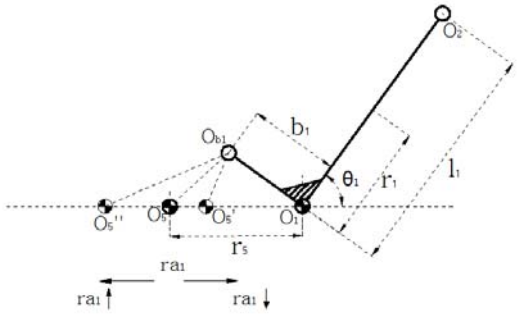

Figure I.4. 1. The balancer layout when ratio ra_1 changes

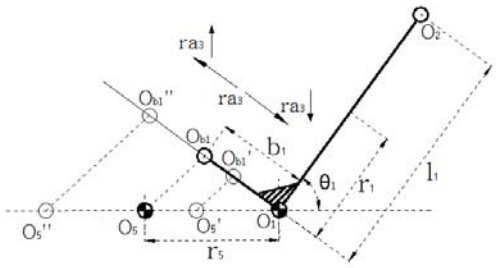

Figure I.4. 2. The balancer layout when the ratio ra_3 changes

According to the conclusion in the Section I. 3, when a mechanical spring produces a variable force, which value is dependent on the spring elongation, the perfect balance is realized at the position where $\alpha_5 = \pi/2$ (Figure I.4. 3). The balance effect is not dependent on the ratio ra_1.

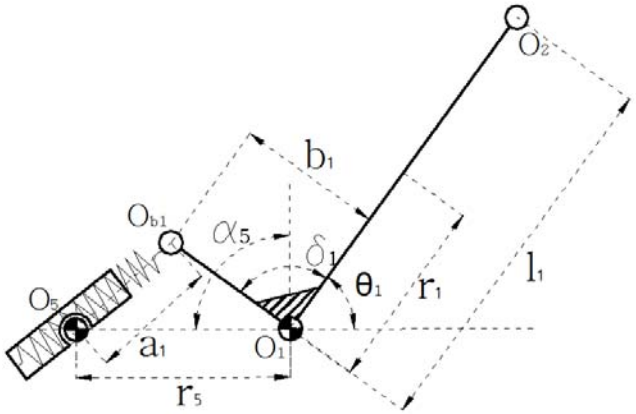

Figure I.4. 3. The perfect balance for the first link

But ra_1 value can influence the moment arm and therefore the force value provided by the spring. When ra_1 is more or less than 1, Table I.4. 1 shows the positions between the spring and the first linkage at three configurations. It is possible to adjust the ratio and choose the proper ratio for spring distribution. For large value of ratio, it means the fixed revolute joint O_5 for the spring is far away from the fixed revolute joint O_1. This layout makes the whole mechanism big. Especially when the length O_1-O_5 is bigger than the length of Link 1, the manipulator is too bulky and should be avoided. On the other hand, if the ratio is too small, this can make the manipulator compact. But in this case, the spring has to provide much force change during the working range, which makes the spring has a very big value of the spring diameter or practically unrealized.

Table I.4. 1. The balancer layout when ra_1 and configurations are different:
$\theta_1 = 0$, $\theta_1 = \pi/2$, $\theta_1 = -\pi/2$

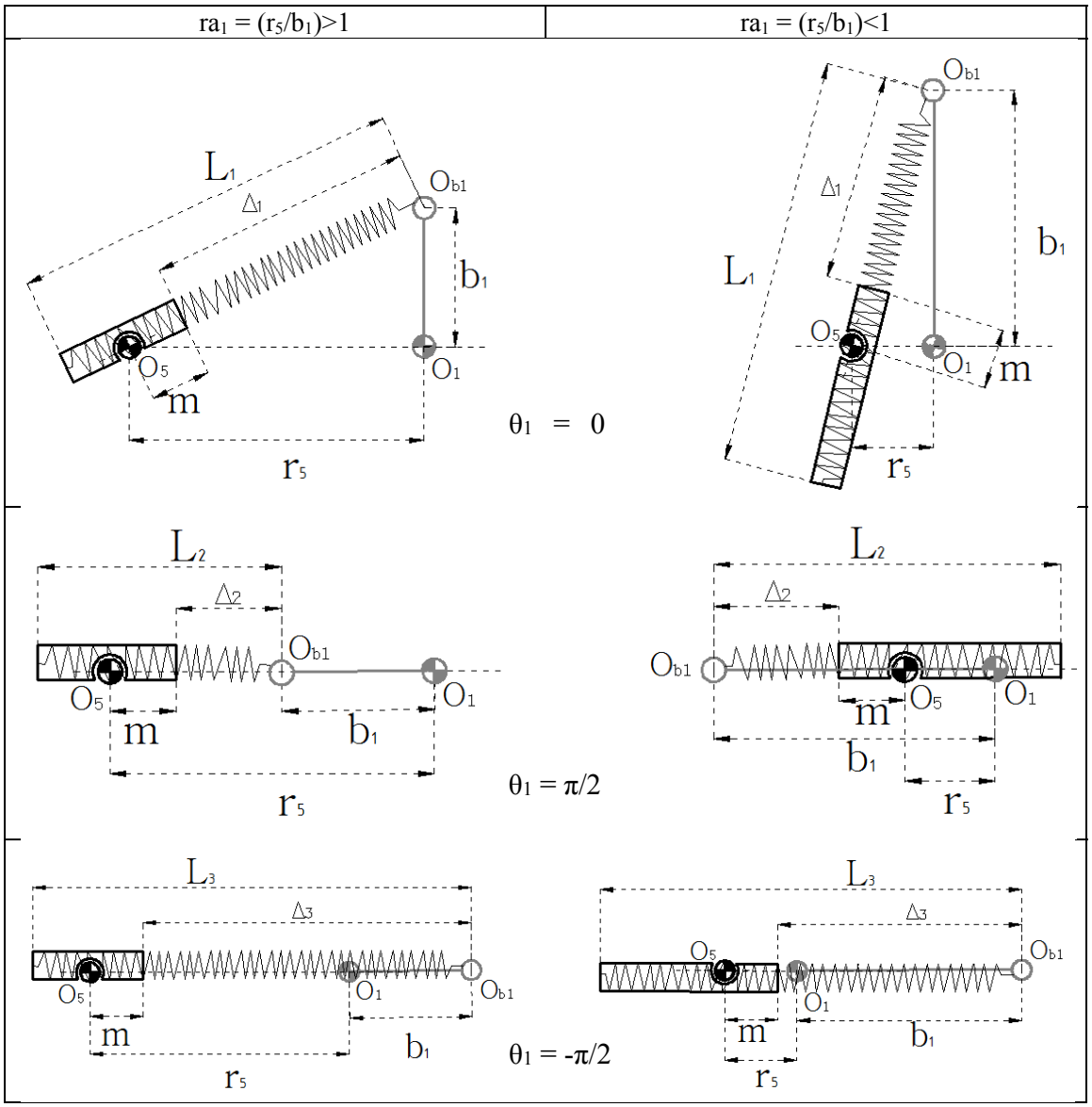

The relation between L, Δ and a_1 (the distance between O_5 and O_{b1}) is shown in Figure I.4. 4. The motion range is assumed as $(-\pi/2, \pi/2)$, the same as that in the Section I. 3. Here, it is marked as black line part in Figure I.4. 4, between Δ_2 and Δ_3. From the Section I. 3, it is known that,

$$a_{10} = \sqrt{r_5^2 + b_1^2} \qquad \text{(I.4. 1)}$$

a_{10} means the length between O_5 and O_{b1} when the manipulator is at the first configuration, $\theta_1 = 0$ (Table I.4. 1). According to the conclusion from the Section I. 3, it

is the configuration when F_{1FO} ($=\frac{C_{1max}}{b_{1F(\theta_1=0)}}$) is produced by the spring. Based on F_{1FO} and a_{10}, we can arrange the spring to follow this equation we obtained in the previous chapter,

$$F_{1FK} = F_{1FO} + k_1 \cdot (a_1 - a_{10}) \quad \text{(I.4. 2)}$$

When the configurations are $\theta_1 = \pi/2$ and $\theta_1 = -\pi/2$, F_{1min} and F_{1max} are known as:

$$F_{1min} = F_{1FO} + k_1 \cdot (|r_5 - b_1| - a_{10}) \quad \text{(I.4. 3)}$$

$$F_{1max} = F_{1FO} + k_1 \cdot (r_5 + b_1 - a_{10}) \quad \text{(I.4. 4)}$$

Where $k_1 = C_{1max}/(r_5 b_1)$, as we already obtained in Section I. 3.

F_{1i} in Figure I.4. 4 is the initial force in the spring when it is at its natural length situation. For an extension spring, it can absorb and store energy by offering resistance to a pulling force. The initial force is the built-in load to hold spring coils tightly together.

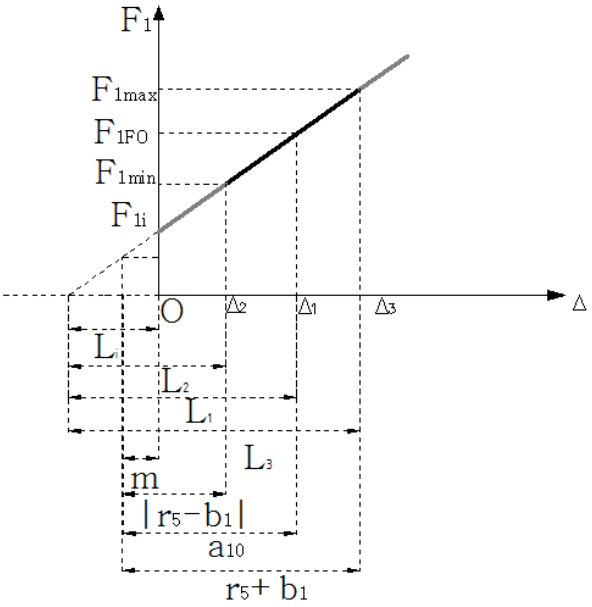

Figure I.4. 4. The relation among length calibration

I.4.2 Methodology

To design such a mechanical extension spring satisfying the requirements in Figure I.4. 4, a solution is proposed ([6][7]). An extension spring is normally designed within the torsional proportional limit of the material, about 40-45 percent of the minimum tensile strength of the material. Once the spring material is chosen, its minimum tensile strength is fixed. Given a certain volume of spring in which the spring will act and a certain

maximum load, the design approach is firstly to find a wire size based on a spring index (I) and a reasonable stress (S):

$$d = \sqrt{\frac{8F_{1max} I}{\pi \cdot S}} \qquad \text{(I.4. 5)}$$

Once d is fixed, D can be obtained by the spring index I. Since the stiffness is already known from the analysis of Section I. 3, the number of the spring coils n and the initial force F_{1i} are therefore evolved as:

$$n_a = \frac{G \cdot d^4}{8k_1 \cdot D^3} \qquad \text{(I.4. 6)}$$

Where G is Young modulus in torsion. k_1 is the stiffness of the first balancing spring. n is an integer, which value is not less than n_a.

$$F_{1i} = \frac{\pi \cdot S_i \cdot d^3}{8D} \qquad \text{(I.4. 7)}$$

Where S_i is the initial tension, it can be obtained from the spring index (Figure I.4. 5). Also S_i can be calculated by the empirical formula for computer programming purposes:

$$S_i = \frac{231}{e^{0.105 \cdot I}} \text{or} \frac{231}{10^{0.0456 \cdot I}} \qquad \text{(I.4. 8)}$$

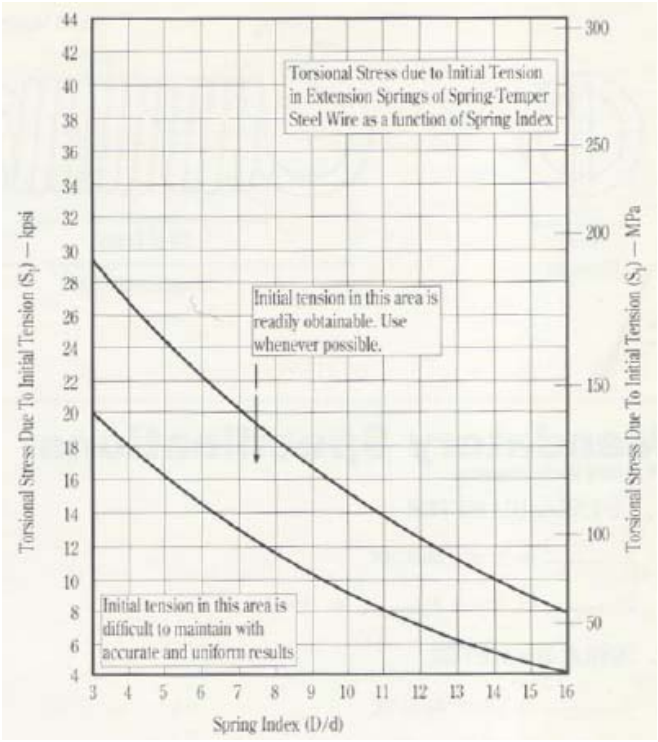

Figure I.4. 5. The relation between the initial tension S_i and the spring index I [7]

Then, we can have the initial length L_i as,

$$L_i = (n + 1 \sim 2) \cdot d \qquad \text{(I.4. 9)}$$

Considering the length of spring ends attaching the spring to the manipulator, L_i is normally set longer than the result of spring coils n multiplying the wire size d.

Finally, after the design of the spring, we can obtain the elongation Δ at every configuration. For example, when $\theta_1 = \pi/2$ (in Table I.4. 1), the elongation Δ_2 can be calculated by the equation (I.4.3), then with the structure dimensions r_5, b_1, the part distance m between the fixed joint O_5 and one end of the spring can be calculated to mount the spring in a correct position.

I.4.3 Numerical examples

Here presents examples to show the spring dimensions, such as D, d, L_i, and its position with respect to the manipulator in space (controlled by the ratios ra_1 and ra_3). This is meaningful for the realization of the perfect balance in a compact way. Assuming a tensile strength of 1500 MPa for oil-tempered wire, the trial design stress is 45 % of the tensile strength. Table I.4. 2 lists the physical parameters in the example.

Table I.4. 2. Physical parameters of the system

Physical parameters	l_1	r_1	b_1	ra_3	m_1	m_2	θ_1
values	1.2	0.6	0.2	1/3	100	40	$(-\pi/2, \pi/2)$

Figure I.4. 6 -Figure I.4. 12 show results about the wire size (d), the spring diameter (D), the number of spring coils (n), the initial length (L_{1i}), the initial force (F_{1i}), the stroke and the stroke rate. The stroke is the error between the maximum elongation and the initial length (L_{1max} - L_{1i}). The stroke rate (or maximum elongation rate) is the ratio of the stroke and the initial length. For a compact layout for the balancing system, we can choose higher I, which means shorter initial length and lighter initial force, but bigger spring diameter and the stroke rate. The situation is converse when we choose lower I. From Figure I.4. 11 and Figure I.4. 12, it is realized when I changes, the stroke replies insensitive, while the stroke rate responds dramatically, varying from around 33% to around 78%. Also, it seems that the stroke rate is unchanged when ra_1 varies, shown from Figure I.4. 11. It is the result when we define the wire size (d) decided by the maximum force F_{1max}, since the stroke is the maximum elongation when F_{1max} is applied. In detail,

$$\frac{\Delta_3}{L_i} = \frac{F_{1max} - F_{1i}}{L_i \cdot k_1} \tag{I.4. 10}$$

L_i is the initial length from the equation (I.4. 9). To investigate the relation between the stroke rate and the spring index, we replace L_i with n_a*d ideally. From the equation (I.4. 5), we have:

$$F_{1max} = \frac{\pi d^3}{8D} S \tag{I.4. 11}$$

Considering the equations (I.4. 6), (I.4. 7) and (I.4. 8), the equation (I.4. 10) is evolved as:

$$\frac{\Delta_3}{L_i} = \frac{1}{\frac{G \cdot d^4}{8k_1 \cdot D^3} \cdot d \cdot k_1} \cdot \frac{\pi \cdot d^3}{8D}(S - S_i) = \frac{\pi}{G} \cdot I^2 \cdot (S - S_i) = \frac{\pi}{G} \cdot I^2 \cdot (S - \frac{231}{10^{0.0456 \cdot I}}) \tag{I.4. 12}$$

So the stroke rate is only dependent on I. Since we use L_i in the equation (I.4. 9) for the spring design and the computer program, the stroke rate does not show strictly straight lines in Figure I.4. 11.

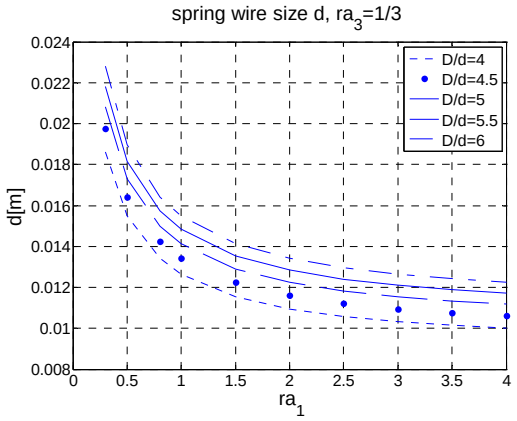

Figure I.4. 6. The changes of the wire size when I and ra_1 vary

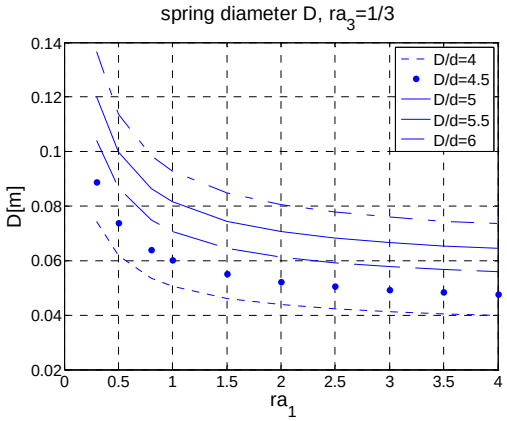

Figure I.4. 7. The changes of the spring diameter when I and ra_1 vary

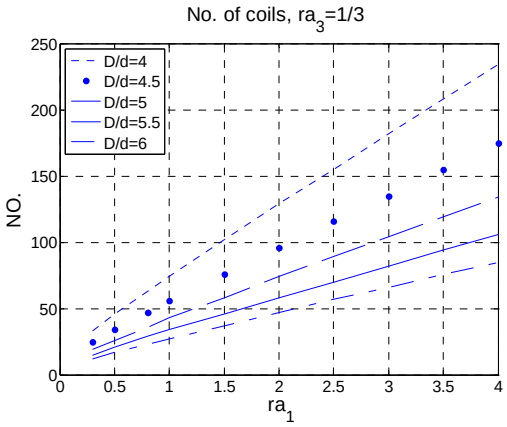

Figure I.4. 8. The number of spring coils when I and ra_1 vary

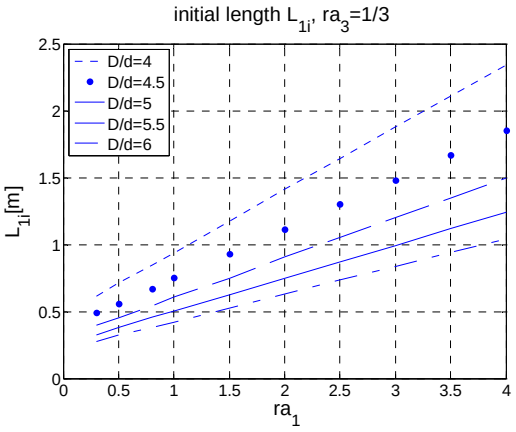

Figure I.4. 9. The initial lengths when I and ra_1 vary

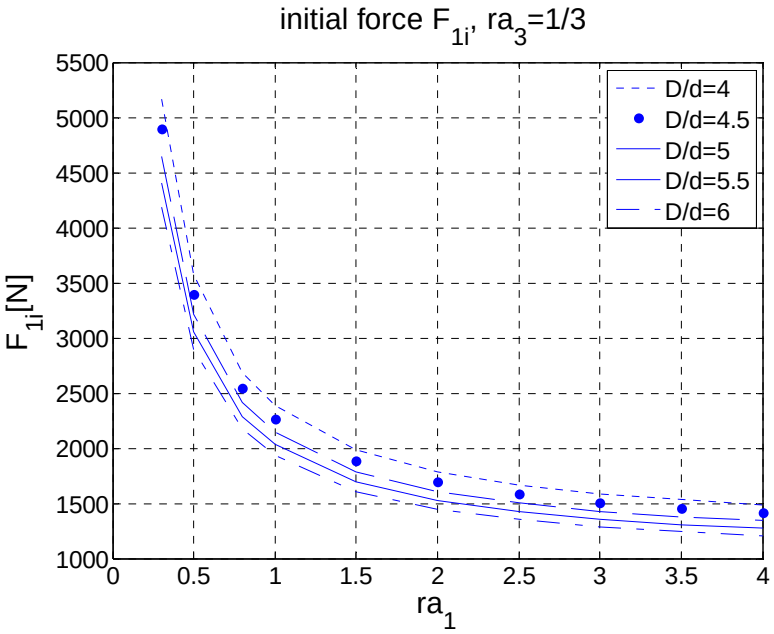

Figure I.4. 10. The initial forces when I and ra_1 vary

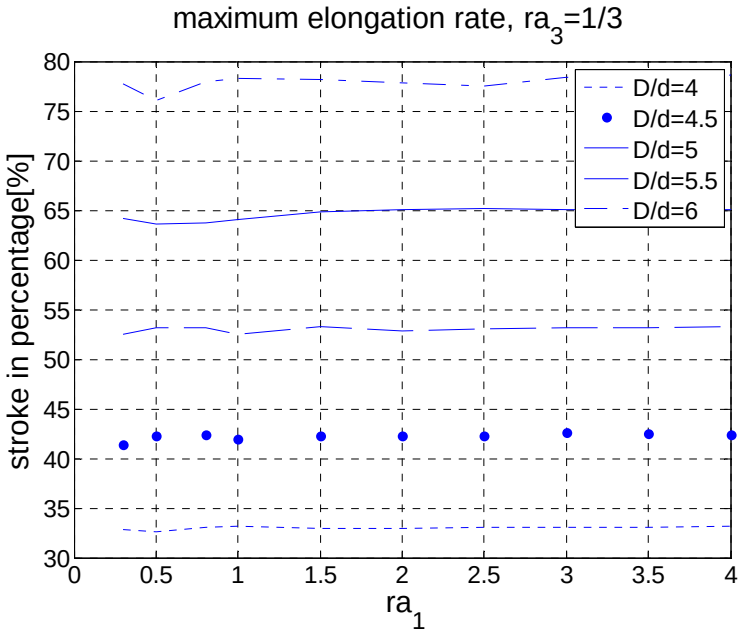

Figure I.4. 11. The maximum elongation rate under different I and ra_1

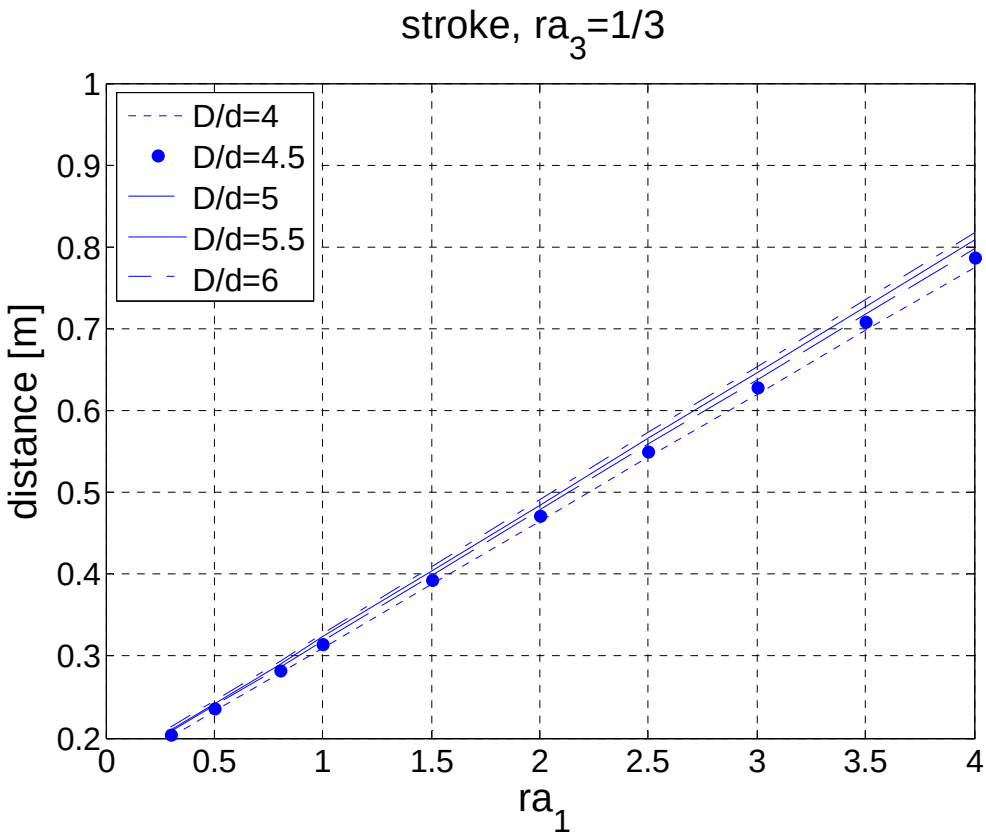

Figure I.4. 12. The spring stroke when I and ra_1 vary

When ra_3 changes, we can find different results from Figure I.4. 13 to Figure I.4. 16.

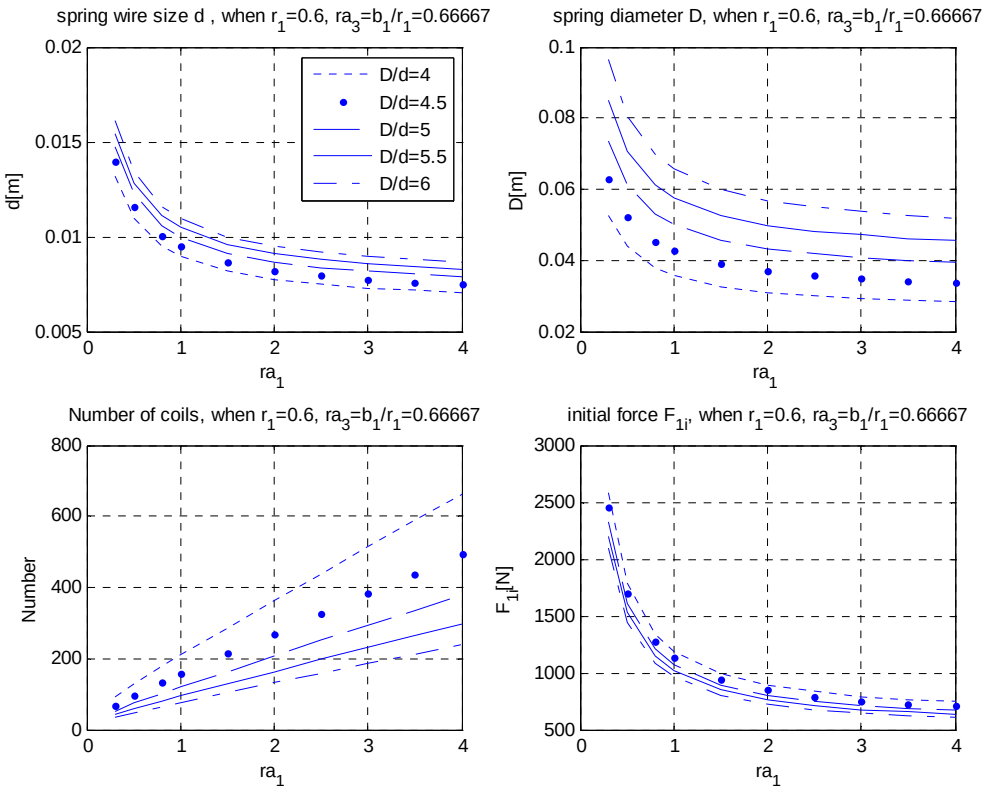

Figure I.4. 13. Spring properties d, D, n, F_{1i}, when $ra_3 = 2/3$

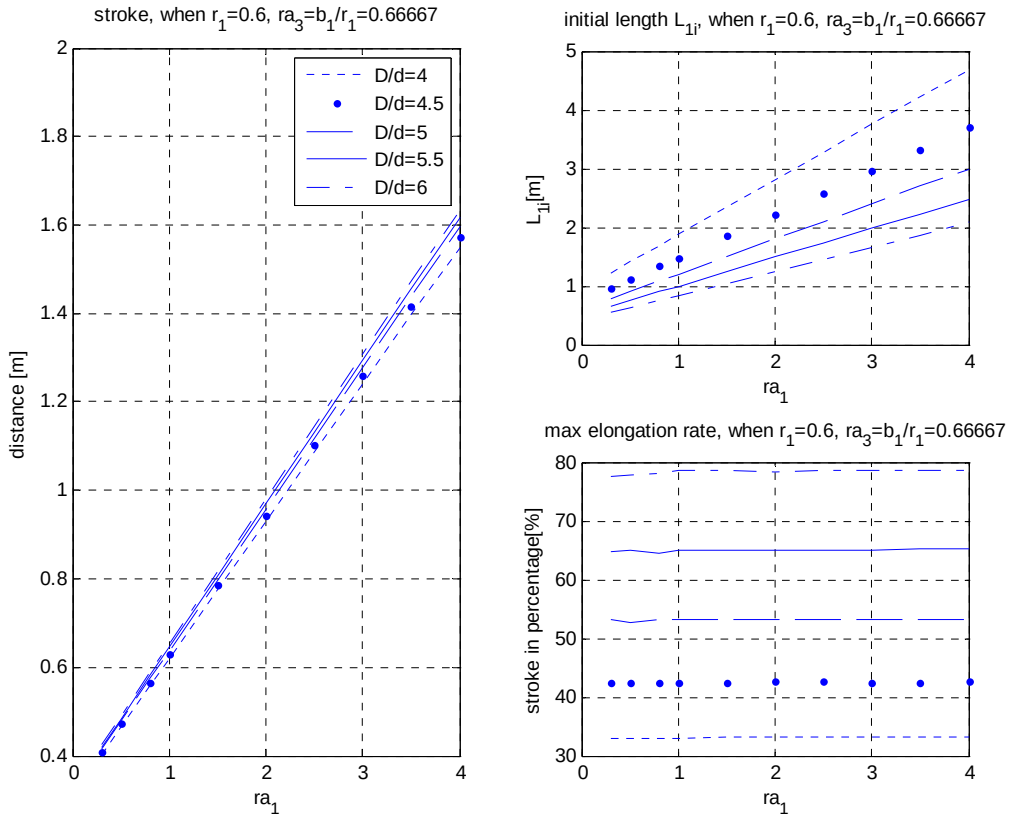

Figure I.4. 14. Spring properties L_{1i}, stroke and stroke rate when $ra_3 = 2/3$

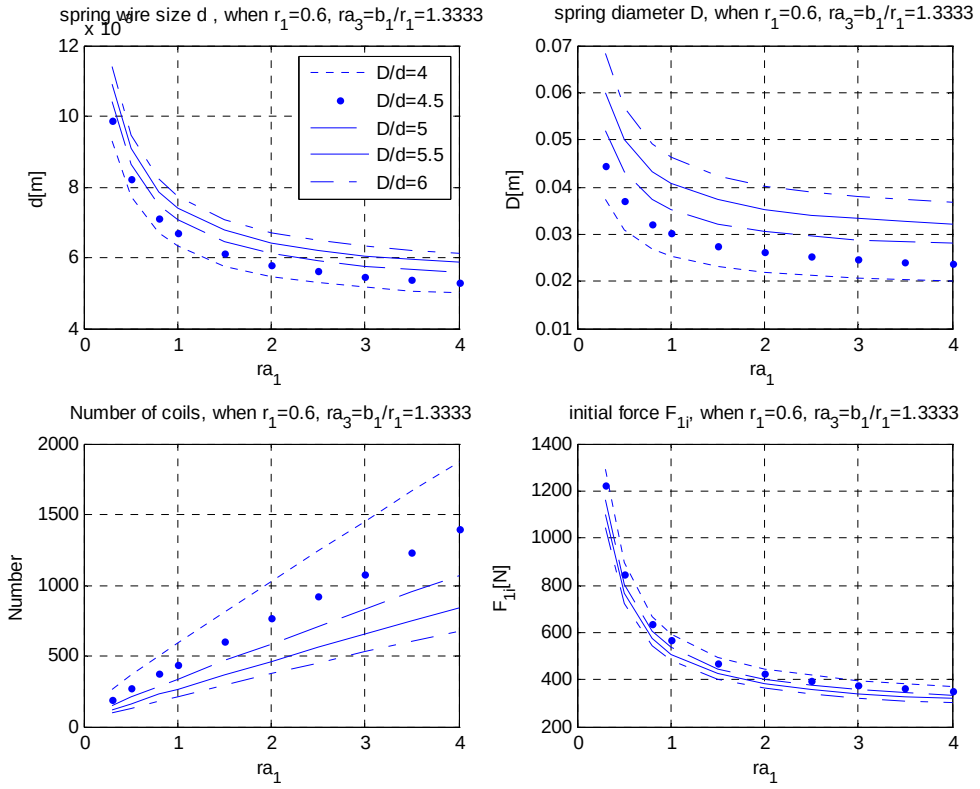

Figure I.4. 15. Spring properties d, D, n, F_{1i}, when $ra_3 = 4/3$

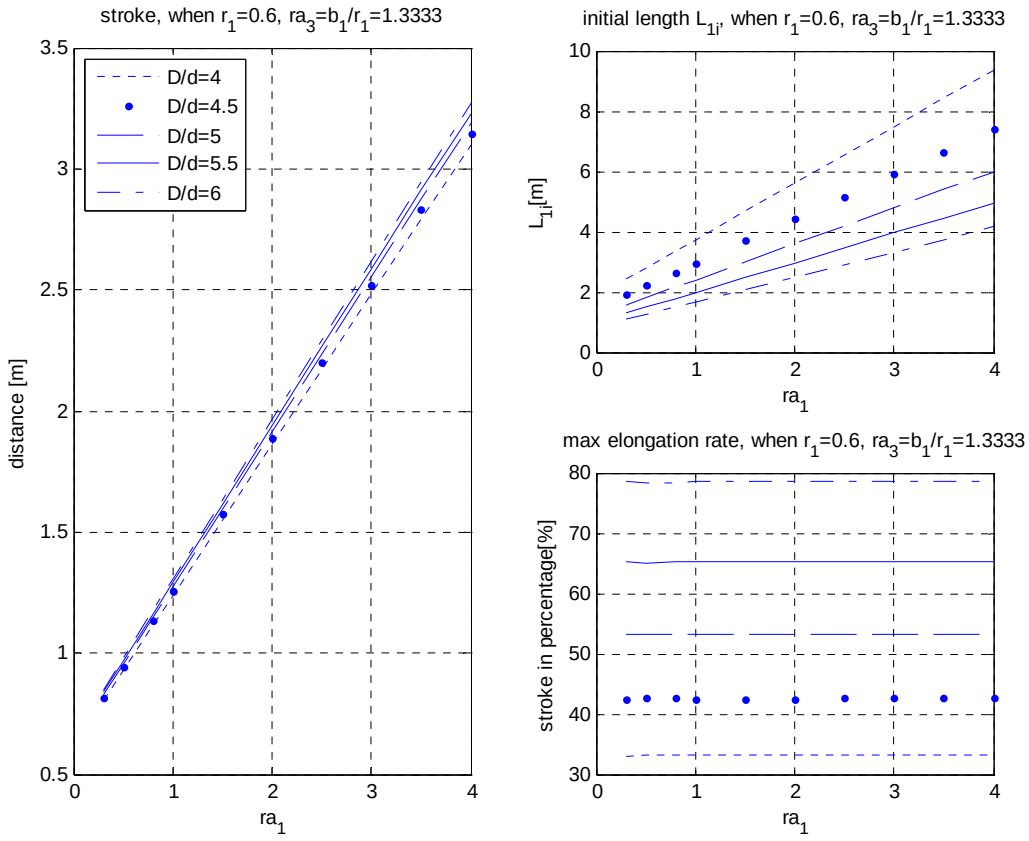

Figure I.4. 16. Spring properties L_{1i}, stroke and stroke rate when $ra_3 = 4/3$

When ra_3 (or b_1) increases, the torque should be balanced by the spring decreases. In this situation, spring wire size d, diameter D and required initial force F_{1i} decrease, but spring coil number n, the stroke and the initial length L_{1i} increase. The stroke rate keeps invariant.

With the spring wire size, diameter, number of coils and its initial length, we can estimate the spring volume in space. The length m (Table I.4. 1) can be also calculated using equations in this chapter and therefore the position of the spring is fixed. This could provide with a clear distribution between the spring and the manipulator and be useful for the balancer designer. For a compact assembly, design factors, such as the ratios (ra_1, ra_3), the spring volume and the length m, should be compromised out of an integrated consideration.

Stress in extension spring ends is not mentioned here, since this chapter focuses on the spring distribution in space. However, stress in the ends is significant for a spring design, since stress is normally higher in spring ends than in the spring body. It could be a meaningful future work to do.

I.4.4 Considerations about the Motion Range of the Balancing Spring

Notice that when ra_1 is more than 1 or less than 1, the motion range γ of the spring is different, as shown in Figure I.4. 17 and Figure I.4. 18. When θ_1 moves between $-\pi/2$ and $\pi/2$, we have: $\gamma_1 < \gamma_2$. In this situation, the first case ($ra_1>1$) is more feasible than the second one since the spring in the first case has a narrower sway than the spring in the second case.

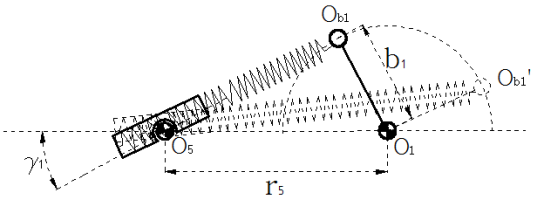

Figure I.4. 17. The motion range γ_1 of the spring, when $ra_1>1$, $-\pi/2<\theta_1<\pi/2$

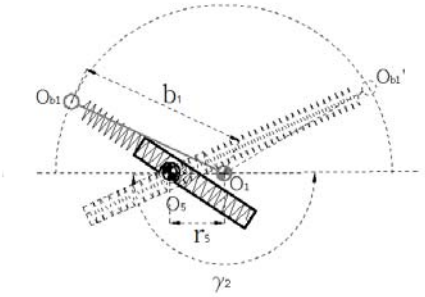

Figure I.4. 18. The motion range γ_2 of the spring, when $ra_1<1$, $-\pi/2<\theta_1<\pi/2$

References:

[1] Sunil. A, Abbas F. Gravity-balancing of Classes of Industrial robots, Proceedings of the IEEE International Conference on Robotics and Automation, May, 2006.

[2] Sunil Agrawal, Abbas Fattah. Gravity-balancing of spatial robotic manipulators. Mech. Mach. Theory. Vol 39, pp. 1331-1344, 2004.

[3] Streit D.A., Gilmore B.J., Perfect Spring Equilibrators for Rotatable Bodies. ASME Journal of Mechanisms, Transmissions, and Automation in Design, Dec, Vol. 111, pp. 451-458, 1989.

[4] T. Wongratanaphisan, Matthew O. Cole. Analysis of a Gravity Compensated Four-bar Linkage Mechanism with Linear Spring Suspension. Journal of Mechanical Design, Jan,2008, Vol. 130, 011006.1-8.

[5] R. Rizk, S. Krut, E. Dombre. Design of a 3D Gravity Balanced Orthosis for Upper Limb, IEEE International Conference on Robotics and Automation, May 19-23, 2008.

[6] Hain, K. 'Force Analysis', 'Spring Mechanism-Point Balancing' and 'Spring Mechanisms-Continuous Balancing', Spring Design and Application, Chironis N. P., McGraw- Hill, New York, 1961, pp. 268-275.

[7] http://www.scribd.com/doc/29044778/Spring-Design-Handbook#outer.

Section I.5 Conclusions of Section I

Section I discusses the design of the balancing systems for the two serial robotic devices. The two robotic structures with 2 DOF are presented. Their kinematic and dynamic characters are studied and simulated with the tools Simulink/Matlab and SimMechanics /Matlab. In the Simulink module, the kinematic and dynamic relation is collected in the matrix form, the simulation results are obtained through solving the matrix equation. In the SimMechanics method, the model is dealt with the module blocks. The two methods have a compared study about the two structures. Based on the motion study, the balancing systems for the both structures are proposed.

In details, the energy transfer principle is illustrated. Based on it, two variants I and II of an articulated robotic structure are equipped with proper balancing systems. Both links of the robot are balanced by means of different springs and auxiliary devices. For the first structure, the design details provide the designer a tool to decide balance accuracy. Approximate and perfect balance are both considered. Numerical examples show the balancing effect. For a constant-force case, the robot can be approximately statically balanced with low-stiffness mechanical springs or pneumatic springs. For a variable-force case, the perfect balance is realized through the spring design. For the second structure, pulley, cable and cross mechanisms, (hydro-) pneumatic springs compose the balancer. The perfect balance can be realized using a constant force generation device.

As a feasible consideration, the spring volume and the influence factors are discussed. The pros and cons between the two variants are presented. According to the methodology presented in this section, articulated robots can be perfectly statically balanced in all configurations.

Section II Rehabilitation Device Using Parallel Wire Robotic Structure

Section II presents a rehabilitation robotics for the human ankle. The robotic device has a parallel structure with wires connecting the fixed and moving platforms. It is designed for the ankle performance and the strength of muscles around the ankle.

There are many devices presented by researchers focusing on the rehabilitation of the ankle joint. Currently, there are two kinds of devices applied for clinic applications: wearable devices and platform based devices. Wearable devices can be installed on the patient lower extremity for gait training and ankle function strength. Platform based devices, on the other hand, is placed under the foot. The patient foot is normally fixed on the moving platform (as a pedal) of the device. This kind of device is applied for the ankle performances. There are advantages and disadvantages for the both kinds of devices.

However, for the most devices, there are some drawbacks should be improved and solved as primary design considerations. One of them is that many rehabilitation devices has the bulky volume. Many devices have attachments, such as sensors, the control system, power sources, etc. These inevitable auxiliary components increase the cost, are normally distributed around the patient ankle and considered as a burden when a patient executes trainings. Moreover, some devices using linkages as parts add more weight on the lower extremity. To improve the disadvantages, the device proposed in this section is a wire robot and therefore has a light weight and a compact volume. The application of Bowden Cable allows to transfer the actuation system far away from the patient, therefore can make the device more suitable for use. As a proposal in this section, the actuation system is worn by the patient. The application of brackets distributes the load universally on the whole lower extremity and make the patient feel comfortable. The wire structure also decreases the cost.

Versatile functions are also considered here. The device proposed here can be not only applied for gait function, but also treated as the muscle strength and ankle performance tool. The proposal is a wearable device and its ergonomics is also stressed. The wire structure with the Bowden Cable makes the device easy donning on and off. Once the system fails to work, the patient can take off the device quickly and make sure the body safety.

As we know, the ankle has a complex motion with three rotational degrees of freedom: dorsiflexion/plantar flexion, eversion/inversion, and adduction/abduction. Like many wearable devices, the proposed device only makes the first two degrees of freedom under control. The adduction/abduction rotation can be added if the device cooperates with a platform based device.

The organization of this section is scheduled in this way:

In Section II.1, the state of the art for the rehabilitation device is studied, two kinds of devices, many platform based devices and wearable devices are graphically shown.

In Section II.2, the biomechanical properties of the ankle are discussed. For the human ankle, the range of motion and torques driving the motion are various and depending on different subjects with different ages and sex. The control system and sensors are also mentioned here.

In Section II.3, a rehabilitation device is proposed based on the ankle properties and training requirements. An ideal model of the proposed device is shown for its kinematic and dynamic analysis. Forward and inverse kinematic equations are built and several numerical examples are shown to verify the simulation of the kinematic model. For the dynamic description, quasi-static equation is described.

In Section II.4, conclusions are highlighted and some future work are shown.

Section II.1 An Investigation on Ankle Rehabilitation Robot

Ankle injury is common among sports' people and paralytics. Ankle injuries are normally also occurred when people have excessive load, over-running, or walking on uneven surfaces, or suffer disease of the nervous system [1]. Insufficient strength, flexibility, and proprioception are the main cause of ankle injury [2]. For patients' recovery, medical facts show medicine and physiotherapy are both important. Physiotherapy is a training skill using rehabilitation devices, mainly referring to motion therapy and muscle strength. Nowadays, rehabilitation devices are becoming popular in the ankle rehabilitation since their effectiveness [3].

There are many mechanisms applied for ankle rehabilitation ([1]-[6]). Generally speaking, seven kinds of devices are using in clinics [1]: elastic bands [4], foam rollers [5], wobble boards [6], ankle rehabilitation pumps, spring-rail rock device, stability systems (such as electronic wobble board, the Bio balance system), and the multi-joint systems. These devices can be classified to four categories, but all mentioned here show two extreme products [1]: one end having less functionalities and the other having a complex and heavy system. Also they cannot provide the passive training for the ankle physiotherapy. They further lack quantitative diagnostic and networking capabilities that would allow therapists to remotely monitor patient's progress. These devices are rarely interactive, making the rehabilitation training repetitive and boring [2]. Based on the drawbacks mentioned above, it is necessary to develop a robot-assisted therapy on ankle rehabilitation. Ankle rehabilitation by means of robotic devices can have some advantages: to release therapists from a tedious and repetitive task, to do controlled ankle training with the accuracy of a closed loop controlled device, to monitor displacements, forces, torques and electromiographic signals for an objective improvement evaluation, to let the patient autonomously carry out the therapy at home, avoiding difficult displacements, to decrease the therapy costs. There are two main kinds of robots widely used, focusing on ankle performance and gait function [3]. The first kind of the device 'platform based ankle rehabilitation robot' is mainly relative with the pedal supported by a parallel robot. A parallel robotics has a fixed and a moving platform with several legs' support between them. The moving platform with several degrees of freedom (DOFs) plays a pedal attached with the patient foot. Ankle performance is trained and controlled by the moving platform. The other kind of the device 'wearable ankle rehabilitation robot' is mounted on the patient leg and foot, mainly consisting of linkages to drive the gait training.

II.1.1 Platform based ankle rehabilitation robot

There are many research groups and work focusing on the development of the platform based robot ([1]-[10]). 'Rutgers Ankle' is a rehabilitation system (Figure II.1. 1) proposed by Girone et al. ([2], [7]-[11]), consisting of a Stewart-robot [12] haptic interface, a host computer, and pneumatic control valves. This system allows patient to perform not only active but also passive activities. For passive activities in the patient term of view, the system plays an active role. The host computer provides a variety of exercises, interacts

with the patient in a virtual environment, controls the movement and the output forces of the robot. For active activities, when the patient tries to move, the system can perform diagnostic functions, measure the ankle's range of motion, force exertion capabilities and coordination. After recording the information, the computer sends it to therapists for a remote evaluation, through a tele-rehabilitation system [13]. Therefore, the rehabilitation robot can be developed for home use by patients. The Stewart robot can provide six DOFs with resistive forces and torques, as shown in Figure II.1. 2. Its moving platform is a haptic interface to take the patient foot. The robot has double-acting pneumatic cylinders between the both platforms. On the robot, there are linear potentiometers as position and force sensors. Valve controllers, signal conditioning electronics are also equipped with the system.

It has been tested successfully in orthopaedic rehabilitation, post-stroke rehabilitation, and rehabilitation of muscular-skeletal injuries. The host computer has a rehabilitation library with many rehabilitation simulation programs in it. Nevertheless the Stewart platform has certain disadvantages, particularly it is redundant for this application, since the ankle has fewer degrees of freedom than six DOFs and consequently there is high complexity and costs. Moreover the pneumatic actuators used are noisy.

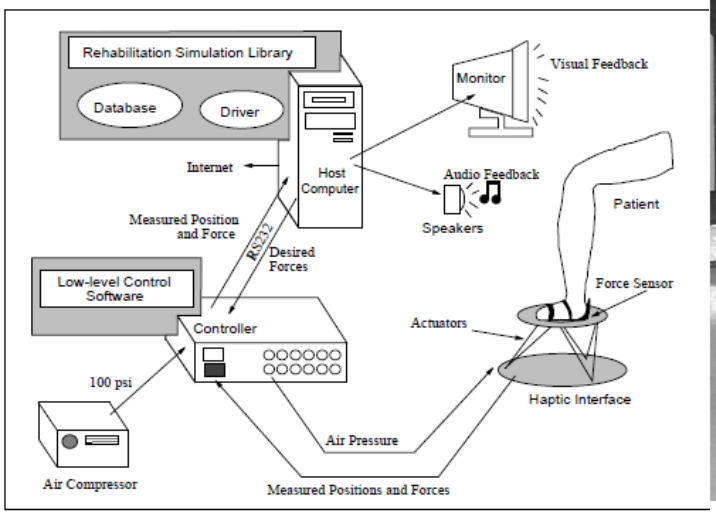

Figure II.1. 1. The 'Rutgers Ankle' Orthopedic Rehabilitation System[2]

Figure II.1. 2. the Stewart platform component for the 'Rutgers Ankle' rehabilitation device[2]

Deutsch et al. focus on the case study and verify the effectiveness of the 'Rutgers Ankle' system ([14]-[17]). Gait speed increased 11% and elevation time decreased 14%. Compared with the situation before the training, the gait and elevation speed improved from 0 to 44% and 3 to 33% respectively. The gait endurance also increased 11%. For study cases, the data such as ankle position, forces, and mechanical work during an exercise, the number of loops completed and the time it took to do that are stored online. A case study was presented of a patient nine months post-stroke. Results showed that, over six rehabilitation sessions, strength and endurance were improved. There were also

substantial improvements in task accuracy and coordination during the simulation and the patient's walking and stair-climbing ability. The second case was for a 14-year old male who was diagnosed with a Grade I inversion sprain that occurred during wrestling. He had injured his ankle two-weeks prior to beginning the trials. Objective measures obtained by the Rutgers Ankle showed improvement in task accuracy to 100% after the training. The third case for a 15-year old female who was diagnosed with a Grade II inversion sprain that occurred while playing softball. She had incurred the sprain five months before the beginning of the trial. After the two-week rehabilitation training, she reached 100% task accuracy and had a fivefold increase in ankle power output. The last test was for a 56-year old female who had a bi-malleolar fracture. The fracture had been reduced with an external fixator two months earlier. After the two-week rehabilitation training, she had a three-fold increase in ankle power output 100% task accuracy was also reached.

Dai et al. ([1], [18]-[22]) proposed various parallel robotic devices which can be applied on the ankle injuries rehabilitation. These devices have lower number of degrees-of-freedom than the Stewart platform, however enough for the whole ankle motion range during therapy. Compared with the previous research group (Girone M and J.E. Deutsch et al.), the research group of Dai et al. focus on the analysis of kinematics and stiffness for the proposed rehabilitation robotic mechanism.

Before parallel robots were proposed, they investigated the range of motion (ROM) described based on the study of ankle structure. In detail, the human ankle mainly has two joints, the ankle joint and the sub talar joint. The both have different functional capacities and roles in movement and should be both considered seriously. They share a close connection functionally and interdependently. For a rehabilitation device, the ankle joint was considered with 3 revolute joints to simulate the human ankle and different joints have different ROMs. Without limitations of the rotation, the rotation can be illustrated as a curved leaf-surface in Figure II.1. 3. In the figure, the φ-axis represents the rotation for adduction and abduction. The θ-axis represents the rotation for inversion and eversion. The ϕ-axis represents the rotation for dorsiflexion and plantar flexion. Considering the biomechanics of the foot ankle, the particular area enclosed by the double dashed curves gives the ROM for the ankle.

Based on these facts, the parallel robot was modelled and its motion and stiffness were analysed. Figure II.1. 4 shows a representative of their work that can rotate within the ROM of the ankle. Between the both platforms there are three SPS (spherical-prismatic-spherical) linkages and a central strut in the middle. The central strut is fixed on the base, and interconnects with the moving platform with a spherical joint. This mechanism has three rotational DOFs.

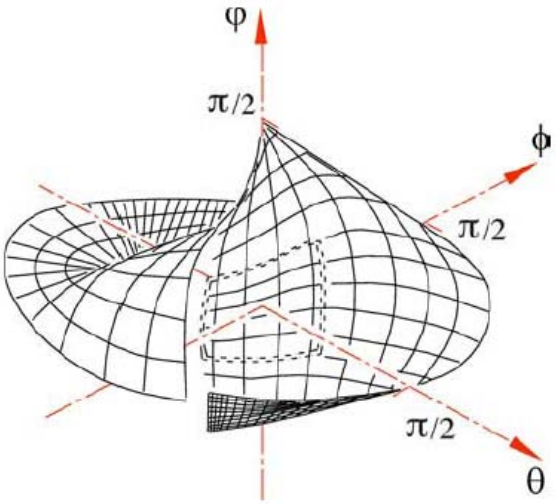

Figure II.1. 3. Orientation range in the rehabilitation therapy[1]

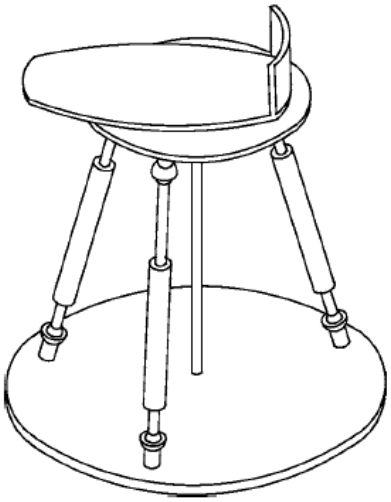

Figure II.1. 4. A 3-SPS/S parallel mechanism for ankle rehabilitation[1]

To increase the DOF to four, a SP (spherical-prismatic) strut is instead in Figure II.1. 5. It is a parallel robot with three linkages and a middle strut between the two platforms. Every linkage is connected to the two platforms with spherical joints. Every linkage itself can stretch and shorten by its prismatic pair in it. This joint can be controlled with an elastic input. An end of the central strut is fixed on the fixed platform, while the other end is spherically connected to the moving one. The moving platform has three revolute DOFs and one prismatic DOF if the central strut has a prismatic joint in it. To decouple the input with respect to the rehabilitation motion, an improved mechanism with four legs and a central strut is replaced in Figure II.1. 6. Take the Figure II.1. 5 as a study object, it is known that the strut constrains the movement of the moving platform in the x-y plane. Therefore the moving platform remains one translation along the z axis and three rotational DOFs (Figure II.1. 7).

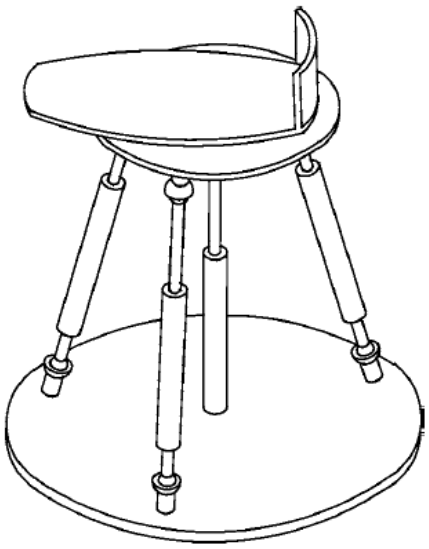

Figure II.1. 5. ankle rehabilitation device based on 3-SPS/SP parallel mechanism[1]

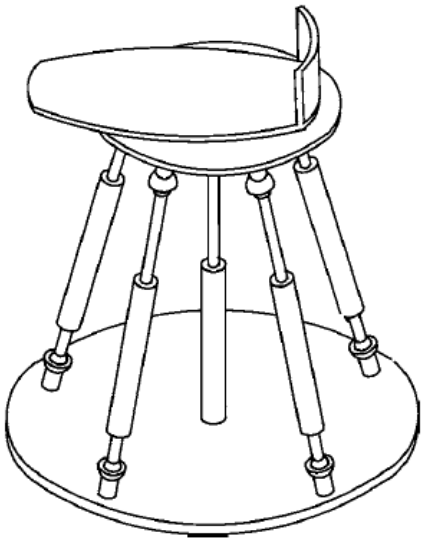

Figure II.1. 6. a 4-SPS/SP parallel mechanism for decoupling motion inputs[1]

With the locations of connecting points and the coordinates shown in Figure II.1. 7, the kinematic model was built and the Jacobian matrix for the model was obtained. After that, the stiffness was also studied. For the control purpose, the effect from the central strut needs to be decomposed. The stiffness matrix of the elastic under-actuated platform mechanism was evolved. The development of the stiffness matrix concluded that the compliance of the under-actuated platform mechanism was related to the structural parameters, joint stiffness and external forces. If the prismatic joint of the strut is designed as an elastic passive joint, the model becomes a mechanism with one passive DOF. Based on this assumption, the stiffness effect in the passive case and its decomposition were discussed. Also, some structure variations and control strategies were studied by the research group of Dai ([20]-[22]).

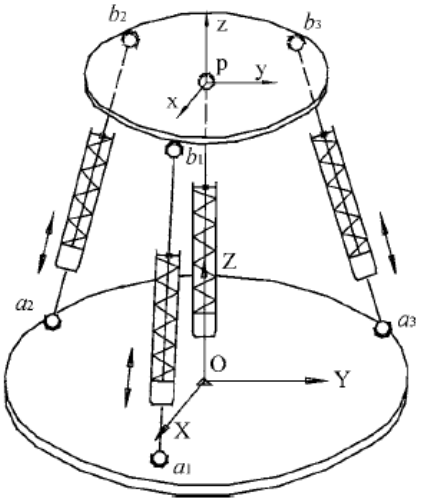

Figure II.1. 7. The kinematic model for the 3-SPS/SP parallel mechanism[1]

Mark E. Stodgell invented a device for ankle rehabilitation [23], as shown in Figure II.1. 8 and Figure II.1. 9. This device can be used for the ankle movement including plantar and dorsiflexion, inversion, eversion and rotation. The amount of resistance to movement and the direction of resistance may be changed without dis-attaching the foot from the device. With the controllable resistance, the muscle strength can be trained. There is a tensioning device (No.18 in Figure II.1. 9) provided to permit use of the device for isometric exercise of the ankle. A spring (No.26 in Figure II.1. 9) connected between the bars is applied to adjust the resistance.

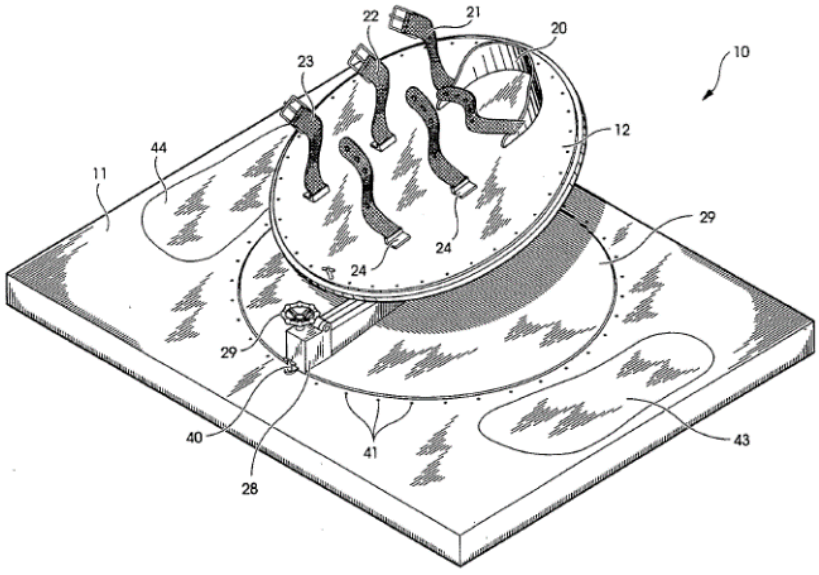

Figure II.1. 8. The upper platform of the rehabilitation device to fix the foot. [23]

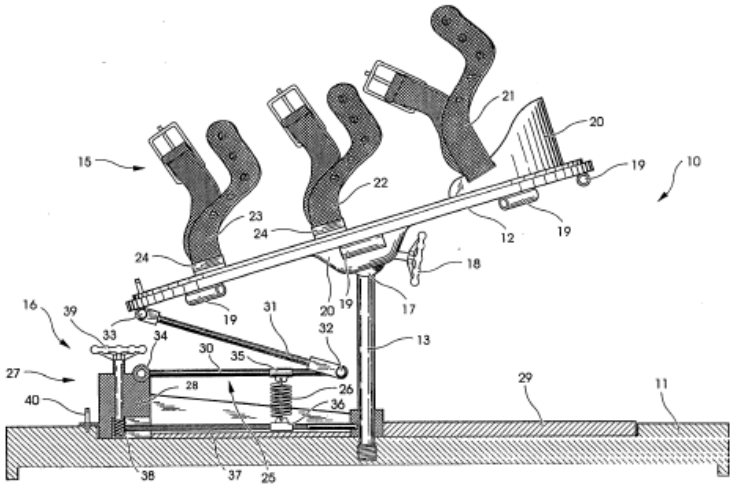

Figure II.1. 9. The structure for an ankle rehabilitation device[23]

Matteo Malosio et al. [24] proposed a complex structure for the ankle rehabilitation, originated from the Agile Eye [25]. This parallel robot PKAnkle (Parallel Kinematic machine for Ankle rehabilitation, shown in Figure II.1. 10) encompasses three parallel legs, each composed of two links, connected to a mobile platform. All the joints are rotational and their axes intersect in the same point, which happens to be the mobile platform rotation centre. The kinematics of the Agile Eye architecture does not depend on the sizes of its links, but only on the alignment angles among its links. The machine therefore can be scaled according to application needs and its final size does not affect the mobility and dexterity of the mechanism.

Figure II.1. 10. PKAnkle prototype[24]

Control strategies were also discussed in their work (Figure II.1. 11). The motion input has two sources. One is from the admittance model (A) and the other is from the database (B). The input path can move the moving platform and act on the patient foot directly. Tests (Table II.1. 1) confirmed that PKAnkle allowed the patient to execute comfortable and physiological movements. But EMG signals and force/torque measures were not mentioned within the robot behaviour and exercises.

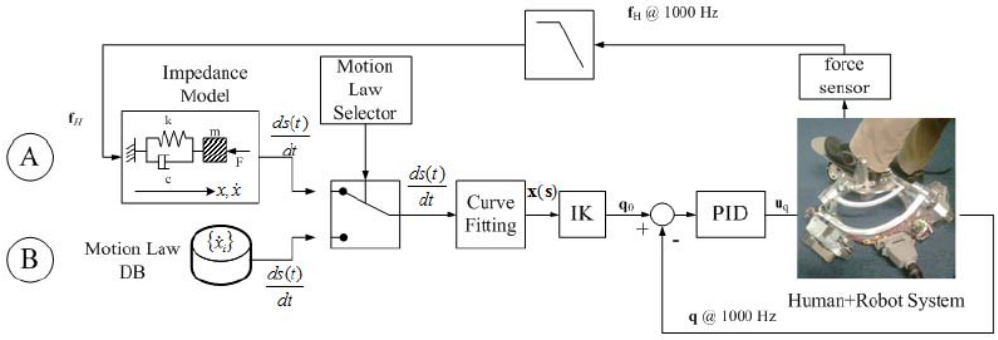

Figure II.1. 11. Robot controller strategies [24]

Table II.1. 1. PKAnkle control characteristic [24]

Current loop rate [kHz]	3
Position loop rate [kHz]	1
Max axis velocity [deg/s]	90
Max roll velocity [deg/s]	20
Max pitch velocity [deg/s]	20
Max yaw velocity [deg/s]	20
Continuous axis torque [Nm]	6.8
Force Acq. Rate [kHz]	1
EMG Acq. Rate [kHz]	1

Jungwon Yoon et al. [26][27] presented a reconfigurable ankle rehabilitation robot to cover various rehabilitation exercise modes (Figure II.1. 12). A four DOF parallel mechanism with two moving platforms receives a foot on them. This device is composed of front and rear platforms, linkages and the base. The robotic device can adjust the two moving platforms to be reconfigured for different exercise activities: kinematic range exercise, strengthening exercise, a balance/proprioception exercise, etc. Not only ankle motion, but also foot motion can be trained with the device (Figure II.1. 13). The front and rear platforms can generate pitch, roll and heave motions: the device can rotate around pitch axis to simulate the motion of plantar flexion (PF) and dorsiflexion (DF); it can also rotate around the roll axis to simulate the motion of eversion (Eve) and inversion (Inv); foot motion around the MTP joint can be simulated with the relative motion between the front and rear platforms. To perform a variety of activities, a unified position-based impedance control system is also developed taking into account the desired position and velocity.

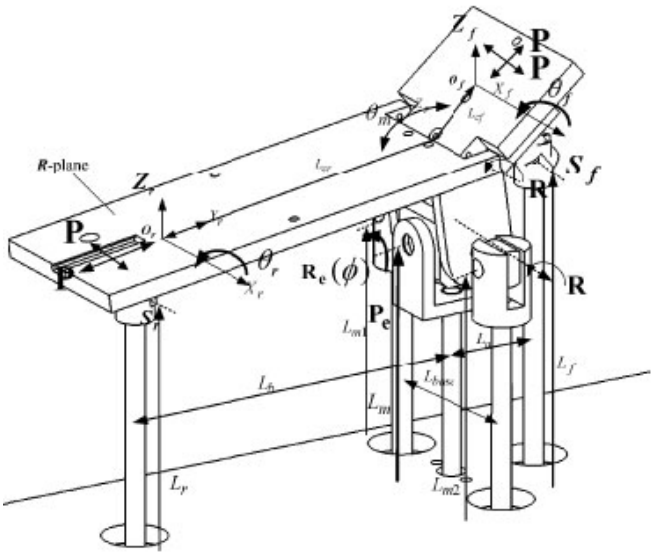

Figure II.1. 12. A four DOF mechanism with the two moving platforms[26]

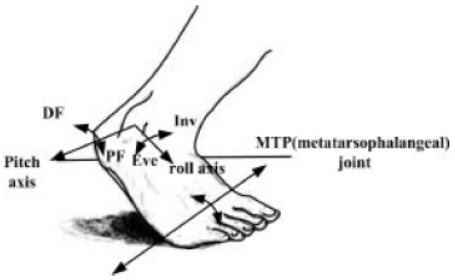

Figure II.1. 13. ankle and foot motions[26]

Li-Qun Zhang et al. [28][29] proposed a suit device for stretching an ankle joint evaluating the treatment outcome (Figure II.1. 14). The seat has 4 DOF to adjust ankle flexion axis to a motor shaft. The device focuses on the recovery of plantar-dorsiflexion rotation. In their work, active and passive ROM, joint stiffness and viscous damping were considered using the system. With this device, the foot under treating is slowly stretched into extreme positions and transited the middle position quickly so that the treatment is focused on the two extreme positions. The paper also suggested, with the appropriate simplification, it is possible to make the device portable, low cost, frequently used in clinics/home and allow more effective treatment and long-term improvement ([30]-[32]).

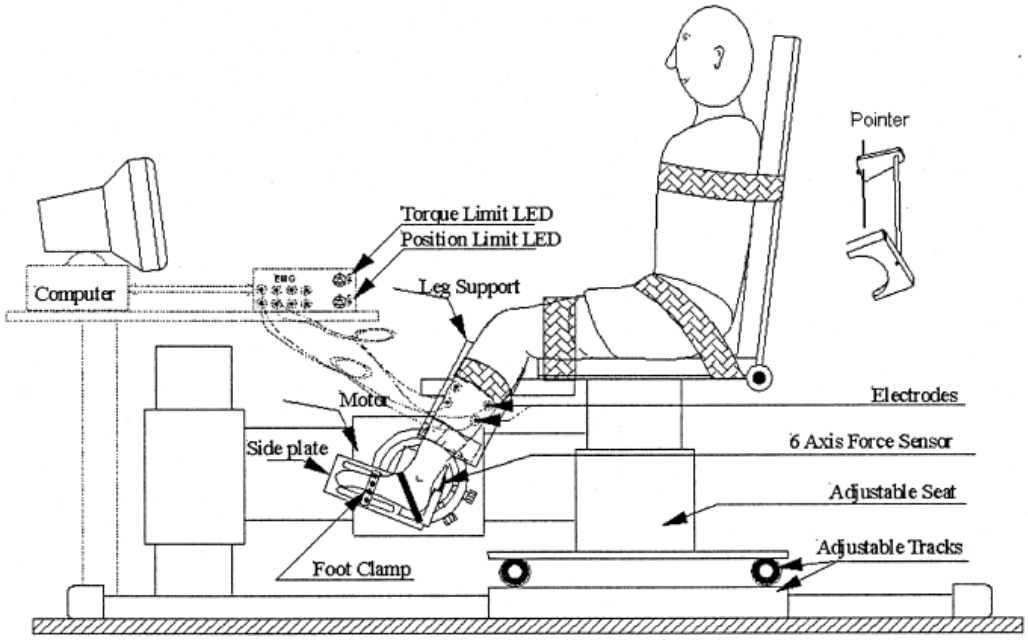

Figure II.1. 14. A suit device for stretching an ankle joint[28]

Saglia J.A. and Dai J.S. et al. ([33]-[37]) proposed a parallel device (Figure II.1. 15) for the ankle rehabilitation with two degree-of-freedom and redundant actuation (Figure II.1. 16), similar with the model in Figure II.1. 5. It is able to reproduce the ankle movements and it makes use of actuation redundancy to eliminate singularity and greatly improve the workspace dexterity.

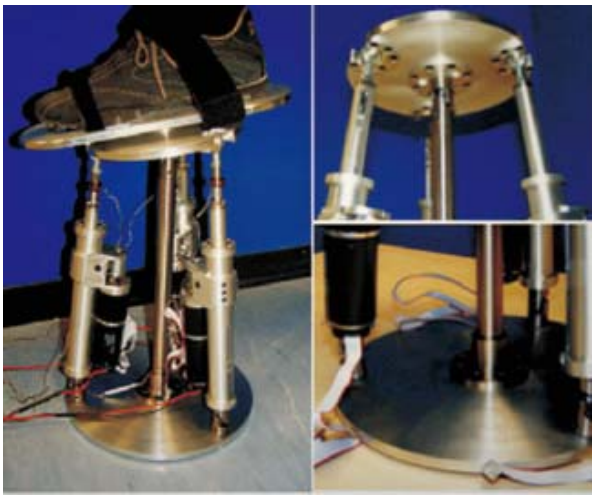

Figure II.1. 15. Prototype of the ankle rehabilitation robot [33]

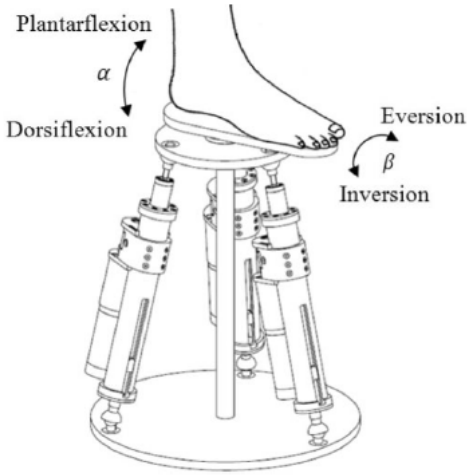

Figure II.1. 16. The two degree-of-freedom and redundant actuation[33]

Syrseloudis, Emiris et al. [38][39] analysed the motions of the foot according to the 2-axes ankle model [40] and the shape of the workspace which it covers. Based on this model, they studied a parallel tripod from Lee and Shah [41]. The Tripod (3-RPS) has

two rotational (pitch, roll) and one translational (z) degrees of freedom. An extra rotation axis was added on the moving platform to provide the necessary extra yaw angle once the yaw angle changes during the foot movements on the platform.

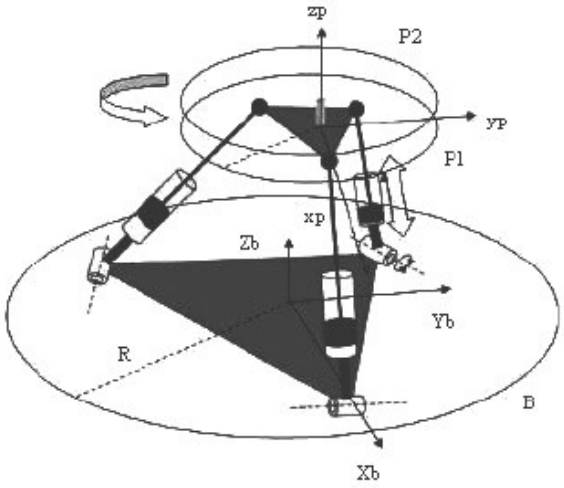

Figure II.1. 17. A prototype of the Tripod (3-RPS) [38]

Malack, Ding et al. [42] patented a two-degree of freedom solution, with two fixed rotation axes. The device is controlled in environment with virtual reality. It has stable or moving mode. In stable mode it works like a force platform and can measure the foot pressure centre during equilibrium exercises. In moving mode it is free to move or with a resistance and the trajectory can be visualized.

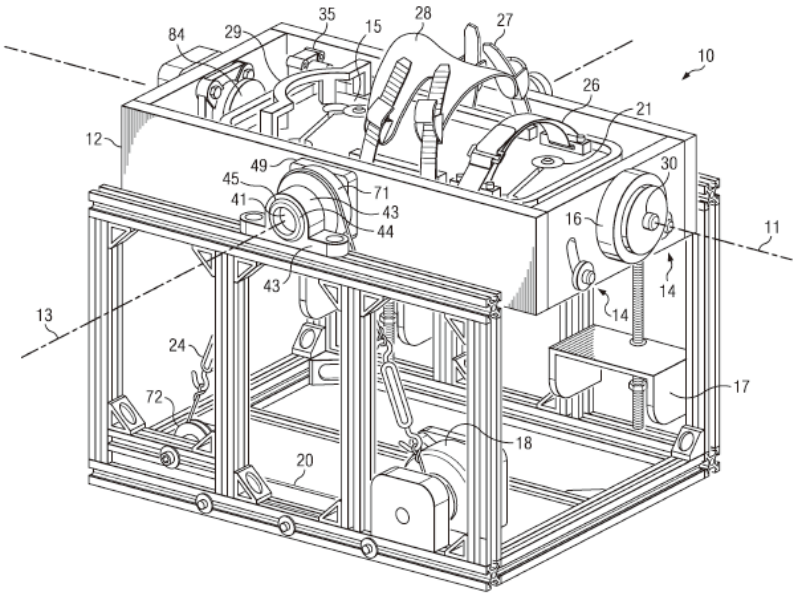

Figure II.1. 18. A rehabilitation system with two DOFs. [42]

Tiecheng Zhu et al. [43][44] patented a passive movement device for the ankle joint, consisting of a fixed disk and two moving disks (Figure II.1. 19). With the disks, the passive movement device can provide passive training in various directions and at different frequencies for an ankle joint, the patient can adjust the rotational speed and the angle according to specific tasks.

They also had an active movement equipment which comprises a movable plate and a fixed plate (Figure II.1. 20). The ball cup is connected with the movable plate through a bolt, which can enable the movable plate to rock forwards and backwards as well as leftwards and rightwards. The movement of the movable plate can be limited by the lateral sides of the fixed plate. The equipment has a simple structure for exercise and rehabilitation.

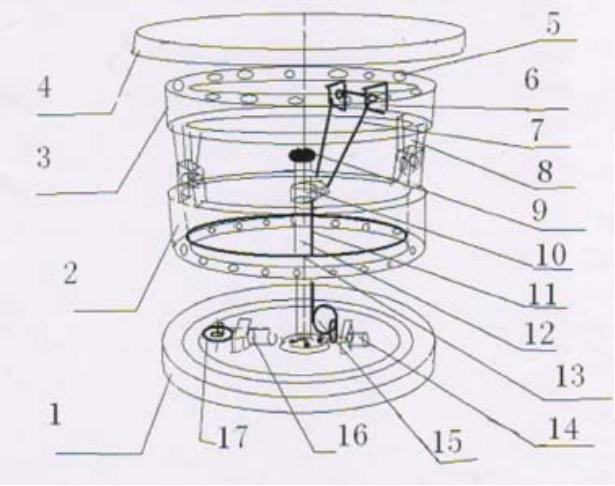

Figure II.1. 19. A passive movement device for the ankle joint. [43]

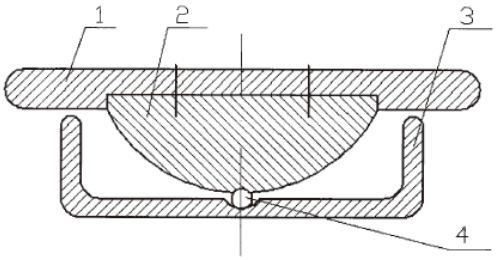

Figure II.1. 20. An active movement equipment for the ankle joint. [43]

The device proposed by Lixun Zhang and Wei Wang [44] is a rope-drawn rehabilitation training machine for an ankle joint (Figure II.1. 21). The machine consists of three main components: a base with a strut welded on it, a mobile platform connected with the strut through a flexible ball hinge, and three ropes with three driving motors of the same model and three same universal wheels uniformly fixed on the bottom plate. A sensor is mounted on the supporting strut to record the up and down motion of the moving platform. The machine can be used for rehabilitation training of sprain and orthotics of the ankle joint,

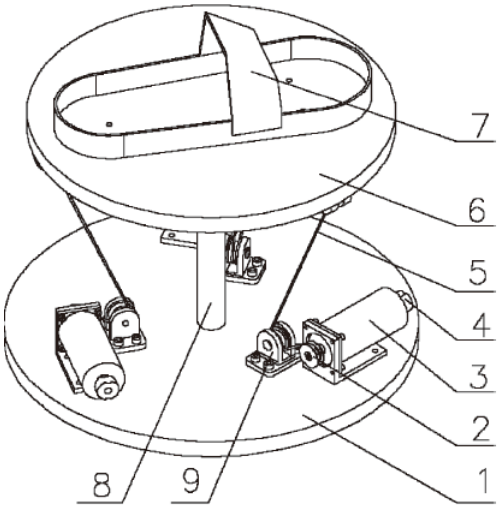

Figure II.1. 21. A rope-drawn rehabilitation training machine [45]

An apparatus (Figure II.1. 22 and Figure II.1. 23) designed by A. Austen [46] is used to strengthen, develop, and rehabilitate the anatomy of the human ankle, comprising a large stable floor base and a foot securing platform. The user is able to move their foot in a vertical and orbital manner against the resistance of the cylinders resulting in rehabilitation and/or strengthening of the muscles, tendons and ligaments surrounding the ankle.

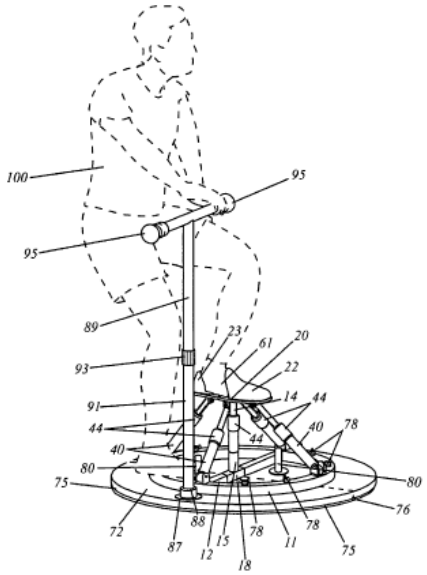

Figure II.1. 22. Shock absorber ankle exercise device. [46]

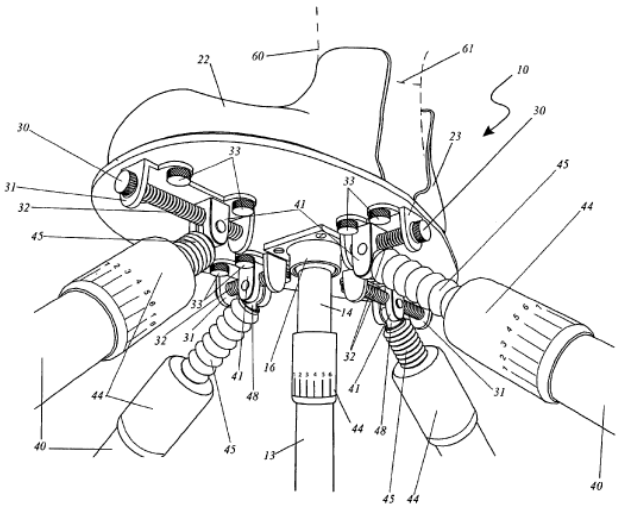

Figure II.1. 23. The connection details of the ankle exercise device. [46]

V. Mikhajlovich et al. [47] designed a rehabilitation device for patients with ankle injuries, as well as for extended range of motions and stimulation of related muscles and ligaments. The apparatus comprises a foot rest, a support and a base. Between the base

and foot rest, there is a vertical strut with a hemispherical slot comprising a ball in its top. The invention can provide high-level mobility of the foot rest, graduated load and simulated ankle muscles and ligaments due to muscle force of a healthy foot.

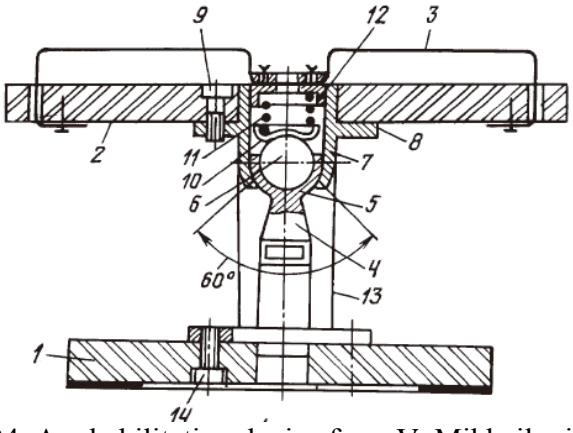

Figure II.1. 24. A rehabilitation device from V. Mikhajlovich et al. [47]

Juan Jose [48] patented a device for an objective assessment of progress made during the rehabilitation of the ankle and leg muscles. The moving platform of the device (Figure II.1. 25) is intended to receive the sole of a person's foot. Calibrations on (10) is for measuring the angle of inclination between the platform and the horizontal of the frame.

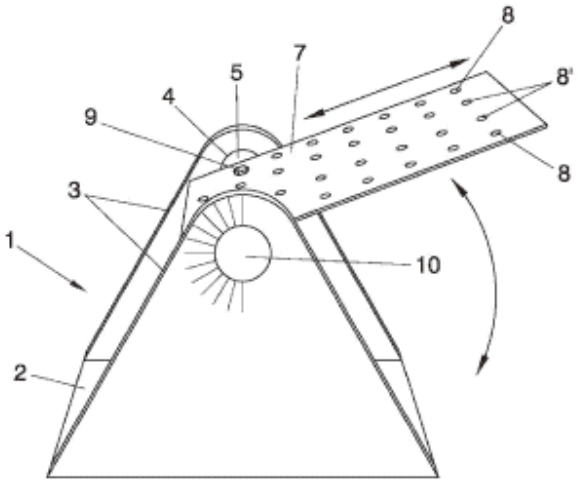

Figure II.1. 25. The device for the measurement of the rehabilitation effect[48]

Hong Yue et al. [49] proposed a 3SRS/S parallel robot for the ankle rehabilitation (Figure II.1. 26). The device has mechanical, control and display parts. Three motors are mounted on the base to drive the three rotational joints on the three linkages. Force/torque sensors are fixed between the moving platform and the pedal. The position sensors are on the three linkages. The display part is for the effect evaluation and the interaction with patients. With the device the ankle joint can be trained in the three rotational directions: pitch, roll and yaw.

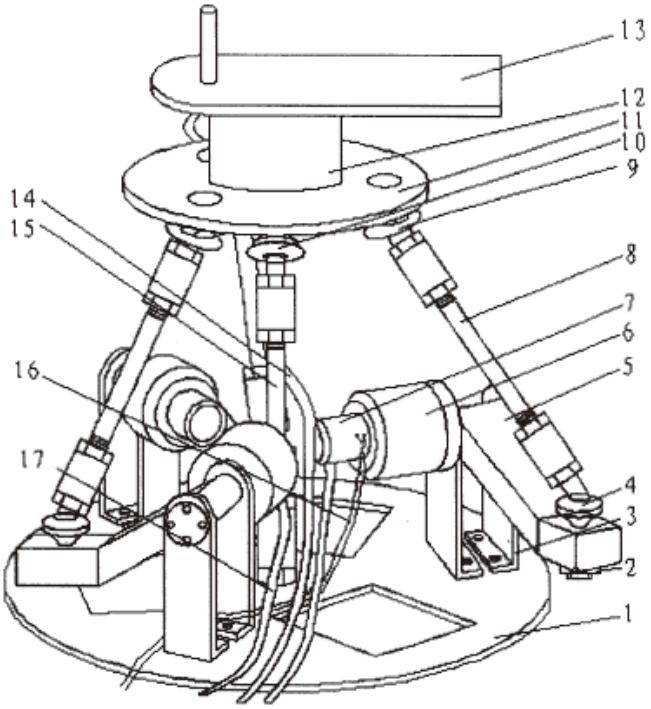

Figure II.1. 26. The 3SRS/S parallel robot for the rehabilitation [49]

Liju Xu et al. [50] patented a 3 DOF device for the ankle rehabilitation (Figure II.1. 27 and Figure II.1. 28). The device has hybrid structure. The lower part is a mechanism with a rotational degree and the upper part is a parallel robot with the two rotational degrees. This device can simulate the reality of the ankle motion for the ankle training.

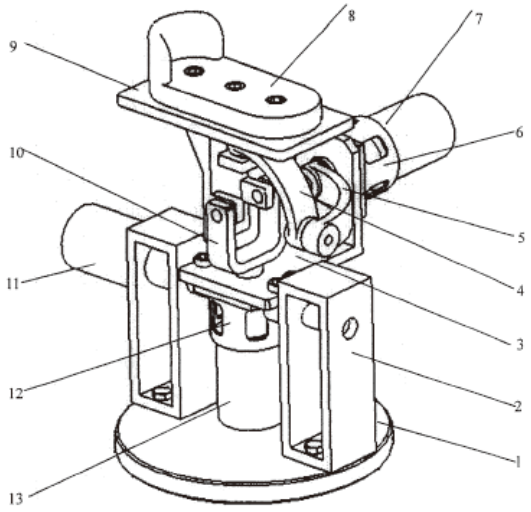

Figure II.1. 27. A hybrid structure of a rehabilitation device[50]

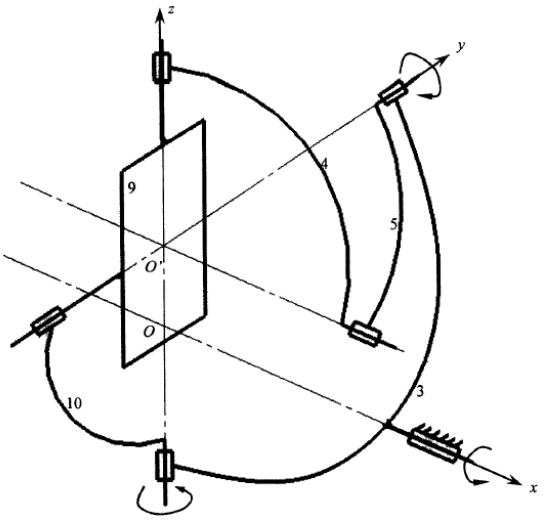

Figure II.1. 28. The three DOFs of the device[50]

H. Craig invented a device [51] including a foot platform disposed on a support arm coupled to and extending upwardly from a base (Figure II.1. 29 and Figure II.1. 30). The foot platform is configured to pivot in the three directions: plantar flexion and dorsiflexion, inversion and eversion, internal and external rotation. The device also includes resistance means to resist movement of the foot platform with respect to the base.

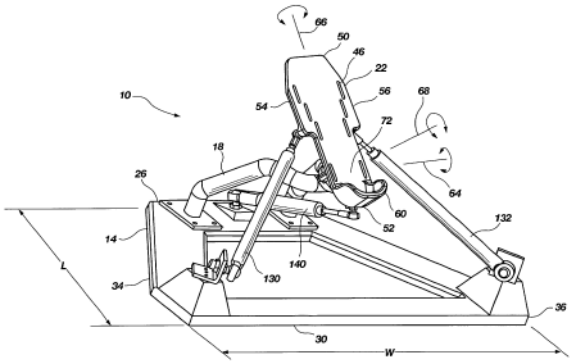

Figure II.1. 29. A 3 DOF device for the ankle rehabilitation, by H. Craig [51]

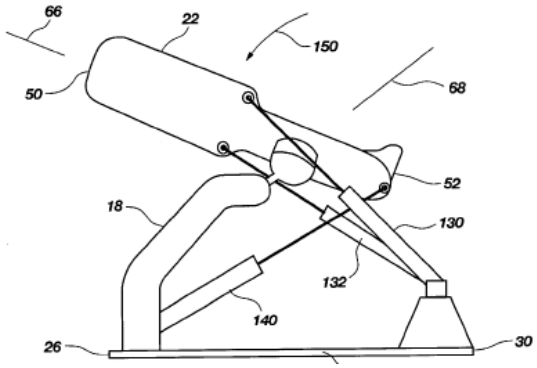

Figure II.1. 30. The detail of the rehabilitation device from H. Craig [51]

Y. Mikio [52] invented a device for a rehabilitation exercise by freely adjusting a swing width and a swing speed. As shown in Figure II.1. 31 and Figure II.1. 32, a rack 8 can be slid by the drive of a linear motor 9. A foot mounting plate 12 can rotate around the shaft 13.

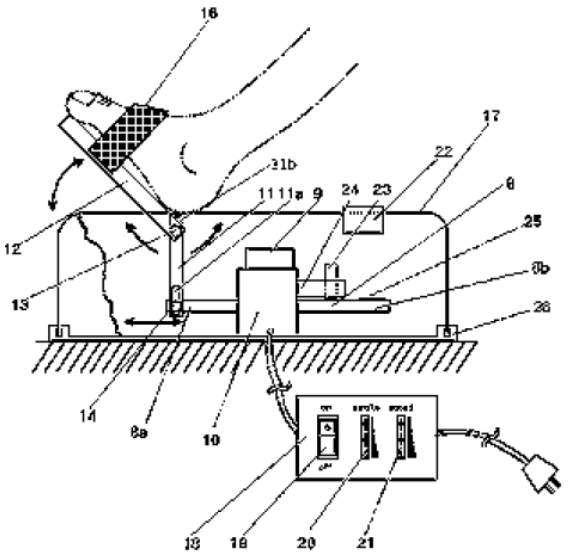

Figure II.1. 31. An invention for a rehabilitation exercise. [52]

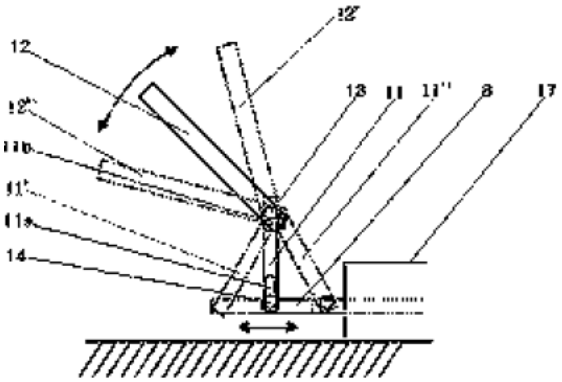

Figure II.1. 32. The motion of the device. [52]

F. Russell [53] invented an exerciser for use in the rehabilitation of the leg, ankle, and foot muscles. It has a foot support connected to a base of a ball and socket joint enabling

the support to be tilted in any direction. The joint includes a threaded member operable to provide selected resistance to such tilting.

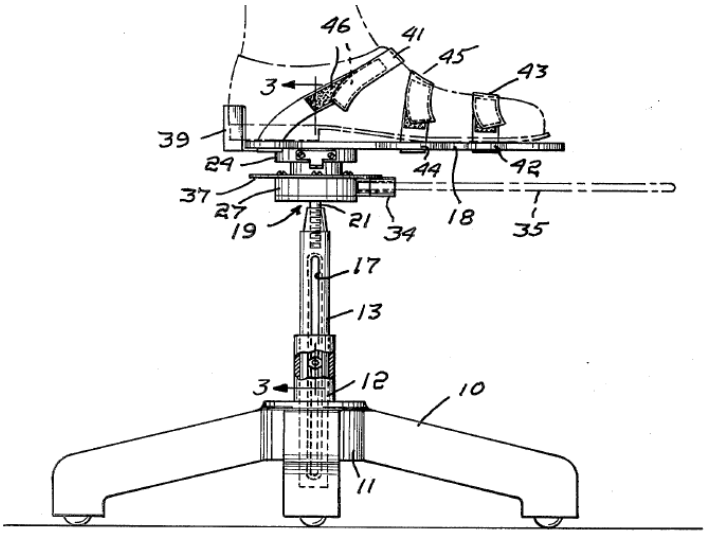

Figure II.1. 33. Exerciser for lower leg, ankle, and foot muscles[53]

A Giguere [54] proposed a device for an ankle re-education. When a person suffers a twist or a bone fracture of the ankle, it is necessary to re-educate the ankle motions after the plastering. In his invention (Figure II.1. 34), a footrest is fastened on a base and may pivot on the base by means of a ball-and-socket joint. The rotation and training can be measured so that the patient or the doctor may follow the re-education progress.

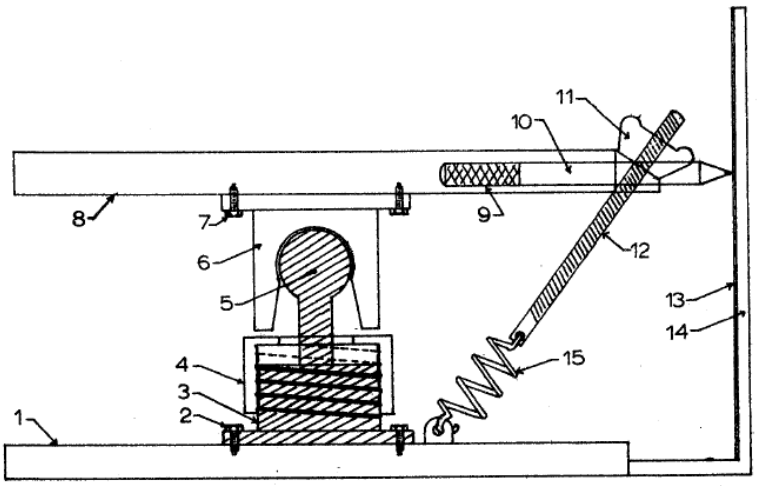

Figure II.1. 34. A device for an ankle re-education. [54]

An exercising machine invented by M. Stewart [55] is for the training of the ankle and knee, comprising a base 11, an upright support 6, a top 7 (Figure II.1. 35). A pair of footrests 21 can rotate and return helped by a spring 38 (Figure II.1. 36). The patient sits

on a chair to the right of the apparatus and places his feet on the footrest 21. Keep his feet against end 24, and the ankles and knees are supported by cushions 26 and 28 respectively. The top 49 of the apparatus serves as a table top and can be adjusted and held rigidly in position by means of rod 59. The tension in spring 38 is adjustable for different requirements.

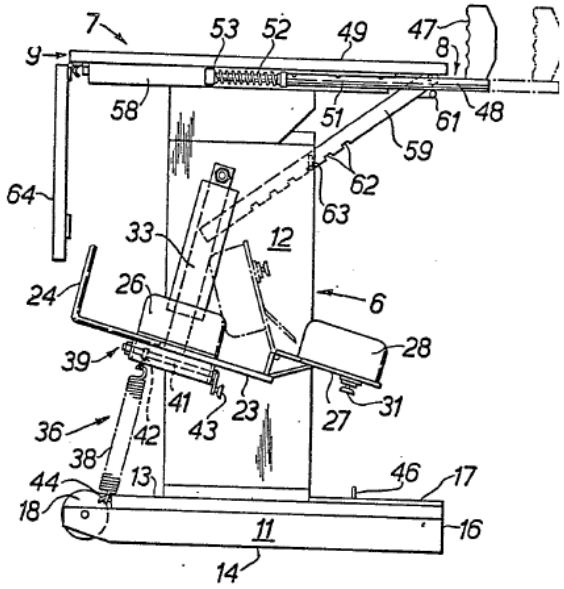

Figure II.1. 35. An exercising machine for the ankle and knee, lateral view[55]

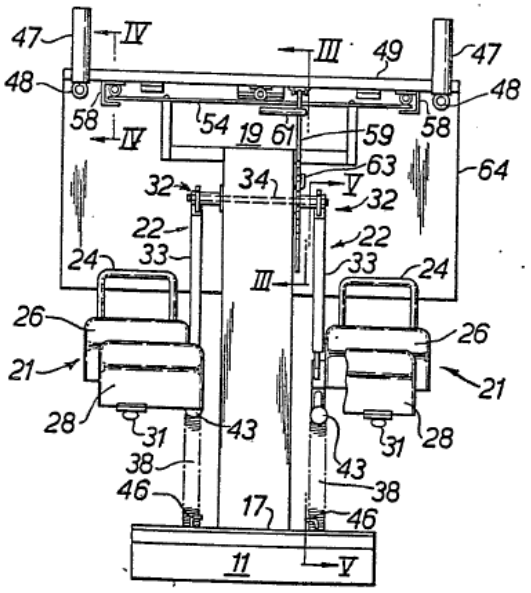

Figure II.1. 36. An exercising machine for the ankle and knee, front view[55]

II.1.2 Wearable ankle rehabilitation robot

A wearable robot (also exoskeleton robot) is a mechatronic system that is designed around the shape and function of the human body, with segments and joints corresponding to those of the person it is externally coupled with [56]. A wearable rehabilitation robot for the lower extremity (LE) is normally mounted on the patient leg for the gait training [3]. The ankle foot orthosis (AFO) is commonly used since the late 1960s [57]. It is a single joint orthosis designed to assist and support movements of the ankle joint. Different robotic orthoses have been developed around the world ([58]-[64]). J. Furusho et al. [58][59] proposed an AFO with the magneto rheological (MR) brake. They measured the ankle angle, reaction force and a bending moment. With this device, the subject can maintain the dorsal flexion and prevent the foot drop during the foot swing phase. The subject can contact the ground at heel. The maximal value of the bending moment and the walking cycle were also improved. Blaya J. and Herr H. [60] proposed an active foot ankle orthosis (AAFO) for the adaptive control of a variable impedance to assist plantar flexion and drop-foot gait. An actuator is attached posteriorly to a conventional AFO (Figure II.1. 37), and provides variable orthotic joint impedance based on position and force sensory information. Their work suggested that a variable-impedance orthosis may have certain clinical benefits for the treatment of drop-foot gait

compared to conventional ankle-foot orthoses having zero or constant stiffness joint behaviors.

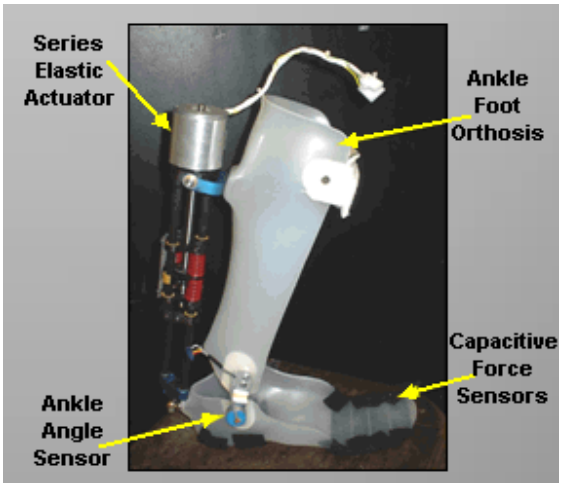

Figure II.1. 37. An AAFO device [60]

A powered ankle foot orthosis (PAFO) was presented by Daniel P. Ferris and J. Ward et al. ([61]-[64]). They presented a PAFO using two pneumatic muscles for supporting a rehabilitation device and the training of an ankle joint (Figure II.1. 38 and Figure II.1. 39). Two muscles actuated and controlled the training of plantar-dorsiflexion rotation.

Figure II.1. 38. a device using pneumatic muscles[61]

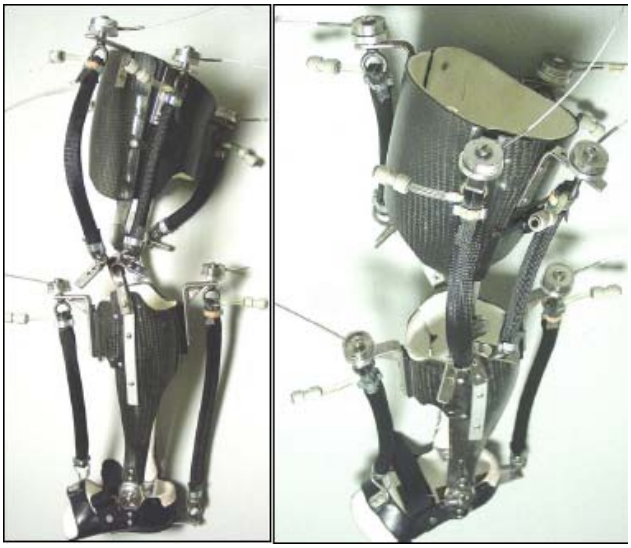

Figure II.1. 39. A pneumatically powered knee-ankle-foot orthosis (KAFO) [61]

A. Roy and H. Krebs et al. ([65]-[67]) invented an ankle robot 'Anklebot' with 3 DOFs (Fig. 10). The device is designed to train the stroke patients to overcome the foot drop and balance problems. Two of 3 DOFs are actuated using the parallel linear actuators for

plantar-dorsiflexion and inversion-eversion rotations. The third DOF provides the assembly convenience. 'Anklebot' supports 25° of dorsiflexion, 45° of plantar flexion (DP), 25° of inversion, 20° of eversion, and 15° of internal or external rotation (IE). The robot has the weight of the device less than 3.6 kg with low intrinsic mechanical impedance. The robot can deliver a continuous net torque of 23 Nm for DP and 15 Nm for IE and the torque capability does not afford the patient weight. Two brushless DC motors were selected to satisfy the technical requirements. The two sets of sensors were provided for the position information collection and matched with rotary encoders and linear incremental encoders respectively.

Safety features were also highlighted in their work. The failure analysis referred to don-on and off processes, body-weight support during gait training and software failures. Multiple protection levels were built to minimize the electrical risk. All mechanical parameters were monitored. The authors also analysed the ankle kinematics and kinetics under the robot. As a clinical application, the passive ankle stiffness was estimated and compared with other published literatures.

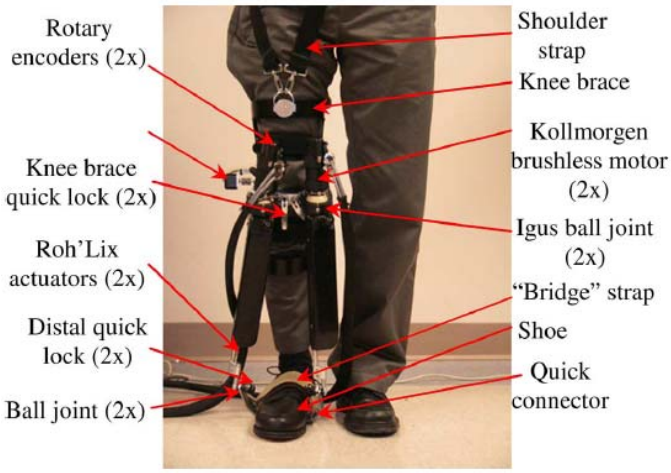

Figure II.1. 40. A 3 DOF rehabilitation device for gait training. [65]

Other prototypes were presented by Jason W. Wheeler and H. Krebs [66] in Wheeler's master thesis (Figure II.1. 41).

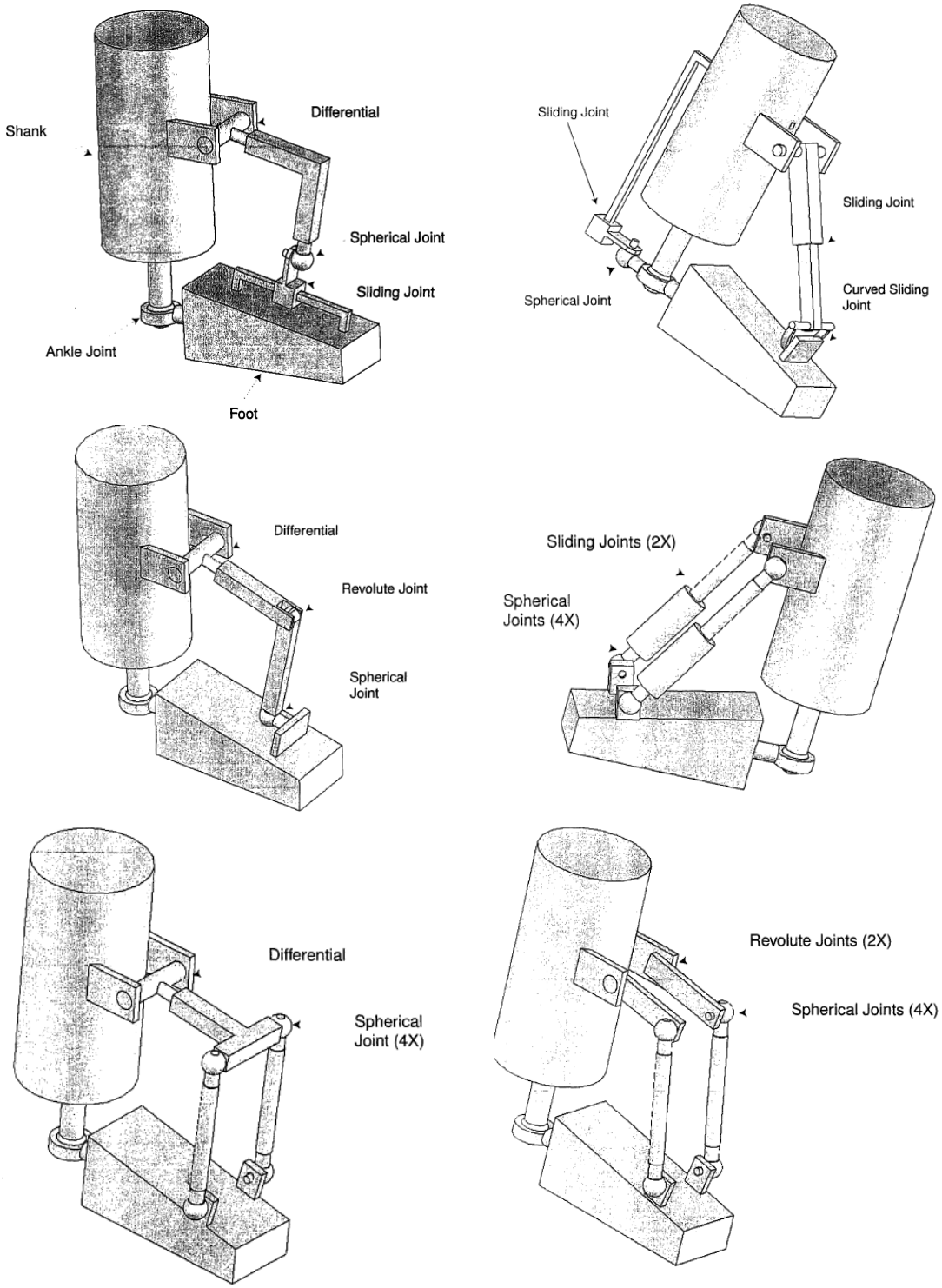

Figure II.1. 41. Mechanism concepts from Jason W. Wheeler[66]

Kartik Bharadwaj et al. [68] proposed a similar device, like the foregoing device (Figure II.1. 40 and Figure II.1. 41). A unique feature in his design is that the human anatomy is a part of the robot, the first fixed link being the patient's leg (Figure II.1. 42). The

kinematics and workspace of the tripod device have been analysed determining its range of motion (Figure II.1. 43. a kinematic model for workspace analysis.). The actual angular position in dorsi/plantar flexion was collected in experiments with a subject Figure II.1. 44.

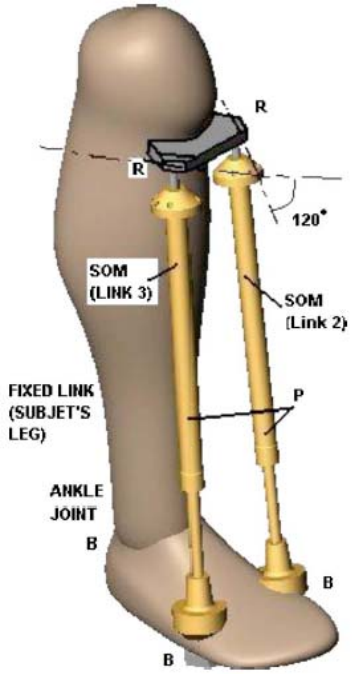

Figure II.1. 42. a proposal device from Kartik Bharadwaj et al. [68]

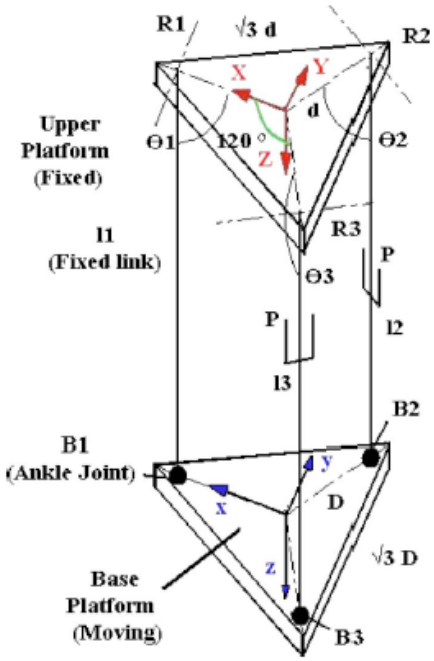

Figure II.1. 43. a kinematic model for workspace analysis. [68]

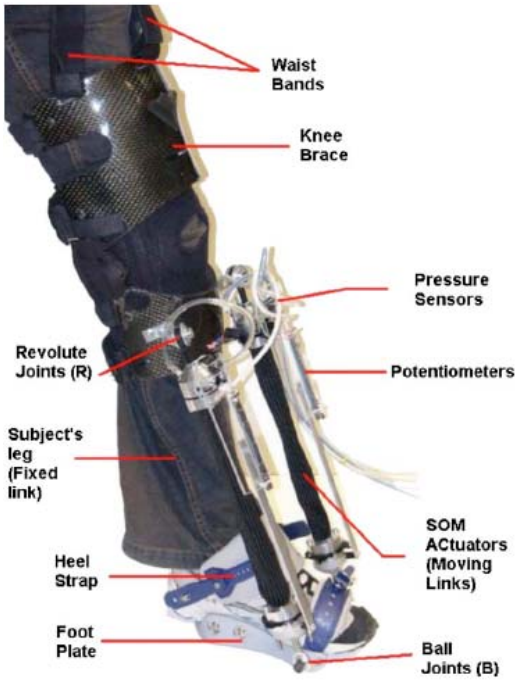

Figure II.1. 44. Robotic gait trainer (RGT) in experiments. [68]

Satici et al. [69] designed an exoskeleton (Figure II.1. 45) for the human ankle. This device is a reconfigurable, parallel mechanism that can either be employed as a balance/proprioception trainer or configured to accommodate range of motion and strengthening exercises. The exoskeleton can be utilized as a clinical measurement tool to estimate dynamic parameters of the ankle and to assess ankle joint properties in physiological and pathological conditions.

Figure II.1. 45. An exoskeleton device for the human ankle[69]

In order to span the whole natural range of motion of the human ankle and to do so robustly for various operators of different ankle and foot dimensions, the proposed 3UPS (Universal/Prismatic/Spherical joints) mechanism has six degrees-of-freedom but only three, the prismatic joints, are actuated. To support to the human weight and to adjust the torques transferred to the ankle joints while covering an acceptable portion of the natural human ankle workspace, a 3UPS-RR parallel mechanism (Figure II.1. 46) is proposed as the kinematic structure of the exoskeleton for balancing exercises.

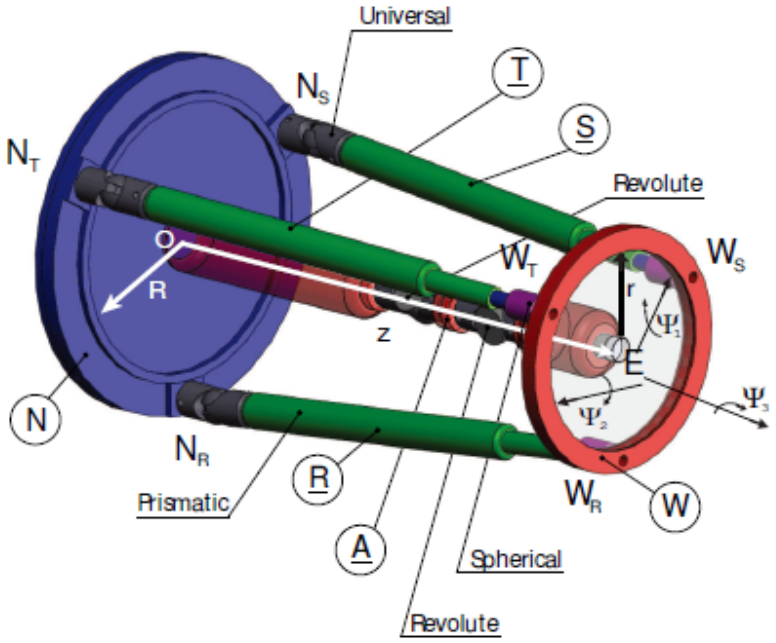

Figure II.1. 46. 3 UPS/RR mechanism in a perspective view. [69]

S. Pittaccio and S. Viscuso [70] designed an active orthosis mounting a pair of motors based on shape memory alloy NiTi wires wrapped on pulleys (Figure II.1. 47). The electromiographic signal of the anterior tibial muscle controls the actuation. With this device, passive and active modes were then studied for the ankle training (Figure II.1. 48).

Figure II.1. 47. A device for ankle dorsiflexion with rotary actuators[70]

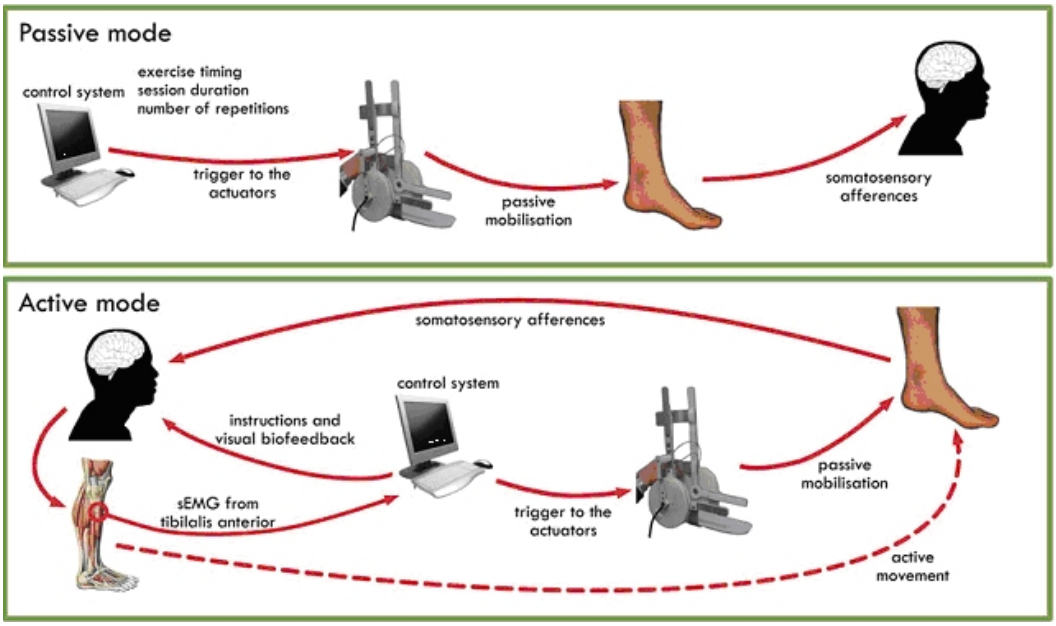

Figure II.1. 48. Passive and active modes for the ankle training. [70]

From the actuation point of view the orthosis proposed by N. Saga et al. [71][72] is interesting. It consists of a tendon-drive system using a pneumatic balloon actuator, power transfer mechanism, and ankle foot orthosis (Figure II.1. 49). A compressed air supplied pneumatic balloon was developed as an actuator of this device, which is simple, compact and lightweight.

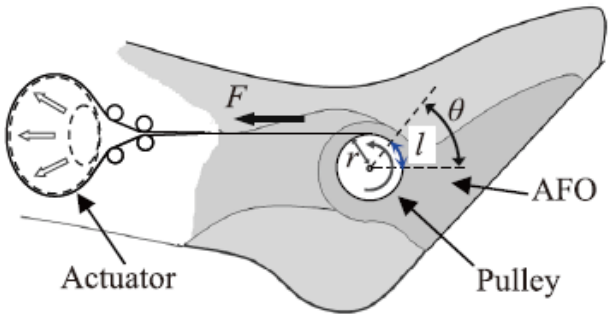

Figure II.1. 49. The tendon driven system[71]

Song Yin et al. [73] proposed a parallel 3-RPS mechanism with 3 DOF, as shown in Figure II.1. 50. In their device, the lower platform is a moving platform that can support plantar-dorsiflexion and inversion-eversion rotations, while the upper platform is fixed with a patient's leg.

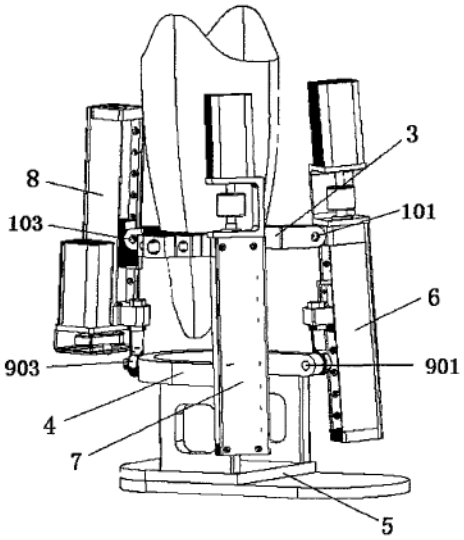

Figure II.1. 50. A parallel 3-RPS mechanism with 3 DOF[73]

Yupeng Ren et al. [74][75] designed a system for acute stroke survivors in bed (Figure II.1. 51). The robot provides controlled passive stretching and active motivating training with proprioceptive and audio-visual feedback (Figure II.1. 52). The patient engage is highlighted during the robot work, which is important in motor recovery (neuroplasticity). The direct physical guidance to help acute patients post stroke regain motor control ability. Changes in active and passive biomechanical properties can also be measured to evaluate the rehabilitation situation.

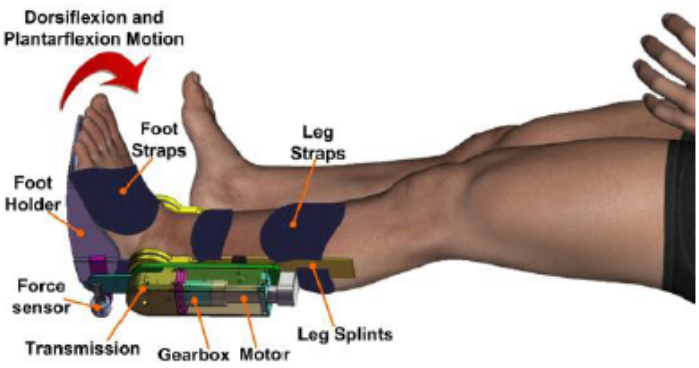

Figure II.1. 51 The ankle rehabilitation system for acute stroke survivors. [74]

Figure II.1. 52. The interface between the patient and the system[74]

A. Agrawal et al. [76] designed an ankle-foot orthosis (AFO) to help subjects with weakness of ankle dorsiflexor muscles. The deformity and muscle weakness of one joint in the lower extremity influences the stability of the adjacent joints, thereby requiring compensatory adaptations. An innovative ankle-foot orthosis (AFO) was designed to allow two degree-of-freedom motion while serving to maintain proper foot position for subjects (Figure II.1. 53). The dorsiflexion/plantar flexion is controlled by an actuator and inversion/eversion with a spring and a damper. Figure II.1. 54 shows the detail about

the rotation axes. The two cubes on the top are used to locate the dorsiflexion-plantar flexion axis, while the cube at the bottom is used to locate the inversion-eversion axis. The dashed lines represents the two joint axes. Control strategies and results were also shown in the paper.

Figure II.1. 53. An innovative AFO proposed by A. Agrawal et al. [76]

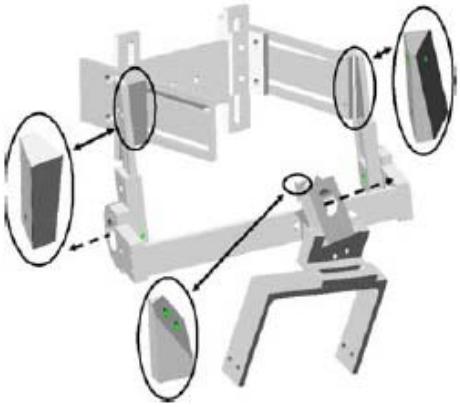

Figure II.1. 54. The detail shows the two rotation axes. [76]

M. Mirbagheri et al. [77] studied the effects of Robotic-Assisted Locomotor (LOKOMAT) Training on persons who suffer problems about the neuromuscular properties and the spastic ankle with incomplete Spinal Cord Injury (SCI). System identification techniques were used to characterize the effects of Lokomat for the physical training of the ankle joint from full plantar flexion to dorsiflexion at maximum speed. Results showed that reflex stiffness, abnormally increased in SCI, was significantly reduced following LOKOMAT training. Active range of motion, peak-velocity and peak-acceleration of voluntary movement increased.

Subjects were fitted in the overhead harness/counterweight system and unloaded by a counterweight. Subjects were fitted into the LOKOMAT by stabilizing and aligning the lower extremity and joints (Figure II.1. 55). During the training, treadmill speed increased gradually from 1 to 2.5 kmph. Total training parameters such as time, speed, distance, and amount of unloading will be recorded. Blood pressure, and heart rate will also be assessed.

Figure II.1. 55. Robotic-assisted locomotor (LOKOMAT) training apparatus. [77]

K. Shorter [78] invented a novel portable powered ankle foot orthosis (PPAFO) for rehabilitation (Figure II.1. 56). The device provides untethered assistance during gait and both plantar flexor and dorsiflexor torque assistance by way of a bidirectional pneumatic rotary actuator. A portable pneumatic power source with a compressed carbon dioxide bottle and embedded electronics is applied to control the actuation of the foot. Collected data demonstrated the PPAFO's capability to provide correctly timed plantar flexor and dorsiflexor assistance during gait.

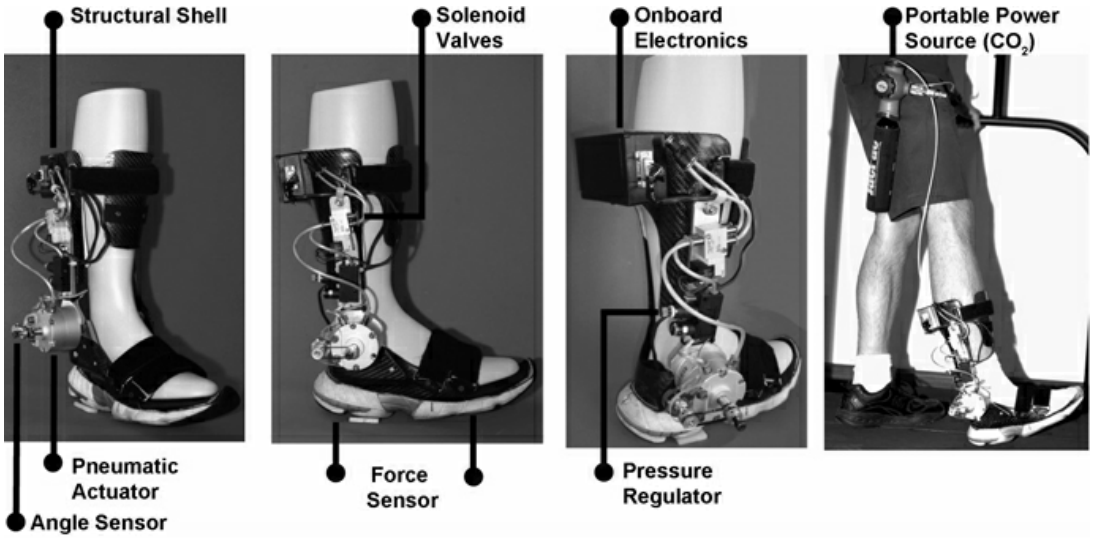

Figure II.1. 56. The components and the structure of the PPAFO robot[78]

Hongbo Wang et al. [79] patented a device (Figure II.1. 57 and Figure II.1. 58) for the ankle training. The motor 13 is housed under the foot pedal 19 and it drives the synchronous pulleys 3 and 15 so that the pedal 19 can rotate around the pin B on the base 14. Sensors 7 and 9 can measure the positive and negative torques during the dorsiflexion and plantar flexion motion.

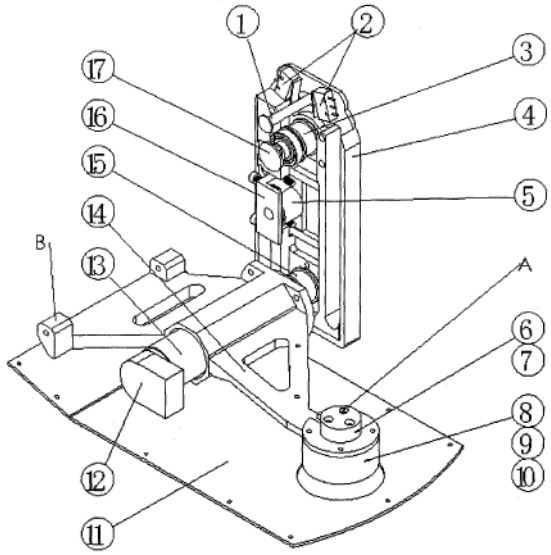

Figure II.1. 57. The inner structure of the training device. [79]

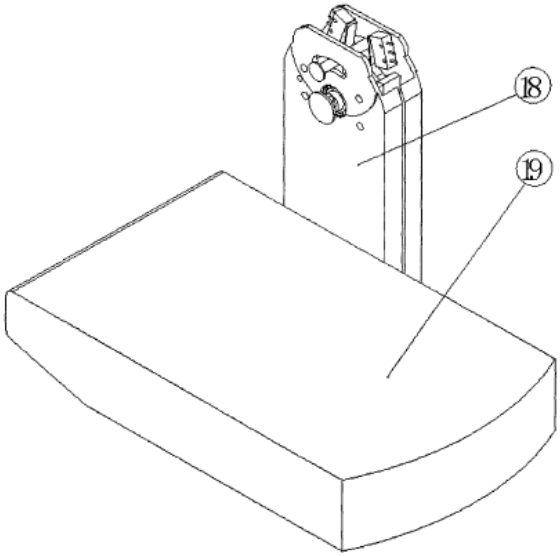

Figure II.1. 58. The prototype of the training device. [79]

Indian Song [80] patented a hybrid structure (Figure II.1. 59) for the ankle rehabilitation. The serial parts 1 and 10 are to hold the patient thigh and calf so that the most mass of the leg is removed from the ankle load. A parallel robot with the structure 3-UPS is designed for the foot. The device can provide three DOFs for the ankle training.

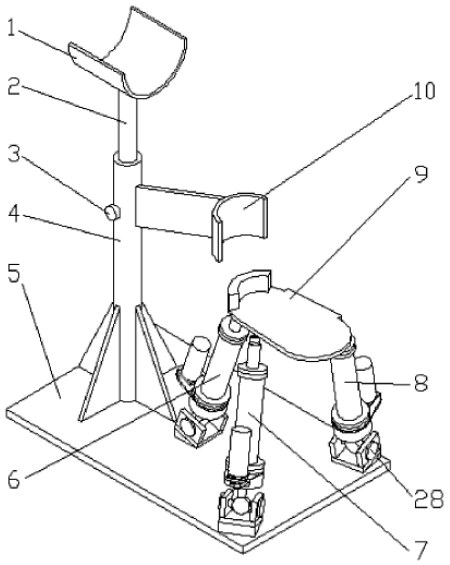

Figure II.1. 59. The hybrid structure for the ankle training. [80]

The orthopaedic device (Figure II.1. 60 and Figure II.1. 61) invented by R. Darelle [81] includes a foot support element to support a user's foot. The foot support element has a first portion and a second portion that are configured to rotate with respect to one another about a pivot point. Guide lines are connected to the foot support. The control member 380 is configured to control the plurality of guide lines to flex the user's ankle in a plurality of directions. There are many holes on the foot support for the line ends to adjust to different sizes of feet.

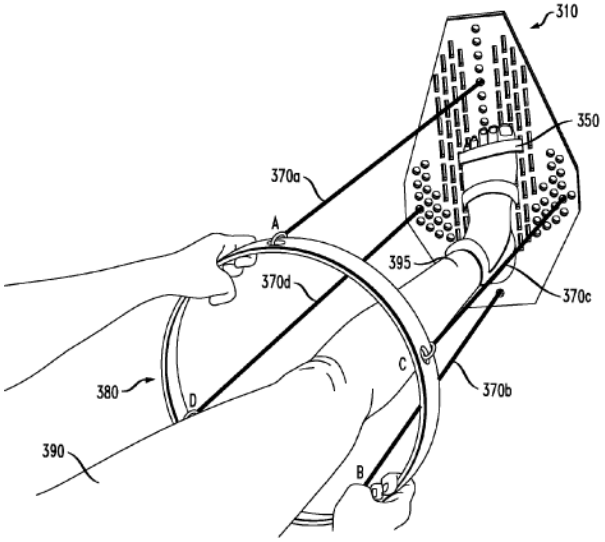

Figure II.1. 60. The prototype of the orthopedic device. [81]

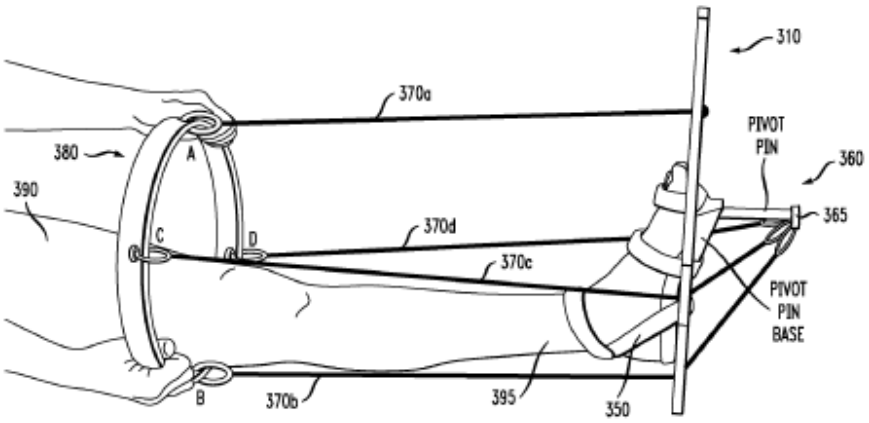

Figure II.1. 61. The lateral view of the device. [81]

An apparatus for calf, shin and ankle rehabilitation and exerciser, invented by Vincent Gibbons [82] is shown below (Figure II.1. 62 and Figure II.1. 63). It is comprised of a rigid sole plate member 12 and a cross brace 20 connected by an ankle pivot adjusting mechanism 32. A sole plate protective pad 40 and a shin protective pad member 36 is to secure the foot and the lower leg. Cross brace 20 engages the toe section 14 of sole plate member 12 via an engaging biasing resistance means 48. In this case, the device can do dorsiflexion, plantar-flexion, inversion or eversion. The invention also provides a means for immobilizing and supporting the foot in a relation substantially at a right angle to the lower leg for walking or rehabilitation.

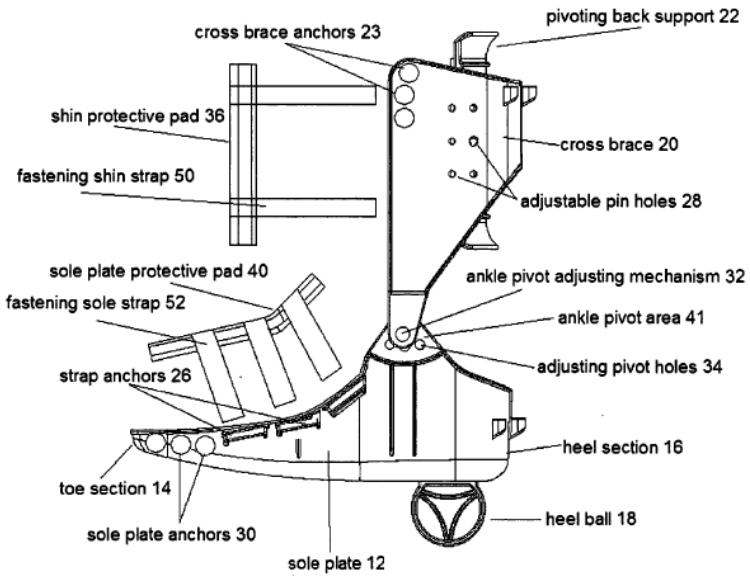

Figure II.1. 62. An apparatus for the rehabilitation and exerciser[82]

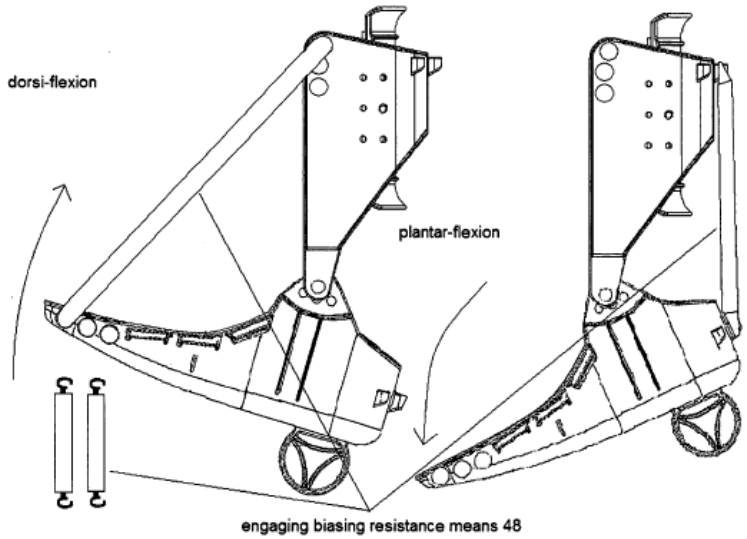

Figure II.1. 63. The connection between the cross brace and the sole plate. [82]

An assistant movement exoskeleton (Figure II.1. 64 and Figure II.1. 65) invented by Jiafan Zhang et al. [83] has three DOFs, controlled by three motors 10, 17, 19. The upper ring and the lower ring are connected with the connectors 15 and 18. The supports 1 and 9 are connected with the axes of the connectors 15 and 18 by bearings. So the two rings can move with respect to the ring gear 7. On the ring gear, there are the two U-shape connectors 16 and 20 connected with the calf supports 5 and 6 through bearings. The motor 17 and 19 are fixed on the U-shape connector 16 and the connector 18 respectively. During the rehabilitation, the motor 19 can make the two rings (therefore the foot) do dorsiflexion/plantar flexion rotation with respect to the ring gear. The motor 17 can make the gear ring (therefore the foot) do eversion and inversion rotation with respect to the calf supports. The motor 10 can realize the adduction and abduction rotation.

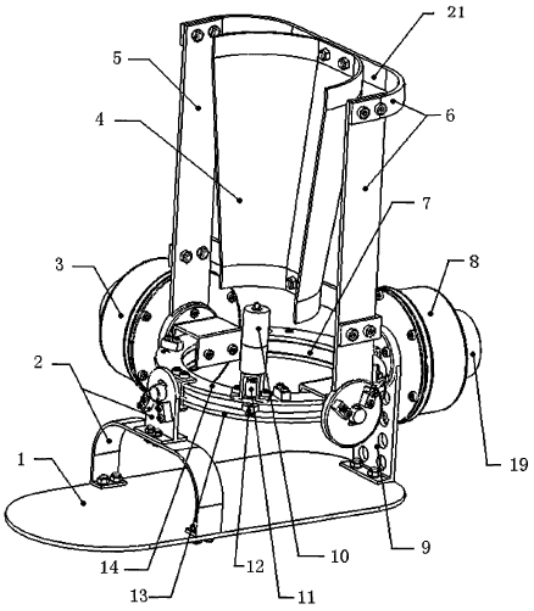

Figure II.1. 64. The assistant movement exoskeleton with a perspective view. [83]

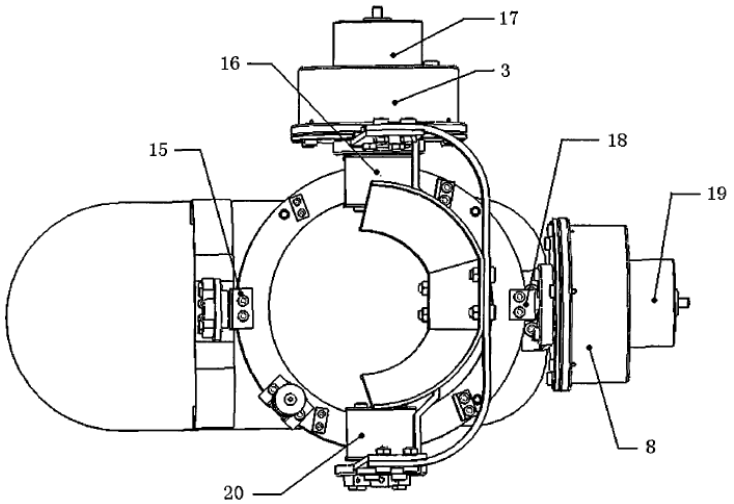

Figure II.1. 65. The assistant movement exoskeleton with a top view. [83]

A medical rehabilitation and treatment apparatus for stretching paralyzed ankle is provided by Yu Cheol [84] to easily supply a proper force to the ankle just by means of an electrical driving. In Figure II.1. 66, the motor 108, fixed with the frame and the calf support, controls the ankle rotation by the connecting rod 103.

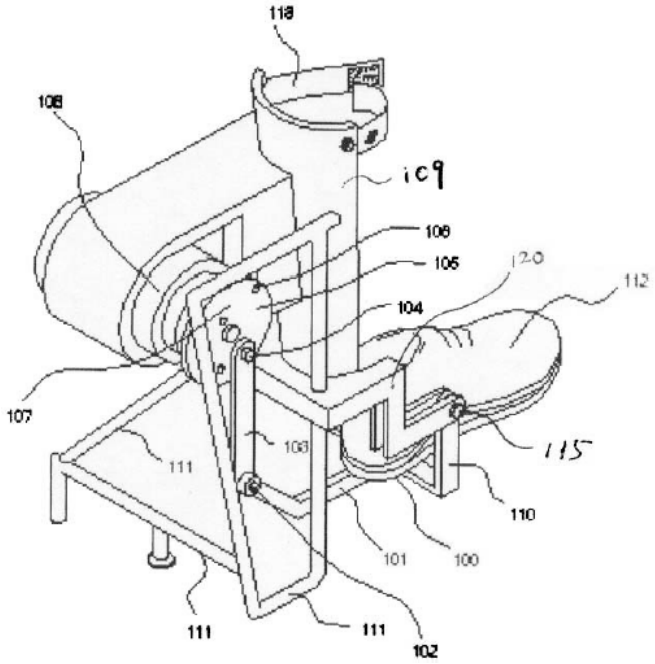

Figure II.1. 66. An apparatus for stretching paralyzed ankle. [84]

T. Herve and L. Gerald [85] patented an orthosis device consisting of an anklet (2) and a sole (4) with an anatomically-shaped layer (7), connected by an elastic, e.g. pneumatic or hydro-pneumatic, power cylinder (10) that assists the movement of the foot (Figure II.1. 67). The connection between the sole and the power cylinder's rod (15) has a universal joint (18). The structure makes the orthosis device compact and portable.

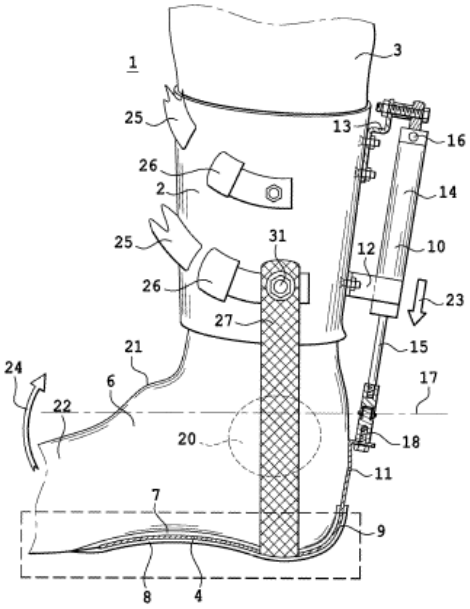

Figure II.1. 67. An orthosis device driven by an elastic actuator. [85]

Jack Bastow [86] patented a device (Figure II.1. 68 and Figure II.1. 69) is to train inversion/eversion rotation of the subtalar joint and dorsal/plantar flexion of the ankle joint. The device uses fluid chambers for hydraulic resistance. A method for strengthening an ankle is also provided.

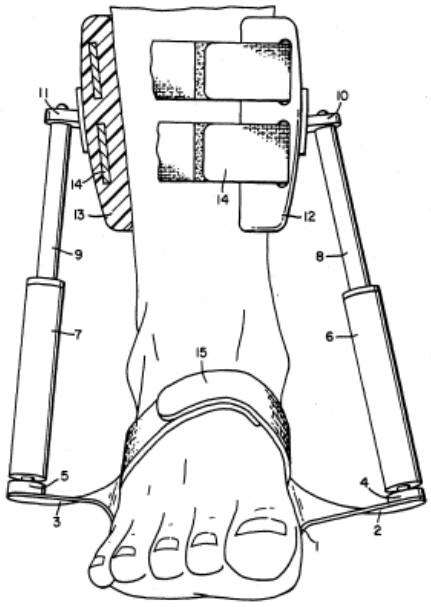

Figure II.1. 68. The frontal view of the device invented by J. Bastow[86]

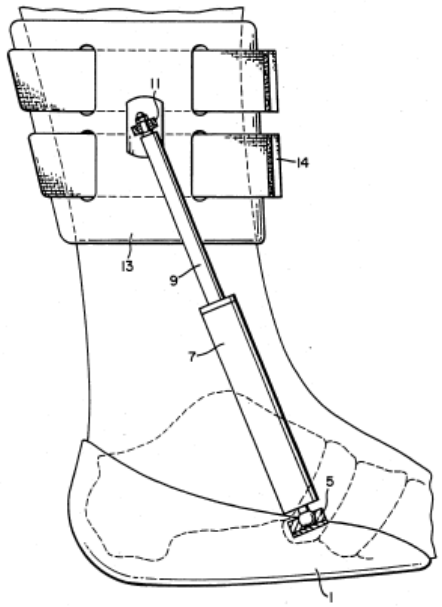

Figure II.1. 69. The lateral view of the device invented by J. Bastow[86]

Among these valuable work, most of them are bulky, especially considering the volume and the mass of the control and interaction components. Some of them can only control one or two DOFs of the ankle joint. A good rehabilitation system should be compact and portable, functionally satisfied, safe, considering the bio-mechanics of the ankle and the foot. Next chapter, we will investigate the characters of the foot and the ankle, including the kinematics and dynamics, ergonomics, safety, torque properties and so on. A good rehabilitation system should be based on the considerations of these factors.

References:

[1] Jian S. Dai, Tieshi Zhao and Christopher Nester. Sprained Ankle Physiotherapy Based Mechanism Synthesis and Stiffness, Autonomous Robots Vol. 16, pp. 207–218, 2004.

[2] Girone M, Burdea G, J. E. Deutsch, et al. Orthopedic rehabilitation using the "Rutgers ankle" interface. In Virtual reality meets Med. Amsterdam, The Netherlands: Ios Press; 2000:89–95.

[3] Mingming Zhang, T Davies, Shane Xie. Effectiveness of robot-assisted therapy on ankle rehabilitation – a systematic review. Journal of Neuroengineering and rehabilitation, 2013, 10-30.

[4] DMSystems, Inc. Ankle Tough, http://dmsystems.com/, 1999.
[5] Perform Better, Biofoam Rollers, http://www.performbetter.com/page11.html, 1999.
[6] Kinetic Health Corporation, Wobble and Rocker Boards, http://www.kinetichealth.com/edu11.html, 1999.
[7] M. Girone, G. Burdea, M. Bouzit, V.G. Popescu, and J. Deutsch, A Stewart Platform-based System for Ankle Tele-rehabilitation, invited article, Special Issue on Personal Robotics, Autonomous Robots, Vol. 10, pp. 203-212, Kluwer, March 2001.
[8] R.F. Boian, C.S. Lee, J.E. Deutsch, G. Burdea and J.A. Lewis, Virtual Reality-based System for Ankle Rehabilitation Post Stroke, 1st International Workshop on Virtual Reality Rehabilitation (Mental Health, Neurological, Physical, Vocational) VRMHR 2002 Lausanne, Switzerland, November 7-8, 2002, pp. 77-86, 2002.
[9] M. Girone, G. Burdea, M. Bouzit, V.G. Popescu, and J. Deutsch, A Stewart Platform-based System for Ankle Telerehabilitation, invited article, Special Issue on Personal Robotics, Autonomous Robots, Vol. 10, pp. 203-212, Kluwer, March 2001.
[10] M. Girone, et al. Ankle rehabilitation system. US patent No. 6162189.
[11] M. Girone, G. Burdea, and M. Bouzit. The "Rutgers Ankle" Orthopedic Rehabilitation Interface. In Proceedings of the Haptics Symposium. DSCD, ASME WAM. Nashville, Tennessee, 1999.
[12] D. Stewart, A platform with 6 degrees of freedom. In Proc. Of the Institution of Mechanical Engineers, 66, 1965.
[13] V. Popescu, G. Burdea, M. Bouzit, and V. Hentz, A Virtual Reality-based Telerehabilitation system with Force Feedback. In IEEE Transactions on Information Technology in Biomedicine, 7, 1999.
[14] Deutsch JE, Paserclia C, Vecchione C, Mirelman A, Lewis JA, Doian R, Burclca G: Improved gait and elevation speed of individuals poststroke after lower extremity training in virtual environments. Journal of Neurological Physical Therapy 2004, 28:185–186.
[15] Deutsch JE, Latonio J, Burdea GC, Boian R: Post-stroke rehabilitation with the Rutgers ankle system: a case study. Presence 2001, 10:416–430.
[16] Deutsch JE, Latonio J, Burdea GC, Boian R: Rehabilitation of musculoskeletal injuries using the Rutgers ankle haptic interface: three case reports. In Eurohaptics conference. Birmingham, UK: 2001:11–16.
[17] Burdea GC, Cioi D, Angad K, Janes WE, Ross SA, Engsberg JR: Robotics and gaming to improve ankle strength, motor control and function in children with cerebral palsy-a case study series. IEEE Transaction on Neural System and Rehabilitation Engineering 2012, pp (99):1.
[18] Zhao, T.S., Dai, J.S., and Huang, Z. Geometric synthesis of spatial parallel manipulators with fewer than six degrees of freedom. Journal of Mechanical Engineering Science, 2002a, 216(C12):1175–1186.
[19] Zhao, T.S., Dai, J.S., and Huang, Z. Geometric analysis of over-constrained parallel manipulators with three and four degrees of freedom. JSME International Journal, 2002b, 45(3): 730–740.

[20] Dai, J.S. and Kerr, D.R. Geometric analysis and optimisation of symmetrical watt 6bar mechanisms. J. Mechanical Engineering Science, 1991, 205(C1):275–280.
[21] Dai, J.S., Sodhi, C., and Kerr, D.R. Design and analysis of a new six-component force transducer for robotic grasping. In Proceedings of the Second Biennial European Joint Conference on Engineering Systems Design and Analysis, London. ASME PD, 1994, vol. 64, no. 8–3, pp. 809–817.
[22] Dai, J.S. and Kerr, D.R. A six-component contact force measurement device based on the Stewart platform. Journal of Mechanical Engineering Science, 2000, IMECHE, 214(C5):687–697.
[23] Mark E. Stodgell. Ankle rehabilitation device. US patent No. 5368536.
[24] Matteo Malosio, Simone Pio Negri, et al. A Spherical Parallel Three Degrees-of-Freedom Robot for Ankle-Foot Neuro-Rehabilitation. 34th Annual International Conference of the IEEE EMBS San Diego, California USA, 28 August - 1 September, 2012.
[25] C. Gosselin, E. S. Pierre, and M. Gagne. On the development of the agile eye, Rob.& Aut. Mag., IEEE, vol. 3, no. 4, pp. 29–37, 1996.
[26] Jungwon Yoon, Jeha Ryu and Kil-Byung Lim. Reconfigurable Ankle Rehabilitation Robot for Various Exercises. Journal of Robotic Systems 22 (Supplement), S15–S33 (2006).
[27] Jungwon Yoon, Jeha Ryu. A New Family of Hybrid 4-DOF Parallel Mechanisms with Two Platforms and Its Application to a Footpad Device. Journal of Robotic Systems 22(5), 287–298, 2005.
[28] Zhang L-Q, Chung SG, Bai Z, Xu D, Rey EMT, Rogers MW, Johnson ME, Roth E J, Intelligent stretching of ankle joints with contracture/spasticity. IEEE Trans Neural Syst Rehabil Eng 2002, 10:149–157.
[29] Selles RW, Li X, Lin F, Chung SG, Roth EJ, Zhang L-Q. Feedback-controlled and programmed stretching of the ankle plantarflexors and dorsiflexors in stroke: effects of a 4-week intervention program. Arch Phys Med Rehabil 2005, 86: 2330–2336.
[30] Wu Y-N, Ren Y, Hwang M, Gaebler-Spira DJ, Zhang L-Q: Efficacy of robotic rehabilitation of ankle impairments in children with cerebral palsy. In 32th Annual international conference of the IEEE engineering in medicine and biology society; august 31-september 4. Buenos Aires, Argentina: 2010:4481–4484.
[31] Wu YN, Hwang M, Ren YP, Gaebler-Spira D, Zhang L-Q: Combined passive stretching and active movement rehabilitation of lower-limb impairments in children with cerebral palsy using a portable robot. Neurorehabil Neural Repair 2011, 25:378–385.
[32] Waldman G, Wu YN, Ren Y, Li Y, Guo X, Roth EJ, Wang L, Zhang LQ: Stroke rehabilitation using a portable robot improves biomechanical and clinical outcome measures. In International stroke conference and nursing symposium poster presentations. Los Angeles, USA: The American Heart Association; 2011:e128.
[33] J. A. Saglia, N. G. Tsagarakis, J. S. Dai, and D. G. Caldwell. A high-performance redundantly actuated parallel mechanism for ankle rehabilitation. International Journal of Robotics Research, vol. 28, no. 9, pp. 1216–1227, 2009.
[34] Saglia JA, Tsagarakis NG, Dai JS, Caldwell DG. Assessment of the assistive performance of an ankle exerciser using electromyographic signals. In

International conference of the IEEE engineering in medicine and biology society. Buenos Aires, Argentina: IEEE; 2010:5854–5858.
[35] Saglia, J. A. and Dai, J. S. Geometry and kinematic analysis of a redundant type parallel mechanism for rehabilitation. Proceedings of the ASME International Design Engineering Technical Conferences and Computers and Information in Engineering Conference, LasVegas,NV, September, 2007.
[36] Saglia, J. A., Dai, J. S., and Caldwell, D. G. Geometry and kinematic analysis of a redundantly actuated parallel mechanism that eliminates singularities and improves dexterity. Transactions of the ASME: Journal of Mechanical Design, 130(12): 124501, 2008.
[37] Saglia, J. A., Tsagarakis, N.G., Dai, J. S., and Caldwell, D. G. Inverse-kinematics-based control of a redundantly actuated platform for rehabilitation. Proceedings of the Institution of Mechanical Engineers, Part I: Journal of Systems and Control Engineering, 223(1): 53–70, 2009.
[38] Syrseloudis C, Emiris I, Maganaris C, Lilas T. Design framework for a simple robotic ankle evaluation and rehabilitation device. Proc. 30th IEEE Intern. Conf. Engineering in Medicine & Biology, 2008. 1410–1413, Vancouver, Canada.
[39] Syrseloudis C, Emiris I. A Parallel Robot for Ankle Rehabilitation: Evaluation and its Design Specifications. 8th IEEE Intern. Conf. Bioinformatics & Bioengineering, 2008. 1-6, Athens, Greece.
[40] Dul J, Johnson GE. A kinematics model of the human ankle. J. Biomedical Engineering, 1985, 7:137–143.
[41] Lee K, Shah D.K. Kinematic Analysis of a three degrees of freedom in parallel actuated manipulator. J. Robotics and Automation, 1988, Vol 4(3) pages 354-60.
[42] Malack, Ding et al. Virtual Ankle and Balance Trainer System. US patent No. US20110256983.
[43] Tiecheng Zhu, Fali Zhu. Ankle joint passive movement device with adjustable fluctuation velocity and Angle. China patent NO. CN201894723U.
[44] Tiecheng Zhu, Gaoyong Cui. Ankle joint active movement equipment. China patent NO. CN201894722U.
[45] Lixun Zhang, Wei Wang. Rope-drawn rehabilitation training machine for ankle joint. China patent NO. CN201870898U.
[46] A. Austen. Shock absorber ankle exercise device. US patent No. US7892154.
[47] V. Mikhajlovich et al. Ankle working out and muscle and ligament stimulation apparatus. Russia patent No. RU2408352.
[48] Gil Alvarez Juan Jose. Rehabilitation device, in particular for the foot. Patent No. ES1072371U.
[49] Hong Yue, Xiaojun Zhang, et al. Rehabilitation robot for anklebone. China Patent No. CN201168163U.
[50] Liju Xu et al. Ankle joint rehabilitation training device. China Patent No. CN101006958.
[51] H. Craig. Ankle rehabilitation device. US patent No. US6277057.
[52] Y. Mikio. Ankle exercising device. Japan Patent No. JP2876204.
[53] F. Russell. Exerciser for lower leg, ankle, and foot muscles. US patent No. US4186920.
[54] A. Giguere. Apparatus for foot rehabilitation. Canada Patent No. CA1021818.

[55] M. Stewart. Rehabilitation machine. Great Britain Patent NO. GB1112288.
[56] J. L. Pons, Wearable Robots: Biomechatronic Exoskeletons. Wiley, New York, NY (2008).
[57] Mohammed S, Amirat Y, Rifai H: Lower-limb movement assistance through wearable robots: state of the Art and challenges. Advanced Robotics 2012, 26:1–22.
[58] Furusho J, Kikuchi T, Tokuda M, Kakehashi T, Ikeda K, Morimoto S, Hashimoto Y, Tomiyama H, Nakagawa A, Akazawa Y. Development of shear type compact MR brake for the intelligent ankle-foot orthosis and its control. In 2007 IEEE 10th international conference on rehabilitation robotics; 12–15 June. Noordwijk, Netherlands: IEEE Computer Society; 2007:89–94.
[59] Tanida S, Kikuchi T, Kakehashi T, Otsuki K, Ozawa T, Fujikawa T, Yasuda T, Furusho J, Morimoto S, Hashimoto Y. Intelligently controllable ankle foot orthosis (I-AFO) and its application for a patient of guillain-barre syndrome. In 2009 IEEE international conference on rehabilitation robotics, ICORR 2009, June 23, 2009 - June 26, 2009. Kyoto, Japan: IEEE Computer Society; 2009:857–862.
[60] Blaya JA, Herr H. Adaptive control of a variable-impedance ankle-foot orthosis to assist drop-foot gait. IEEE Trans Neural Syst Rehabil Eng 2004, 12:24–31.
[61] Daniel P. Ferris et al. An Ankle-Foot Orthosis Powered by Artificial Pneumatic Muscles. J Appl Biomech. 2005 May, 21(2): 189–197.
[62] Gregory S Sawicki, Daniel P Ferris. A pneumatically powered knee-ankle-foot orthosis (KAFO) with myoelectric activation and inhibition. Journal of NeuroEngineering and Rehabilitation, 2009, 6-23.
[63] Sawicki GS, Domingo A, Ferris DP. The effects of powered ankle-foot orthoses on joint kinematics and muscle activation during walking in individuals with incomplete spinal cord injury. Journal of Neuro engineering and Rehabilitation 2006, 3:3.
[64] Ward J, Sugar T, Standeven J, Engsberg JR. Stroke survivor gait adaptation and performance after training on a powered ankle foot orthosis. In 2010 IEEE international conference on robotics and automation; 3–8 May. Anchorage, USA: IEEE; 2010:211–216.
[65] Anindo Roy, Hermano Igo Krebs, et al. Robot-Aided Neurorehabilitation: A Novel Robot for Ankle Rehabilitation. IEEE TRANSACTIONS ON ROBOTICS, VOL. 25, NO. 3, 569-583, 2009.
[66] Jason W. Wheeler, Hermano Igo Krebs. An Ankle Robot for a Modular Gait Rehabilitation System. For the degree of Master of Science in Mechanical Engineering at the Massachusetts Institute of Technology.
[67] Roy A, Forrester LW, Macko RM. Short-term ankle motor performance with ankle robotics training in chronic hemiparetic stroke. J Rehabil Res Dev 2011, 48:417–430.
[68] Kartik Bharadwaj et al. Design of a Robotic Gait Trainer using spring over Muscle Actuators for Ankle Stroke Rehabilitation. Journal of Biomechanical Engineering, 1009-1014, Vol. 127, NOVEMBER 2005.
[69] Aykut Satici, Ahmetcan Erdogan, Volkan Patoglu. Design of a Reconfigurable Ankle Rehabilitation Robot and Its Use for the Estimation of the Ankle

Impedance. 2009 IEEE 11th International Conference on Rehabilitation Robotics. Japan, June 23-26, 2009.
[70] Simone Pittaccio, Stefano Viscuso. Shape Memory Actuators for Medical Rehabilitation and Neuroscience. Smart Actuation and Sensing Systems – Recent Advances and Future Challenges, pp: 83-120, InTech Press.
[71] Norihiko Saga. Development of a Tendon Driven System using a Pneumatic Balloon. Journal of Intelligent Material Systems and Structures 2007, 18: 171.
[72] Saga, N., Saito, N., and Nagase, J. Ankle Rehabilitation Device to Prevent Contracture Using a Pneumatic Balloon Actuator. Int. J. of Automation Technology, Vol.5, No.4, 2011.
[73] Song Yin et al. Parallel type multi-freedom artificial limb exoskeleton ankle joint. China patent, NO. 200810034002.7.
[74] Yupeng Ren, Tao Xu, Liang Wang, et al. Develop a wearable ankle robot for in-bed acute stroke rehabilitation. Engineering in Medicine and Biology Society, EMBC, 2011 Annual International Conference of the IEEE, pp: 7483-7486, 2011.
[75] Yupeng Ren, Liqun Zhang. Wearable and convertible passive and active movement training robot: apparatus and method. US Patent No. US20120165158.
[76] Abhishek Agrawal, Sai K. Banala, Sunil K. Agrawal. Design of a Two Degree-of-freedom Ankle-Foot Orthosis for Robotic Rehabilitation. Proceedings of the 2005 IEEE 9th International Conference on Rehabilitation Robotics, 2005, Chicago, IL, USA.
[77] Mirbagheri MM, Tsao C, Pelosin E, Rymer WZ. Therapeutic effects of robotic-assisted locomotor training on neuromuscular properties. International Conference on rehabilitation robotics. Chicago, USA. 2005, pp: 561–564.
[78] Shorter KA, Kogler GF, Loth E, Durfee WK, Hsiao-Wecksler ET. A portable powered ankle-foot orthosis for rehabilitation. J Rehabil Res Dev 2011, 48:459–472.
[79] Hongbo Wang, Qing Guo, Lin Yuan et al. The lower limb recovery trains the robot ankle joint device. China Patent No. CN102028607.
[80] Indian Song. Workout trainer of rehabilitation of multi-variant ankle joint of parallel type. China Patent NO. CN101999970.
[81] Rodgers Darelle. Orthopaedic rehabilitation mechanism employing a foot support having a first portion and second portion configured to rotate with respect to one another. US Patent No. US20110071441.
[82] Vincent Gibbons. Calf enhancer for the lower extremity. US Patent No. US20110040225.
[83] Jiafan Zhang, Yu Zhang. Assistant movement exoskeleton of three-degree of freedom ankle joint. China Patent No. CN101596139.
[84] Yu Seung Cheol. Medical treatment apparatus for stretching paralyzed ankle. Patent No. KR20050033113.
[85] Teyssedre Herve, Lefort Gerald. Dynamic orthesis. Patent NO. EP1382317.
[86] Jack Bastow. Ankle rehabilitation device. US Patent NO. US5215508.

Section II.2 Design requirements of the rehabilitation robot

This chapter focuses on the design requirements of the rehabilitation robot. A proper rehabilitation robot should be designed based on a clear investigation of the ankle structure and its biomechanics. The robotic structure should take care of the interface and safety issues, matched with the patient ankle. The actuation system should provide the suitable torques and power considering the ankle properties. The sensors and control system should also be designed and have a proper layout to aim to train and evaluate the ankle with all possible activities (such as active or passive activities).

This chapter firstly investigates properties of the foot ankle. The foot ankle is a part of lower extremity. It has close connection with other parts in structure and biomechanics points of view. Therefore, it is inevitable to refer to other parts of the lower extremity when we analyse the ankle properties. After the structure of foot ankle is introduced, biomechanics of the foot ankle is studied, consisting of static and dynamic parts. In static part, load distribution and inner-function of the foot ankle during ambulation is discussed. In dynamic part, not only the normal dynamics is included, but also the abnormal dynamics. Range of motion (RoM) is shown according to different rotational degrees of freedom (DOF). After that, torques used to drive the ankle are also classified and discussed. This part could be a good guideline for the choice of the motor. Then, control strategies and other details are presented.

II.2.1 Structure of the foot ankle

The ankle, or talocrural region [1], is the region where the foot and the leg meet (Figure II.2. 1). The ankle includes three joints: the ankle joint or talocrural joint, the subtalar joint, and the Inferior tibiofibular joint. In common usage, the term ankle refers exclusively to the ankle region. In medical terminology, "ankle" (without qualifiers) can refer broadly to the region or specifically to the talocrural joint. The main bones of the ankle region are the talus (in the foot), and the tibia and fibula (in the leg). The talus is also called the ankle bone. The talocrural joint, is a synovial hinge joint that connects the distal ends of the tibia and fibula in the lower limb with the proximal end of the talus. The articulation between the tibia and the talus bears more weight than between the smaller fibula and the talus.

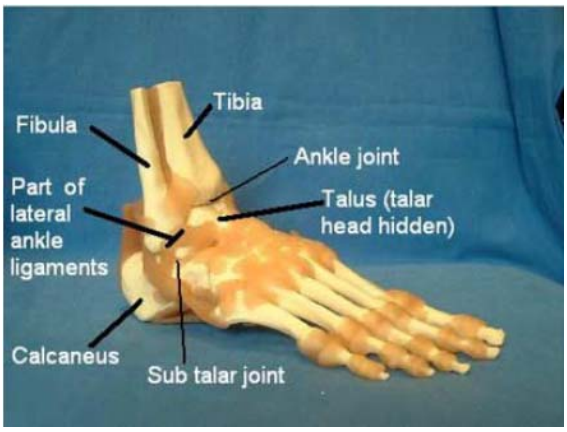

Figure II.2. 1. The ankle structure[1]

II.2.2 Biomechanics of the foot ankle

The design of the rehabilitation robot for ankle must be based on a deep investigation of ankle's structure and its biomechanics. Biomechanics of the foot and ankle is important for weight bearing and ambulation. Basically speaking, the biomechanics can be divided into static and dynamic components [2].

II.2.2.1 Statics of the foot ankle

Static structure mainly includes bones, joint surface congruity, ligaments and fascia. Research shows [3] that muscle activity does not support the full load at rest. The arch on foot, maintained by passive ligamentous and osseous support, plays a necessary role in weight bearing. The stress of weight bearing, in details, is mainly supported by two resources: the beam action of the metatarsals (25%) and the tensile strength of the plantar aponeurosis (60%), in static stance position [5][6]. The plantar and the calcaneonavicular ligaments are also assistive in the passive maintenance of the arch. Moreover, the tension in the plantar aponeurosis is helpful for the supination of the subtalar joint during ambulation. As aponeurosis becomes taut with toe extension, its ability to absorb stress increases. For the stabilization of the foot, the joint alignment and congruity of the metatarsal and tarsal bones (Figure II.2. 2) play a critical role.

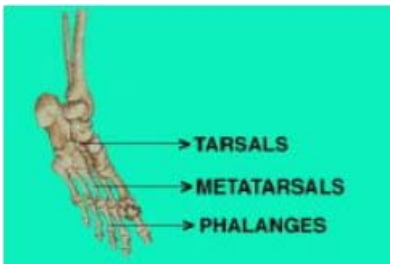

Figure II.2. 2. The structure of foot bones[35]

II.2.2.2 Dynamic of the foot ankle

II.2.2.2.1 Normal dynamic structure

Movement of the foot and ankle is a complex action involving many joints, which are mainly called pronation and supination. Both processes refer to a combination of motions in sagittal, frontal, transverse planes (Figure II.2. 12). Pronation includes abduction, dorsiflexion, eversion, while supination includes adduction, plantar flexion, and inversion (Figure II.2. 9-Figure II.2. 11). These motions involve complex rotation of the ankle. Five tri-plane joints and five joints are identified by Root et al. [7].

Pronation occurs in the stance of gait for shock absorption, ground terrain changes and balance [2]. About 60% of the gait cycle is weight bearing, as the stance phase of gait (Figure II.2. 3).

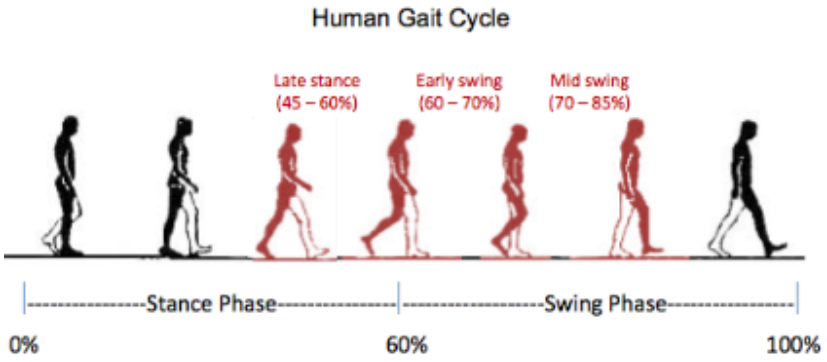

Figure II.2. 3. A cycle of gait[36]

Four basic forces act on the foot and the lower limb from heel strike to toe strike. Firstly, upon heel strike, 80% of body weight acts directly on the calcaneous, producing a vertical force against the ground. Interaction of the tibia, talus, and calcaneous attenuates the vertical compressive forces in a safe way. The force of weight bearing is then gradually distributed between the calcaneous and the matatarsals, which makes the tarsals and the metatarsals are in a mutual compression. Secondly, an anterior shearing force is also from the tibia, acting on the talus. This force is decelerated mainly by the gastroc/soleus muscle group. Thirdly, a medial shearing to the foot, from the internal rotation of the lower limb, is absorbed by the subtalar joint consisting of the talus (5) and the calcaneous (4). As a result, the calcaneous moves laterally or into valgus. The talus also rolls with some angle. Finally, these motions result in the sustentaculum tali (3) falling along with the talus. The rotation of the talus and the calcaneous is described as the torque converter of the lower limb (Figure II.2. 4).

During ambulation, the foot does not rotate in the stance phase of gait. The transverse rotations of the tibia and the femur are transmitted and reduced at the sub-talar joint. The transverse rotations of the lower limb are converted into the tri-plane motions of

pronation and supination. During pronation, the foot moves from the heel strike to the toe strike, three muscles are active and control the motion. These muscles are called supinators, including anterior tibialis, extensor digitorium longus, and extensor hallicus longus.

Supination occurs at the end of the stance phase of gait [2]. Electromyography (EMG) shows that many muscles, including extrinsic and intrinsic muscles, involve the supination, especially gastroc/soleus, posterior tibialis, flexor digitorium longus, and the flexor hallicus longus. Moreover, the external rotation of lower limb plays an important role in supination. The contralateral limb swings forward and an external rotation force occurs, which causes a lateral shearing force within the foot. The calcaneous inverts and the subtalar joint initiates supination. A locking mechanism occurs between the cuboid (1) and the navicular (2), making bones act as rigid levers and more efficiently pull the peroneus longus and the posterior tibialis (Figure II.2. 5). The MTP (metatarsal phalangeal) joint also helps supination. Because the joint's dorsiflexion increases the tension of the plantar aponeurosis and therefore assists the subtalar joint supination. During the stance phase of gait, the foot pronates at heel strike, passes through neutral and starts to supinate at mid-stance.

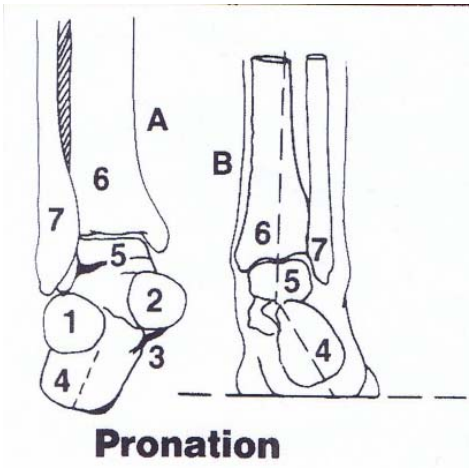

Figure II.2. 4. Dynamic analysis of pronation.[2]

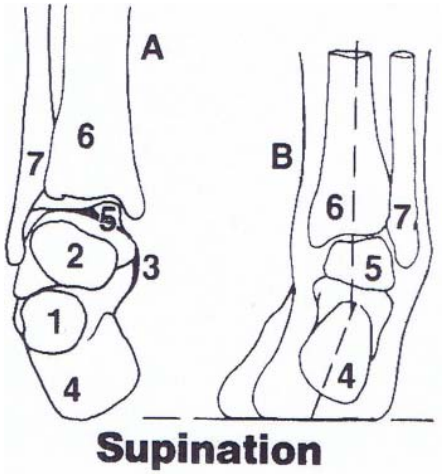

Figure II.2. 5. Dynamic analysis of supination. [2]

II.2.2.2.2 Abnormal dynamic structure

The investigation for abnormal biomechanics of the foot and ankle is helpful for use of orthotics to re-establish the normal mechanics and recover the normal functions of the foot and ankle. It is also useful to study pathologies of some neurological injuries such as heel spurs, hallux valgus, neuromas, hallux limitus, shin splints, and nonspecific knee pain [8].

Abnormal pronation is a compensation for a soft tissue or osseous deformity [4]. In this case, excessive pronation occurs at the subtalar joint and result in pathology. If the foot

pronates beyond 25% of the stance phase, it has excessive pronation. Maximum pronation happens at foot flat. Excessive pronation results in the inability of the foot to effectively attenuate the stress of weight bearing. Many factors can explain the etiology of abnormal pronation. Congenital, developmental, intrinsic (within the foot), and/or extrinsic (outside the foot) are common categories. Intrinsic congenital deformities commonly include convex pes valgus, tarsal coalitions, and congenital metatarsus varus. Convex pes valgus is a primary dorsal and lateral dislocation of the talocaneonavicular joint. The navicular articulates with the dorsal aspect of the talus, locking it in the vertical position. Tarsal coalitions include complete or incomplete fusion of the major tarsal bones. The coalitions producing a flatfoot are, calcaneonavicular or talocalcaneal at the middle, anterior, or posterior facet. Congenital metatarsus varus is medial subluxation of the tarsometatarsal joints with adduction and inversion deformity of the metatarsals. An important clinical finding is the inability of the forefoot to be passively abducted to the neutral position.

The developmental deformities intrinsic to the foot include talipes calcaneovalgus, talipes calcaneovarus, postural metatarsus adduction, and forefoot varus [4]. Calcaneovalgus is a common postural deformity. Its appearance is one of dorsiflexion and eversion. In this deformity, the range of the plantarflexion is usually limited to 90° or less at the ankle joint. Calcaneovarus is the inversion of the entire foot. Forefoot varus is the most common intrinsic deformity, resulting in abnormal pronation. It is an inversion of the forefoot on the rear-foot with the subtalar joint in neutral, deformed in a frontal plane [7]. It is normally compensated at the subtalar joint by eversion or a valgus position of the calcaneus in weightbearing, causing mechanical pain and dysfunction within the foot. McCrea [8] defined forefoot varus as a sagittal plane deformity of the first ray. Due to the inability of the peroneus longus to stabilize the first ray, the first ray has hypermobility. A cuboid pulley (1) allows the peroneus longus (P) to plantarflex and abduct the first ray with stability, as shown in part A of Figure II.2. 6. During the supination of the subtalar joint, the mid-tarsal joint locks the pulley. Abnormal or excessive pronation reduces the ability of the foot to return to supination. In this case, the cuboid is in a poor position, causing instability of the first ray, as shown in part B of Figure II.2. 6. F and C are plantar flexion and abduction vectors. The dorsiflexed and hypermobile first ray causes a hallux valgus, which inability results the shift of the weight from the first to the second metatarsal. But the second ray is not designed to take the excessive forces of weight-bearing. Therefore, a callus or keratosis is a common result.

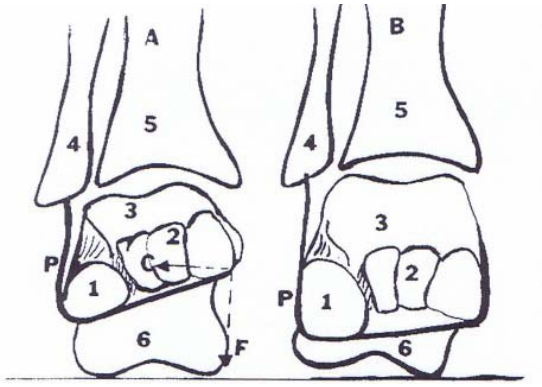

Figure II.2. 6. Cuboid pulley. [4]

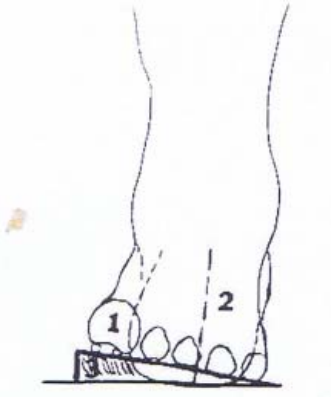

Figure II.2. 7. The correction of a forefoot varus with a medial post[4]

Extrinsic congenital or developmental deformities, such as hip dysplasia, pelvic imbalances, and muscle imbalances within the pelvis and lower extremity, can also result in abnormal pronation. These deformities produce a rotation of the lower limb that could be compensated by pronation of the subtalar joint. The excessive kinematic movements occur between four bones: calcaneus, talus, navicular and cuboid. The weight-bearing stress is more medial causing a medial force to the heel, resulting in a valgus heel. These excessive kinematic movements also cause some changes in the mechanics of the foot that can be observed, such as valgus position of the calcaneus, abduction of the forefoot on the rearfoot, a reduction in the height of the medial arch.

Abnormal supination has three cases. The first one is a pes cavus foot with a fixed plantarflexed forefoot (or an equinus forefoot) and a neutral rearfoot under weightbearing. The second one is pes cavo varus with a fixed plantarflexed medial column or first ray and a varus calcaneus under weightbearing. Root et al. defined the inversion of the calcaneus is a compensation of a forefoot valgus. Pes qeuinovarus is the third case with a fixed plantarflexed forefoot and rearfoot. Abnormal supination is the inability of the foot to pronate. In normal situation, the foot starts pronation at heel strike. An excessive supination lasts through the stance phase or late in stance. In this case, more trauma happen to the foot.

A functional biomechanical orthotic is designed to restore normal alignment of the subtalar and midtarsal joints, controlling excessive pronation and supination, reducing the abnormal forces through the kinetic chain. The general function of an orthotic is to support the forefoot varus or valgus deformity and reposition the rearfoot (subtalar joint) as close as possible to neutral. Figure II.2. 7 shows an example to correct a forefoot varus with a medial post (3), bring the ground up to the first ray (1) and keeping the calcaneus (2) in neutral. A post or support is designed as a wedge with the same angle as measured forefoot varus deformity.

It is also important to evaluate muscle imbalances extrinsic and intrinsic to the foot for the improvement of the forefoot and rear foot deformities. The treatment, therefore, includes correction with the foot and the lower extremity. Basically speaking, the muscles

are responsible for foot and ankle movement up and down (dorsiflexion and plantar flexion) and turning in and out (inversion and eversion). Tendons are the part of the muscle that attaches the muscle to the bone.

In addition to movement, strong muscles provide active stability to the ankle as opposed to the passive stabilization of the ligaments. The major muscles of the ankle include the gastrocnemius and soleus (calf) muscles, which push the foot down and allow us to go up on our toes. These two large muscles join at the ankle to form the Achilles tendon. The two peroneal muscles, longus and brevis, are located on the outside of the ankle, and push the foot down (plantar flexion) and turn it out (eversion). They also support the lateral ankle to prevent sprains. The posterior tibialis is located on the inside of the ankle, and supports the arch of the foot and helps turn the ankle in (inversion). The anterior tibialis muscle attaches to the front of the foot, and helps lift it up (dorsiflexion).

II.2.3 Range of motion (RoM) for the ankle joint

Basically speaking, the ankle joint which controls the rotation of a foot is usually considered as a single joint. But actually, the rotation of a foot is governed by two joints, the ankle joint and the sub talar joint which both have close relation and play different roles in motion (Figure II.2. 8). These two joints operate three rotation directions, dorsiflexion and plantar flexion, eversion and inversion, internal and external rotation (Figure II.2. 9-Figure II.2. 11). Take the right foot as an example, the range for every rotation is listed in Table II.2. 1.

Figure II.2. 8. X-ray for the relative positions of ankle and sub talar joints in the lateral view.[1]

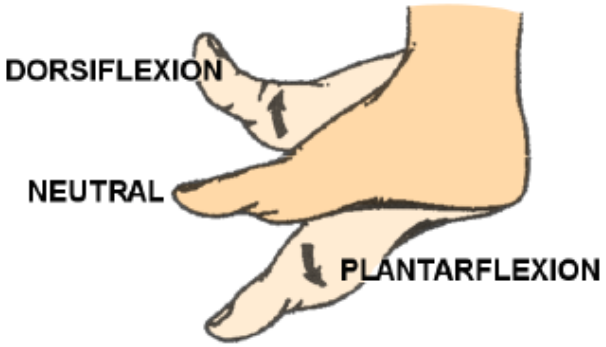

Figure II.2. 9. Dorsiflexion and plantar flexion[34]

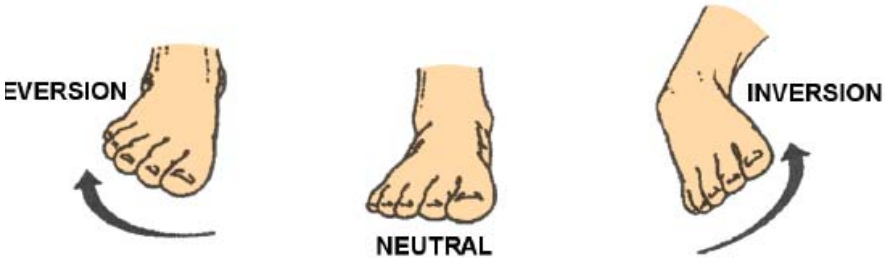

Figure II.2. 10. Eversion and inversion[34]

Figure II.2. 11. Abduction and adduction[34]

Table II.2. 1. The RoM for different degrees of freedom

Degrees of Freedom	Dorsiflexion(-) plantarflexion(+)	Eversion(-) inversion (+)	Abduction(-) adduction(+)
Range of Motion			
Normal subjects[9]	-25°, 45°	-20°, 25°	-15°, 15°
Normal subjects[10]	(-42°, -30°), 35°	-25°, 25°	(-30°, -25°), (25°, 30°)
Male subjects, 30-40 years [11]	(-40°, -5°), (10°, 55°,)	(-50°, -15°), (15°,50°)	--
Standard reference from AAOS [12]	-18°, 48°	-18°, 33°	--
Male subjects [13]	(-17°, -8.2°), (50.1°, 62.3°)	(-25.7°, 15.7°), (32.3°, 41.3°)	--
Male subjects no more than 19 years[13]	(-17.7°, -9.7°), (52.1°, 64.3°)	(-26.9°, -17.7°) (32.8°, 42.2°)	--
Male subjects more than 19 years[13]	(-16.3°, -8.1°), (48.4°, 60.2°)	(-24.1°, -14.1°) (32°, 40.4°)	--

From the table, we know that the RoM from different research groups normally has different values. The specific values of the RoM normally depend on the subject age, sex and healthy conditions. Any rehabilitation device should be designed to reach the ROM

for every degree of freedom (DOF). There are three planes to define the motion range of the ankle joint, as shown in Figure II.2. 12 and Figure II.2. 13. In detail, sagittal plane is defined by x and z and movements occur around the y axis. Transverse plane is defined by x and y and movements in this plane occur around the z axis; and frontal plane is defined by y and z and movements in this plane occur around the x axis.

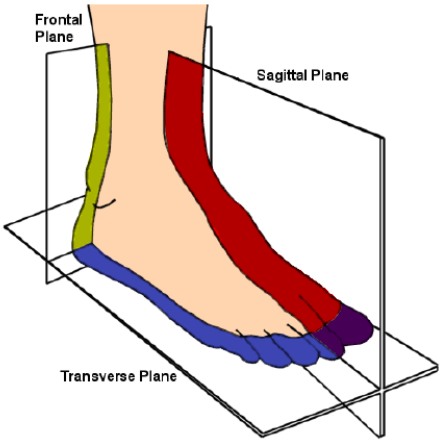

Figure II.2. 12. Three planes to define the ankle motion.[34]

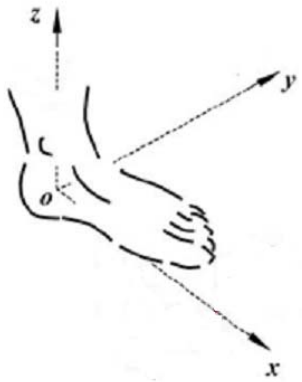

Figure II.2. 13. Cartesian coordinate for the motion description of the ankle joint[1]

II.2.4 The ankle torque

Torques are applied by muscles in the lower extremity to drive the motion of the foot ankle. In rehabilitation of the foot ankle, the ranges of torques supplied by rehabilitation devices are based on the investigation of the ankle's dynamics. Muscles which are normally distributed around the lower extremity can drive the ankle with torques. This part will support the choices of motors for the rehabilitation device.

Many references ([10], [14]-[17]) show a universal range for torques needed to actuate the ankle joint. But based on the same ranges of the torques, different research groups designed respective devices using different ranges ([15]-[17]) as shown in Table II.2. 2. Mainly because the ankle motion shows wide variation among humans conditions, such as size and orientation of the foot bones, shape of the articulated surfaces, constraints from ligaments, tendons etc. All these factors impose some influence on the choice of torque limits and required RoM.

Table II.2. 2.The ranges of torques

Motion of ankle joint	Dorsiflexion (-)	Plantarflexion (+)	Eversion (-)	Inversion (+)
Range of Motion (RoM) [10][14]	-20°	40°	-25°	35°
Joint torque limits [10][14]	-97.6~ -	20.3 -- 36.6Nm	Max -	Min -

	40.7Nm		34Nm	48Nm
Designed torque limits [15]	-100Nm	50Nm	-50Nm	50Nm
Designed RoM [15]	-40°	40°	-35°	35°
Designed torque limits [16]	-104Nm	104Nm	-248Nm	248Nm
Designed RoM [16]	-50°	50°	-55°	55°
Designed torque limits, no bearing weight [17]	-23Nm	23Nm	-15Nm	15Nm
Designed RoM [17]	-25°	45°	-20°	25°

S. Miyazaki et al. [6] investigated the dynamic change in the moment generated by ankle musculature referring to the active ankle movement during walking with or without ankle-foot orthosis (AFOs). Only dorsi/plantar direction is discussed. The subjects are male and female in 38-76 years old with hemiparesis and they participated in the measure of ankle moment after stroke. Active ankle moment was measured with some subjects around 63kg weight and 1.65m tall. The active moment varied from 0 to 50 Nm during the gait for dorsiflexion and the maximum moment can reach to 70 Nm for plantarflexion.

C. Kim and J. Eng [18] investigated the relationship of lower-extremity muscle torque and locomotor performance in people after stroke. They evaluated the participants with criterion 'ICIDH-2' and 'Chedoke-McMaster Stroke Assessment'. An angular velocity 60 degree/s was used to mimic the peak angular velocity of ankle joints during the gait of people with stroke. 30 degree/s was the second choice for those cannot produce torque at 60 degree/s. gait performance and stair-climbing ability were measured for data collection. Male and female were both considered. Paretic and non-paretic people were classified and compared. The mean mass of participants was 76.2 kg. Its standard derivation (SD) was 13.8 kg and the range was 52.0-99.4 kg. For the torque measures, average torque values were normalized to body mass. The motion of range is 10 to 33 degrees of plantar flexion for the ankle. The results were shown in Table II.2. 3. The speed for different tasks were shown in Table II.2. 4.

Table II.2. 3. Average torque (in N.m/kg) for ankle joint and motion direction (subjects number N: 20)[18]

Side	Test	Mean value	SD	Range
Paretic	Ankle plantar flexion	0.19	0.14	0.00-0.51
	Ankle dorsiflexion	0.15	0.13	0.00-0.42
Non-paretic	Ankle plantar flexion	0.93	0.29	0.21-1.46
	Ankle dorsiflexion	0.49	0.13	0.22-0.76

Table II.2. 4. Gait speed (m/s) and stair-climbing speed (stairs/s) (N=20)[18]

Task	Pace	Mean value	SD	Range

Gait	Self-selected	0.45	0.25	0.20-1.10
	Maximum	0.69	0.35	0.26-1.56
Stair-climbing	Self-selected	0.63	0.23	0.31-1.18
	Maximum	0.83	0.26	0.36-1.50

Bohannon [19] measured the strength of the muscles group for plantar flexion and dorsiflexion of the ankle in kg, as shown in Table II.2. 5.

Table II.2. 5. The strength of the muscle group for the ankle, the paretic lower extremity of 20 hemi-paretic stroke patients.[19]

Muscle group	Actual strength scores (kg)			Standardized strength scores		
	Mean value	SD	Range	Mean value	SD	Range
Ankle dorsiflexors	5.2	7.8	0-23.5	0.07	0.11	0-0.30
Ankle plantar flexors	8.3	13.2	6.2-49.6	0.37	0.17	0.08-0.70

Bäckman E and Oberg B [20] investigated the muscles torques in dorsiflexion of the ankle for 6-15 years' children. The best parameters for torques' prediction are age, weight and height (Table II.2. 6). Torques were tested with children sitting in a standard position, fastened and stabilized with padded straps. Here shows the ankle dorsiflexion torque for different ages (Table II.2. 7). Six different speeds were applied during measurement.

Table II.2. 6. Number of subjects, their age, weight and height [20]

	6 years		9 years		12 years		15 years	
	girls	boys	girls	boys	girls	boys	girls	boys
n	20	23	21	15	15	16	15	12
weight (kg)	23.8 ±3.7	21.7 ±2.4	31.4 ±6.5	29.7 ±4.1	40.3 ±6.1	39.0 ±4.4	54.2 ±8.8	53.5 ±8.5
height (cm)	119.6 ±4.4	118.1 ±3.1	135.6 ±6.5	135.9 ±6.6	152.9 ±6.8	150.1 ±6.1	165.5 ±6.0	168.8 ±7.3

Table II.2. 7. Ankle dorsiflexor torque in Nm for different ages [20]

	6 years		9 years		12 years		15 years	
°/sec	Dom	ND	Dom	ND	Dom	ND	Dom	ND
Girls								
0	6.8 NS	7.5	11.6*	12.9	19.3 NS	20.7	23.6**	26.9
	±2.0	±2.3	±3.7	±3.3	±3.1	±5.1	±5.2	±6.7
15	6.0 NS	6.3	10.0**	11.2	15.4*	16.9	18.3**	21.8
	±1.6	±1.4	±3.0	±3.0	±3.3	±5.0	±4.1	±5.4
30	5.3 NS	5.5	9.0**	10.2	14.7 NS	16.1	17.9**	20.4

	±1.3	±1.5	±2.2	±3.0	±3.7	±4.9	±3.9	±5.0
60	4.8 NS	4.5	8.6 NS	8.8	13.5*	15.0	17.9 NS	19.4
	±1.7	±1.3	±2.7	±2.5	±4.0	±4.4	±4.6	±4.9
120	4.7 NS	4.2	7.7 NS	7.8	11.6 NS	13.2	15.4 NS	15.9
	±1.7	±1.7	±2.2	±2.5	±2.6	±3.5	±4.6	±4.4
180	4.3 NS	3.7	6.4 NS	6.4	10.2 NS	11.4	14.1 NS	13.6
	±1.9	±1.5	±2.1	±2.1	±3.1	±5.3	±5.0	±4.4
240	3.9 NS	3.8	5.6 NS	5.8	8.8 NS	8.5	11.2 NS	10.9
	±1.9	±1.9	±1.9	±2.3	±2.4	±2.2	±4.0	±3.5
Boys								
0	6.9 NS	7.3	12.7 NS	12.5	18.7*	20.7	30.9 NS	34.5
	±1.5	±1.5	±3.6	±2.2	±3.7	±5.1	±9.1	±9.3
15	5.7 NS	6.1	9.8 NS	10.6	14.8**	17.1	24.7*	28.6
	±1.4	±1.2	±2.2	±2.2	±3.7	±4.4	±8.2	±8.0
30	5.1 NS	5.2	9.8 NS	9.9	14.8*	17.0	23.7 NS	25.7
	±1.7	±1.2	±3.3	±2.0	±3.4	±4.6	±8.5	±8.7
60	4.9 NS	4.7	9.3 NS	9.5	13.8*	15.5	22.7 NS	24.7
	±1.4	±1.2	±2.6	±3.2	±4.5	±4.5	±9.3	±6.8
120	4.6 NS	4.5	8.8 NS	9.1	13.4 NS	14.6	21.2 NS	22.1
	±1.4	±1.1	±2.7	±2.4	±3.9	±4.7	±7.1	±5.0
180	4.5*	3.7	8.8 NS	7.6	11.5 NS	12.4	18.0 NS	18.1
	±1.8	±1.6	±2.6	±2.6	±4.3	±4.9	±4.8	±4.0
240	3.9*	3.0	7.7 NS	6.4	10.6 NS	10.2	15.1 NS	15.6
	±1.5	±1.4	±2.4	±2.4	±4.3	±3.7	±5.1	±4.1
Dom = dominant side, ND = non-dominant side, *p<0.05, **p<0.01.								

A. Ferri et al. [21] measured the strength and power changes of the human plantar flexors in response to resistance training. The subjects were 16 older men aged 65–81 years with a 16-week resistive programme. Methods and measurements were clearly demonstrated in their work. The subjects were divided into three groups as a comparison: before training (B), after 4 weeks of training (WK4), and 16 weeks of training (WK16). Figure II.2. 14-Figure II.2. 16 show the results.

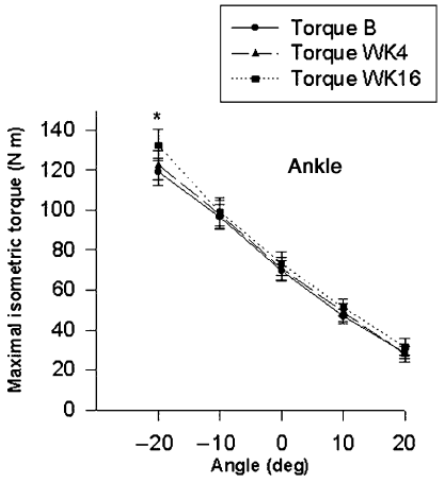

Figure II.2. 14. Peak torques at different angles[21]

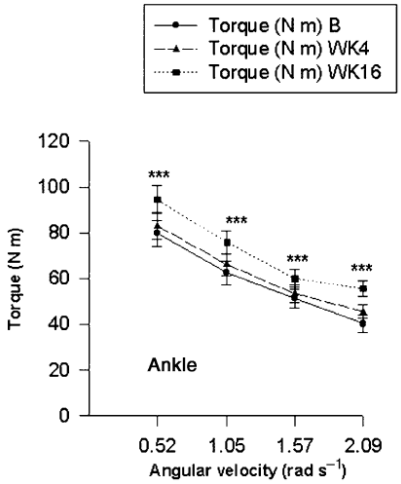

Figure II.2. 15. Peak torques at different velocities[21]

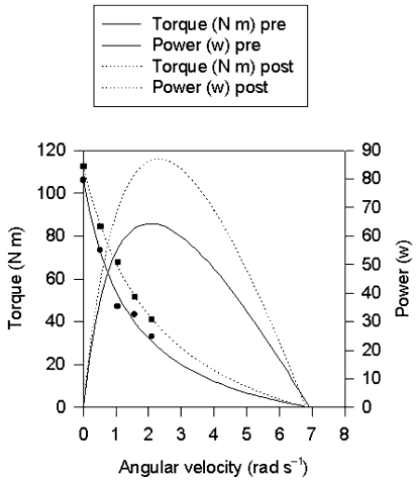

Figure II.2. 16. Torque–velocity relationships and derived mechanical power curves before (continuous lines) and after (interrupted lines) training for plantar flexor muscles in a representative subject.[21]

II.2.5 Considerations about control strategies and sensors

Control strategies should be planned and executed according to different tasks and targets. Before the control strategies are planned, we should know clearly that which kind of injuries a patient suffers and which parts of the foot-ankle should be trained during rehabilitation.

II.2.5.1 Injury category

Recoverable ankle injuries are normally musculoskeletal or neurologic injuries [22]. Musculoskeletal injuries are sustained in sports and daily active life, from walking or

running on uneven road surfaces, walking under excessive load. In injuries, muscles and/or ligaments are damaged. Concomitant nerve terminal is influenced too. For the recovery, long-term physiotherapy and daily use of rehabilitation techniques are necessary. Clinical devices, for example, platform based mechanisms are applied. Both active and passive physical exercises are important to achieve a total recovery. These exercises are stressed to train ankle ligaments, working muscles for providing stability, the development of neural feedback and neuromuscular control of ankle function [31]. Therefore, long durable and repetitive training is effective to promote propioception. Due to damaged muscles and tendon, low-load on ankle exercises is considered. The majority of the total body weight should be supported by extra devices, not taken on an injured ankle. Resistive training is considered for the aim of strengthening muscles.

If the ankle is unable to dorsiflex (bend backward) properly it will not allow the knee to travel forward enough for the body to move its center of mass over the foot, hence making the forward motion of the body difficult [3]. In such a case, the foot is forced to pronate excessively and as a result the knee will drift medially (toward midline) and the hip will have to excessively adduct (move toward midline) and internally (turn inward) rotate. This of course continues into the rest of kinetic chain and results in other abnormalities in motion mechanics. In this particular instance of lack of ankle flexibility, making a correction through shoes and orthotics is often asking for nothing but trouble. The over pronation in this case is a needed compensation for a lack of mobility elsewhere in the body. So taking this compensatory element away without first addressing and correcting the true underlying cause will force compensation (frequently accompanied by pain) in another part of the body.

Neurologic injuries such as stroke and spinal cord injury are normally treated in a wearable rehabilitation device [23]. For patients who suffer this kind of injuries, muscles and ligaments are not damaged so severely as nervous system and still have potential to take more weight, compared with them in musculoskeletal injuries. Neural feedback is highlighted and therefore gait training is necessary to promote the feedback for joint position and motion. But at the early stage in which neural feedback is weak [29][30], patients fail to get enough strong feedback from haptic training. A machine support is still helpful and can be realized using a treadmill. With some assistive machine support, weight of patients and acceleration of body motion can be supported and patients can pay more attention on gait training [24]. Active physical exercise from patients is stressed to improve the recovery of nervous system during locomotion on the treadmill [1][25][26]. Normally, dorsiflexion and plantar flexion are focused during gait training [27][28]. Eversion and inversion are also considered. The reasons of these considerations are complicated [17]. In many neurological injuries such as stroke, cerebral palsy, multiple sclerosis, traumatic brain injury, or peripheral nerve pathology, 'drop foot' is a common impairment, caused by a weak muscle in the dorsiflexor that lift the foot. Two common complications of drop foot are slapping of the foot after heel strike (foot slap) and dragging of the toe during swing (toe swing). In addition to inadequate dorsiflexion (“toe-up”), the paretic ankle also suffers from excessive inversion (heel toward midline). This begins in the swing phase and results in toe contact (as opposed to heel contact) and lateral instability in stance. Therefore, ankle rehabilitation in both the sagittal and frontal

planes should be under control. At least a rehabilitation device with 2 DOF is necessary for functional recovery.

II.2.5.2 Interaction between muscles and the actuation system

The rehabilitation robot is not only designed to train the motion of the ankle joint, but also considered for the training of muscles around the ankle. During the ankle motion, those muscles also act as well as deform to drive and/or match the according ankle motion. Therefore the muscles play various, but all important roles to control the ankle motion, provide enough torques and make the ankle reach the every configuration within the ankle RoM. During the training, the muscles can play active or passive roles, depending on different tasks. When the muscles play an active role, the actuation system plays a passive role, which means that the actuation system provides resistant forces and/or torques to train the muscle strength. When the actuation system plays an active role, the ankle joint is driven and controlled by the actuation system to move with the RoM. So the muscles and the actuation system are required to cooperate during rehabilitation. They play different roles in different rehabilitation training. For example, if muscles around the ankle play an active role during muscles training, the rehabilitation robot acts as a breaking system. In detail, when muscles which control the plantar flexion motion work as an active resource, the rehabilitation system provides a resistant effect. In this case, the back muscle groups distributed on shank's back (mainly consisting of two layers of muscles, gastrocnemius, soleus on the shallow layer, tibialis posterior, flexor digitorum longus, flexor hallucis longus on the deep layer) are obtained training. When muscles which control the dorsiflexion motion work as an active resource, the robot produces force/torque against the dorsiflexion motion. In this case, the frontal muscle groups distributed on the shank's front (mainly consisting of tibialis anterior muscle, extensor digitorum longus and extensor hallucis longus) are obtained training. For inversion and eversion motion, lateral muscles (mainly fibularis longus and fibularis brevis) act as an active role, and can be obtained training.

In the motion training, the ankle is trained to move within RoM and reach its boundaries of its ROM under the control of the rehabilitation robot. When the actuation system works in an active way, the muscles around the ankle play a breaking role. In this case, the motion of the ankle is trained, since patients who suffer a sprained ankle cannot actively drive the ankle move to its extreme positions. The actuation system should work and move the ankle in a slow way. With the proper control of the wires, dorsiflexion and plantar flexion, inversion and eversion can be trained.

II.2.5.3 A proposal of control strategy

A good rehabilitation robot should provide enough activities for the ankle rehabilitation. Force control and position control are the two common control strategies. Force control loop is shown here as an example.

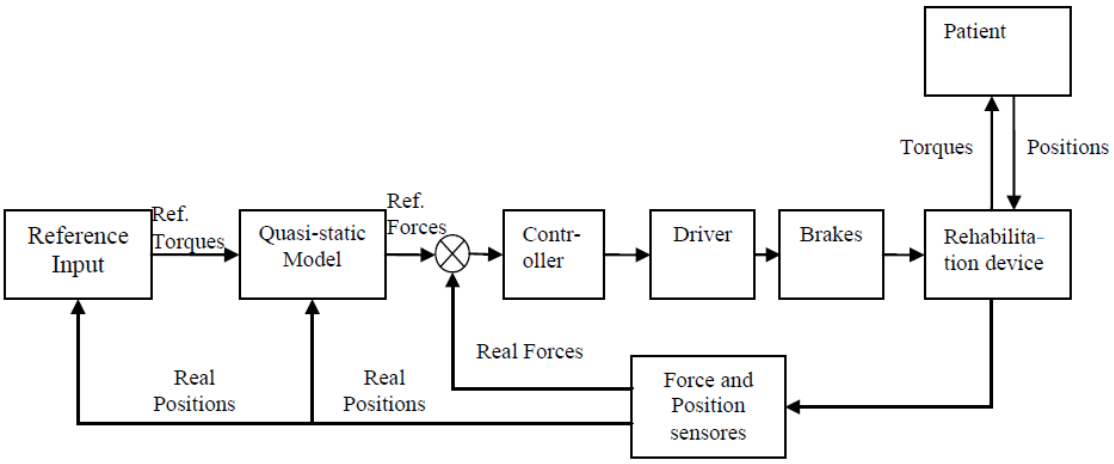

Figure II.2. 17. Force control loop

Figure II.2. 17 shows the force control loop. During the loop, the patient plays an active role to drive the ankle, while the rehabilitation robot plays a passive role to break the patient motion. From the start, 'reference input' is to show which kind of exercise is involved. Here we take dorsiflexion motion as an example. The actuation system provides torques and therefore reference forces through a quasi-static model. After the comparison with forces from the device, the error is increased or decreased through the controller. With an actuation system (normally consisting of driver and brakes), real forces are produced for the device. On the other hand, the patient is prepared to apply a dorsiflexion to train the muscles in the front of the calf. So the patient drives his muscles to do a dorsiflexion. During his motion, he will receive breaking torques from the device. Then the patient has to strength his muscles to finish the dorsiflexion. Once the effect from the patient becomes stronger than the breaking torques, the foot is moved. At the same time, its position is measured by position sensors mounted on the device. The sensors transfer the information back and make it have a comparison with the dorsiflexion requirement. The loop will not stop until the foot ankle reaches the required position.

II.2.5.4 Sensors

Sensors are applied to measure physical parameters for control targets. Therefore, we define the parameters to be measured according to different control tasks. The position of the ankle should be measured for force and position control. We describe the position of the ankle using the dimensional changes of the device or the three angles of the ankle position. The linear lengths can be measured by means of length change ΔL. Two kinds of position sensors are commonly used [17]. The first kind is normally rotary encoders mounted on coaxial with the motors. The other is linear incremental encoders mounted on the traction drive for collecting the linear changes as feedback to the controller. We can obtain the angular position of the ankle using their linear information through its forward kinematic model (which will be developed in the next chapter).

Torque can be measured by analog current sensors, which provide a measure of motor torque. Also, Jennifer M. Newton et al. [31] presented the use of a magnetic resonance system to measure the torques of joints for low extremities (including torques of ankle, knee, hip), and at the same time provided visual feedback of torques at relevant joints to the subject. Forces applied on the ankle are necessary to be measured as a feedback in force control loop. We can use strain gauge to measure the voltage change caused by the ankle during motion, then forces can be obtained and imported to controller for force loop control. Velocity and acceleration of the ankle motion are also considered. What's more, EMG (Electromyography) signal needs to be collected to observe muscle and ligament situations. Use of electrogoniometers has been proved successful for monitoring and providing feedback of movements of the ankle ([28]-[30]).

References:

[1] S. Miyazaki, S. Yamamoto, T. Kubota. Effect of ankle-foot orthosis on active ankle moment in patients with hemiparesis. Medical & Biological Engineering & Computing, July 1997, 381-385.

[2] Donatelli R A. Normal biomechanics of the foot and ankle. The Journal of Orthopaedic and Sports Physical Therapy, 1985, 7(3):91-95.

[3] Mann RA, Inman VT. Phasic activity of intrinsic muscles of the foot. J Bone Joint Surg (Am), 46-469, 1964.

[4] Donatelli R A. Abnormal biomechanics of the foot and ankle. The Journal of Orthopaedic and Sports Physical Therapy, 1987, 9(1):11-16.

[5] Hicks JH. The mechanics of the foot. I. The joints. J Anat 87, 1953, 345-357.

[6] Hicks JH. The mechanics of the foot. II. The plantar aponeurosis. J Anat 88, 1954: 25-30.

[7] Root ML, Orien WP, Weed JN. Clinical Biomechanics. Vol. II: Normal and abnormal Function of the Foot. Los Angles: Clinical Biomechanics Corp, 1977.

[8] McCrea JD. Pediatric Orthopaedics of the lower extremity. Mt Kisco, NY: Future Publishing Co, 1985.

[9] J. Stein,H. I.Krebs, W. R. Frontera, S. E. Fasoli, R. Hughes, and N.Hogan, "Comparison of two techniques of robot-aided upper limb exercise training after stroke," Amer. J. Phys. Med. Rehabil., vol. 83, pp. 720–728, Sep. 2004.

[10] Donatelli, R. A., 1996. The Biomechanics of the Foot and Ankle, Philadelphia.

[11] Asbjorn Roaas, Gunnarb. J. Andersson. Normal Range of Motion of the Hip, Knee and Ankle Joints in Male Subjects, 30-40 years of age. Acta orthop. scand. 53, 205-208, 1982.

[12] American Academy of Orthopaedic Surgeons (1965). Joint Motion: Method of Measuring and Recording. Chicago: American Academy of Orthopaedic Surgeons.

[13] Boone, Donna C.; Stanley P. Azen (July 1979). Normal range of motion of joints in male subjects. The Journal of Bone and Joint Surgery 61–A: 756–759. Retrieved 24 October 2012.

[14] C.S. Parenteau, D.C. Viano, and P. Petit, Biomechanical properties of human cadaveric ankle-subtalar joints in quasi-static loading, Journal of Biomechanical Engineering, 120, (1), 1998: 105–111.

[15] Aykut Cihan Satici, Ahmetcan Erdogan, Volkan Patoglu. Design of a Reconfigurable Ankle Rehabilitation Robot and Its Use for the Estimation of the Ankle Impedance. 2009 IEEE 11th International Conference on Rehabilitation Robotics. Kyoto International Conference Center, Japan, June 23-26, 2009.

[16] Jungwon Yoo, Jeha Ryu, Kil-Byung Lim. Reconfigurable Ankle Rehabilitation Robot for Various Exercises. Journal of Robotic Systems 22(Supplement), 2006, 15-33.

[17] Anindo Roy, Hermano Igo Krebs, et al. Robot-Aided Neurorehabilitation: A Novel Robot for Ankle Rehabilitation. IEEE transactions on robotics, vol. 25, no. 3, 569-583, 2009.

[18] C Maria Kim, Janice J Eng. The Relationship of Lower-Extremity Muscle Torque to Locomotor Performance in People with Stroke. Physical Therapy. Volume 83. Number 1. January 2003, 49-61.

[19] Richard W. Bohannon. Strength of lower limb related to gait velocity and cadence in stroke patients. Physiotherapy Canada, July/August 1986, Vol. 38, No. 4, 204-206.

[20] Bäckman E, Oberg B. Isokinetic muscle torque in the dorsiflexors of the ankle in children 6-15 years of age. Normal values and evaluation of the method. Scandinavian Journal of Rehabilitation Medicine, 1989, 21(2):97-103.

[21] A. Ferri, G. Scaglioni et al. Strength and power changes of the human plantar flexors and knee extensors in response to resistance training in old age. Acta Physiol Scand 2003, 177, 69–78.

[22] Zhang et al. Effectiveness of robot-assisted therapy on ankle rehabilitation: a systematic review. Journal of Neuro Engineering and Rehabilitation 2013, 10-30.

[23] Laura Marchal-Crespo, David J Reinkensmeyer. Review of control strategies for robotic movement training after neurologic injury Journal of NeuroEngineering and Rehabilitation 2009, 6-20.

[24] Stefan Hesse, Henning Schmidt, Cordula Werner and Anita Bardeleben. Upper and lower extremity robotic devices for rehabilitation and for studying motor control, Current Opinion in Neurology 2003, 16:705-710.

[25] Robert W. Teasell, Norine C. Foley et al. An Evidence-Based Review of stroke rehabilitation. Top Stroke Rehabil 2003; 10(1): 29–58.

[26] Chiung-Ling Chen et al. Anterior ankle-foot orthosis effects on postural stability in hemiplegic patients. Arch Phys Med Rehabil, Vol 80, December, 1999, 1587-1593.

[27] Bruce H. Dobkin, Ann Firestine, Michele West, Kaveh Saremi, et al. Ankle dorsiflexion as an fMRI paradigm to assay motor control for walking during rehabilitation. NeuroImage 23 (2004) 370–381.

[28] Bradley J. Macintosh, Richard Mraz, Nicole Baker et al. Optimizing the experimental design for ankle dorsiflexion fMRI. NeuroImage 22 (2004) 1619–1627.

[29] Christensen, M.S., Lundbye-Jensen, J., Petersen, N., Geertsen, S.S., Paulson, O.B., Nielsen, J.B., 2006. Watching your foot move—an fMRI study of visuomotor interactions during foot movement. Cereb. Cortex. 17 (8), 1906 – 1917.

[30] Debaere, F., Swinnen, S.P., Beatse, E., Sunaert, S., Van Hecke, P., Duysens, J., 2001. Brain areas involved in inter-limb coordination: a distributed network. Neuroimage 14, 947 – 958.
[31] Jennifer M. Newton, Yun Dong, Joseph Hidler, Prudence Plummer-D'Amato et al. Reliable assessment of lower limb motor representations with fMRI: Use of a novel MR compatible device for real-time monitoring of ankle, knee and hip torques. NeuroImage 43 (2008) 136 – 146.
[32] Tobias Bruckmann, Lars Mikelsons, Thorsten Brandt, Manfred Hiller and Dieter Schramm (2008). Wire Robots Part I: Kinematics, Analysis & Design, Parallel Manipulators, New Developments, Jee-Hwan Ryu (Ed.), ISBN: 978-3-902613-20-2, InTech.
[33] Tobias Bruckmann, Lars Mikelsons, Thorsten Brandt, Manfred Hiller and Dieter Schramm (2008). Wire Robots Part II: Dynamics, Control & Application, Parallel Manipulators, New Developments, Jee-Hwan Ryu (Ed.), ISBN: 978-3-902613-20-2, InTech.
[34] Foot Health Practitioner Diploma Course. www.stonebridge.uk.com.
[35] Zeuter Development Corporation. www.alientravelguide.com
[36] Hofstad, C., Weerdesteyn, V., van der Linde, H., Nienhuis, B., Geurts, A., & Duysens, J. (2009). Evidence for bilaterally delayed and decreased obstacle avoidance responses while walking with a lower limb prosthesis. Clinical Neurophysiology, 120 (5), 1009-1015.

Section II.3 Modeling and Simulation of the Wearable Robotic Device for the Ankle Rehabilitation

Nomenclature:

ψ	deg	rotation angle around axis Z, in the transverse plane
θ	deg	rotation angle around axis X, in the frontal plane
ϕ	deg	rotation angle around axis Y, in the sagittal plane
T_i	--	Transformation matrix, around axis i, i=z,x,y
R_{zxy}	--	Transformation matrix, from the local coordinate to global coordinate.
L_i, l_i	m	The length of two points O and i.
L'_i	m/s	The linear velocity of the wire i.
α, β, γ	rad	Physical parameters to describe positions
s, c	--	Short for sin, cos
(x, y, z)	--	The position description in the local coordinate O-xyz
(X, Y, Z)	--	The position description in the global coordinate O-XYZ
$\boldsymbol{\omega}$	--	Angular velocity vector of the moving platform
$\mathbf{s_{ij}}$	--	Unit vector, pointing from the point i to the point j.
$\mathbf{n_I}$	--	The normal vector to a plane defined by the triangle ΔOI_1I_2, I=A, B, C.
$\mathbf{J_I}$	--	Inverse kinematic matrix
$\mathbf{J_\omega}$	--	Forward kinematic matrix
$\mathbf{n_O}$	--	The moment vector around the ankle joint O
n_J	N.m	The component of the moment $\mathbf{n_O}$ around the axis J. J=X, Y, Z.
$\mathbf{F_I}$	--	The force vector applied by the wire I. I = A, B,C.
f_i	N	The scalar value for the force vector $\mathbf{F_I}$
$\mathbf{F_J}$	--	The force vector applied by the ankle joint O. J=X, Y, Z.

This chapter proposes an innovative wearable device for rehabilitation, based on ankle properties and requirements mentioned in the Section II.2, then focuses on the ideal model and its simulation of the wearable device. The wearable device can be assumed as a parallel robot with wires connecting the moving platform with the fixed base. An ideal model of the device is studied in terms of inverse and forward kinematics. Numerical examples are shown to simulate the motion process with multi degrees of freedom (DOF). The quasi-static force model is also proposed as force model for the dynamic analysis.

II.3.1 The Proposal and the Model Description

Based on the considerations mentioned in the Section II.2, this part introduces a wearable robotic device for the ankle rehabilitation (Figure II.3.1). The device drives the motion of the ankle by controlling three wires (Bowden Cable). The Bowden Cable connects the foot to the device through spherical joints. The load of the wearable device is distributed at the whole lower extremity by brackets: the motors are mounted on the thigh through a wearable bracket, while the spherical joints are on the calf. In this case, the load is not intensive, the patient feels easy to afford the load for long time during the rehabilitation device. Also, the device employs wires as connecting parts, instead of solid linkages, so that the device is light-weight, not bulky. The rehabilitation device is also available for different sizes. So the wires of the device are adjusted to different individuals.

Ergonomic is considered seriously since the rehabilitation device works on the patient body. Safety is the first issue under consideration. In this case, forces applied by the device should be under control to make sure that they cannot be over a threshold. Also, the motion of the ankle should be restricted within the range of motion. This goal can be realized by the control of lengths of the wires. The wire structure with the Bowden Cable makes the device easy donning on and off. Once the system fails to work, the patient can take off the device quickly and make sure the body safety.

Versatile functions are also considered here. The device proposed here can be available for gait function, the muscle strength and ankle performance tool. According to the wire drive theory [4][5], three wires can only control two degrees of freedom, here three wires tries to control two rotational DOFs: dorsiflexion/plantar flexion and eversion/inversion, releasing flexibility for the ankle adduction/abduction, which aims at making the patient feel comfortable during the rehabilitation training. The adduction/abduction rotation can be added if the device cooperates with a platform based device.

The rehabilitation device can be modelled ideally, as shown in Figure II.3. 2. The upper tetrahedron O-$A_1B_1C_1$ can be considered as the shank part of the leg. The lower tetrahedron O-$A_2B_2C_2$ is assumed as the foot of the patient. In this case, the point O is abstracted as the ankle joint. So the joint O is a spherical joint with three rotational DOFs. The universal coordinate O-XYZ is attached on the tetrahedron O-$A_1B_1C_1$. On the foot there is a local coordinate O-xyz. The three rotational directions are described as dorsiflexion and plantar flexion, eversion and inversion, adduction and abduction (Table II.3. 1). When the foot moves around the ankle joint, the local coordinate O-xyz moves around the universal coordinate O-XYZ. So in this case, the upper tetrahedron can be treated as a fixed platform, while the lower tetrahedron is the moving platform. Take the right foot as an example, the positions A1, A2, B1, B2, C1 and C2 in Figure II.3. 2 are considered as spherical joints since they can rotate freely in 3 DOFs as wires work. Also the parallel robot has a spherical joint connecting the two platforms together. Between the both platforms, three wires, controlled by actuators can shorten or extend to drive the moving platform perform activities. Therefore, the model is a wire robot with a parallel structure.

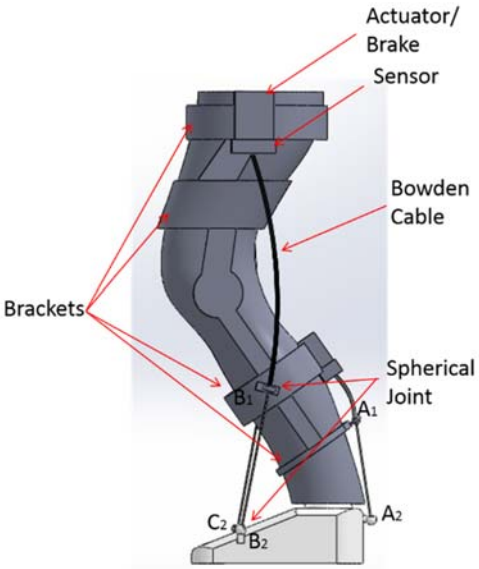

Figure II.3. 1. the wearable rehabilitation device

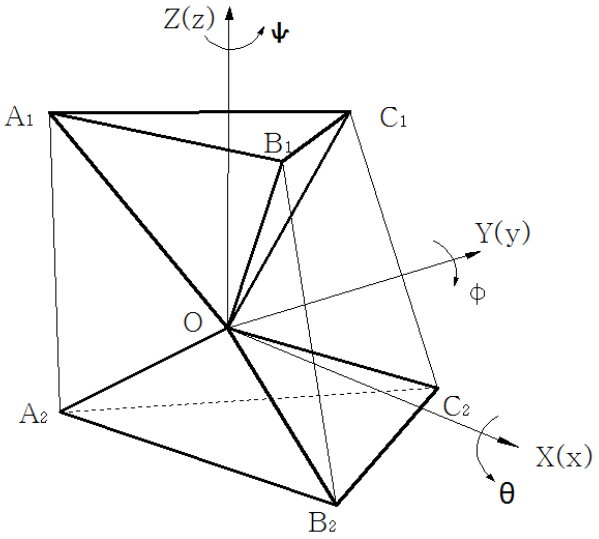

Figure II.3. 2. The ideal model for the wearable device at the initial location

Table II.3. 1. Rotation direction

Degree of Freedom	inversion	plantarflexion	adduction
	eversion	dorsiflexion	abduction
Around x axis (θ)	+		
	-		
Around y axis (ϕ)		+	
		-	
Around z axis (ψ)			+
			-

II.3.2 The kinematic study

The transformation matrix from the moving platform to the fixed base can be described by a rotation matrix defined in this way: assume that the initial position of the moving frame coincides with the fixed one and the final position is obtained by a rotation of ψ around z axis, followed by a second rotation of θ around the displaced x axis, finally followed by a third rotation of ϕ around the displaced y axis. The three steps are described by matrixes as:

$$T_z = \begin{bmatrix} c\psi & -s\psi & 0 \\ s\psi & c\psi & 0 \\ 0 & 0 & 1 \end{bmatrix}, \quad T_x = \begin{bmatrix} 1 & 0 & 0 \\ 0 & c\theta & -s\theta \\ 0 & s\theta & c\theta \end{bmatrix}, \quad T_y = \begin{bmatrix} c\phi & 0 & s\phi \\ 0 & 1 & 0 \\ -s\phi & 0 & c\phi \end{bmatrix}$$

The resultant transformation matrix from the moving platform to the fixed base is,

$$R_{zxy} = T_z \cdot T_x \cdot T_y = \begin{bmatrix} c\psi c\phi - s\psi s\theta s\phi & -s\psi c\theta & c\psi s\phi + s\psi s\theta c\phi \\ s\psi c\phi + c\psi s\theta s\phi & c\psi c\theta & s\psi s\phi - c\psi s\theta c\phi \\ -c\theta s\phi & s\theta & c\theta c\phi \end{bmatrix} \quad \text{(II.3. 1)}$$

Assume that A_1, the fixed point in the fixed base, is in the plane XOZ, while A_2 is in the local plane xOz. The angle between the vector OA_1 (the length is l_{A1}) and Z axis is assumed as α_1, in the global coordinate O-XYZ, and the angle between the vector OA_2 (the length is l_{A2}) and z axis is assumed as α_2, in the local coordinate O-xyz. In this case, the positions of A_1 and A_2 can be expressed in this way:

$A_1 = (X_{A1}, 0, Z_{A1})$ and $A_2 = (x_{A2}, 0, z_{A2})$.

Where,

$$X_{A1} = -l_{A1} \cdot s\alpha_1, \quad Z_{A1} = l_{A1} \cdot c\alpha_1$$

And,

$$x_{A2} = -l_{A2} \cdot s\alpha_2 , \quad z_{A2} = -l_{A2} \cdot c\alpha_2$$

Also, we assume that B_1 and C_1 are distributed at the symmetric positions with respect to the plane XOZ. As well as B_1 and C_1, B_2 and C_2 are the symmetric positions with respect to the plane xOz, as shown in Figure II.3. 3 and Figure II.3. 4.

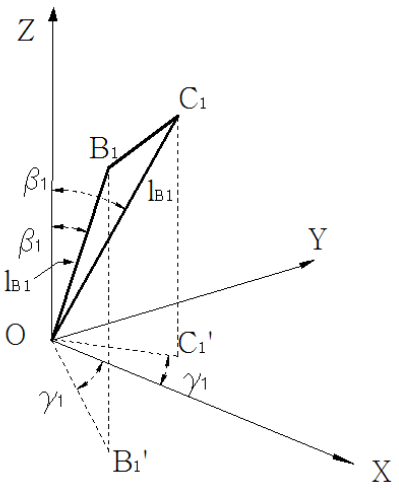

Figure II.3. 3. The positions of B_1 and C_1 in the coordinate O-XYZ

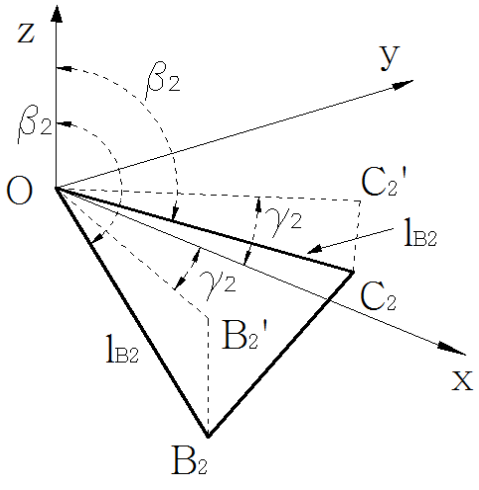

Figure II.3. 4. The positions of B_2 and C_2 in the coordinate O-xyz

In Figure II.3. 3, we can obtain the positions of B_1 and C_1:

$B_1 = (X_{B1}, Y_{B1}, Z_{B1})$. $C_1 = (X_{C1}, Y_{C1}, Z_{C1})$ or $(X_{B1}, -Y_{B1}, Z_{B1})$

Where,

$X_{B1} = l_{B1} \cdot s\beta_1 \cdot c\gamma_1$, $Y_{B1} = -l_{B1} \cdot s\beta_1 \cdot s\gamma_1$, $Z_{B1} = l_{B1} \cdot c\beta_1$.

$X_{C1} = X_{B1}$, $Y_{C1} = -Y_{B1}$, $Z_{C1} = Z_{B1}$.

In Figure II.3. 4, B_2 and C_2 are obtained as,

$B_2 = (x_{B2}, y_{B2}, z_{B2})$. $C_2 = (x_{C2}, y_{C2}, z_{C2})$ or $(x_{B2}, -y_{B2}, z_{B2})$

Where,

$x_{B2} = l_{B2} \cdot s\beta_2 \cdot c\gamma_2$, $y_{B2} = -l_{B2} \cdot s\beta_2 \cdot s\gamma_2$, $z_{B2} = -l_{B2} \cdot c\beta_2$.

$x_{C2} = x_{B2}$, $y_{C2} = -y_{B2}$, $z_{C2} = z_{B2}$.

Any position (x, y, z) on the foot can be expressed in the fixed base as (X, Y, Z),

$(X, Y, Z)^T = R_{zxy} \bullet (x, y, z)^T$.

$$\begin{bmatrix} X \\ Y \\ Z \end{bmatrix} = \begin{bmatrix} (c\psi c\phi - s\psi s\theta s\phi)x - s\psi c\theta y + (c\psi s\phi + s\psi s\theta c\phi)z \\ (s\psi c\phi + c\psi s\theta s\phi)x + c\psi c\theta y + (s\psi s\phi - c\psi s\theta c\phi)z \\ -c\theta s\phi x + s\theta y + c\theta c\phi z \end{bmatrix} \quad \text{(II.3. 2)}$$

With this way, A_2, B_2, C_2 are expressed in the global coordinate as

$A_2 = (X_{A2}, Y_{A2}, Z_{A2})$, $B_2 = (X_{B2}, Y_{B2}, Z_{B2})$, $C_2 = (X_{C2}, Y_{C2}, Z_{C2})$

II.3.2.1 The inverse kinematic analysis

For inverse kinematics, the position of the moving platform is known, and the problem is to find the wire lengths l_A, l_B, l_C [1][2].

$$\begin{aligned} l_A^2 &= (\mathbf{OA_2} - \mathbf{OA_1})^2 \\ &= \mathbf{OA}_2^2 + \mathbf{OA}_1^2 - 2 \cdot \mathbf{OA_2} \cdot \mathbf{OA_1} \\ &= (X_{A2}^2 + Y_{A2}^2 + Z_{A2}^2) + (X_{A1}^2 + 0 + Z_{A1}^2) - 2(X_{A2} \quad Y_{A2} \quad Z_{A2}) \cdot (X_{A1} \quad 0 \quad Z_{A1})^T \end{aligned}$$

Here, $\mathbf{OA}_1$ and $\mathbf{OA}_2$ are the vectors pointing from O to A_1, A_2. Only positive solution of l_A is acceptable, as:

$$l_A = \sqrt{(X_{A2}^2 + Y_{A2}^2 + Z_{A2}^2) + (X_{A1}^2 + 0 + Z_{A1}^2) - 2(X_{A2} \quad Y_{A2} \quad Z_{A2}) \cdot (X_{A1} \quad 0 \quad Z_{A1})^T} \quad \text{(II.3. 3)}$$

With the same way, we can obtain the lengths of l_B, l_C.

$$l_B = \sqrt{(X_{B2}^2 + Y_{B2}^2 + Z_{B2}^2) + (X_{B1}^2 + Y_{B1}^2 + Z_{B1}^2) - 2(X_{B2} \quad Y_{B2} \quad Z_{B2}) \cdot (X_{B1} \quad Y_{B1} \quad Z_{B1})^T} \text{ (II.3. 4)}$$

$$l_C = \sqrt{(X_{C2}^2 + Y_{C2}^2 + Z_{C2}^2) + (X_{C1}^2 + Y_{C1}^2 + Z_{C1}^2) - 2(X_{C2} \quad Y_{C2} \quad Z_{C2}) \cdot (X_{C1} \quad Y_{C1} \quad Z_{C1})^T} \text{ (II.3. 5)}$$

That is to say, if the orientation of the model is known, we can obtain the wire lengths with the above equations. Here, numerical examples show the length changes when the moving platform performs different rotation. Table II.3. 2 shows the dimension conditions of six positions. With the known conditions, the model is executed three examples (Table II.3. 3) to present the motion and the length change of the three wires.

Table II.3. 2. Positions of wire ends on the fixed base and the moving platform

	Position in O-XYZ, mm		Position in O-xyz, mm
A_1	(100, 0, 120)	A_2	(-120, 0, -100)
B_1	(120, -60, 200)	B_2	(60, -80, -100)
C_1	(120, 60, 200)	C_2	(60, 80, -100)

Table II.3. 3. The motion range of the three orientation angles

Rotation description	ψ	θ	ϕ
Example 1	0	(-20°, 25°)	0
Example 2	(-5°, 5°)	(-15°, 10°)	(-20°, 20°)
Example 3	0	(-20°, 25°)	(-20°, 45°)

As the first example, the model (Figure II.3. 5) is set to perform one rotational degree of freedom from the inversion position to the eversion position. From Figure II.3. 6, it is realized that during the motion, the length of the wire l_C (between C_1 and C_2) continues to decrease. As we know that the wire can only provide pulling force instead of pushing force, the wire l_C contributes the motion as the driving wire. It is necessary to find the driving wire during the model motion. Since without the driving wire, the parallel robot cannot be moved and controlled by wires.

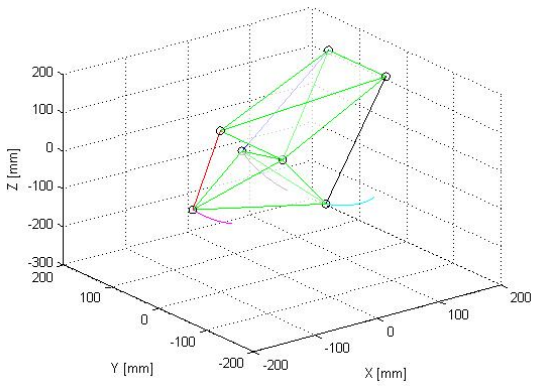

Figure II.3. 5. The motion model

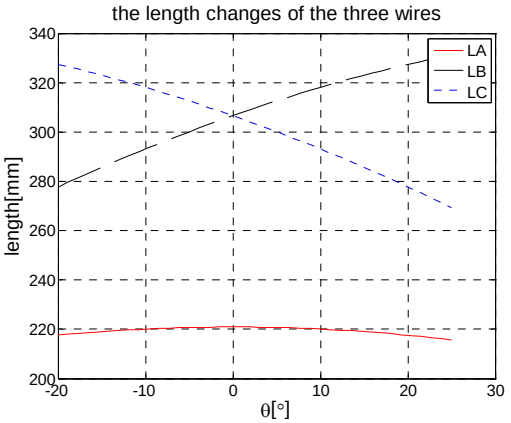

Figure II.3. 6. The changes of the wire lengths

In the second example, we set the motion as a combination of the three rotational DOFs. During the motion, we can observe every detail of wire lengths at every position (Figure II.3. 7-Figure II.3. 9). The motion is physically realizable since the wire l_A can shorten continuously to ensure the motion under control.

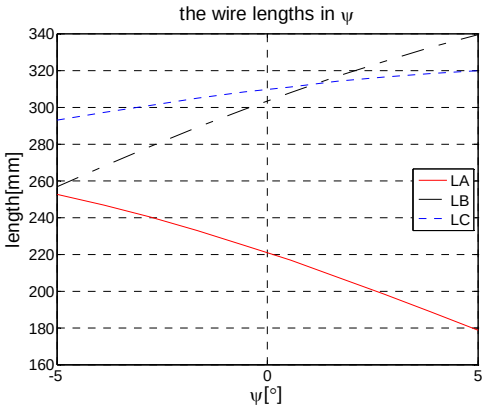

Figure II.3. 7. The length changes of wires as ψ varies

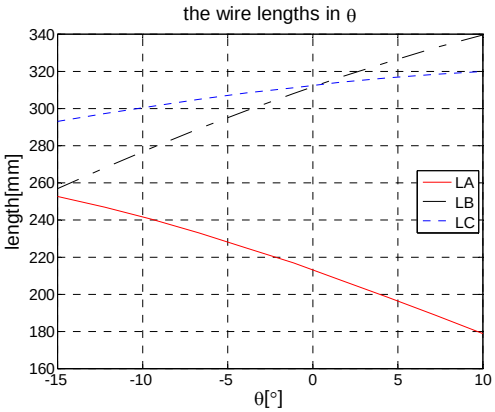

Figure II.3. 8. The length changes of wires as θ varies

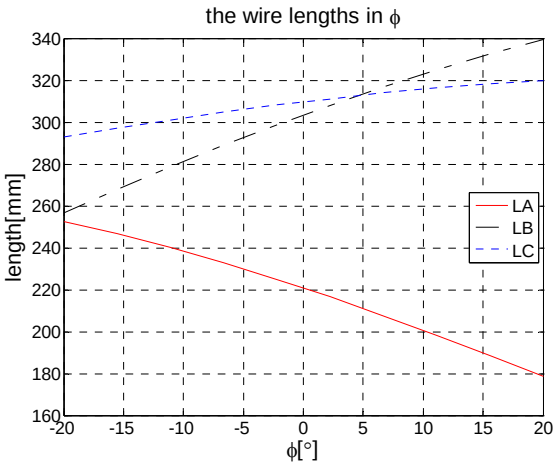

Figure II.3. 9. The length changes of wires as ϕ varies

The third example presents the length changes considering the two angle variants. This is the improvement of Example 1, adding the influence of the angle ϕ (Figure II.3. 10). From the change of the angle θ, l_C is driven to control the motion, as the same conclusion we obtain from the Example 1. From the change of the angle ϕ, the wire l_A controls the motion.

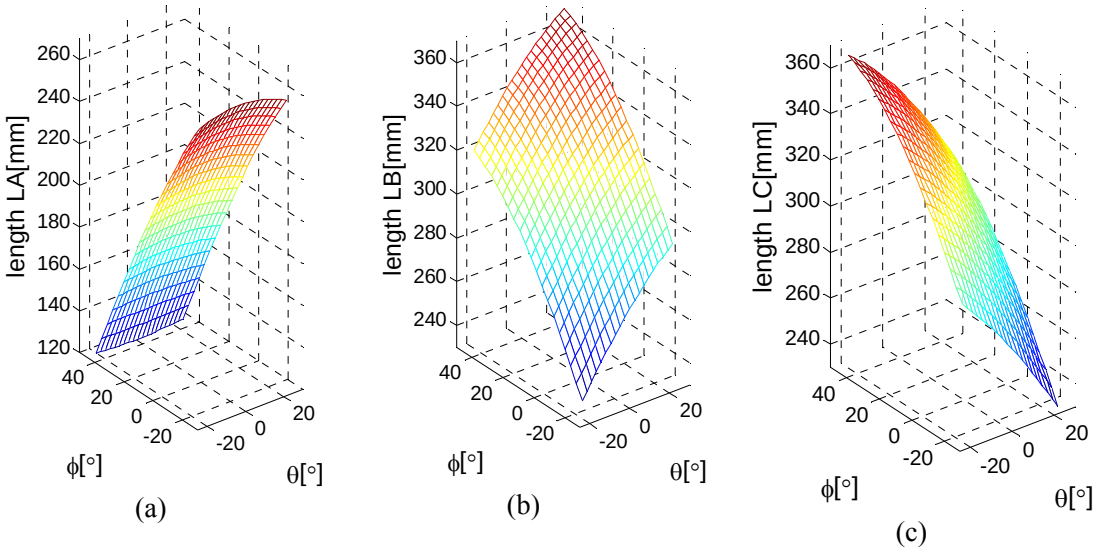

Figure II.3. 10. (a) the length changes of the wire l_A, (b) the length changes of the wire l_B, (c) the length changes of the wire l_C.

II.3.2.2 The forward kinematic analysis

The forward kinematics refers to the calculation of the orientation if the wire lengths l_A, l_B, l_C are known. It is difficult to solve the equations (II.3.3)-(II.3.5) to obtain the angle solutions since these equations refers multi solutions and much considerations should be taken seriously during the calculation process. Therefore, a numerical approach called 'Newton-Raphson Method' [3] is applied to solve the forward problems.

'Newton-Raphson Method' is an iterative approach to solve the non-linear equation set. Starting from the initial values, it obtains an increment as a step size and concludes the updated results. Then, the method repeats the process until the final results approach the exact values as expected. The exact values as expected are decided by required numerical accuracy and engineering practice. An increment is obtained normally by 'Taylor extension' of the non-linear equation set. Generally speaking, assume that an equation set with two variables q_1, q_2 in the following form:

$$\begin{cases} f_1(q_1, q_2) = 0 \\ f_2(q_1, q_2) = 0 \end{cases} \qquad \text{(II.3. 6)}$$

At the first step, organize variables q_1, q_2 in this way: express q_i with the two components, the estimated value q_{iest} and the error Δq_i describing the increment between the estimated value and the equation solution.

$$\begin{cases} q_1 = q_{1est} + \Delta q_1 \\ q_2 = q_{2est} + \Delta q_2 \end{cases} \qquad \text{(II.3. 7)}$$

With the Taylor series, the equation set (II.3.6) can be expressed at the position (q_{1est}, q_{2est}) as:

$$\begin{cases} f_1(q_1,q_2) = f_1(q_{1est},q_{2est}) + \dfrac{\partial f_1}{\partial q_1}(q_{1est},q_{2est})\cdot\Delta q_1 + \dfrac{\partial f_1}{\partial q_2}(q_{1est},q_{2est})\cdot\Delta q_2 + o(q_1^2,q_2^2) \\ f_2(q_1,q_2) = f_2(q_{1est},q_{2est}) + \dfrac{\partial f_2}{\partial q_1}(q_{1est},q_{2est})\cdot\Delta q_1 + \dfrac{\partial f_2}{\partial q_2}(q_{1est},q_{2est})\cdot\Delta q_2 + o(q_1^2,q_2^2) \end{cases} \quad \text{(II.3. 8)}$$

In this equation, $o(q_1^2, q_2^2)$ is the high order item and can be neglected. In this way, the equations $f_1(q_1, q_2)$ and $f_1(q_1, q_2)$ are expressed only with their linear components. The equation set (II.3.8) is used to replace $f_1(q_1, q_2)$ and $f_1(q_1, q_2)$ in (II.3.6) during the iterative process. Put them in matrix form:

$$\begin{bmatrix} f_1(q_{1est},q_{2est}) \\ f_2(q_{1est},q_{2est}) \end{bmatrix} + \begin{bmatrix} \dfrac{\partial f_1}{\partial q_1}(q_{1est},q_{2est}) & \dfrac{\partial f_1}{\partial q_2}(q_{1est},q_{2est}) \\ \dfrac{\partial f_2}{\partial q_1}(q_{1est},q_{2est}) & \dfrac{\partial f_2}{\partial q_2}(q_{1est},q_{2est}) \end{bmatrix} \cdot \begin{bmatrix} \Delta q_1 \\ \Delta q_2 \end{bmatrix} = \begin{bmatrix} 0 \\ 0 \end{bmatrix} \quad \text{(II.3. 9)}$$

Then the error Δq_i can be obtained as:

$$\begin{bmatrix} \Delta q_1 \\ \Delta q_2 \end{bmatrix} = \begin{bmatrix} \dfrac{\partial f_1}{\partial q_1}(q_{1est},q_{2est}) & \dfrac{\partial f_1}{\partial q_2}(q_{1est},q_{2est}) \\ \dfrac{\partial f_2}{\partial q_1}(q_{1est},q_{2est}) & \dfrac{\partial f_2}{\partial q_2}(q_{1est},q_{2est}) \end{bmatrix}^{-1} \cdot \begin{bmatrix} -f_1(q_{1est},q_{2est}) \\ -f_2(q_{1est},q_{2est}) \end{bmatrix} \quad \text{(II.3. 10)}$$

Considering the forward kinematic analysis for the parallel robot, we can have the flow chart describing the process in Figure II.3. 11:

(i) choose the initial values ψ_i , θ_i , ϕ_i and input the values as estimated ones in the forward kinematic analysis.

(ii) with the equation (II.3.10), obtain the error as the step length.

(iii) obtain the updated values ψ_i , θ_i , ϕ_i consisting of the estimated values and the error.

(iv) consider the updated values ψ_i , θ_i , ϕ_i in (iii) as the new estimated values for objective functions f_1, f_2, f_3 which will be shown later.

(v) compare the value of $f_1(f_2, f_3)$ obtained in (iv) with the required accuracy ς, if the requirement is satisfied, move the process to (vi), otherwise, go back to (ii).

(vi) consider the values in (iv) as final values and export them as results.

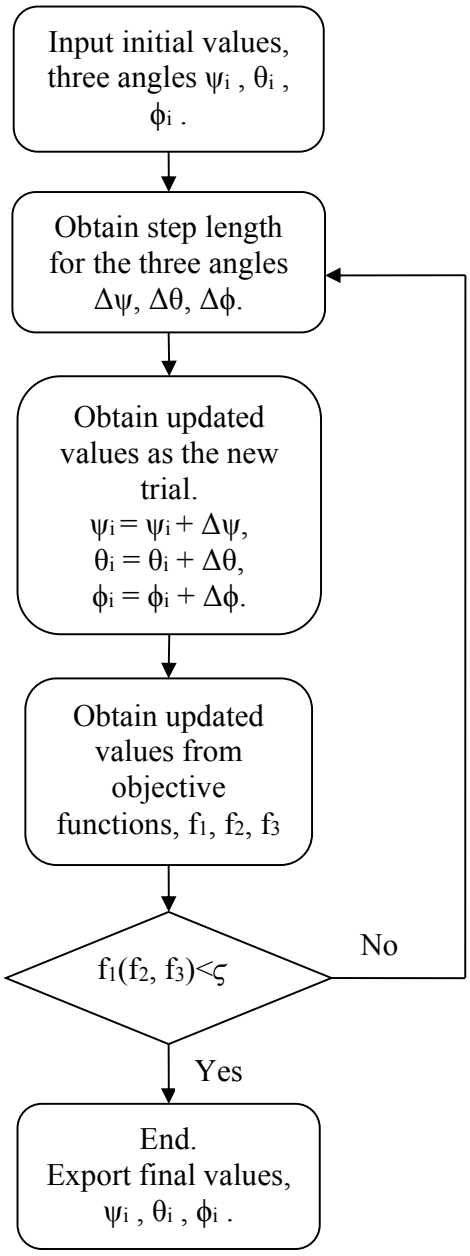

Figure II.3. 11. The flow chart for the forward kinematic analysis

Here we obtain the objective functions from (II.3.3)-(II.3.5) as:

$$f_1 = (c\psi\, c\phi - s\psi\, s\theta\, s\phi)\, x_{A2}\, X_{A1} + (c\psi\, s\phi + s\psi\, s\theta\, c\phi)\, z_{A2}\, X_{A1} - c\theta s\phi x_{A2} Z_{A1} + c\theta c\phi z_{A2} Z_{A1} - \frac{1}{2}(l_{A2}^2 + l_{A1}^2 - l_A^2) = 0 \quad \text{(II.3. 11)}$$

Where l_{A1} and l_{A2} are the lengths of the vectors $\mathbf{OA}_1$ and $\mathbf{OA}_2$.

$$
\begin{aligned}
f_2 &= (c\psi\, c\phi - s\psi\, s\theta\, s\phi)\, x_{B2}\, X_{B1} - s\psi c\theta y_{B2} X_{B1} + (c\psi\, s\phi + s\psi\, s\theta\, c\phi)\, z_{B2}\, X_{B1} \\
&+ (s\psi\, c\phi + c\psi\, s\theta\, s\phi)\, x_{B2}\, Y_{B1} + c\psi c\theta y_{B2} Y_{B1} + (s\psi\, s\phi - c\psi\, s\theta c\phi)\, z_{B2}\, Y_{B1} \\
&- c\theta s\phi x_{B2} Z_{B1} + s\theta y_{B2} Z_{B1} + c\theta c\phi z_{B2} Z_{B1} - \frac{1}{2}(l_{B2}^2 + l_{B1}^2 - l_B^2) = 0
\end{aligned}
\qquad \text{(II.3. 12)}
$$

Where l_{B1} and l_{B2} are the lengths of the vectors $\mathbf{OB}_1$ and $\mathbf{OB}_2$.

$$
\begin{aligned}
f_3 &= (c\psi\, c\phi - s\psi\, s\theta\, s\phi)\, x_{C2}\, X_{C1} - s\psi c\theta y_{C2} X_{C1} + (c\psi\, s\phi + s\psi\, s\theta\, c\phi)\, z_{C2}\, X_{C1} \\
&+ (s\psi\, c\phi + c\psi\, s\theta\, s\phi)\, x_{C2}\, Y_{C1} + c\psi c\theta y_{C2} Y_{C1} + (s\psi\, s\phi - c\psi\, s\theta c\phi)\, z_{C2}\, Y_{C1} \\
&- c\theta s\phi x_{C2} Z_{C1} + s\theta y_{C2} Z_{C1} + c\theta c\phi z_{C2} Z_{C1} - \frac{1}{2}(l_{C2}^2 + l_{C1}^2 - l_C^2) = 0
\end{aligned}
\qquad \text{(II.3. 13)}
$$

Where l_{C1} and l_{C2} are the lengths of the vectors $\mathbf{OC}_1$ and $\mathbf{OC}_2$.

Arrange the functions f_1, f_2, f_3 in the form (II.3.6),

$$
\begin{cases}
f_1(\psi, \theta, \phi) = 0 \\
f_2(\psi, \theta, \phi) = 0 \\
f_3(\psi, \theta, \phi) = 0
\end{cases}
\qquad \text{(II.3. 14)}
$$

Each function can be extended according to the Taylor extension (II.3.8). Take the first function as an example.

$$
\begin{aligned}
f_1(\psi, \theta, \phi) &= f_1(\psi_i, \theta_i, \phi_i) + \frac{\partial f_1}{\partial \psi}(\psi_i, \theta_i, \phi_i) \cdot \Delta\psi + \frac{\partial f_1}{\partial \theta}(\psi_i, \theta_i, \phi_i) \cdot \Delta\theta \\
&+ \frac{\partial f_1}{\partial \phi}(\psi_i, \theta_i, \phi_i) \cdot \Delta\phi + o(\psi^2, \theta^2, \phi^2)
\end{aligned}
\qquad \text{(II.3. 15)}
$$

Where the first item $f_1(\psi_i, \theta_i, \phi_i)$ is the function value when the function $f_1(\psi, \theta, \phi)$ has its estimated angles ψ_i, θ_i, ϕ_i.

$\frac{\partial f_1}{\partial \psi}(\psi_i, \theta_i, \phi_i)$ is the coefficient of the second item when the partial differential function $\frac{\partial f_1}{\partial \psi}(\psi, \theta, \phi)$ has its estimated value. Here we have the partial differential functions as:

$$
\frac{\partial f_1}{\partial \psi} = (-s\psi\, c\phi - c\psi\, s\theta\, s\phi)\, x_{A2}\, X_{A1} + (-s\psi\, s\phi + c\psi\, s\theta\, c\phi)\, z_{A2}\, X_{A1}
$$

$$\frac{\partial f_1}{\partial \theta} = -s\psi\, c\theta\, s\phi\, x_{A2}\, X_{A1} + s\psi c\theta c\phi\, z_{A2}\, X_{A1} + s\theta s\phi x_{A2}\, Z_{A1} - s\,\theta c\phi z_{A2} Z_{A1}$$

$$\frac{\partial f_1}{\partial \phi} = (-c\psi\, s\,\phi - s\psi s\theta c\phi)\, x_{A2}\, X_{A1} + (c\,\psi c\phi - s\psi s\theta s\phi)\, z_{A2}\, X_{A1} - c\theta c\phi x_{A2}\, Z_{A1} - c\theta s\phi z_{A2} Z_{A1}$$

The equations (II.3.12), (II.3.13) share the same format. We can know all partial differential functions. Take the equation (II.3.12) as an example, we have:

$$\frac{\partial f_2}{\partial \psi} = (-s\,\psi\, c\,\phi - c\,\psi\, s\,\theta\, s\,\phi)\, x_{B2}\, X_{B1} - c\psi c\theta y_{B2} X_{B1} + (-s\,\psi\, s\,\phi + c\,\psi\, s\,\theta\, c\,\phi)\, z_{B2}\, X_{B1}$$
$$(c\,\psi\, c\,\phi - s\,\psi\, s\,\theta\, s\,\phi)\, x_{B2}\, Y_{B1} - s\psi c\theta y_{B2} Y_{B1} + (c\,\psi\, s\,\phi + s\,\psi\, s\,\theta\, c\,\phi)\, z_{B2}\, Y_{B1}$$

$$\frac{\partial f_2}{\partial \theta} = -s\,\psi\, c\,\theta\, s\,\phi\, x_{B2}\, X_{B1} + s\psi s\theta y_{B2} X_{B1} + s\psi c\theta c\phi\, z_{B2}\, X_{B1} + c\psi c\theta s\phi x_{B2} Y_{B1}$$
$$-c\psi s\theta y_{B2} Y_{B1} - c\psi c\theta c\phi z_{B2} Y_{B1} + s\theta s\phi x_{B2}\, Z_{B1} + c\theta y_{B2} Z_{B1} - s\,\theta c\phi z_{B2} Z_{B1}$$

$$\frac{\partial f_2}{\partial \phi} = (-c\psi\, s\,\phi - s\psi s\theta c\phi)\, x_{B2}\, X_{B1} + (c\,\psi c\phi - s\psi s\theta s\phi)\, z_{B2}\, X_{B1} + (-s\psi s\phi + c\psi s\theta c\phi)\, x_{B2}\, Y_{B1}$$
$$+(s\,\psi\, c\,\phi + c\,\psi\, s\,\theta\, s\,\phi)\, z_{B2}\, Y_{B1} - c\theta c\phi x_{B2}\, Z_{B1} - c\theta s\phi z_{B2} Z_{B1}$$

Write the equation (II.3.15) three times with the start of f_1, f_2, f_3. Considering (II.3.14), we can obtain the step length for the three angle variables in matrix form:

$$\begin{bmatrix} \Delta\psi \\ \Delta\theta \\ \Delta\phi \end{bmatrix} = \begin{bmatrix} \frac{\partial f_1}{\partial \psi} & \frac{\partial f_1}{\partial \theta} & \frac{\partial f_1}{\partial \phi} \\ \frac{\partial f_2}{\partial \psi} & \frac{\partial f_2}{\partial \theta} & \frac{\partial f_2}{\partial \phi} \\ \frac{\partial f_3}{\partial \psi} & \frac{\partial f_3}{\partial \theta} & \frac{\partial f_3}{\partial \phi} \end{bmatrix}^{-1}_{\psi i, \theta i, \phi i} \cdot \begin{bmatrix} -f_1 \\ -f_2 \\ -f_3 \end{bmatrix}_{\psi i, \theta i, \phi i} \qquad \text{(II.3. 16)}$$

With these details (the equations (II.3.11)-(II.3.16)), we can execute the flow chart and finally obtain the proper results. Here shows examples in Table II.3. 4 and the comparison with the inverse counterparts in Table II.3. 5.

Table II.3. 4. The forward kinematic examples

	Lengths of the three wries			Forward kinematic results		
Examples	LA(mm)	LB(mm)	LC(mm)	ψ(rad)	θ(rad)	ϕ(rad)
1	215.0751	314.2350	308.8812	0.1738	0.0869	0.0525
2	218.9051	310.2206	306.1812	0.0975	0.0552	0.0170

3	201.0768	317.8856	322.4417	-0.1990	-0.0948	0.1712

Table II.3. 5. The inverse kinematic examples

Examples	Inverse kinematic results		
	ψ(rad)	θ(rad)	ϕ(rad)
1	0.1745	0.0873	0.0524
2	0.0873	0.0524	0.0175
3	-0.1745	-0.0873	0.1745

II.3.3. Jacobian matrix

This part is devoted to the Jacobian and quasi-statics analysis. The Jacobian matrix of the structure can be obtained in this way. From Figure II.3. 2, we can have:

$$\begin{cases} \mathbf{OA_2} = \mathbf{OA_1} + \mathbf{A_1A_2} \\ \mathbf{OB_2} = \mathbf{OB_1} + \mathbf{B_1B_2} \\ \mathbf{OC_2} = \mathbf{OC_1} + \mathbf{C_1C_2} \end{cases} \quad \text{(II.3. 17)}$$

Taking the derivative of the equation (II.3.17) with respect to time yields a velocity vector equation. With the first part in Eq. (II.3.17), it can be evolved as:

$$\boldsymbol{\omega}_A \times \mathbf{OA_2} = L_A \cdot \boldsymbol{\omega}_{A1A2} \times \mathbf{s}_{A1A2} + L'_A \cdot \mathbf{s}_{A1A2} \quad \text{(II.3. 18)}$$

Where $\boldsymbol{\omega}_A$ means that the angular velocity of the moving platform, contributed by the wire A. $\boldsymbol{\omega}_{A1A2}$ denotes the angular velocity of the wire A with respect to the fixed base. L'_A is the linear velocity of the wire A. $\mathbf{s}_{A1A2}$ is a unit vector along the wire A, pointing from A_1 to A_2. To eliminate $\boldsymbol{\omega}_{A1A2}$, we dot-multiply both sides of the equation (II.3.18) by $\mathbf{s}_{A1A2}$:

$$(\mathbf{OA_2} \times \mathbf{s}_{A1A2}) \cdot \boldsymbol{\omega}_A = L'_A \quad \text{(II.3. 19)}$$

Write the equation (II.3.19) three times, for each wire A, B and C, and arrange the three equation in matrix form as:

$$\mathbf{J}_\omega \boldsymbol{\omega} = \mathbf{J}_1 \mathbf{L}' \quad \text{(II.3. 20)}$$

In details,

$$\mathbf{J}_\omega = \begin{bmatrix} (\mathbf{OA_2} \times \mathbf{s}_{A1A2})^T \\ (\mathbf{OB_2} \times \mathbf{s}_{B1B2})^T \\ (\mathbf{OC_2} \times \mathbf{s}_{C1C2})^T \end{bmatrix}, \quad \mathbf{J}_1 = \mathbf{I} \text{ (3×3 identity matrix).}$$

$\boldsymbol{\omega} = [\omega_x, \omega_y, \omega_z]^T$ is the angular velocity of the moving platform. $L' = [L'_A, L'_B, L'_C]^T$ is the linear velocity of the three wires.

As we know,

$$\mathbf{OA_2} = (X_{A2}, Y_{A2}, Z_{A2})^T$$

$$\mathbf{s_{A1A2}} = \frac{1}{L_A}(X_{A2} - X_{A1}, Y_{A2} - Y_{A1}, Z_{A2} - Z_{A1})^T$$

So, here we have,

$$\begin{aligned}\left(\mathbf{OA_2} \times \mathbf{s_{A1A2}}\right)^T = \frac{1}{L_A}[&(Z_{A2} - Z_{A1})Y_{A2} - (Y_{A2} - Y_{A1})Z_{A2},\\ &(X_{A2} - X_{A1})Z_{A2} - (Z_{A2} - Z_{A1})X_{A2},\\ &(Y_{A2} - Y_{A1})X_{A2} - (X_{A2} - X_{A1})Y_{A2}]\end{aligned}$$

Finally, we can have the relation between the angular velocity of the moving platform and the wire linear velocity in the equation (II.3.20).

For simplicity, in the matrix $\mathbf{J_\omega}$, we can use $\mathbf{n_A}$, $\mathbf{n_B}$ and $\mathbf{n_C}$ representing every row of the matrix. For example,

$$\mathbf{n_A} = \left(\mathbf{OA_2} \times \mathbf{s_{A1A2}}\right) \qquad \text{(II.3. 21)}$$

$\mathbf{n_A}$ means a vector is normal to the plane defined by the triangle ΔA_1OA_2.

A limitation of a parallel structure is that the singular configurations may exist within its workspace where the structure gains one or more DOFs and loses its stiffness completely. Due to the existence of the two Jacobian matrices in the equation (II.3.20), the structure is said to be at a singular configuration below the following three situations [1]:

(i). the inverse kinematic singularity occurs when the determinant of $\mathbf{J_I}$ is zero, $\det(\mathbf{J_I}) = 0$. Since $\mathbf{J_I}$ is an identity matrix, it does not exist inverse kinematic singularity within the workspace of the structure. However, at the workspace boundary, one or more wires are fully stretched or retracted, the singularities may occur. This kind of singularity can be avoided for the rehabilitation device we focus on, since the motion range of the foot ankle (see Section II.2) is normally limited by biomechanics and the physical structure of the foot ankle.

(ii) the forward kinematic singularity occurs when the determinant of $\mathbf{J_\omega}$ is zero, $\det(\mathbf{J_\omega}) = 0$. Considering the equation (II.3.20), (II.3.21), the determinant could go to zero in three cases:

(1). One of the three vectors, $\mathbf{n_A}$ (or $\mathbf{n_B}$ or $\mathbf{n_C}$) vanishes. In this situation, the three points A_1, O and A_2 lie on a straight line. With all actuators locked, the moving platform can make an infinitesimal rotation about a line of intersection of the two planes defined by the other two triangles ΔB_1OB_2 and ΔC_1OC_2, shown in Figure II.3. 12. In fact, for the rehabilitation device, the foot cannot go to the singular situation with the three points on a straight line. So this case is not happened during the rehabilitation process.

(2). Any two of the three vectors, $\mathbf{n_A}$ and $\mathbf{n_B}$ (or $\mathbf{n_C}$) are linearly dependent. It is possible when the two planes defined by the triangles ΔA_1OA_2 and ΔB_1OB_2 are coincident, the structure can get one DOF. With all actuators locked, the moving platform can make an infinitesimal rotation about a line of intersection of the two planes defined by the two triangles ΔA_1OA_2 and ΔC_1OC_2, shown in Figure II.3. 13.

For the design of the rehabilitation device, since the ends of the wires B_1B_2 and C_1C_2 are at the two sides of the calf and the ankle joint is between the wires, the planes defined by the triangles ΔB_1OB_2 and ΔC_1OC_2 always have intersection during the motion. The two planes would coincide unless the ends B_1 and C_1, B_2 and C_2 are coincident respectively. This design prototype is therefore not accepted. We can choose the positions of the spherical joints at the calf and the foot to ensure this kind of the singular situation avoided. The other possibility is the singular problem between the planes defined by the triangles ΔA_1OA_2 and ΔB_1OB_2 (or ΔA_1OA_2 and ΔC_1OC_2). In this configuration, the positions of the points A_2 and B_2 in the workspace should be included in the fixed plane defined by the fixed points A1, O and B_1. It is impossible considering the existence of the bone and muscle structure of the calf and the foot. Therefore, the singular configuration in this case is not physically realized.

(3). the three vectors, $\mathbf{n_A}$, $\mathbf{n_B}$ and $\mathbf{n_C}$ are linearly dependent. This condition happens when the three planes defined by the triangles ΔA_1OA_2 , ΔB_1OB_2 and ΔC_1OC_2 intersect in a common line. The vectors $\mathbf{n_A}$, $\mathbf{n_B}$ and $\mathbf{n_C}$ lie on the same plane. In this situation, the moving platform can make an infinitesimal rotation about the common line. In the design of the rehabilitation device, this could be happened when the ends B_1, C_1, B_2 and C_2 of the wire B1B1, C1C2 are designed in symmetric positions with respect to the sagittal plane of the foot. Also considering the properties of the wire connection, n wires can only control (n-1) DOF [4][5]. The three wires are used to control the rotation in the frontal and sagittal planes. The rotation in the transverse plane is expected to be controlled by a pedal device applied under the foot during the rehabilitation process.

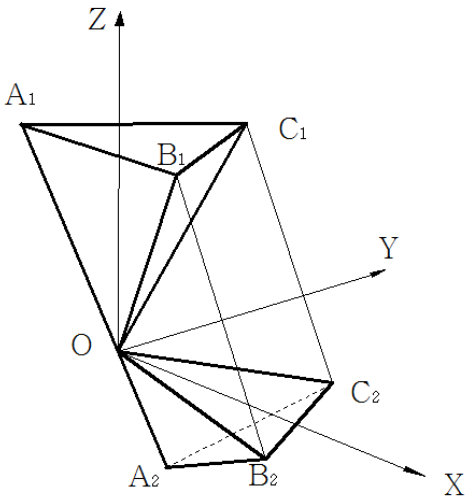

Figure II.3. 12. The singular situation when the points A_1, O and A_2 on a straight line.

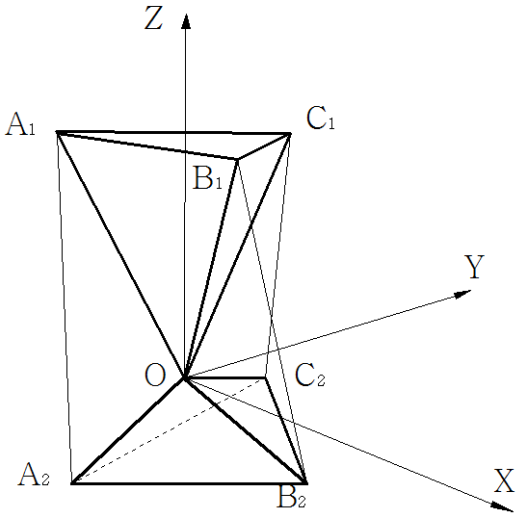

Figure II.3. 13. The singular situation when the two planes defined by the triangles ΔA_1OA_2 and ΔB_1OB_2 are coincident

(iii) Combined singularities. Combined singularities consider a combination of inverse and forward singularities. This could be happened at the workspace boundary if the following three conditions are satisfied simultaneously: 1. the moving tetrahedron is similar to the fixed one; 2. The three planes defined by the three triangles intersect at a common line; 3. One of the three wires is at its extreme reach. Considering the physical realization of the rehabilitation device, this kind of singularities can be avoided.

II.3.4. Quasi-statics study

Here we focus on the study of the quasi-statics since the foot equipped with the rehabilitation device is moved and treated slowly during the training work. The gravity of the foot is negligible. The foot is applied by forces from the wires and the ankle joint (Figure II.3. 14).

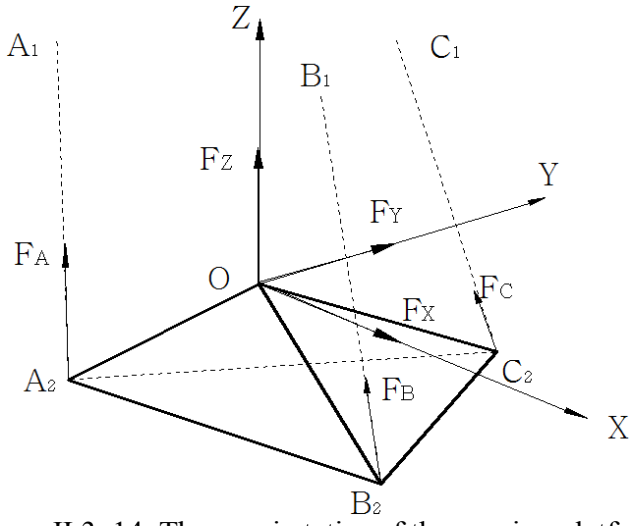

Figure II.3. 14. The quasi-statics of the moving platform

Assume that every force is the result of the scalar value multiplying the unit vector along the direction of the force:

$$\mathbf{F_A} = f_A \cdot \mathbf{s_{A2A1}}\ ,\ \ \mathbf{F_B} = f_B \cdot \mathbf{s_{B2B1}}\ ,\ \ \mathbf{F_C} = f_C \cdot \mathbf{s_{C2C1}}\ ,\ \ \mathbf{F_X} = f_X \cdot \mathbf{X}\ ,\ \ \mathbf{F_Y} = f_Y \cdot \mathbf{Y}\ ,\ \ \mathbf{F_Z} = f_Z \cdot \mathbf{Z}\ .$$

Where,

$$\mathbf{s_{A2A1}} = \frac{\mathbf{A_2A_1}}{L_A}\ ,\ \ \mathbf{s_{B2B1}} = \frac{\mathbf{B_2B_1}}{L_B}\ ,\ \ \mathbf{s_{C2C1}} = \frac{\mathbf{C_2C_1}}{L_C}\ .$$

Therefore, the resultant force applied on the moving platform is :

$$\begin{aligned}\mathbf{F} &= \mathbf{F_A} + \mathbf{F_B} + \mathbf{F_C} + \mathbf{F_X} + \mathbf{F_Y} + \mathbf{F_Z} \\ &= \frac{f_A}{L_A}\begin{bmatrix} X_{A1} - X_{A2} \\ Y_{A1} - Y_{A2} \\ Z_{A1} - Z_{A2} \end{bmatrix} + \frac{f_B}{L_B}\begin{bmatrix} X_{B1} - X_{B2} \\ Y_{B1} - Y_{B2} \\ Z_{B1} - Z_{B2} \end{bmatrix} + \frac{f_C}{L_C}\begin{bmatrix} X_{C1} - X_{C2} \\ Y_{C1} - Y_{C2} \\ Z_{C1} - Z_{C2} \end{bmatrix} + \begin{bmatrix} f_X \\ 0 \\ 0 \end{bmatrix} + \begin{bmatrix} 0 \\ f_Y \\ 0 \end{bmatrix} + \begin{bmatrix} 0 \\ 0 \\ f_Z \end{bmatrix} \\ &= \begin{bmatrix} \frac{X_{A1} - X_{A2}}{L_A} & \frac{X_{B1} - X_{B2}}{L_B} & \frac{X_{C1} - X_{C2}}{L_C} \\ \frac{Y_{A1} - Y_{A2}}{L_A} & \frac{Y_{B1} - Y_{B2}}{L_B} & \frac{Y_{C1} - Y_{C2}}{L_C} \\ \frac{Z_{A1} - Z_{A2}}{L_A} & \frac{Z_{B1} - Z_{B2}}{L_B} & \frac{Z_{C1} - Z_{C2}}{L_C} \end{bmatrix} \cdot \begin{bmatrix} f_A \\ f_B \\ f_C \end{bmatrix} + \begin{bmatrix} f_X \\ f_Y \\ f_Z \end{bmatrix}\end{aligned} \qquad \text{(II.3. 22)}$$

The moments applied on the foot can be evolved around the ankle joint O, as:

$$\begin{aligned}\mathbf{n_O} &= \begin{bmatrix} n_X & n_Y & n_Z \end{bmatrix}^T = \mathbf{OA_2} \times \mathbf{F_A} + \mathbf{OB_2} \times \mathbf{F_B} + \mathbf{OC_2} \times \mathbf{F_C} \\ &= f_A \cdot \mathbf{OA_2} \times \mathbf{s_{A2A1}} + f_B \cdot \mathbf{OB_2} \times \mathbf{s_{B2B1}} + f_C \cdot \mathbf{OC_2} \times \mathbf{s_{C2C1}} \\ &= \begin{bmatrix} \mathbf{OA_2} \times \mathbf{s_{A2A1}} \\ \mathbf{OB_2} \times \mathbf{s_{B2B1}} \\ \mathbf{OC_2} \times \mathbf{s_{C2C1}} \end{bmatrix}^T \cdot \begin{bmatrix} f_A \\ f_B \\ f_C \end{bmatrix} = \mathbf{J_\omega} \cdot \begin{bmatrix} f_A \\ f_B \\ f_C \end{bmatrix}\end{aligned} \tag{II.3. 23}$$

Where,

$$\begin{aligned}n_X = &\frac{(Z_{A2} - Z_{A1}) Y_{A2} - (Y_{A2} - Y_{A1}) Z_{A2}}{L_A} \cdot f_A + \frac{(Z_{B2} - Z_{B1}) Y_{B2} - (Y_{B2} - Y_{B1}) Z_{B2}}{L_B} \cdot f_B \\ &+ \frac{(Z_{C2} - Z_{C1}) Y_{C2} - (Y_{C2} - Y_{C1}) Z_{C2}}{L_C} \cdot f_C\end{aligned} \tag{II.3. 24}$$

$$\begin{aligned}n_Y = &\frac{(X_{A2} - X_{A1}) Z_{A2} - (Z_{A2} - Z_{A1}) X_{A2}}{L_A} \cdot f_A + \frac{(X_{B2} - X_{B1}) Z_{B2} - (Z_{B2} - Z_{B1}) X_{B2}}{L_B} \cdot f_B \\ &+ \frac{(X_{C2} - X_{C1}) Z_{C2} - (Z_{C2} - Z_{C1}) X_{C2}}{L_C} \cdot f_C\end{aligned} \tag{II.3. 25}$$

$$\begin{aligned}n_Z = &\frac{(Y_{A2} - Y_{A1}) X_{A2} - (X_{A2} - X_{A1}) Y_{A2}}{L_A} \cdot f_A + \frac{(Y_{B2} - Y_{B1}) X_{B2} - (X_{B2} - X_{B1}) Y_{B2}}{L_B} \cdot f_B \\ &+ \frac{(Y_{C2} - Y_{C1}) X_{C2} - (X_{C2} - X_{C1}) Y_{C2}}{L_C} \cdot f_C\end{aligned} \tag{II.3. 26}$$

II.3.5 Conclusions

In this chapter, a wire robot with a parallel structure and its ideal model are proposed. Inverse and forward kinematic analysis is presented respectively. In the inverse kinematics, the rotational angles are assumed as the known conditions and the wire lengths are supposed to obtain. The vector relation between the moving platform and the fixed base is used to develop the accurate solutions for the wire lengths. Numerical examples are followed to verify the conclusions. With the inverse kinematic model as a simulation tool, any range of motion can be simulated and the according length changes can be obtained. As for the forward kinematics, the iterative method called 'Newton-Raphson Method' is applied to solve the nonlinear kinematic problems in an approximated way. After an introduction of the method, the flow chart is shown. Examples are provided and compared with the inverse counterparts. The error between the forward and inverse kinematics is acceptable. Then, the singularities problems are discussed in three categories. Finally, the quasi-statics model is presented and the forces and moments applied on the foot are studied. The kinematic and force model introduced in this chapter are useful tools for the proposal of the control strategies based on different rehabilitation tasks.

References:

[1] Tsai, L. W Robot Analysis: The mechanics of Serial and Parallel Manipulators, Wiley-Intersecience Publication, John Wiley and Sons, 1999.

[2] John Craig. Introduction to Robotics: Mechanics and Control. Pearson Education Inc., 2005.

[3] John F. Gardner. Simulations of Machines Using Matlab and Simulink. Books/Cole. Thomson Learning, 2002.

[4] Tobias Bruckmann, Lars Mikelsons, Thorsten Brandt, Manfred Hiller and Dieter Schramm (2008). Wire Robots, Part I: Kinematics, Analysis & Design, Parallel Manipulators, New Developments, Jee-Hwan Ryu (Ed.), ISBN: 978-3-902613-20-2, InTech Education and Publishing.

[5] Tobias Bruckmann, Lars Mikelsons, Thorsten Brandt, Manfred Hiller and Dieter Schramm (2008). Wire Robots, Part II: Dynamics, Control & Application, Parallel Manipulators, New Developments, Jee-Hwan Ryu (Ed.), ISBN: 978-3-902613-20-2, InTech Education and Publishing.

Section II.4 Conclusions of Section II

This section focuses on the design of a parallel robotic structure for the ankle rehabilitation. A wire robot with a parallel structure is proposed based on the ankle properties and its training requirements. The biomechanics is discussed and also its motion and torque ranges.

The innovative proposal is replaced with an ideal model for its kinematic and dynamic analysis. Then, inverse and forward kinematic analysis is presented respectively. In the inverse kinematics, the vector relation between the moving platform and the fixed base is used to develop the accurate solutions for the wire lengths. Numerical examples are followed to verify the ankle motion. As for the forward kinematics, an iterative method is applied to solve the nonlinear kinematic problems in an approximated way. Examples are provided and compared with the inverse counterparts. The error between the forward and inverse kinematics is acceptable. The singularities problems are discussed in three categories. The quasi-statics model is presented and the forces and moments applied on the foot are studied. The kinematic and force model are useful tools for the proposal of the control strategies based on different rehabilitation tasks.

Closure

This thesis tries to design and develop robotic devices in their applications. For the Section 1, the thesis makes some contribution to the design of the energy saving system for serial robotic structures and present some interesting conclusions. This section showed the design details and the balancing system for the two robotic structures with 2 DOF. The energy transfer principle was illustrated. This section also provided the designer a tool to decide balance accuracy. Approximate and perfect balance were both considered. Numerical examples showed the balancing effect. As a feasible solution, the spring volume and the influence factors were discussed. The pros and cons between the two variant structures were presented. According to the methodology presented in this section, articulated robots with similar structures can be designed and equipped with perfectly statically balancers.

Section II focuses on the design of a parallel robotic structure for the ankle rehabilitation. A wire robot was proposed based on the ankle properties and its training requirements. The proposal is innovative with a light weight and a compact volume. Its kinematic and dynamic analysis was presented. For the kinematic analyses, inverse and forward kinematics was presented and compared with numerical examples. For the dynamic analyses, the quasi-statics model was presented and the forces and moments applied on the foot were studied. The kinematic and force model are useful tools for the ankle rehabilitation.